

## Offshore Wind Farm

## Eneco Luchterduinen

Ecological monitoring of seabirds

T0 report



February 2015

This report has been prepared under the DHI Business Management System certified by DNV to comply with ISO 9001 (Quality Management)



DNV Business Assurance, Danmark A/S

# Offshore Wind Farm

## Eneco Luchterduinen

Ecological monitoring of seabirds

T0 report

Prepared for            ENECO  
 Represented by        Ms. Sytske van den Akker



*Photo by Tom Wezo*

Project manager	Henrik Skov
Author	Henrik Skov   Stefan Heinänen   Lotte Nyborg   Martin Lazcny
Quality supervisor	Ramunas Zydelis
Project number	11813060
Approval date	2 February 2015
Revision	Final
Classification	Confidential

## Executive summary

The Offshore Wind Farm Eneco Luchterduinen (LUD) is scheduled for construction in summer 2014, with the 43 turbines expected to be fully operational by summer 2015. According to the license permit, LUD is obliged to carry out a 3-5 year monitoring program on seabirds focused on assessing any location specific and cumulative avoidance behaviour which can be measured in LUD and the two existing offshore wind farms (OWEZ and PAWP). For this purpose, a ship-based line transect monitoring program of wintering seabirds has been approved by the Competent Authority, which covers pre-construction (baseline), construction and post-construction phases. This report covers the results of the first winter of seabird monitoring (LUD-T0) carried out between October 2013 and January 2014.

The three surveys undertaken supplemented PAWP-T0 and PAWP-T1 data as well as OWEZ-T0 and OWEZ-T1 data near these two wind farms, while the area south of PAWP and OWEZ received much more coverage compared to earlier surveys. Additionally, more data were collected on the utilisation of the two wind farms by seabirds; data which largely corroborated earlier findings, and now form part of LUD-T0 (Leopold et al. 2013). The greatest challenge for the seabird monitoring at LUD will be to decipher 'natural' variability in distributions from changes induced by LUD. LUD is located at 18-22 m water depth in an area characterised by being at the deeper end of the gradient between coastal and North Sea water masses found along the Dutch mainland coast. Thus, distributions of seabirds at the LUD may oscillate in response to the dynamics of coastal and North Sea water masses. In addition to the influence of local oceanographic features ship traffic affects the distribution of several seabird species negatively, while fisheries affect the distribution of seabirds in both positive and negative ways. In order to describe the LUD-T0 situation for seabirds, and enable the identification of potential impacts of LUD on seabird distribution a semi-dynamic model framework was established. The model framework has been based on multiple regression models for all seabird species matched with modelled hydrodynamic habitat parameters and pressure data on wind farms, anchoring sites and patterns of ship traffic. The models have utilized all existing data which have been collected over the last 10 years.

After LUD-T1, the power of the monitoring data will be assessed. All primary transects were covered, as were a number of the secondary transects, especially in the southern part of the area. Thus, the collected data should form a solid basis for assessing any habitat displacement of seabirds from the LUD. This can be determined by testing for changes in densities at increasing distances from the wind farms while taking account of changes in oceanographic properties of the area as well as seasonal and year-to-year variation. Judged from the model results the winter distribution of seabirds at the LUD may be characterised by high densities of Common Guillemot and low densities of other species of seabirds. However, the distribution of several species of seabirds in the area is closely associated with features of the local current and hydrographic regime, especially surface salinity and eddy activity seem to be important features. Almost all species which occur in higher densities inshore from LUD have a tendency to extend their distribution westwards during periods with a strong coastal current, whereas the more pelagic species show the opposite response and extend their distribution eastwards during periods with a weak coastal current.

# CONTENTS

<b>Executive summary</b> .....	<b>ii</b>
<b>1 Abbreviations</b> .....	<b>v</b>
<b>2 Introduction</b> .....	<b>6</b>
<b>3 Materials and methods</b> .....	<b>7</b>
3.1 Monitoring approach.....	7
3.2 Survey design and available data.....	7
3.3 Seabird counting techniques .....	9
3.4 Quality control and post-processing of survey data .....	11
3.5 Distance analysis .....	11
3.6 Statistical analysis .....	13
3.7 Presentation of data.....	16
<b>4 Results</b> .....	<b>16</b>
4.1 Effort and sample sizes .....	16
4.2 Distance analysis .....	18
4.3 Species accounts.....	20
4.3.1 Divers: Red-throated <i>Gavia stellata</i> and Black-throated Divers <i>Gavia arctica</i> .....	20
4.3.2 Great Crested Grebe <i>Podiceps cristatus</i> .....	22
4.3.3 Northern Fulmar <i>Fulmarus glacialis</i> .....	24
4.3.4 Northern Gannet <i>Morus bassanus</i> .....	25
4.3.5 Great Cormorant <i>Phalacrocorax carbo</i> .....	28
4.3.6 Common Scoter <i>Melanitta nigra</i> .....	30
4.3.7 Little Gull <i>Hydrocoloeus minutus</i> .....	32
4.3.8 Black-headed Gull <i>Chroicocephalus ridibundus</i> .....	34
4.3.9 Common Gull <i>Larus canus</i> .....	37
4.3.10 Lesser Black-backed Gull <i>Larus fuscus</i> .....	40
4.3.11 Herring Gull <i>Larus argentatus</i> .....	42
4.3.12 Great Black-backed Gull <i>Larus marinus</i> .....	45
4.3.13 Black-legged Kittiwake <i>Rissa tridactyla</i> .....	48
4.3.14 Sandwich Tern <i>Sterna sandvicensis</i> .....	51
4.3.15 ‘Commic’ terns: Common Tern <i>Sterna hirundo</i> and Arctic Tern <i>Sterna paradisaea</i> .....	51
4.3.16 Common Guillemot <i>Uria aalge</i> .....	52
4.3.17 Razorbill <i>Alca torda</i> .....	55
4.3.18 Marine mammal observations .....	58
<b>5 Discussion and Conclusions</b> .....	<b>59</b>
5.1 Characterisation of LUD site .....	59
5.2 Monitoring design .....	60
<b>6 References</b> .....	<b>62</b>

## APPENDICES

APPENDIX A – Detailed methods for species distribution models .....	65
APPENDIX B – Detailed results of species distribution models .....	87
APPENDIX C – Historic T0 data .....	135
APPENDIX D – Survey effort 2002-2010 134 .....	154

# 1 Abbreviations

AIC	Akaike Information Criterion
AUC	Area Under Curve. Probability of correctly predicting presence of species
CDS	Conventional Distance Sampling engine
EEZ	Dutch Exclusive Economic Zone
EIA	Environmental Impact Assessment
ESASD	European Seabirds at Sea Database
ESW	Effective Strip Width
GAM	Generalized Additive Model
LAT	Lowest Astronomical Tide
LUD	Offshore Wind Farm Eneco Luchterduinen
MEP	Monitoring and Evaluation Program
MCDS	Multiple Covariates Distance Sampling engine
OWF	Offshore Wind Farm
PAWP	Prinses Amalia wind farm
TOR	Terms of Reference
UTM	Universal Transverse Mercator
WTG	Wind Turbine Generator

## 2 Introduction

The Offshore Wind Farm Eneco Luchterduinen (LUD) is scheduled for construction in summer 2014, and the 129 MW (43 turbines) are expected to be fully operational by summer 2015. The wind farm will cover an area of 16 km<sup>2</sup>. The proposed location for the LUD is 17 km south of the existing Prinses Amaliawindpark (PAWP), roughly 23km off the coast of IJmuiden in block Q10 of the Netherlands Continental Shelf (NCS) in the Dutch Exclusive Economic Zone (EEZ). The water depth at this location ranges between 19 m and 24 m relative to LAT. The water depth and composition of the sediment underground allows for steel mono-piles to be used in conjunction with the preferred wind turbine generator (WTG) type which, under these circumstances, is the most cost effective solution. At a water depth of 25 m the WTGs require mono-piles of 51.5 m in length, with a diameter between 4.2 and 4.6 m and a transition piece of 19.1 m in length with a diameter of 4.5 m. Pile penetration in the seabed is approximately 23 m. An offshore high voltage station (OHVS) will collect the generated energy at all WTGs and transforms the voltage from MV level to HV level, suited for export to shore. The wind farm shall be connected to the 150 kV onshore substation in Sassenheim.

OWEZ was constructed between April and August 2006, while PAWP was constructed between October 2006 and June 2008. The two wind farms have very different designs; PAWP has a much higher turbine density than OWEZ, and has been built in slightly deeper waters (19-24 m versus 18-20 m) and further offshore (ca 23 km versus ca 15 km) than OWEZ.

As part of the Wbr-permit application an ‘Environmental Impact Assessment’ (EIA) and an ‘Appropriate Assessment’ were carried out. The outcome of these studies resulted in the requirement by the Competent Authority for a ‘Monitoring and Evaluation Program’ (MEP). The MEP is undertaken in conjunction with and for approval by the Competent Authority. Currently the MEP consists of eleven monitoring topics, of which seabirds is one topic. LUD is obliged to carry out a 3-5 year monitoring program on seabirds. According to the license permit the objective of the Luchterduinen seabird monitoring program is to conduct the seabird monitoring program in a way that location specific and cumulative avoidance behaviour can be measured in LUD and the two existing offshore wind farms (OWEZ and PAWP). For this purpose, a ship-based line transect monitoring program of seabirds focusing on the winter season has been proposed by the Client’, and approved by the Competent Authority. The program covers pre-construction (baseline), construction and post-construction phases. This report covers the results of the first winter of seabird monitoring (T0) carried out between October 2013 and January 2014.

As documented during the most comprehensive monitoring program in the North Sea at the Horns Rev 1 and 2 offshore wind farms in Denmark between 2000 and 2012, a between species of seabirds diversity of distribution responses to the wind farms should be expected at the LUD (Petersen et al. 2006, Piper et al. 2008, Skov et al. 2009, Skov et al. 2012). Most pelagic seabirds and waterbirds like Red-throated Diver and Common Scoter displayed clear avoidance patterns, with only few birds irregularly entering the Horns Rev 1 and Horns Rev 2 wind farms. Similar results were obtained at the PAWP wind farm (Krijgsveld et al. 2011, Leopold et al. 2013). As LUD is located in a dynamic oceanographic region at the interface between coastal and North Sea water masses, the challenge of the monitoring programme will be to separate changes in the distribution of seabirds which can be attributed to the wind farm rather than to natural changes in the location of feeding habitats.

## 3 Materials and methods

### 3.1 Monitoring approach

The TORs for the seabird monitoring are to study the distribution and abundance of seabirds in the region of the three wind farms before, during and after construction of the LUD wind farm. After the post-construction surveys, the results will be evaluated (once or twice) to determine to what extent the behavioural responses of species of seabirds have been determined, and whether the ship-based surveys can be curtailed. The collected data should be used to assess the avoidance behaviour of seabirds both in relation to the LUD wind farm and as a secondary priority cumulatively to the LUD, OWEZ and PAWP wind farms. The study should be undertaken using three sets of four NE-SW oriented transects traversing the three wind farms. Each of the proposed transects measures approximately 20 km. Results of the monitoring of habitat displacement of seabirds and waterbirds at other offshore wind farms have strongly indicated displacements to a distance of 1-2 kilometers (Petersen et al. 2006, Skov et al. 2012). Hence, the use of relatively short transect lines in the three wind farms is suitable for detecting gradients in abundance which can be attributed to the wind farms. This means that the degree of habitat displacement from all three wind farms can be tested statistically by gradient analysis.

In addition to the three series of four 20 km long primary transects through each of the LUD, OWEZ and PAWP wind farms, the monitoring approach includes a number of 30-40 km long secondary transects running east-west through the entire survey region. As habitat displacement of seabirds from offshore wind farms is typically short-scaled, this survey design provides a good basis for determining to what degree the different species of seabirds are impacted by habitat displacement, which can be determined by testing for changes in densities at increasing distances from the wind farms. However, the distribution of seabirds like Red-throated Divers *Gavia stellata* and Great Crested Grebe *Podiceps cristatus* in the coastal waters of the eastern North Sea is controlled by the distribution of feeding habitats. As these habitats are typically associated with hydrographic structures and water masses (Skov & Prins 2001, Skov et al. 2009), any changes in the distribution of the seabirds may be caused by other factors than the three wind farms. This could lead to a type II error – a result erroneously pointing at an impact. This has been corroborated by power tests of aerial monitoring data of seabirds associated with wind farms in the United Kingdom which documented low power in the detection of descending trends in abundance of seabirds caused by wind farms (MacLean et al. 2012). These tests showed that fair power could only be achieved in cases where large concentrations were regularly observed and/or where monitoring was continued over a very long period of time. It was therefore concluded that detection of changes in the distribution of seabirds induced by the construction of a wind farm would require the collection of in situ co-variables describing the variation in the location of feeding habitats. Therefore dynamic habitat data computed by a dedicated habitat model has been integrated into the LUD monitoring scheme.

### 3.2 Survey design and available data

The survey design is given in Figure 1, showing the three series of four dense primary transects through LUD, OWEZ and PAWP designed to detect habitat displacement and the coarse set of secondary transects covering a larger region surrounding the three wind farms designed to describe distributions over a wider region. Between LUD and PAWP-OWEZ the shipping lane to/from IJmuiden is located. Two anchoring sites are associated with the shipping lane. The study area extends from about 52°30'N (Noordwijk) to about 52°45'N (Hondsbossche Zeewering) and from the shore to circa 18 nm out to sea. The size of the study area is circa 725 km<sup>2</sup>. The primary transects are oriented NE-SW to capture the expected density gradient in seabirds, whereas the secondary transects are largely perpendicular to the main physical and ecological parameters, such as distance from the coast, water depth, temperature and salinity.

Three surveys with 2 months interval were planned to be undertaken during the 2013-2014 winter in October, December and February. Each survey was planned for a period of five days (if permitted by the weather). The survey strategy has been to cover primary transects during all surveys, and as many of the secondary transects as possible. The primary transects were surveyed first, and surveying of the secondary

transects was only initiated once the primary transects had been surveyed. The primary transects measure 209 km (+ 11 km transit) which can be covered in 12-14 hours of survey time. The secondary transects measure 660 km (+ 48 km transits). It was the strategy to achieve as much coverage as possible in the coastal and offshore environment surrounding the Luchterduinen survey area. The coverage of the secondary transects was therefore designed to achieve as much survey effort as possible on the secondary transects in the southern part of the survey region.

In order to avoid survey artefacts due to effects of diurnal patterns in distribution each survey started with different primary transects. When crossing PAWP and OWEZ a safety distance of 250 m was kept to the turbines. During crossing of the shipping lane a minimum distance of 1000 m was maintained to all vessels in the shipping lane.

Surveys were initiated only on the basis of a forecasted weather window (less than Beaufort 5, good visibility ( $\geq 2$  km), no heavy precipitation) of at least 2 days. Surveys should only be undertaken during sea states less than or equal to 4 and visibility of 2 km or more. Cancellation of a survey would only take place in situations with adverse weather conditions in relation to surveying (sea state above 4, visibility  $< 2$  km) extending beyond the 5 day period of a survey.

Ship-based seabird survey data collected as part of the OWEZ-T0 and OWEZ-T1 as well as PAWP-T0 and PAWP-T1 monitoring were kindly made available to us by the Dutch Ministry of Infrastructure and the Environment. It was therefore possible to include all recent survey data into the LUD-T0 models describing the present distribution of seabirds in the survey region. Both historic and new LUD-T0 data were treated in the same way, i.e. only data collected in sea states less than or equal to 4 were retained (see chapter 3.5 and 3.6 for details). Data from the short-list monitoring programme [http://www.informatiehuismarien.nl/Images/Zeevogeltellingen%20schip\\_2030.pdf](http://www.informatiehuismarien.nl/Images/Zeevogeltellingen%20schip_2030.pdf) are expected to be included in the model framework in 2015.

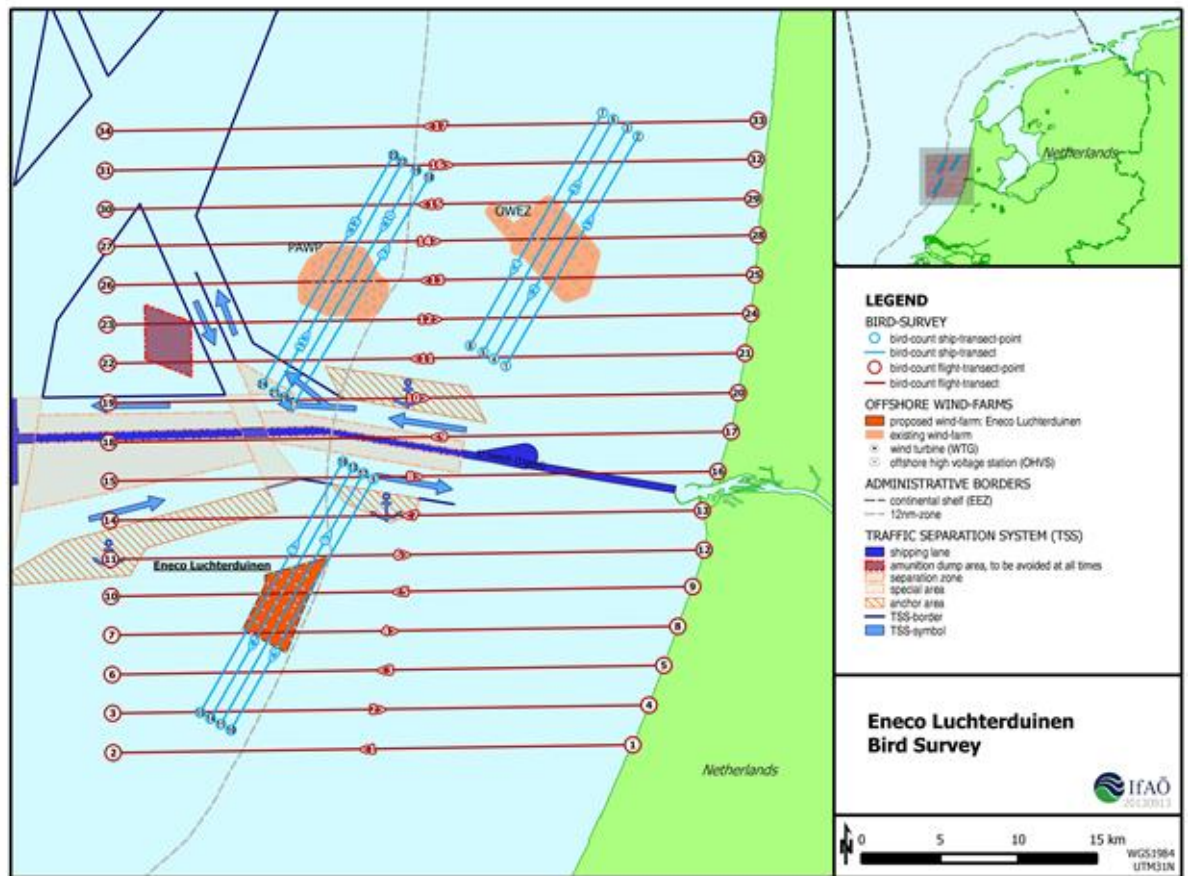


Figure 1. Primary (blue) and secondary (red) transects with indications of Luchterduinen, Prinses Amalia and Egmond aan Zee wind farms indicated.

### 3.3 Seabird counting techniques

Seabirds were recorded according to the method for surveying seabirds from ship by means of the strip-transect method as suggested by Tasker et al. 1984, Camphuysen & Garthe 2004, Camphuysen et al. 2004 and Leopold et al. 2004, and implemented as a standard by the European Seabirds at Sea Database (ESASD). As the search mode used during previous surveys for OWEZ and PAWP was ‘naked-eye’ (Leopold et al. 2013) this mode was also used during the monitoring of seabirds for LUD. The observation height was between 6.5 and 10 m above sea level. The method is a modified strip transect with a width of 300 meter, and five perpendicular distance sub-bands:

- A. 0-50 m;
- B. 50-100 m;
- C. 100-200 m;
- D. 200 – 300 m;
- E.  $\geq$  300 m.

Transect lines were broken up into 1 minute (time) stretches and birds seen “in transect” in each individual 1 minute count were pooled (from t=0 to t=1 mins and for portside and starboard). At t=1 mins, the next count commenced, from t=1 mins to t=2 mins, etc. Densities were calculated as numbers seen in transect, divided by area surveyed. Area surveyed is the segment length covered in that particular 1 minute period, depending on sailing speed (average 9 knots) and strip width (300 m), which were both continuously monitored, corrected for the proportion of birds that were missed by the observers (see next

section: distance sampling). The location of each count was taken as the mid-position between the positions at  $t=0$  and  $t=1$  mins, for each count, on the ship's transect line.

Birds were counted from the roof of the survey ship by four bird observers (Table 1), two on each side of the ship (Figure 2). Swimming seabirds were counted on both sides of the ship, and snap-shot counts of flying birds were made whereby every minute all birds will be counted within an area of 300 by 300 m transverse and directly in front of the ship (Figure 3).



Figure 2. The 'Coastal Vanguard' used as the survey ship.

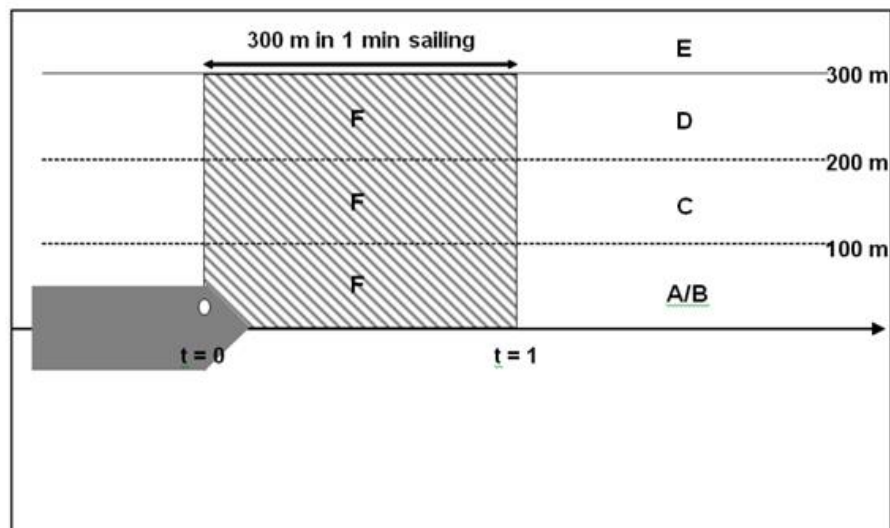


Figure 3. Schematic overview of the seabird survey method (see above for definitions of bands A-E).

Table 1. List of observers engaged in the LUD-T0 seabird surveys.

Survey	Observers
LUD-T0-01	Jörn Hartje*, Thomas Schubert, Troels Eske Ortvad, Ernst Eric Schrijver
LUD-T0-02	Jörn Hartje*, Thomas Schubert, Troels Eske Ortvad, Henrik Knudsen
LUD-T0-03	Jörn Hartje*, Graeme Pogram, Ernst Eric Schrijver, Henrik Knudsen

\*Cruise leader

### 3.4 Quality control and post-processing of survey data

General quality assurance and management were conducted and documented in accordance with internationally accepted principles for quality and environmental management as described in the DS/EN ISO 9001 standard. Post-processing of the survey data followed Leopold et al. (2013) as far as possible in order to harmonise all T0 data on seabirds and secure comparability across data sets.

Before and after every survey an equipment check was carried out following an approved checklist. On the ship all routines followed strictly briefing rules with the party chief as outlined in the Work Method Statement. All observations of seabirds, marine mammals and ships were recorded on sheets and the ship's position and speed in a GPS. After each survey the GPS-track was downloaded to a computer and checked for completeness. As soon as possible after the survey the sheets were transcribed by one of the observers directly into a special developed database. Unusual data were marked and commented and the observers were asked for clarification or confirmation if needed. This procedure is very important to get rid of erroneous data as soon as possible. Later on, the data sets were run through different automated routines to detect mistyping and other errors.

All observations and GPS positions were stored in a special SQL geo-database (FULMAR) held by IfaÖ for aerial and ship-based surveys, which is linked to ArcGIS, and which exports the results to a Microsoft Access® database. The post-processing chain starts by transcribing the general survey data (e.g. date, observer, observation height etc.) from the observation sheets into the database. The next step is to import the GPS-track into the database by using a special extension for ArcGIS, which is started by the database. In ArcGIS the whole track is shown. The start and end points of each transect lines are marked and then the track points with their position and time are imported into the database. The user of the database can now view track points, time and the columns for the sightings. Every observation will be sorted by time to the nearest 1 minute count period. Also the weather conditions are stored into the database during this step.

After finishing the data input, different tools are used to visualize the observed seabirds along the transect lines. The next step is the validation of the data by a senior biologist, who will also check the weather conditions along all the transect lines on each side of the ship according to sea state, glare and visibility. If the observations of parts of the lines are affected by strong glare, sea state over Bft 4 or poor visibility, he will mark that period as "invalid". After the evaluation, and if necessary by additional confirmation of the observer, the data will be exported to a report-file, which is a Microsoft Access® database file. Here, all common types of results are generated by queries. Two tools are generating the export files for ArcGIS and population estimation in Distance.

### 3.5 Distance analysis

The term 'Distance analysis' used in this report refers to analyses conducted using Distance software (Distance v.6. r2, <http://www.ruwpa.st-and.ac.uk>, Thomas et al. 2010). These analyses were conducted to calculate distance detection functions for swimming seabirds. Sitting seabirds like auks or divers may be difficult to detect in the outer distance bands, and hence the collected densities of sitting seabirds are

biased. As flying seabirds are comparatively easy to detect the collected densities of flying seabirds have been treated as unbiased, and no distance correction was applied. The Distance software takes account of the effect of distance by integration of the sources of variance for three parameters: encounter rate, detection probability, and cluster size. By dividing the detection probability function by the integral of the function over the survey area, a probability density function was estimated. Uniform, Hazard rate and half-normal functions available in the Conventional Distance Sampling engine (CDS) and in the Multiple Covariates Distance Sampling engine (MCDS) were tested, and the best fitting function was chosen on the basis of the smallest Akaike Information Criterion (AIC) values (Burnham and Anderson 2002). Parameter estimates were obtained by maximum likelihood methods. As detection probabilities for seabirds vary depending on weather conditions, estimation of detection probabilities can be done by either stratifying data into subsets showing different detection functions or by application of sea state as a covariate (Buckland et al. 1993). In line with Leopold et al. (2013), sea state was evaluated as a covariate using the MCDS engine.

Detection functions were calculated for the entire dataset for each species with sufficient number of observations, assuming that detectability of bird species was similar among surveys, as the majority of observers were the same during all three surveys. For the historic data the detection functions estimated by Leopold et al. (2013) were used. Estimated detection functions were used to estimate species-specific effective strip widths (ESW), which represent the width within which the expected number of detected seabirds would be the same as the numbers actually detected within the full width of 300 m (Buckland et al. 2001). Correction factors were then calculated by  $1/(ESW/300)$ . In line with Leopold et al. (2013), seabird species were pooled into species groups before Distance analysis and sea state was evaluated as a covariate in the Distance analysis (Table 2).

Table 2. Grouping of species for distance analysis. Some individuals were only identified to species group level, but could be used in distance analyses for groups: small divers (*G. stellata*/*G. arctica*), ‘commic’ terns (*S. hirundo*/*S. paradisaea*) and large auks (*U. aalga*/*A. torda*).

Group	Species
Divers	Red-throated Diver ( <i>Gavia stellata</i> )
Divers	Black-throated Diver ( <i>Gavia arctica</i> )
Grebes	Great Crested Grebe ( <i>Podiceps cristatus</i> )
Fulmars	Northern Fulmar ( <i>Fulmarus glacialis</i> )
Gannets	Northern Gannet ( <i>Morus bassanus</i> )
Cormorants	Great Cormorant ( <i>Phalacrocorax carbo</i> )
Scoters	Common Scoter ( <i>Melanitta nigra</i> )
Small gulls	Little Gull ( <i>Hydrocoloeus minutus</i> )
Small gulls	Black-headed Gull ( <i>Chroicocephalus ridibundus</i> )
Small gulls	Common Gull ( <i>Larus canus</i> )
Small gulls	Black-legged Kittiwake ( <i>Rissa tridactyla</i> )
Large gulls	Herring Gull ( <i>Larus argentatus</i> )
Large gulls	Lesser Black-backed Gull ( <i>Larus fuscus</i> )
Large gulls	Great Black-backed Gull ( <i>Larus marinus</i> )
Terns	Sandwich Tern ( <i>Sterna sandvicensis</i> )
Terns	Common Tern ( <i>Sterna hirundo</i> )
Terns	Arctic Tern ( <i>Sterna paradisaea</i> )
Auks	Common Guillemot ( <i>Uria aalge</i> )
Auks	Razorbill ( <i>Alca torda</i> )

### 3.6 Statistical analysis

By integrating dynamic habitat characteristics in the monitoring of changes in the distribution of seabirds the statistical power of the monitoring program at LUD will be significantly enhanced. For the assessment of potential impacts from LUD and cumulative impacts with PAWP and OWEZ, fine-scale distribution models capable of describing the distribution during the LUD baseline were developed on the basis of all available data including the PAWP and OWEZ monitoring data. Detailed description of the model framework is given in Appendix A. As the developed models integrate dynamic habitat features and baseline pressures from OWEZ and PAWP as well as from anchoring sites and ship traffic they will be capable of predicting changes in distributions of seabirds attributable to LUD rather than to changes in habitats or other pressures. In order to map the monthly distribution of seabirds during the LUD-T0 winter of 2013-2014, prediction models were applied taking both habitat conditions and current infrastructures in the survey area into account. Generalized additive models (GAMs) were used as these are capable of fitting different family distributions and nonlinear responses (Hastie & Tibshirani 1990), which are expected between seabirds and habitat variables. To account for zero inflation a two-step model was fitted consisting of a presence-absence model and a positive model part (densities) where all zeroes were excluded.

The species specific models (all data used) were finally used for predicting the distribution of mean densities in the whole study area during the 2013-2014 winter. In addition to the winter distribution models which were developed on the basis of mean annual environmental conditions in order to map baseline distributions across a large range of years, models based on instantaneous environmental conditions (closest spatio-temporal match) were developed. These models which will form the basis for assessment of changes in distributions of seabirds during the post-construction survey periods which can be attributed to LUD, were used to investigate the variation of seabird distribution in response to the variation in local oceanography. These models were developed for periods with contrasting extent of the coastal water mass (extensive/narrow). An extensive coastal water mass reaching the LUD wind farm is typically observed in the area during periods of easterly winds when brackish water from the river Rhine is advected offshore from the coastal areas. A narrow coastal water mass dominates during periods of westerly winds when North Sea water masses cover the area of the LUD wind farm.

Studies on the biological oceanography of seabirds have documented that the distribution of seabirds is correlated with oceanographic characteristics at both large and small spatial scales. Some seabird species like Red-throated Divers are associated with specific water masses (Skov & Prins 2001) and several species feed mainly at hydrographic fronts, upwelling and eddies (Schneider 1982, Kinder et al. 1983, Skov & Prins 2001, Camphuysen et al. 2006). So, by statistically relating hydrodynamic variables to the observed distribution of seabirds, the development of distribution models has been possible which both accurately describe discrete areas of concentration of the species, and which captures the year-to-year and seasonal variation in the location of these areas on account of the temporal changes in the regional physical oceanography of the Luchterduinen area. Similar dynamic distribution models have been developed for harbour porpoise in the German Bight (Skov et al. 2014). The model results in terms of explanatory and predictive power were evaluated separately for the presence-absence and density parts. The explanatory power was rated as fair-good with explanation degrees above 20% and predictive power was rated as fair-good with AUC values above 0.7 and Spearman's correlation coefficients above 0.25.

A prerequisite for the dynamic predictors to be useful in predictive modelling is their availability as GIS data layers covering the entire model area during the whole survey period. The selection of predictors is based on experience from modelling seabird distribution in the North Sea and Baltic Sea (Skov et al. 2009, Skov et al. 2011). The habitat predictor variables are listed in Table 3.

More detailed description of the species distribution models and predictor variables are found in Appendix A.

Table 3. List of predictor variables included in the prediction models

Predictor variable	Description	Rationale for inclusion	Included in “mean model”	Included in “dynamic model”
Water depth	Static – meter below mean sea level	Key topographic feature	X	
Seabed relief	Static - slope (in degrees) of sea floor	Interaction with frontal dynamics which concentrate prey	X	(included in the binomial model for razorbill)
Surface salinity	Mean seasonal surface salinity (psu) averaged across years	Water mass characteristic potentially determining distribution range of species	X	X
Current speed	Seasonal-yearly mean of magnitude of horizontal current speed (m/s) integrated over the whole water column	Hydrodynamic structure determining variation in prey availability		X
Current gradient	Seasonal-yearly mean of horizontal gradient of currents (m/s/m) integrated over the whole water column	Hydrodynamic structure concentrating prey		
Eddy potential	Seasonal-yearly mean of eddy activity measured as the local vorticity (m/s/m) integrated over the whole water column	Hydrodynamic structure concentrating prey	X	X
Distance to wind farm	Euclidean distance to closest turbine in OWEZ or PAWP	Potential stressor deteriorating suitability of habitat	X	X
Distance to anchoring area	Euclidean distance to closest anchoring area	Potential stressor deteriorating suitability of habitat	X	X
Number of ships	Total number of ships for period December-February	Potential stressor deteriorating suitability of habitat	X	X

### 3.7 Presentation of data

Maps showing mean distributions (mean observed and modelled densities) during the T0 surveys in the winter 2013-2014 have been produced in UTM 32N WGS84 projection. The mean density is presented for cells with a resolution of 1 km. For the observed densities, parts of the area which were not surveyed are shown as blank. The three disturbance areas (LUD, PAWP, OWEZ and the anchorage areas found along the shipping to/from IJmuiden) and the 20 m depth contour are indicated.

## 4 Results

### 4.1 Effort and sample sizes

Three surveys were undertaken during the 2013-2014 winter. The first survey was undertaken between 18<sup>th</sup> and 22<sup>nd</sup> of October 2013 using the Sara Maatje VI. All primary transect lines and the seven southern secondary transect lines plus half of the second transect line no. 8 were finalised. Due to adverse weather conditions, the second survey had to be postponed until the period 10<sup>th</sup> to 14<sup>th</sup> January 2014. This survey was undertaken using the Coastal Vanguard. All primary transect lines and the secondary transect lines no. 3-6 plus half of the second transect line no. 7 were finalised. The third survey was undertaken between 19<sup>th</sup> and 23<sup>rd</sup> of January 2014 using the Coastal Vanguard. All primary transect lines and the secondary transect lines 1-8 and 10 were finalised. The fact that the second and third surveys were undertaken with a much shorter interval than originally planned is not expected to have had any effect on the outcome of the analyses of LUD-T0 data due to the good temporal coverage of available data. Contrary to the plan, the LUD-T0-01 & LUD-T0-02 were started with the same transect. Again, due to the large sample of T0 data from OWEZ and PAWP available this is unlikely to have had any effect on the data analyses.

An overview of the survey effort is given in Table 4 and Figure 4.

Table 2. Survey effort (km<sup>2</sup> covered by observation transect) obtained during the three ship-based surveys in the first winter season (2013-2014).

Period	Survey	Area covered (km <sup>2</sup> )
LUD-T0-01	18-22/10 2013	272.53
LUD-T0-02	10-14/1 2014	213.34
LUD-T0-03	19-23/1 2014	312.36

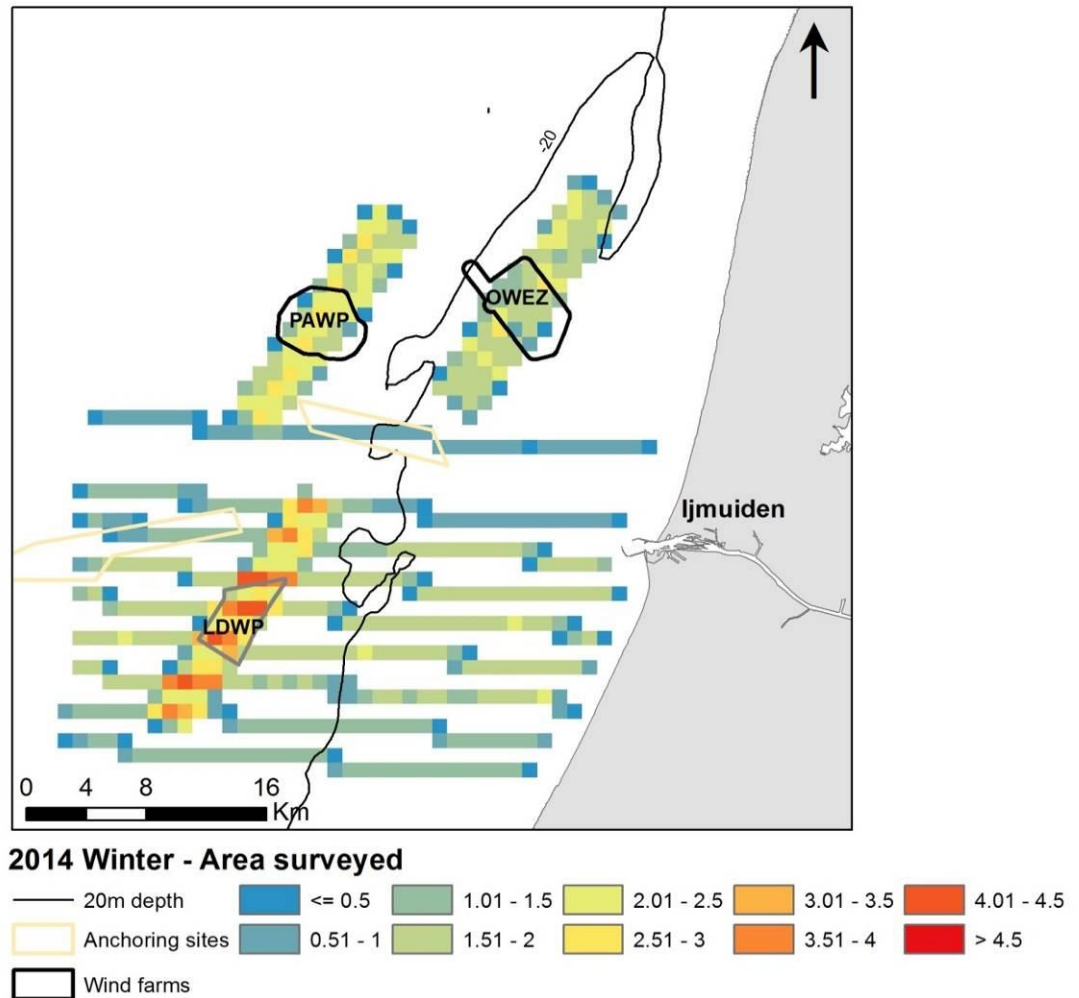


Figure 4. The spatial coverage of survey effort (km) obtained during the ship-based surveys in the first winter season (2013-2014).

Observed abundance (uncorrected) of each species is given in Table 5. Seen over all three surveys Common Guillemot *Uria aalge* was by far the most numerous species. The Great Crested Grebe is next most abundant, concentrated in coastal waters. The observed abundance varied a lot between the first survey in October 2013 and the second/third survey in January 2014. This was especially the case for species moving through the survey region on autumn migration, like for example Northern Gannet *Morus bassanus* and Lesser Black-backed Gull *Larus fuscus* which were uncommon in January. On the contrary, species which mainly use the region for wintering, like Great Crested Grebe and Common Guillemot were much more numerous during the LUD-T0-1 and LUD-T0-2/3 surveys.

Table 3. Numbers of seabirds observed within the 300 m transect in OWEZ and PAWP, LUD, coastal and offshore areas. The wind farm sites included a 2 km buffer. The 20 m depth contour marked the boundary between coastal and offshore areas. The totals for the coastal areas excluded OWEZ.

Species	Group	OWEZ+PAWP depth >20m	LUD depth >20m	COASTAL depth <20m	OFFSHORE depth > 20m	LUD-T0 TOTAL
Red-Black-throated Diver	Divers	0	0	63	37	100
Great Crested Grebe	Grebes	2	1	579	27	609
Northern Fulmar	Fulmars	0	0	0	2	2
Northern Gannet	Gannets	3	1	10	68	82
Great Cormorant	Cormorants	28	0	112	17	157
Common Scoter	Seaducks	2	0	104	29	135
Little Gull	Small gulls	2	9	38	183	232
Black-headed Gull	Small gulls	15	0	23	24	62
Common Gull	Small gulls	33	0	150	62	245
Lesser Black-backed Gull	Large gulls	15	3	53	53	124
Herring Gull	Large gulls	12	1	84	52	149
Great Black-backed Gull	Large gulls	35	15	75	73	198
Black-legged Kittiwake	Small gulls	22	19	62	189	292
Common Guillemot	Auks	242	765	908	4437	6352
Razorbill	Auks	8	4	73	162	247
<b>Total</b>		<b>419</b>	<b>818</b>	<b>2334</b>	<b>5415</b>	<b>8986</b>

Table5. Numbers of rare bird species and marine mammals observed.

## 4.2 Distance analysis

Table 4 gives an overview of the selected models used for estimating detection of sitting birds with distance for the different species groups. For Northern Fulmar *Fulmarus glacialis* and Common Scoter *Melanitta nigra* the sample of sitting birds was insufficient for distance analysis. The final models did not include sea state as a covariate for any group. The fact that sea state was not maintained in the models may have been due to the relatively small range of sea states (0-4) covered during the LUD-T0 surveys.

Table 4. Distance statistics for sitting birds in each species group.

Species group	Sample size	Key function*	Adjustment term	Effective strip width (ESW)	% CV ESW
Divers	13	HN	polynomial	140	22.8
Grebes	74	HN	cosinus	152	15.7
Gannets	12	HN	polynomial	187	27.0
Cormorants	18	HN	cosinus	300	28.3
Small gulls	109	HN	cosinus	146	12.5
Large gulls	91	HR	Polynomial	145	24.0
Auks	2086	HN	cosinus	123	2.5

\* HN=Half normal, HR= Hazard rate

## 4.3 Species accounts

In this chapter an account of the results of the analyses and modelling of the LUD-T0 data is given. For each species the description of the LUD-T0 status starts with a general introduction in which the known distribution and seasonality of the species in the southern North Sea is summarised. A summary of the findings during the PAWP-T0/T1 and OWEZ-T0/T1 surveys and the reported assessments of the impact of these wind farms on the distribution of the species in the region are provided based on Leopold et al. (2013). Then follows a description of the results of the LUD-T0 surveys during the 2013-2014 winter. The results of the species distribution models are given in a separate subsection called ‘model results’.

### 4.3.1 Divers: Red-throated *Gavia stellata* and Black-throated Divers *Gavia arctica*

Both species of divers spend the winter frequently in shallow coastal waters of northern Europe. Yet, the Red-throated Diver is more numerous in most areas, including Dutch waters. The extensive shallow estuaries found in the Wadden Sea, the Thames and the Gulf of Riga host the largest concentrations in mid winter (Skov et al. 1995, Skov et al. 2011). Outside the main areas, divers are found in similar densities, yet due to the limited areas of shallow (< 20 m) water total numbers in these areas are rarely of international significance.

The PAWP-T0/T1 and OWEZ-T0/T1 surveys revealed distribution patterns off the Dutch mainland coast which largely follow the above trends (Leopold et al. 2013). During these surveys, however, more divers were observed further offshore, and OWEZ was found to have a negative effect on the distribution of divers (Leopold et al. 2013). The shift to a more offshore distribution in spring involves the entire German Bight and takes place parallel to an influx of Black-throated Divers *Gavia arctica* (Skov et al. 1995).

The LUD-T0 surveys in 2013-2014 showed distribution patterns similar to those described for the winter surveys from 2002-2011 and earlier (Figure 5, Appendix C, Skov et al. 1995, Leopold et al. 2013).

#### Model results

The explanation degree of the mean winter distribution model for the Red- and Black-throated Diver was fair, as judged from the deviance explained by the presence-absence as well as the positive model parts (Appendix B). The predictive accuracy was good, particularly the AUC value was high. The modelling results indicated a dome-shaped or linear response of presence of divers to water depth, slope and eddy activity, indicating highest probability during winter in slope areas of 10-15 m water depth and intermediate eddy activity. As indicated by the distance to wind farm and ships parameters, wind farms and ship traffic affected the probability of diver presence negatively. Within the areas of high probability the highest densities seem to be related to intermediate eddy activity, shallow depth and higher surface salinity.

The predicted patterns of mean density in the LUD-T0 period show high densities close to the coast and low densities at the LUD. Densities were, however, predicted to be much higher during mid winter (January 2014) than during late autumn (October 2013) (Figure 6). Areas of very low densities were predicted around a 2 km zone off OWEZ and in the main shipping lanes. Model uncertainty was reasonably low, but higher west of the wind farm areas and higher in October in comparison to January (Appendix B). The modelled comparison between distributions during periods of different extent of the coastal water mass shows higher peak densities but much narrower distribution of divers during periods of narrow extent of the coastal current (Appendix B). Accordingly, at the LUD, the densities of divers were predicted to be two-three times higher during periods when the coastal current was wide as compared to when it was narrow.

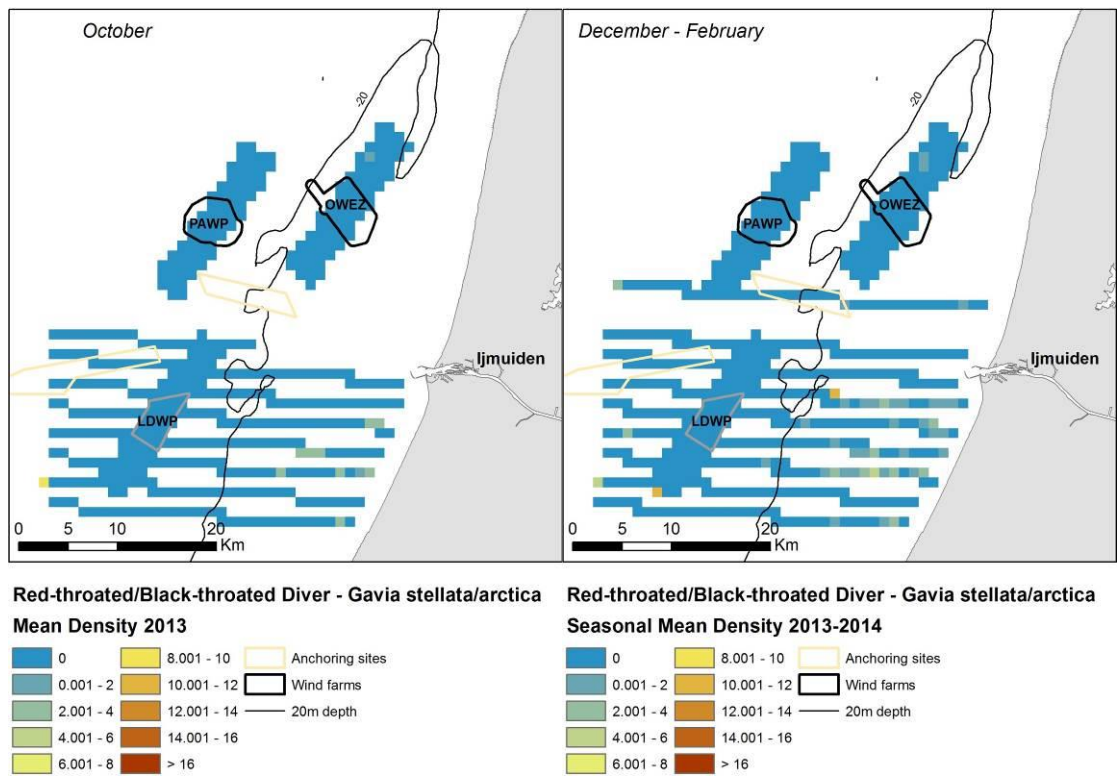


Figure 5. Seasonal mean observed density ( $n/km^2$ ) of Red-/Black-throated Diver during baseline surveys 2013-2014. Densities have been corrected for distance bias.

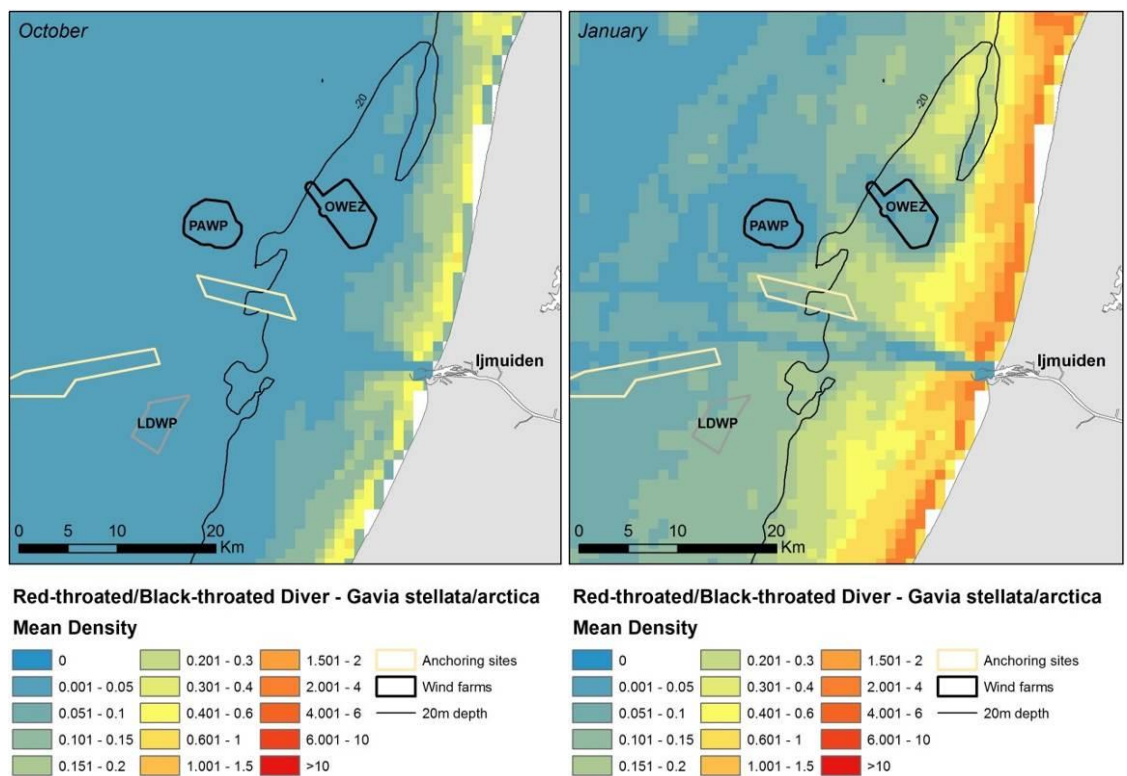


Figure 6. Predicted monthly distribution ( $n/km^2$ ) of wintering divers during October 2013 and January 2014.

### 4.3.2 Great Crested Grebe *Podiceps cristatus*

The Great Crested Grebe has one of its main wintering sites in Europe along the Dutch mainland coast (Leopold et al. 2011). The species only occurs here in large numbers during mid winter, when it is mainly found in waters shallower than 10 m. As a result, the species is not typically seen entering PAWP and OWEZ, although some birds have been observed in the area around OWEZ during late autumn. The PAWP-T1 and OWEZ-T1 surveys did indicate a negative effect of OWEZ on the distribution of grebes (Leopold et al. 2013).

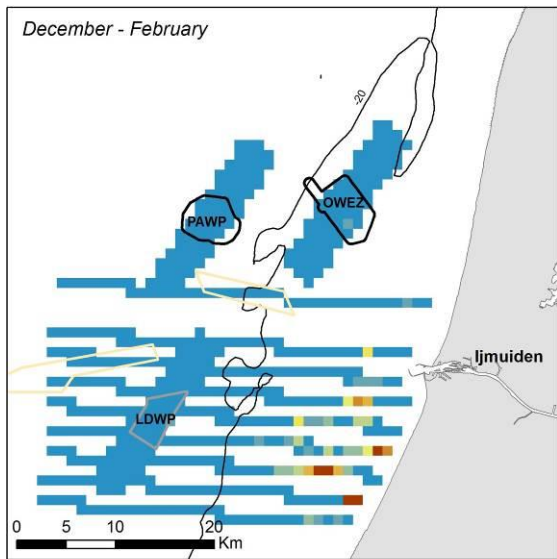
The LUD-T0 surveys in 2013-2014 showed distribution patterns similar to those described for the winter surveys from 2002-2011 and earlier with all observations in coastal waters shallower than 10 m (Figure 7, Appendix C, Leopold et al. 2011, Leopold et al. 2013).

#### Model results

The explanatory power of the winter distribution model for the Great Crested Grebe was fair, as judged from the deviance explained by the presence-absence as well as the positive model parts (Appendix B). According to the AUC value, the binomial model part had a ‘very good’ at ability of distinguishing between presence and absence, while the Spearman’s correlation coefficient was fairly low (Appendix B), indicating that the model was better at describing distribution patterns than accurate densities. The modelling results indicated that low water depth and eddy activity had the strongest positive effect on the presence of grebes, while depth and salinity were the most important factors (negative effects) for the positive part of the distribution model. The responses indicate high probability in shallow waters with intermediate eddy activity, and the highest densities in shallowest areas with higher surface salinity. Neither wind farms nor ship traffic appeared to have a profound negative effect on the distribution of grebes.

The predicted patterns of mean density in the LUD-T0 period showed high densities of Great Crested Grebes along the entire coast of the study area, yet most extensive south of IJmuiden (Figure 8). Very low densities were predicted in October, reflecting the observations well. The western edge of the predicted mean winter distribution overlapped with OWEZ predicting densities factor 10 below densities in the coastal areas, but not with PAWP or LUD wind farms. No visible negative effect of OWEZ could be identified on the predicted distribution of grebes, yet the densities in the main shipping lanes were negatively affected (albeit ship density was not a significant factor). Model uncertainty was reasonably low, mostly below 50%, within the eastern half of the surveyed area, while it was quite high in the western part, reflecting the survey effort. The uncertainty in October was very high all over due to very few observations (Appendix B).

The modelled comparison between distributions during period of different extent of the coastal water mass indicated that the distribution of Great Crested Grebes changes markedly with the current regime, and the range extends further offshore during periods when the coastal current covers a wide space. This means that during these periods densities of grebes in OWEZ may be several times higher, and grebes start to appear in the PAWP and LUD wind farms (Appendix B).



**Great Crested Grebe - Podiceps cristatus**

**Seasonal Mean Density 2013-2014**

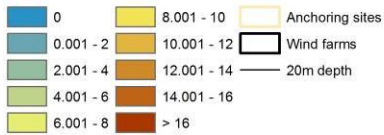
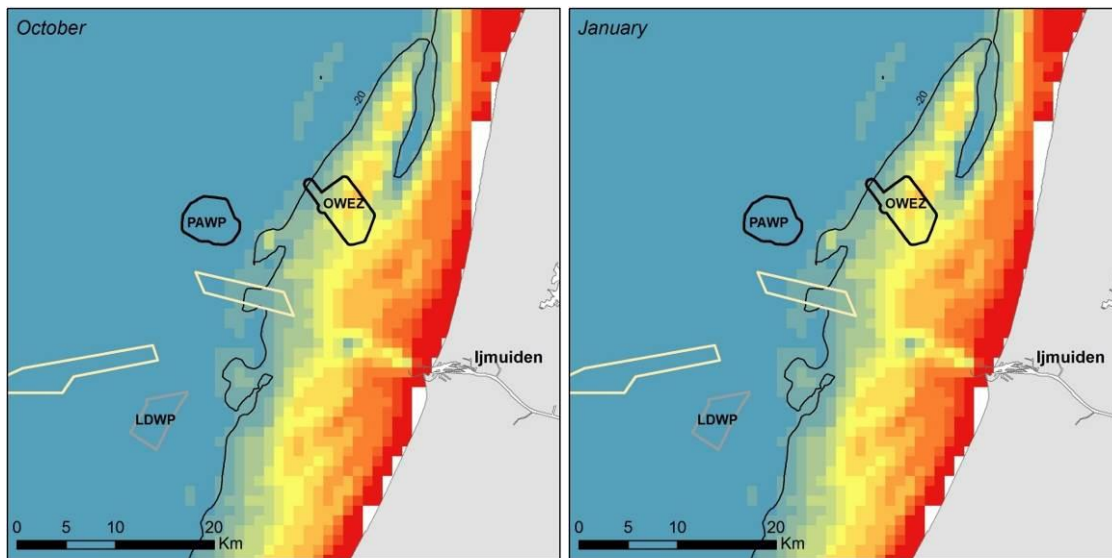
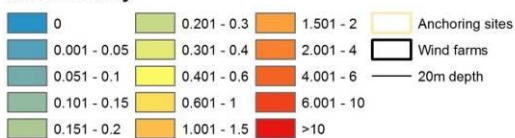


Figure 7. Seasonal mean observed density ( $n/km^2$ ) of Great Crested Grebe during baseline surveys 2013-2014. Very few Great Crested Grebes were observed during the survey in October 2013. Densities have been corrected for distance bias.



**Great Crested Grebe - Podiceps cristatus**

**Mean Density**



**Great Crested Grebe - Podiceps cristatus**

**Mean Density**

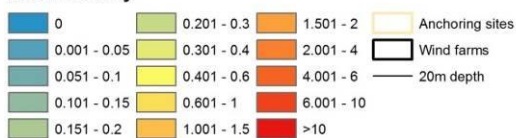


Figure 8. Predicted monthly distribution ( $n/km^2$ ) of wintering Great Crested Grebe during the baseline surveys 2013-2014.

### 4.3.3 Northern Fulmar *Fulmarus glacialis*

Northern Fulmars are abundant in the North Atlantic, and they occur commonly everywhere in the North Sea where water masses from the North Atlantic occur. Hence, the species avoid more estuarine and estuarine waters like the coastal waters off the Netherlands, and generally a strong gradient in distribution of Fulmars is seen from the coast and offshore (Camphuysen & Leopold 1994). As all three wind farms are located on the distribution gradient, the number of Northern Fulmars occurring in the wind farm area varies a lot (Appendix C). Although Leopold et al. (2013) found indications of a negative effect of PAWP and OWEZ on the distribution of Northern Fulmars, the modelling results were inconclusive (Leopold et al. 2013).

During the LUD-T0 surveys in 2013-2014, few Northern Fulmars were observed in the south-western part of the area (Figure 9). The number of observed Northern Fulmar during the LUD-T0 surveys was insufficient for modelling distributions.

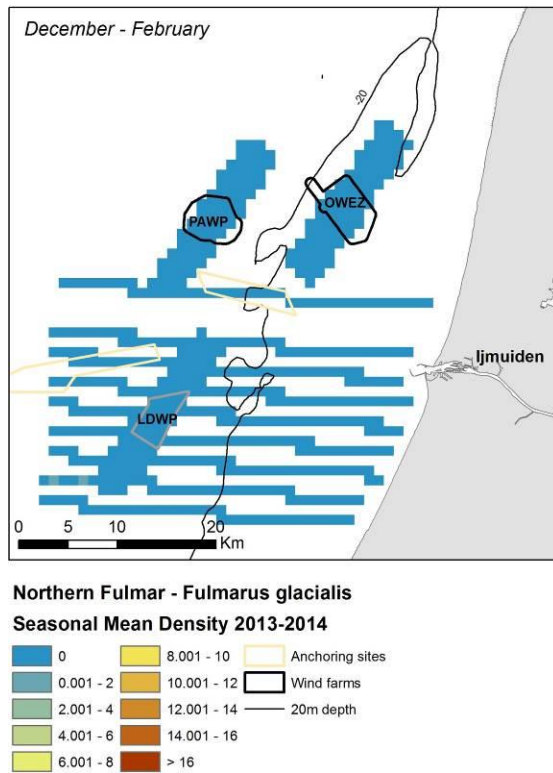


Figure 9. Seasonal mean observed density ( $n/km^2$ ) of Northern Fulmar during baseline surveys 2013-2014. Very few Northern Fulmars were observed during the survey in October 2013. Densities have been corrected for distance bias.

#### 4.3.4 Northern Gannet *Morus bassanus*

Northern Gannets breed in the eastern and western North Atlantic, including the north-western North Sea, and occur in Dutch waters throughout the year with a peak in coastal waters during autumn migration (Camphuysen & Leopold 1994, Leopold et al. 2013). Avoidance of PAWP and OWEZ by Gannets has been determined although single birds are seen entering the wind farms. The T1 surveys documented a negative effect of OWEZ and PAWP on the distribution of Northern Gannets (Leopold et al. 2013).

The LUD-T0 surveys in 2013-2014 showed a wide offshore distribution pattern similar to that described for the winter surveys from 2002-2011 and earlier, and single birds were observed in OWEZ and PAWP (Figure 10, Appendix C, Camphuysen & Leopold 1994, Leopold et al. 2013). Densities were generally higher during the LUD-T0-1 survey as compared to the LUD-T0-2 and LUD-T0-3 surveys.

##### Model results

The explanatory power of the mean winter distribution model for the Northern Gannet was fair for the positive part, whereas the deviance explained was poor for the presence-part of the model (Appendix B). The AUC indicated that the binomial model part had a fair predictive ability while the Spearman's correlation coefficient indicated that predicted densities are similar to the observed, although not very accurate (Appendix B). The modelling results indicated a strong negative effect of the wind farms to a distance of at least 2 km, and much higher probabilities in saline water masses of North Sea origin (>32 psu) (Appendix B). The responses to the positive part indicated highest densities in North Sea water masses.

The predicted patterns of mean density in the LUD-T0 period described the general increasing density gradient from the coast and offshore with the LUD located on the lower part of the gradient with predicted densities below 0.2 birds/km<sup>2</sup> (Figure 10). Model uncertainty was reasonably low in the whole study area (Appendix B).

The modelled comparison between distributions during periods of different extent of the coastal water mass did not indicate an increase in densities of Gannets at the LUD during periods characterised by different width of the coastal current (Appendix B).

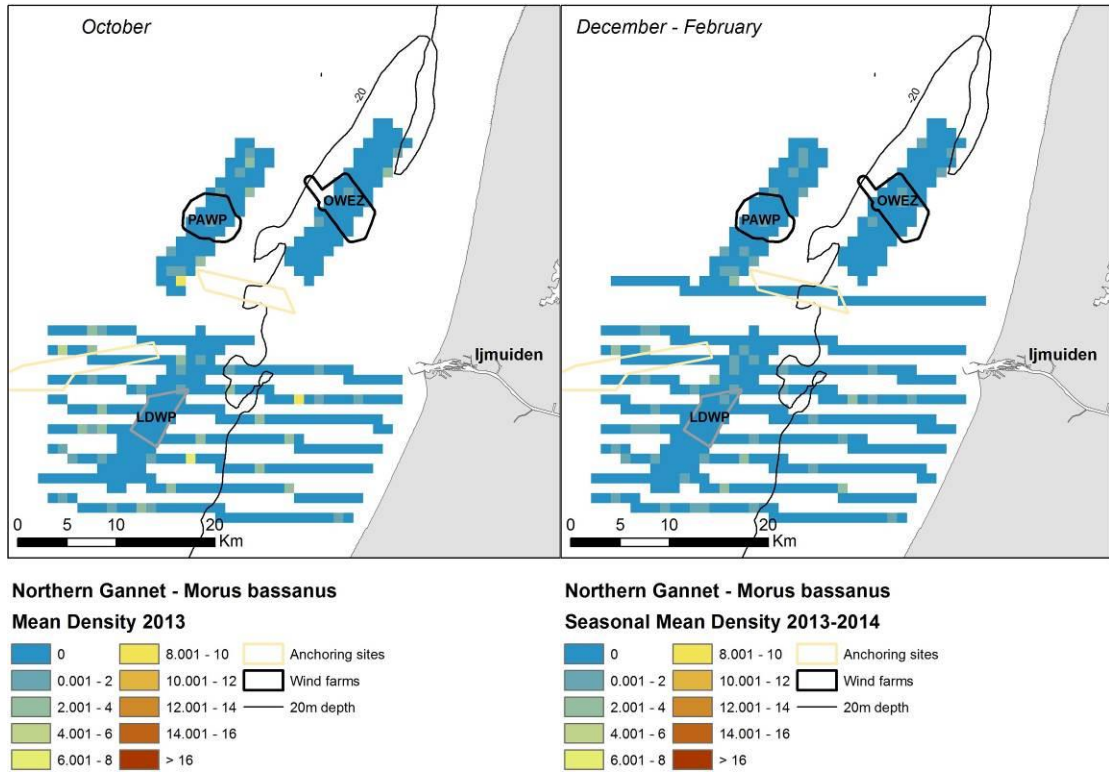


Figure 10. Seasonal mean observed density ( $n/km^2$ ) of Northern Gannet during baseline surveys 2013-2014. Densities have been corrected for distance bias.

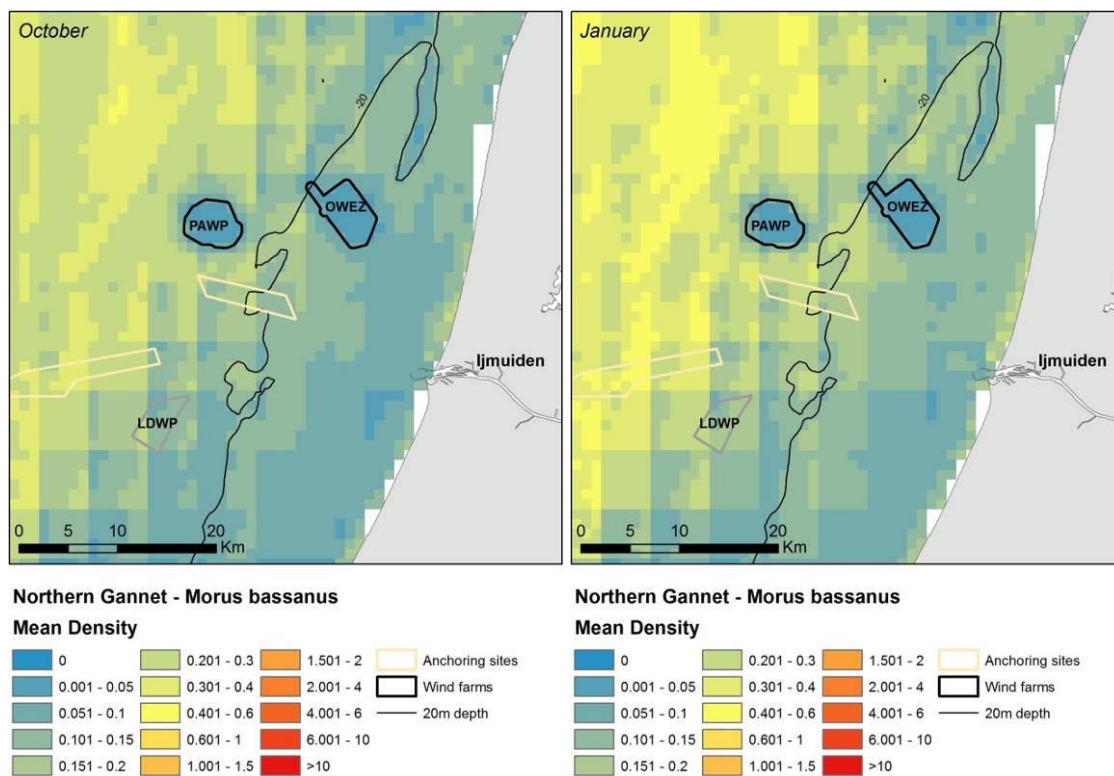


Figure 11. Predicted monthly distribution ( $n/km^2$ ) of wintering Northern Gannet during the baseline surveys 2013-2014.

#### 4.3.5 Great Cormorant *Phalacrocorax carbo*

Great Cormorants *Phalacrocorax carbo* of the *sinensis* race now occur commonly along the Dutch coast all-year round. After the construction of the PAWP and OWEZ wind farms the birds have shown a positive response to the turbines and associated structures due to the fact that they have started using the structures for resting and drying their feathers (Leopold et al. 2013). The effect of attracting Cormorants has been most significant at PAWP as very few birds used these offshore waters before the wind farm was built. The degree to which the Cormorants are actually feeding in offshore waters has not been determined (Leopold et al. 2013).

The LUD-T0 surveys in 2013-2014 reflected the association with PAWP and OWEZ, and also indicated few Cormorants outside the footprint of the wind farms in offshore waters (Figure 12, Appendix C).

##### Model results

The explanatory power of the winter distribution model for the Great Cormorant was fair for both model parts (Appendix B). The predictive accuracy of the binomial part was good according to the AUC statistics while the accuracy of the density predictions was fair, indicating that patterns were better predicted than the densities (Appendix B). The modelling results stressed the importance of PAWP and OWEZ for the presence of cormorants, and also indicated a strong positive effect of low depth and eddy activity on both the presence and abundance of cormorants (Appendix B). The responses to water depth displayed maximum densities both in shallowest areas and areas of 12-15 m, the latter likely reflecting the wind farm areas. The responses to eddy activity showed maximum densities in areas of highest eddy activity.

The predicted patterns of mean density in the LUD-T0 period indicated low density of cormorants in autumn and no birds in winter (Figure 13). Overall, predicted densities in the region were lower during mid winter as compared to early winter/autumn, yet patterns were similar during the two seasons showing a combination of a along-shore concentration in shallow water and localised concentrations at OWEZ and PAWP. Model uncertainty was reasonably low except for smaller coastal areas which received comparably less effort (Appendix B).

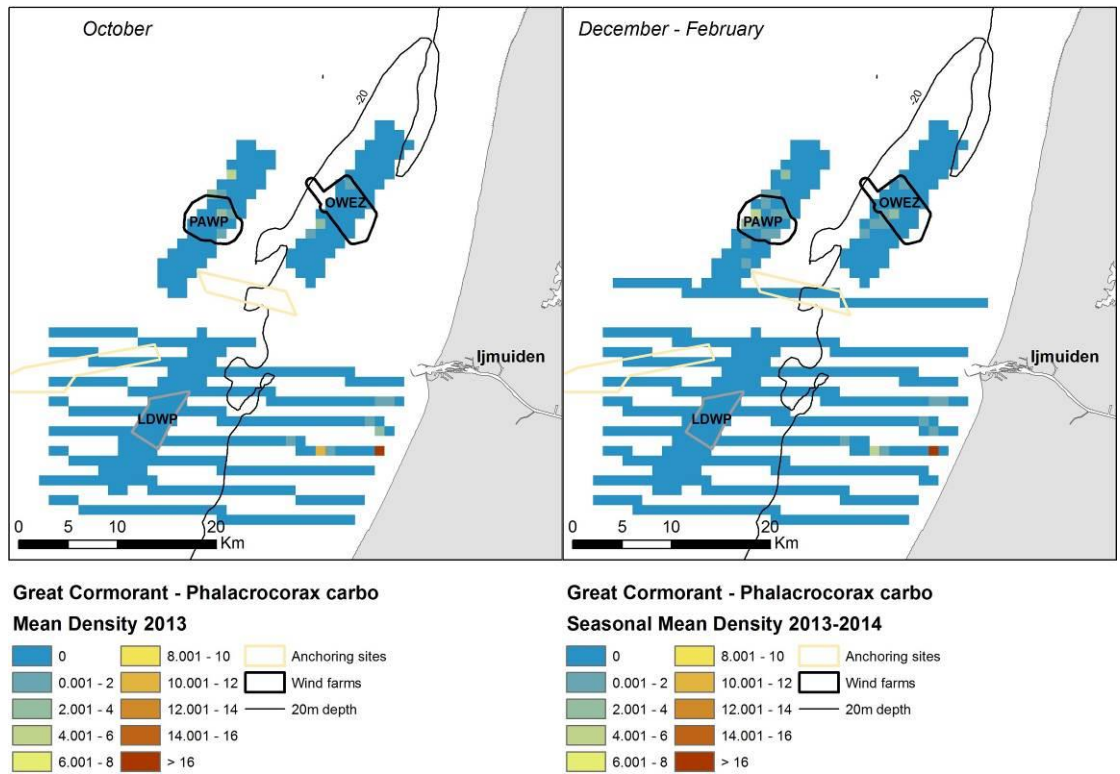


Figure 12. Seasonal mean observed density ( $n/km^2$ ) of Great Cormorant during baseline surveys 2013-2014. Densities have been corrected for distance bias.

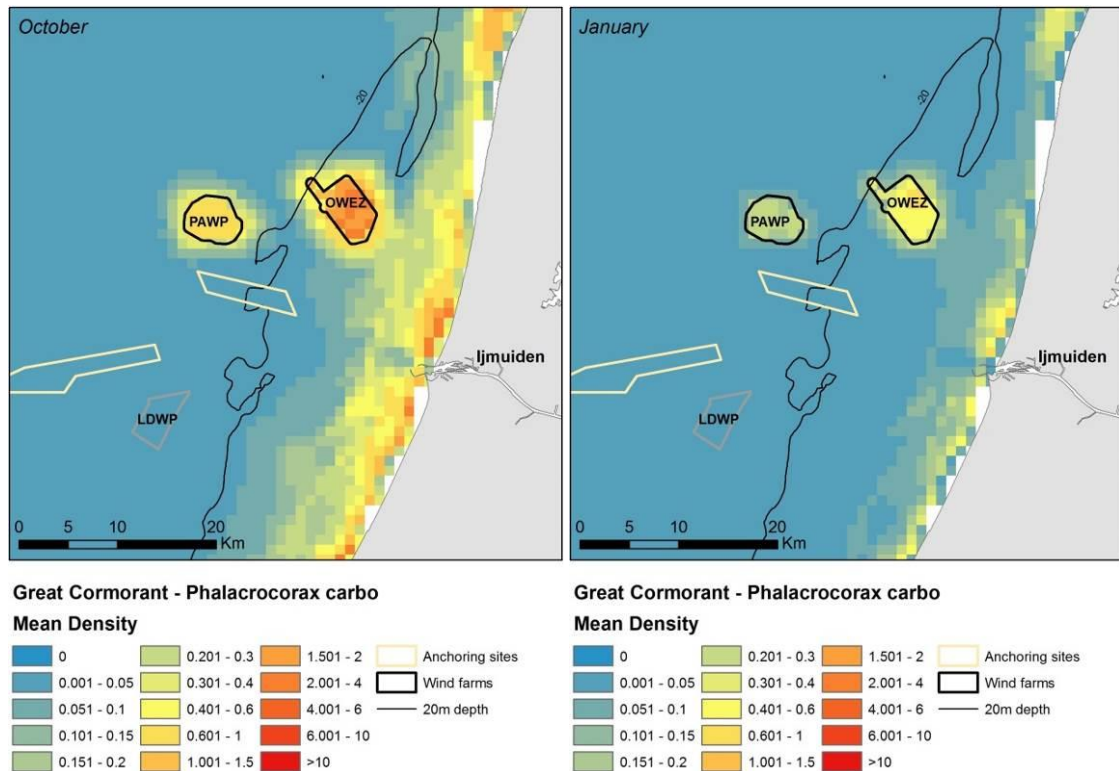


Figure 13. Predicted monthly distribution ( $n/km^2$ ) of wintering Great Cormorant during the baseline surveys 2013-2014.

#### 4.3.6 Common Scoter *Melanitta nigra*

In the eastern North Sea Common Scoters are mainly feeding on *Spisula subtruncata*, although recently the introduced American razorclam *Ensis americanus* has turned up in their diets (Leopold et al. 1995, Skov et al. 2009). Due to declining spisula stocks along the Dutch coast during the 1990s, numbers of wintering Common Scoters were reduced from up to 100,000 to just few birds. Accordingly, no significant numbers were recorded during the PAWP-T0/ T1 and OWEZ-T0/T1 surveys, and scoters were mainly recorded as flying along the coast (Leopold et al. 2013).

The LUD-T0 surveys in 2013-2014 reflected the same lack of concentrations of feeding Common Scoter, and birds were mainly recorded flying along the coast (Figure 14, Appendix C).

##### Model results

The explanatory power of the mean winter distribution model for the Common Scoter was poor for the presence-absence part, and fair for the positive part (Appendix B). The evaluation statistics indicated however that the predictive accuracy of the binomial part was fair while the accuracy of the density predictions was poor (Appendix B). The modelling results indicated a strong positive effect of low water depth and slope of seafloor on the distribution of the birds (Appendix B).

The predicted patterns of mean densities showed peak densities in inshore waters and a distribution range defined approximately by the 18 m depth contour both during late autumn and winter (Figure 15). Very low densities were predicted for the LUD. The proportional model uncertainty was mostly between 40 and 50% during January and more than 50% in October (Appendix B).

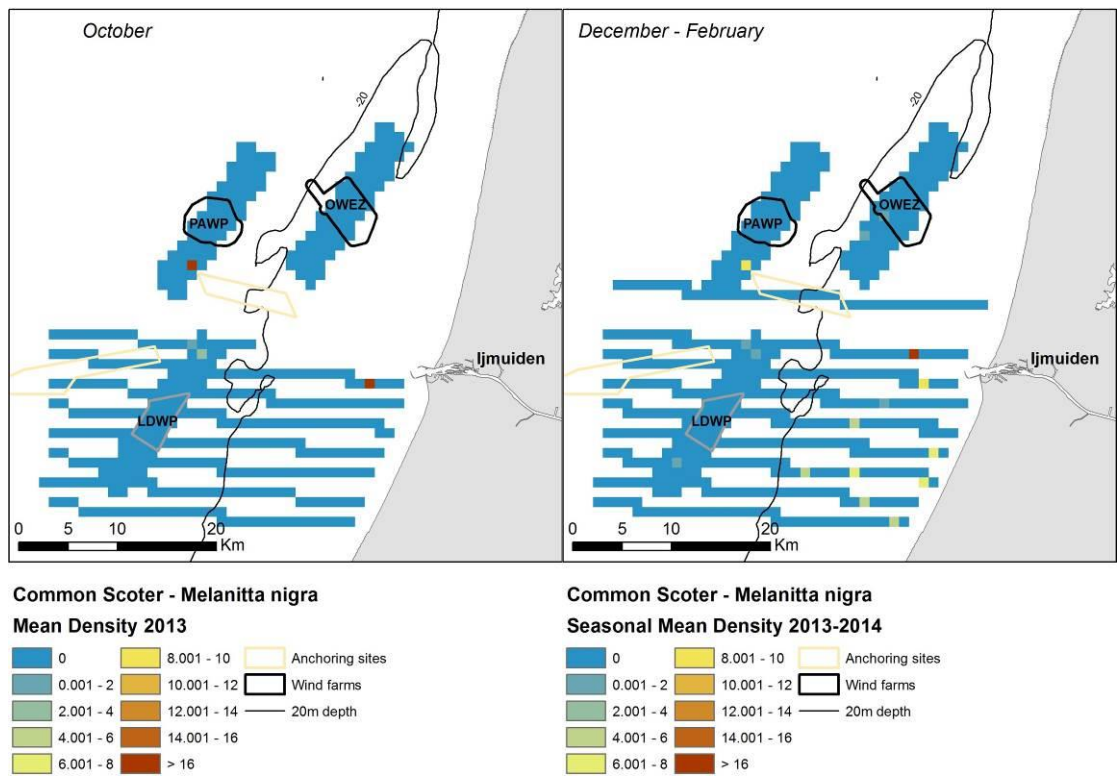


Figure 14. Seasonal mean observed density ( $n/km^2$ ) of Common Scoter during baseline surveys 2013-2014. Densities have been corrected for distance bias.

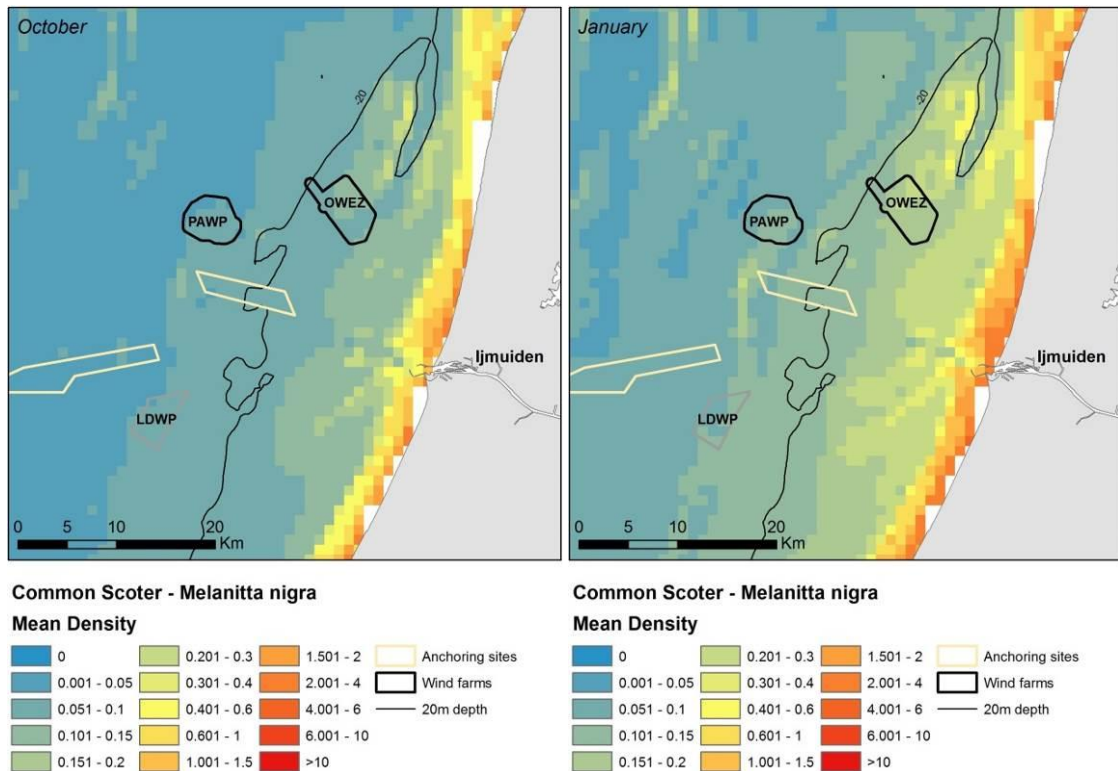


Figure 15. Predicted monthly distribution ( $n/km^2$ ) of wintering Common Scoter during the baseline surveys 2013-2014.

#### 4.3.7 Little Gull *Hydrocoloeus minutus*

The north-west Palearctic flyway of Little Gulls brings tens of thousands of birds through Dutch offshore waters *en route* between their primary breeding areas in Belarus and wintering grounds along the southern part of the Northeast Atlantic coast. The aggregations in Dutch waters are largest in spring (April, Keijl & Leopold 1997, Camphuysen 2009). During the PAWP-T0/ T1 and OWEZ-T0/T1 surveys, Little Gulls were observed throughout the area, including within PAWP and OWEZ (Appendix C). No negative effect of the wind farms on the distribution of the birds was detected (Leopold et al. 2013).

During the LUD-T0 surveys in 2013-2014 Little Gulls were seen scattered over the area with most birds being observed to the south (Figure 16).

Sample sizes were too low to allow for modelling of distribution patterns.

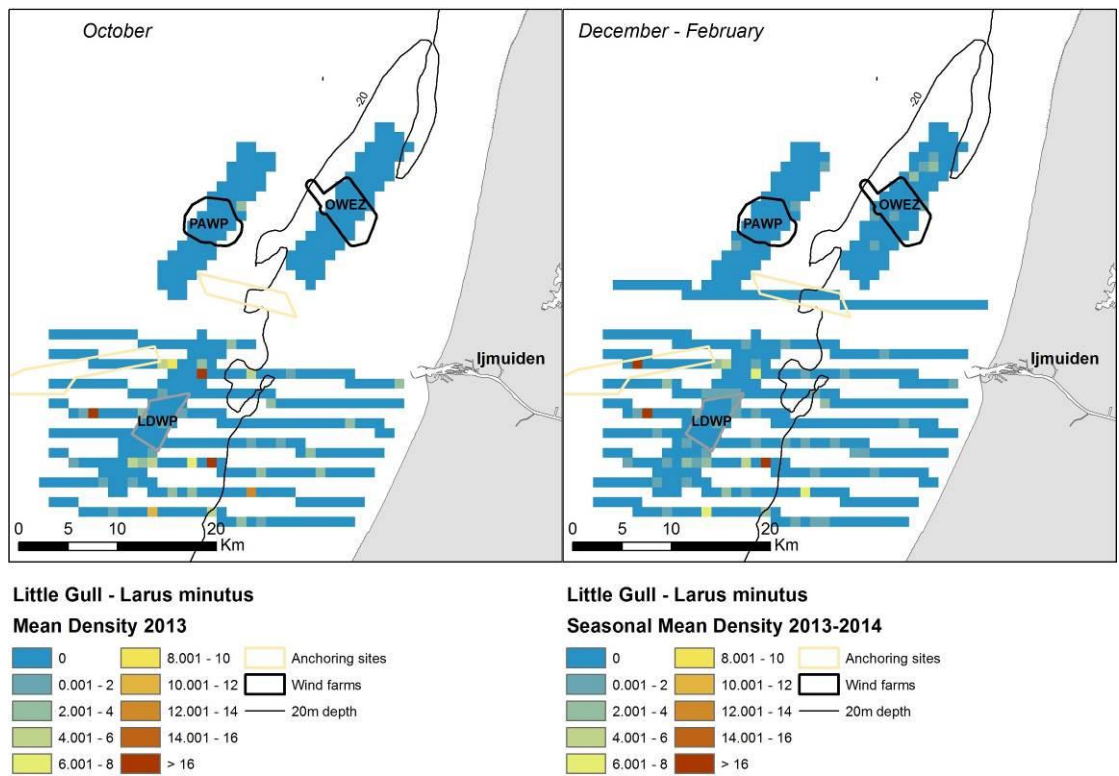


Figure 16. Seasonal mean observed density ( $n/km^2$ ) of Little Gull during baseline surveys 2013-2014. Densities have been corrected for distance bias.

#### 4.3.8 Black-headed Gull *Chroicocephalus ridibundus*

Although Black-headed Gulls *Chroicocephalus ridibundus* are mainly observed in coastal waters shallower than 10 m, they do occur everywhere in the region. During the PAWP-T0/ T1 and OWEZ-T0/T1 surveys, Black-headed Gulls were most common during autumn and winter (Appendix C). No negative effect of the wind farms on the distribution of the birds was detected (Leopold et al. 2013).

During the LUD-T0 surveys in 2013-2014 the distribution of Black-headed Gulls was similar to the one found during the earlier surveys, and birds were seen both in OWEZ and PAWP (Figure 17).

##### Model results

The explanatory power of the winter distribution model for the Black-headed Gull was fair for the presence-absence part, but good for the positive part of the model (Appendix B). The predictive accuracy of the binomial part was good according to the AUC statistics while the Spearman's correlation coefficient indicated that the accuracy of the density predictions was fair (Appendix B). The modelling results indicated a strong positive effect of low water depth, surface salinity and eddy activity on the distribution of the birds (Appendix B). The response to water depth and surface salinity clearly indicated association with estuarine water masses below 30 psu and a water depth shallower than 10 m. A moderate effect of wind farms was indicated for the positive part. Additionally, for the positive part a slight increase with salinity was noted, indicating higher densities in the more saline part of the coastal water mass.

The predicted patterns of mean densities showed peak densities in inshore waters and a distribution range defined approximately by the 22 m depth contour (Figure 18). The predicted offshore distribution around the 20 m depth contour seems not to be continuous with the coastal distribution. Very low densities were predicted for the LUD. Model uncertainty was reasonably low (between 40-50% in the wind farm area) except for the north-westernmost part and a few inshore areas (Appendix B).

The modelled comparison between distributions during periods of different extent of the coastal water mass did not indicate major changes in the distribution of Black-headed Gulls between the periods, yet predicted densities at the LUD were higher during periods characterised by an extensive width of the coastal current (Appendix B).

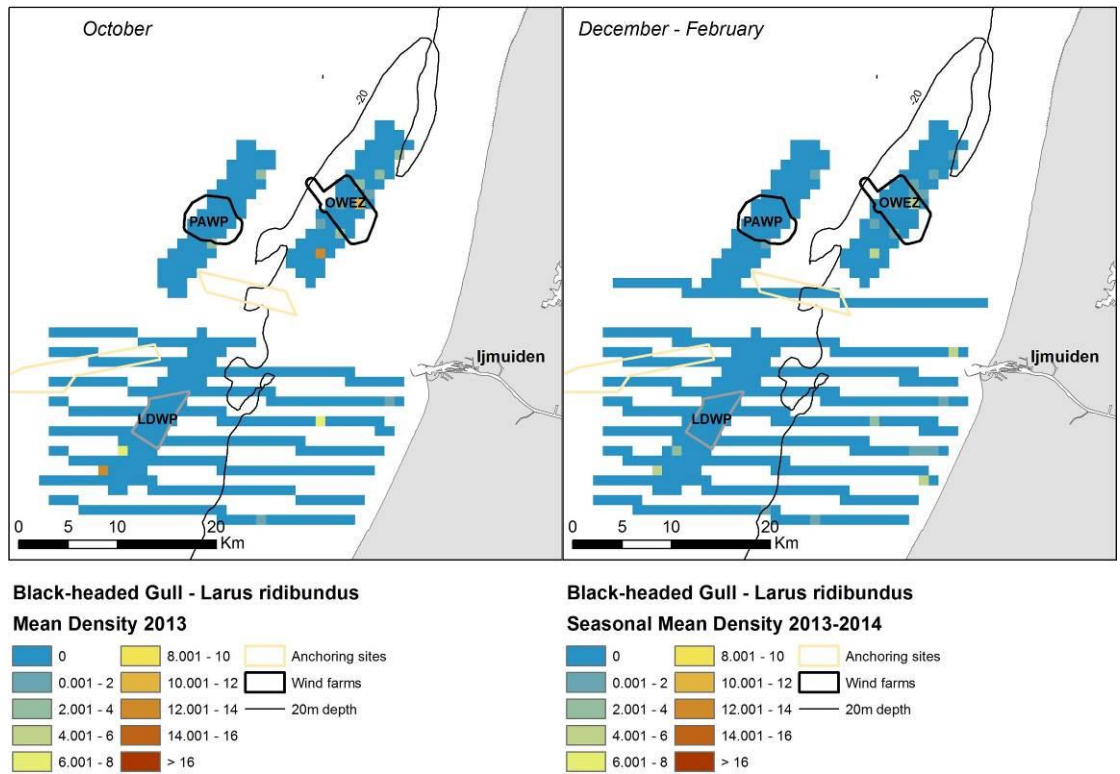


Figure 17. Seasonal mean observed density ( $n/km^2$ ) of Black-headed Gull during baseline surveys 2013-2014. Densities have been corrected for distance bias.

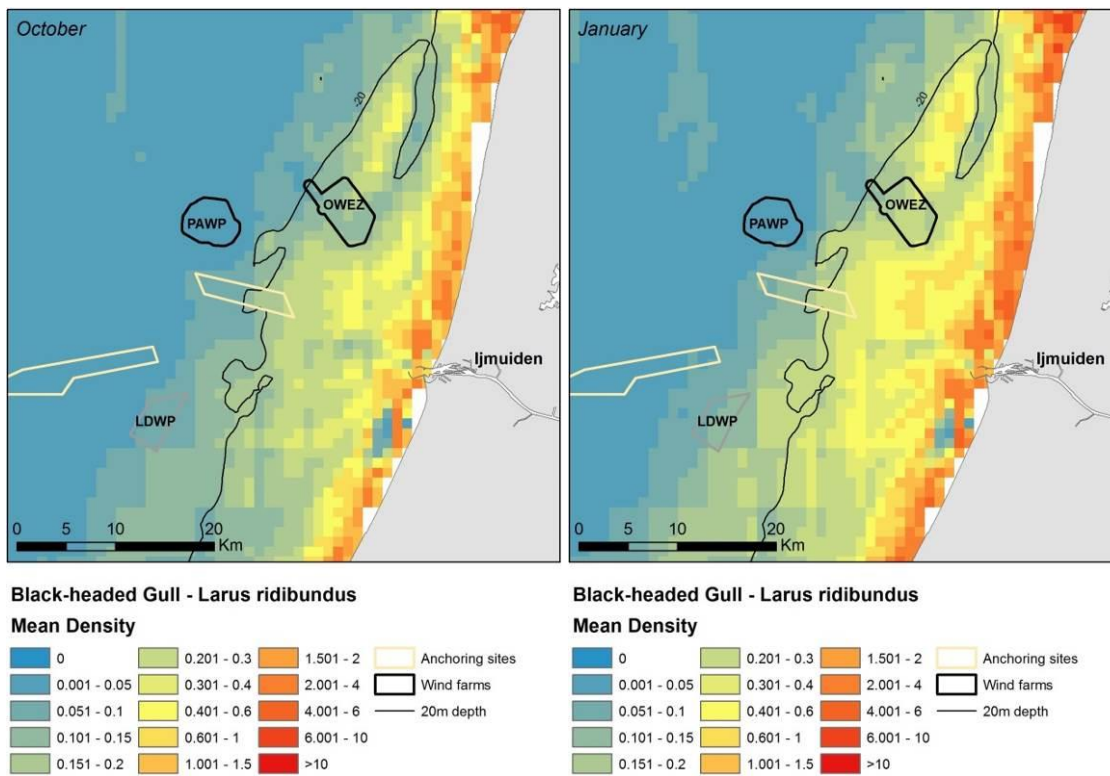


Figure 18. Predicted monthly distribution ( $n/km^2$ ) of wintering Black-headed Gull during the baseline surveys 2013-2014.

#### 4.3.9 Common Gull *Larus canus*

The distribution of the Common Gull *Common Gull* in the study area is rather similar to that of the Black-headed Gull with the highest densities being observed along the coast in waters less than 10 m deep. Compared to the Black-headed Gull, intermediate densities of the Common Gull occur over a wider area between the 10 m and 20 m depth contours. Beyond the 20 m contour the species may be found irregularly. During the PAWP-T0/ T1 and OWEZ-T0/T1 surveys, Common Gulls were most common during winter (Appendix C). No negative effect of the wind farms on the distribution of the birds was detected (Leopold et al. 2013).

During the LUD-T0 surveys in 2013-2014 the distribution of Common Gulls was similar to the one found during the earlier surveys, densities were highest in mid winter and birds were seen both in OWEZ and PAWP (Figure 19).

##### Model results

The explanatory power of the winter distribution model for the Common Gull was low for the presence-absence part, but good for the positive part of the model (Appendix B). According to the evaluation statistics the predictive accuracy was fair regarding both the presence absence part and the combined density predictions (Appendix B). The modelling results indicated a strong positive effect of slope of seafloor, low surface salinity and eddy activity on the distribution of the birds (Appendix B). The response to eddy activity and surface salinity clearly indicated association with estuarine water masses below 30 psu and medium to high eddy activity.

The predicted patterns of mean densities showed peak densities in waters shallower than 10 m, medium densities in waters between 10 m and 20 m water depth, and few birds in deeper parts of the North Sea, including the LUD (Figure 20). The predicted densities in January were much higher than in October. Model uncertainty was reasonably low in the whole area (Appendix B).

The modelled comparison between distributions during periods of different extent of the coastal water mass did not indicate major changes in the distribution of Common Gulls between the periods, yet predicted densities at the LUD were slightly higher during periods characterised by an extensive width of the coastal current (Appendix B).

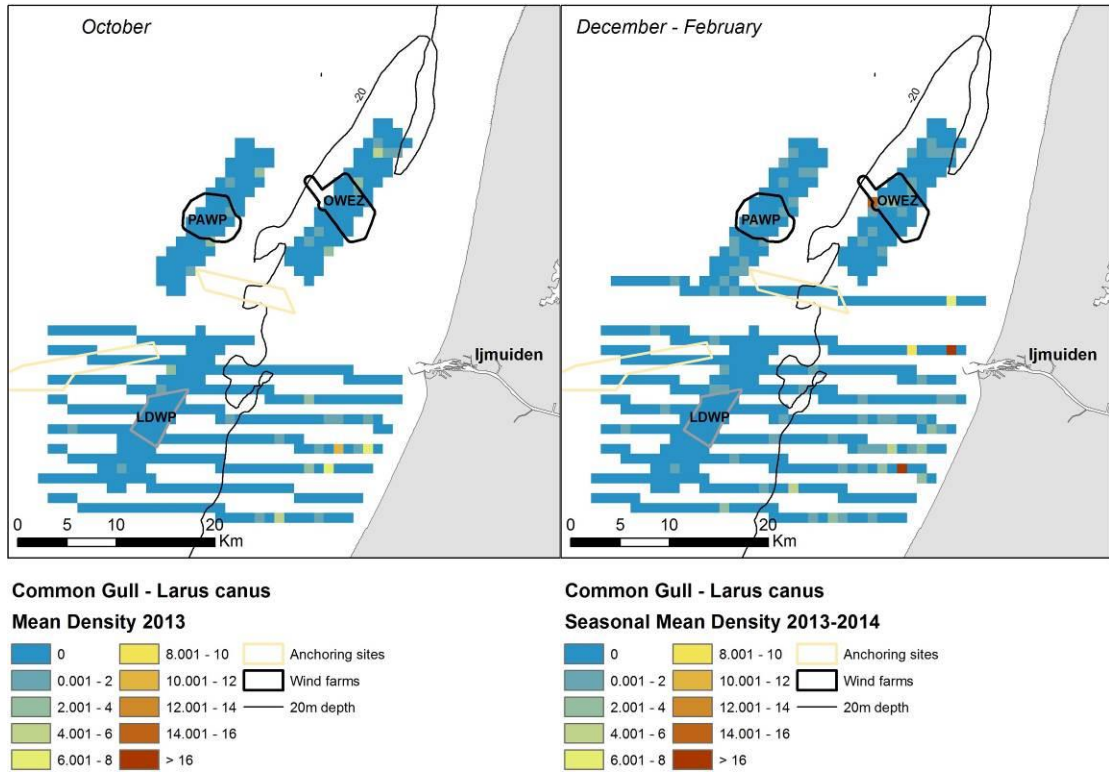


Figure 19. Seasonal mean observed density ( $n/km^2$ ) of Common Gull during baseline surveys 2013-2014. Densities have been corrected for distance bias.

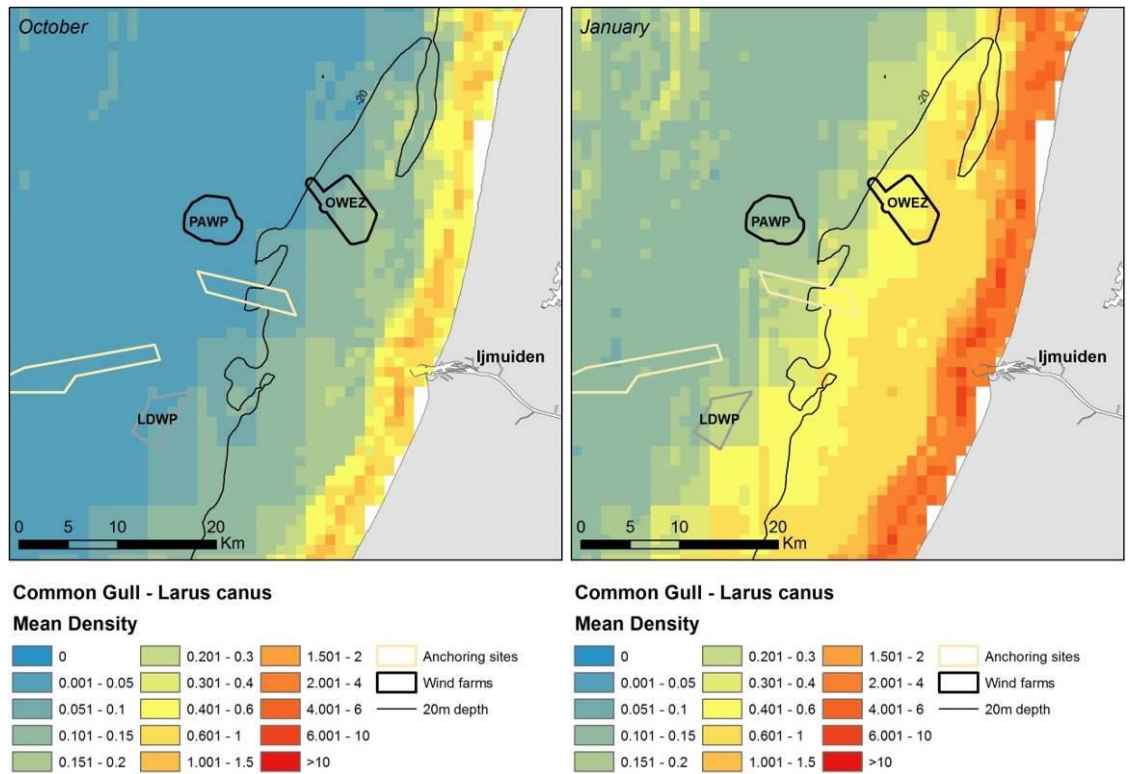


Figure 20. Predicted monthly distribution ( $n/km^2$ ) of wintering Common Gull during the baseline surveys 2013-2014.

#### 4.3.10 Lesser Black-backed Gull *Larus fuscus*

The Lesser Black-backed Gull does not occur in the study area during mid winter. During the rest of the year the birds are mainly seen associated with fishing trawlers (Leopold et al. 2013, Appendix C). A drop in fishing effort was observed in the area between T0 and T1 surveys related to the PAWP and OWEZ wind farms with a notable negative effect on numbers of Lesser Black-backed Gulls seen. As fishing activities were not allowed within the footprint of the wind farms concentrations of the species were not observed in the wind farms during the PAWP-T1 and OWEZ-T1 surveys. A negative effect of OWEZ, due largely to the prohibition of trawling activities in the wind farm, on the distribution of the species was detected during OWEZ-T1 (Leopold et al. 2013).

During the LUD-T0 surveys in 2013-2014 densities of Lesser Black-backed Gulls were highest during the LUD-T0-1 survey in October 2013 (Figure 21).

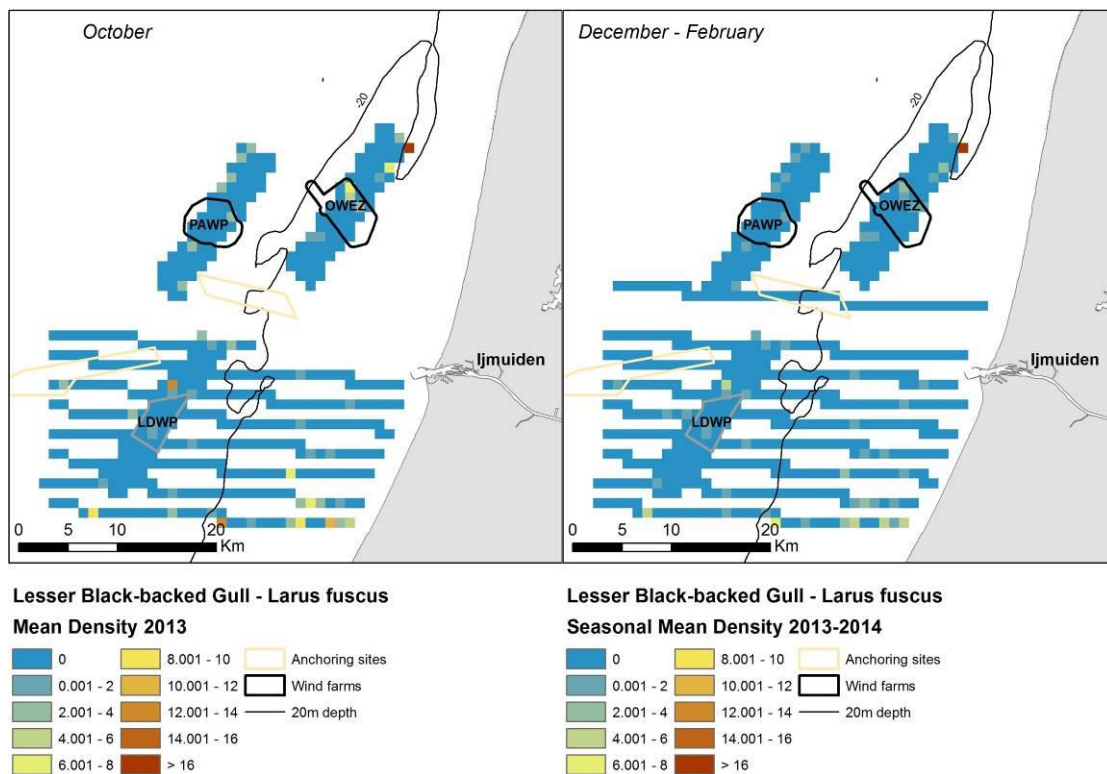


Figure 21. Seasonal mean observed density ( $n/km^2$ ) of Lesser Black-backed Gull during baseline surveys 2013-2014. Densities have been corrected for distance bias.

#### 4.3.11 Herring Gull *Larus argentatus*

Herring Gulls *Larus argentatus* in the study area are associated with both natural food sources and discards from commercial fishing activities (Leopold et al. 2013). The largest numbers of Herring Gulls are seen during winter time, and the species can be observed everywhere in the region, including within the wind farms. High densities are almost entirely associated with fishing vessels, and so densities within the wind farms dropped during PAWP-T1 and OWEZ-T1 when fishing with the footprints of the wind farms was prohibited (Camphuysen & Leopold 1994, Leopold et al. 2013). A coherent zone of higher densities is found at the 10 m contour during large parts of the year (Appendix C).

During the LUD-T0 surveys in 2013-2014 the distribution of Herring Gulls was similar to the one found during the earlier surveys, yet with seemingly fewer birds clustered (at fishing vessels) in offshore waters and more birds at the 10 m depth contour (Figure 22). Few birds were seen both in OWEZ and PAWP.

##### Model results

The explanatory power of the winter mean distribution model for the Herring Gull was fair for the presence-absence part, but good for the positive part of the model (Appendix B). The evaluation statistics also indicated that the predictive accuracy of the model was fair (Appendix B). The modelling results indicated a strong association of presence of Herring Gulls with the environment close to the coast, i.e. low water depth and surface salinity and high eddy activity, whereas the positive part indicated dual responses to characteristics in both the coastal and offshore environments (Appendix B). In addition, a negative response to density of ships was indicated by the positive part. It should be noted that the ship density data reflected cargo traffic rather than commercial fishing activities.

The predicted patterns of mean densities showed peak densities in waters shallower than 10 m, intermediate densities in waters between 10 m and 20 m water depth, and scattered lower densities in the deeper parts of the North Sea, including the LUD (Figure 23). The predicted densities in January were higher than in October. Model uncertainty was reasonably low in the whole area (Appendix B).

The modelled comparison between distributions during periods of different extent of the coastal water mass did not indicate major changes in the distribution of Herring Gulls between the periods, yet predicted densities at the LUD were slightly higher during periods characterised by an extensive width of the coastal current (Appendix B).

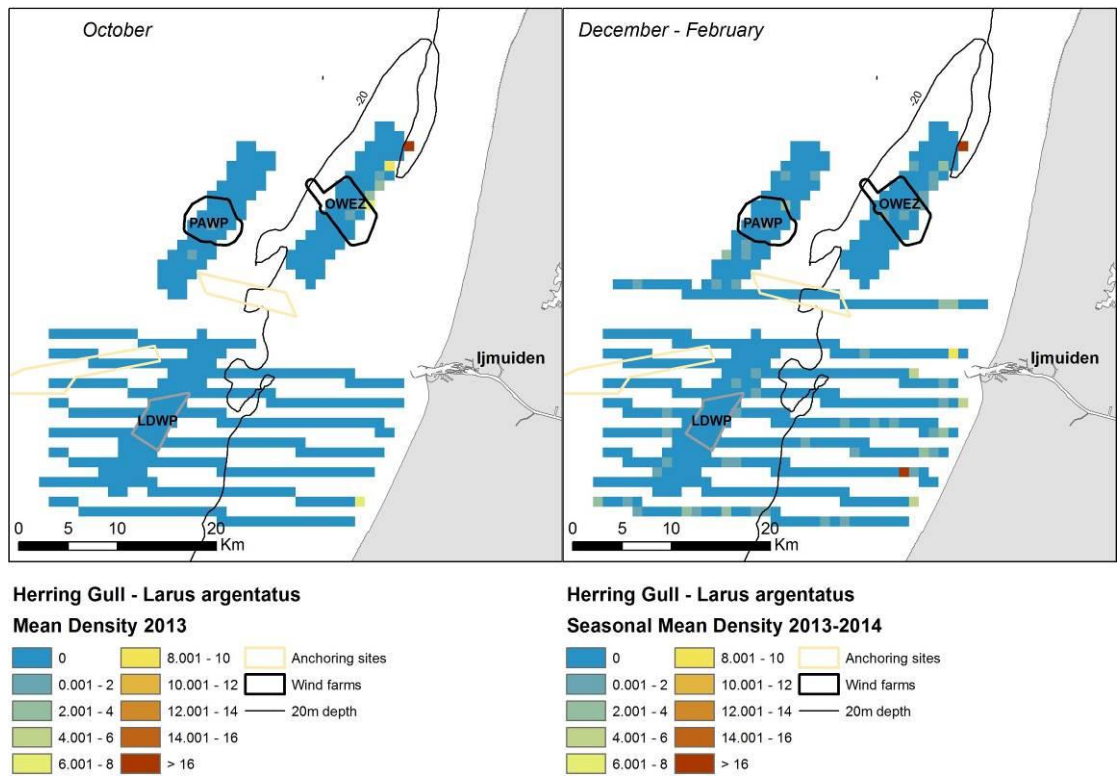


Figure 22. Seasonal mean observed density ( $n/km^2$ ) of Herring Gull during baseline surveys 2013-2014. Densities have been corrected for distance bias.

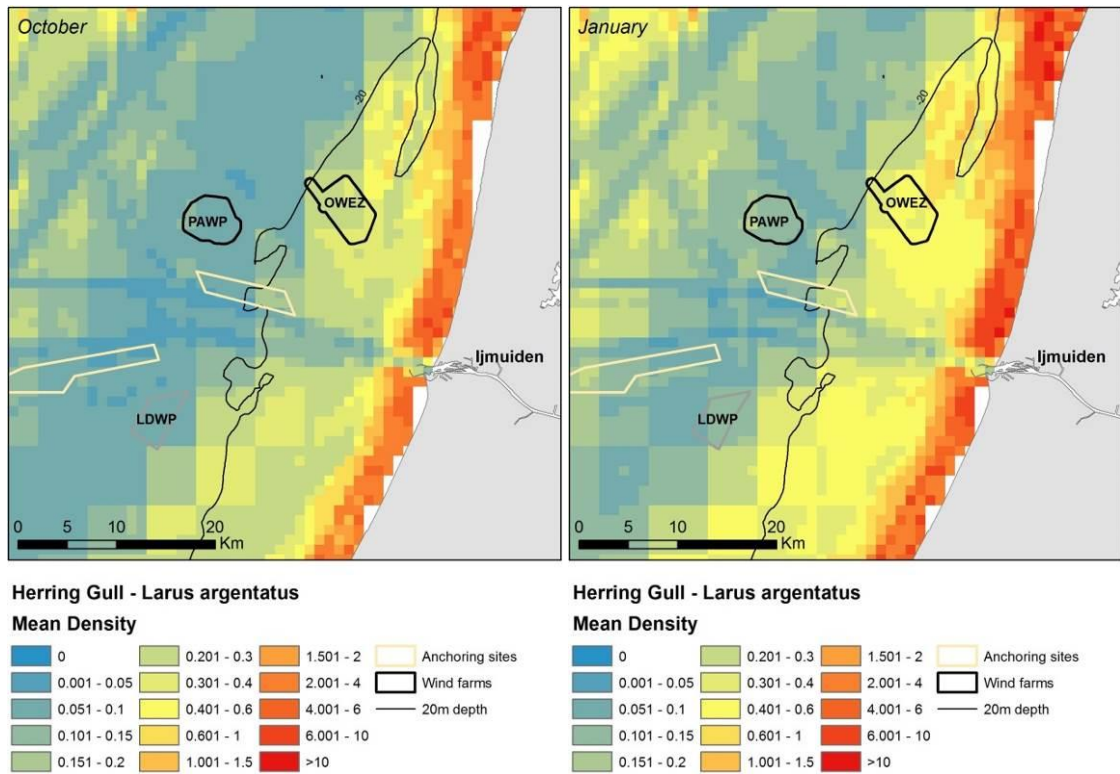


Figure 23. Predicted monthly distribution ( $n/km^2$ ) of wintering Herring Gull during the baseline surveys 2013-2014.

#### 4.3.12 Great Black-backed Gull *Larus marinus*

The distribution and habitat associations of Great Black-backed Gulls *Larus marinus* resemble those of Herring Gulls in the study area, as the species is both utilising the nearshore environment as well as fishing activities in all parts of the area (Leopold et al. 2013). The largest numbers of Great Black-backed Gulls are seen during autumn, and the species can be observed everywhere in the region, including within the wind farms. High densities are almost entirely associated with fishing vessels, and so densities within the wind farms dropped during T1 when fishing with the footprints of the wind farms was prohibited (Camphuysen & Leopold 1994, Leopold et al. 2013). A coherent zone of higher densities is found at the 10 m contour during large parts of the year (Appendix C).

During the LUD-T0 surveys in 2013-2014 the distribution of Great Black-backed Gulls was similar to the one found during the earlier surveys, yet with seemingly fewer birds clustered (at fishing vessels) in offshore waters and more birds at the 10 m depth contour (Figure 24). Few birds were seen both in OWEZ and PAWP

##### Model results

The explanatory power of the winter mean distribution model for the Great Black-backed Gull was low for the presence-absence part, but good for the positive part of the model (Appendix B). The evaluation statistics indicated fair predictive accuracy (Appendix B). The modelling results indicated a strong association of presence of Great Black-backed Gulls with the environment close to the coast, i.e. low water depth and surface salinity and intermediate eddy activity, whereas the positive part indicated dual responses to characteristics in both the coastal and offshore environments (Appendix B). Negative effects of density of ships were indicated by both model parts, and a negative effect of the anchoring area was indicated for the presence part. It should be noted that the ship density data reflected cargo traffic rather than commercial fishing activities.

The predicted patterns of mean densities showed peak densities in waters shallower than 10 m, medium densities in waters between 10 m and 20 m water depth, and scattered lower densities in the deeper parts of the North Sea, including the LUD (Figure 25). The predicted densities in October 2013 were higher than in January 2014. Model uncertainty was reasonably low in the whole area (Appendix B).

The modelled comparison between distributions during periods of different extent of the coastal water mass did not indicate major changes or changes in the density level of the species at the LUD between the periods (Appendix B). Yet, the predicted densities for the January periods were much higher than for the periods in February.

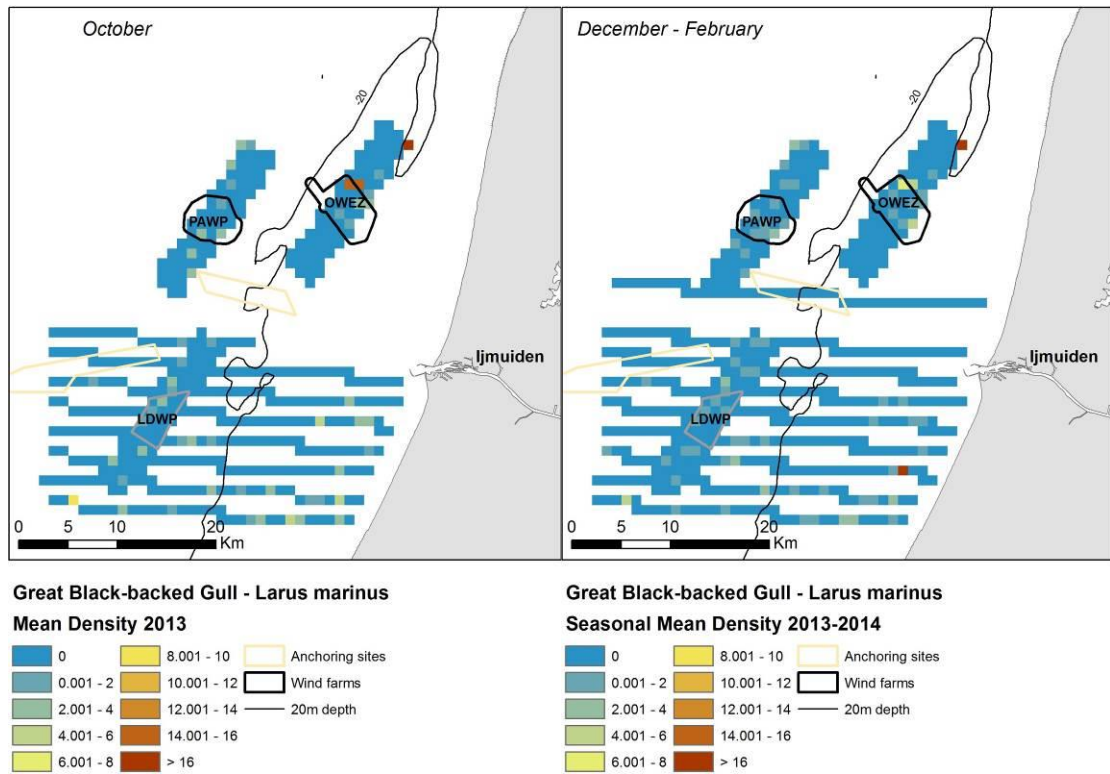


Figure 24. Seasonal mean observed density ( $n/km^2$ ) of Great Black-backed Gull during baseline surveys 2013-2014. Densities have been corrected for distance bias.

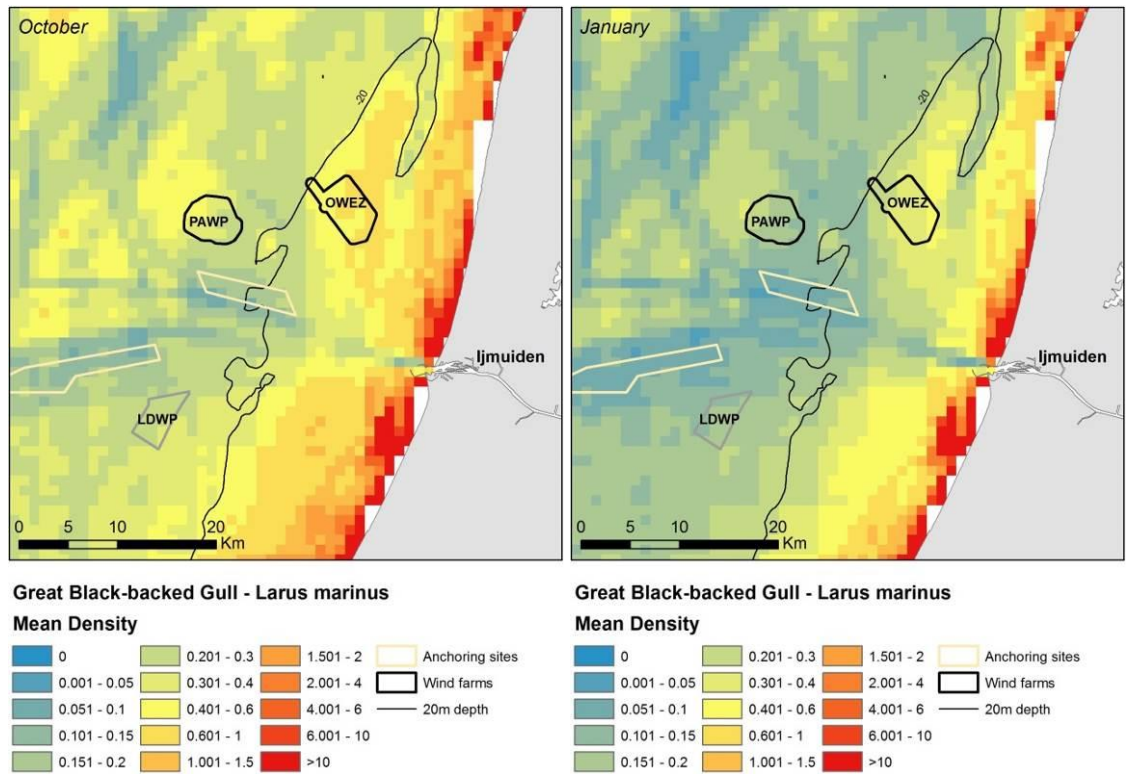


Figure 25. Predicted monthly distribution ( $n/km^2$ ) of wintering Great Black-backed Gull during the baseline surveys 2013-2014.

#### 4.3.13 Black-legged Kittiwake *Rissa tridactyla*

The Black-legged Kittiwake *Rissa tridactyla* is rather dispersed in the study area, and its distribution is similar to that of the Herring Gull and the Great Black-backed Gull with a dual distribution inshore and offshore (Appendix C). However, the distribution of the Black-legged Kittiwake appears to be less influenced by fishing activities than that of the two large gull species (Leopold et al. 2013). Largest numbers visit the area during autumn and winter. Although the birds do not avoid the wind farms, a slight negative effect of PAWP has been detected (Leopold et al. 2013).

During the LUD-T0 surveys in 2013-2014 the distribution of Black-legged Kittiwakes was similar to the one found during the earlier surveys, and birds were both dispersed, seen in OWEZ and PAWP and concentrated at the 10 m depth contour (Figure 26). Observed densities were highest during the LUD-T0-2 and LUD-T0-3 surveys.

##### Model results

The explanatory power of the winter mean distribution model for the Black-legged Kittiwake was low for the presence-absence part, but fair for the positive part of the model (Appendix B). The evaluation statistics indicated fair predictive accuracy (Appendix B). The modelling results indicated some positive effect of water depth and surface salinity on the presence of the birds, and a response of densities to low salinity, high eddy potential and intermediate slope (Appendix B). The latter responses indicate association with the inshore environment. A moderately negative effect of the anchoring site was indicated by the presence part, and a strong negative effect of the density of ships was indicated by the positive part. In addition, a notable but insignificant negative effect of the wind farms was indicated by the positive part.

The predicted patterns of mean densities showed peak densities in waters shallower than 10 m, and low (October 2013) or intermediate (January 2014) densities in deeper waters, including the LUD, OWEZ and PAWP (Figure 27). The predicted densities in January were much higher than in October. Model uncertainty was reasonably low in the whole area, except close to the coast (Appendix B).

The modelled comparison between distributions during periods of different extent of the coastal water mass indicated major changes in the abundance of Kittiwakes between the periods beyond what may be explained by changes in the local oceanography (Appendix B). Much higher densities were predicted in the whole area during periods when the coastal current was narrow.

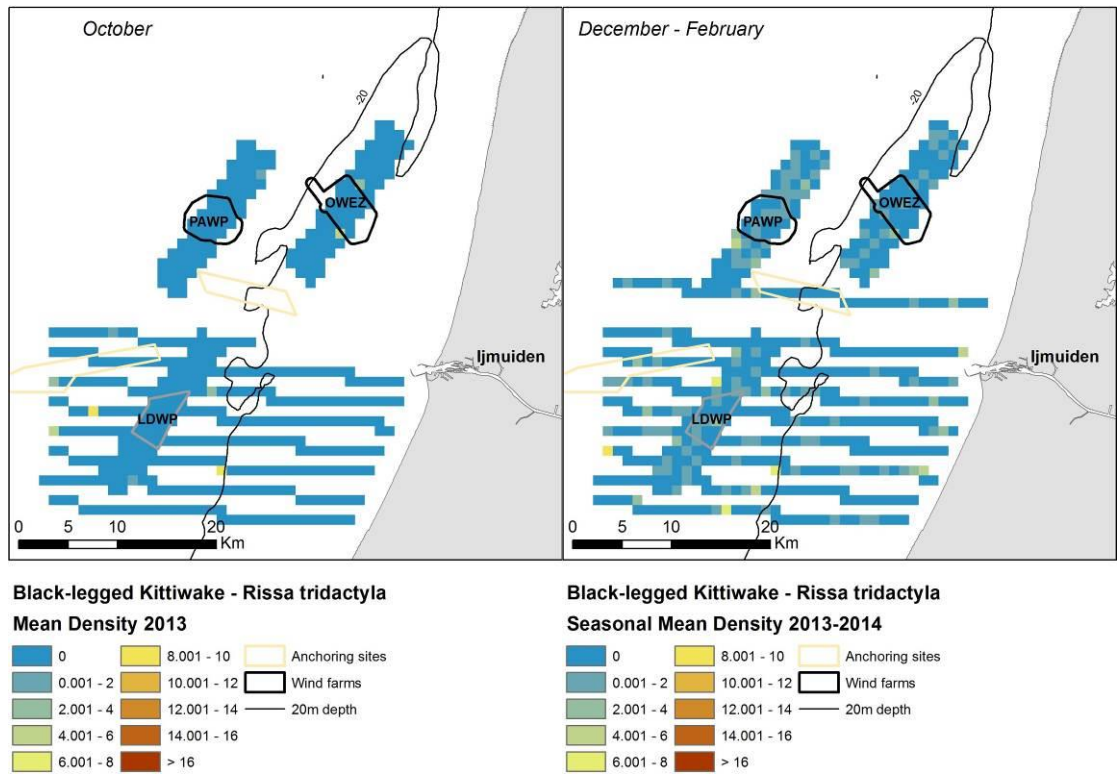


Figure 26. Seasonal mean observed density ( $n/km^2$ ) of Black-legged Kittiwake during baseline surveys 2013-2014. Densities have been corrected for distance bias.

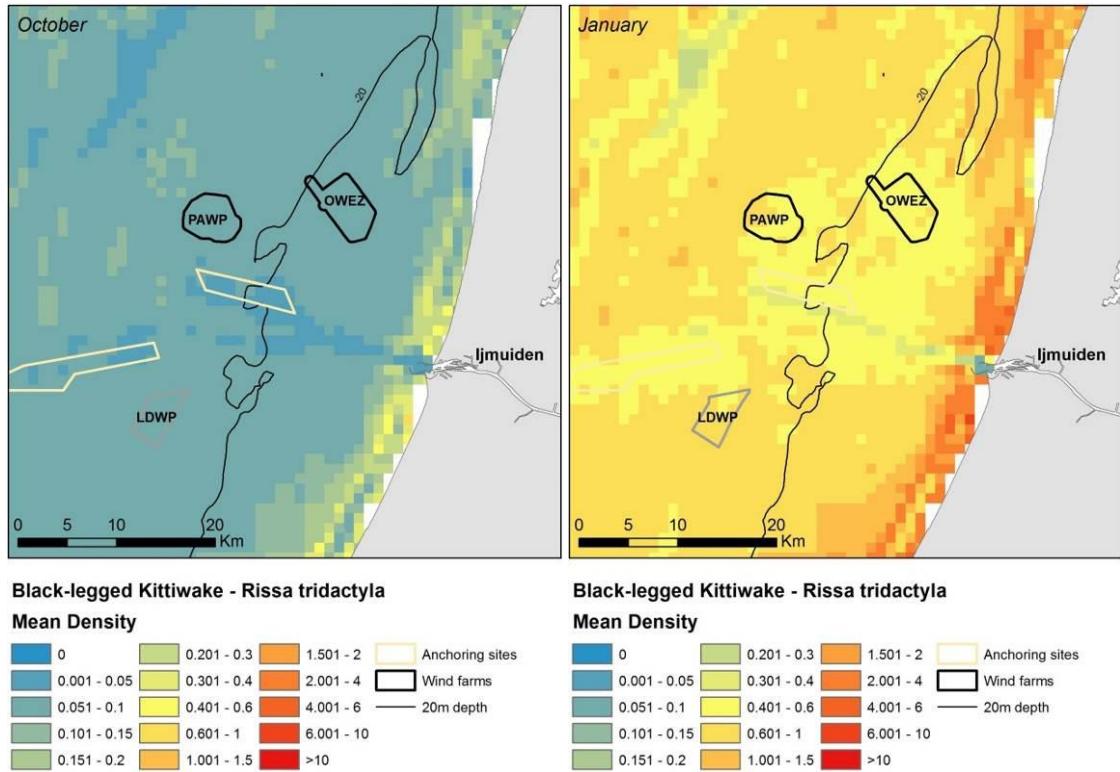


Figure 27. Predicted monthly distribution ( $n/km^2$ ) of wintering Black-legged Kittiwake during the baseline surveys 2013-2014.

#### 4.3.14 Sandwich Tern *Sterna sandvicensis*

Breeding Sandwich Terns from the Wadden Sea or the Delta only visit the inshore area infrequently, and birds on migration are most often observed dispersed over the whole area (Leopold et al. 2013, Appendix C). No negative effect of the wind farms on the distribution of the birds was detected (Leopold et al. 2013).

#### 4.3.15 ‘Commic’ terns: Common Tern *Sterna hirundo* and Arctic Tern *Sterna paradisaea*

Like for the Sandwich Tern breeding Common and Arctic Terns from the Wadden Sea or the Delta do not often visit the inshore area, while birds on migration are most often observed dispersed over the whole area (Leopold et al. 2013, winter (Appendix C, Leopold et al. 2013). A negative effect of OWEZ on the distribution of the birds was detected during OWEZ-T1 (Leopold et al. 2013).

#### 4.3.16 Common Guillemot *Uria aalge*

The Common Guillemot is a very common wintering guest in the area, and may be seen anywhere from the coast to the western boundary of the area (Leopold et al. 2013). However, during all seasons the species is most common in waters deeper than 10 m (Appendix C). Although Guillemots do enter the wind farms, a negative effect of both PAWP and OWEZ was detected during PAWP-T1 and OWEZ-T1 (Leopold et al. 2013). In addition, a negative effect of anchoring areas was identified.

During the LUD-T0 surveys in 2013-2014 the densities of Common Guillemot increased markedly between October 2013 and January 2014, and birds were seen both in OWEZ and PAWP (Figure 28). The overall distribution reflected higher mean densities in the southern part, including LUD, than recorded during earlier surveys in the region.

##### Model results

The explanatory power of the winter mean distribution model for the Common Guillemot was fair for both the presence-absence and the positive part of the model (Appendix B). The predictive accuracy was fair according to the evaluation statistics (Appendix B). The modelling results indicated a strong positive effect of water depth and distance to wind farm on both the presence and density of the birds, while density of ships was an additional important negative factor for density (Appendix B). The response to water depth indicates high use of areas deeper than 13 m with a prominent sloping terrain, and avoidance of wind farms to a distance of several kilometres.

The predicted patterns of mean densities showed high densities throughout the study area in January 2014, and very high densities in a zone just west of the 20 m depth contour, including the LUD (Figure 29). Model uncertainty was reasonably low in the whole area (Appendix B).

Like for the Black-legged Kittiwake, the modelled comparison between distributions during periods of different extent of the coastal water mass indicated major changes in the abundance of Common Guillemots between the periods beyond what may be explained by changes in the local oceanography (Appendix B). Much higher densities were predicted in the whole area during periods when the coastal current was narrow.

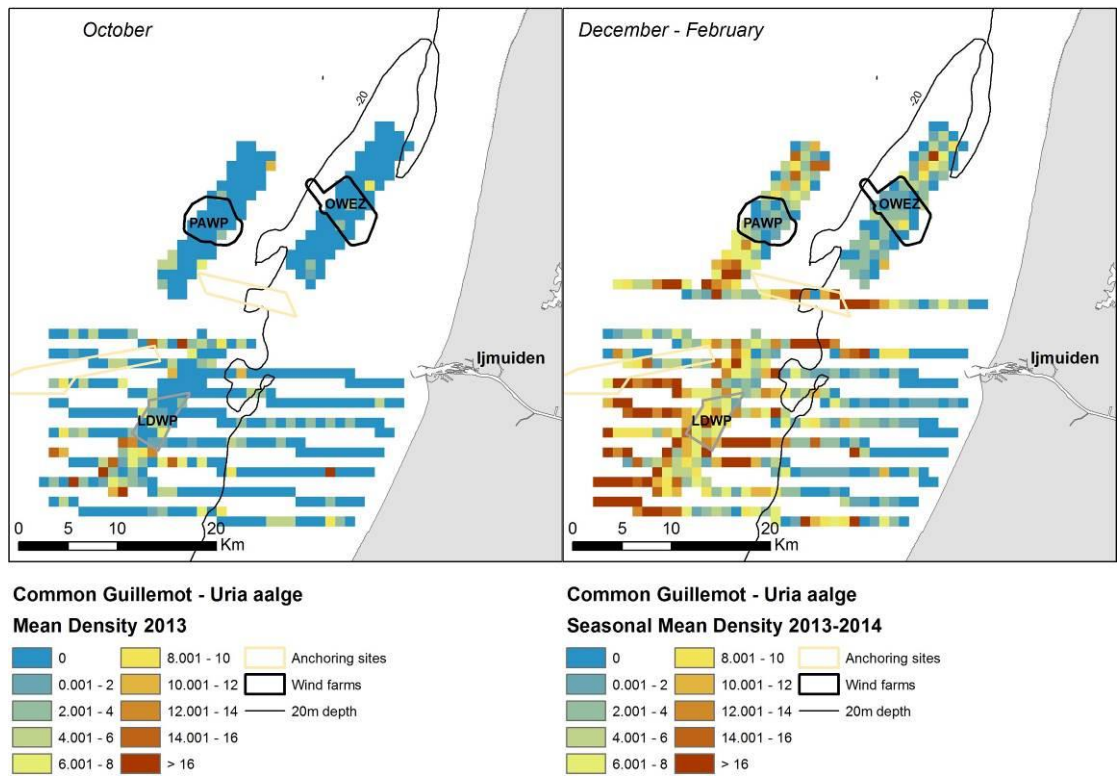


Figure 28. Seasonal mean observed density ( $n/km^2$ ) of Common Guillemot during baseline surveys 2013-2014. Densities have been corrected for distance bias.

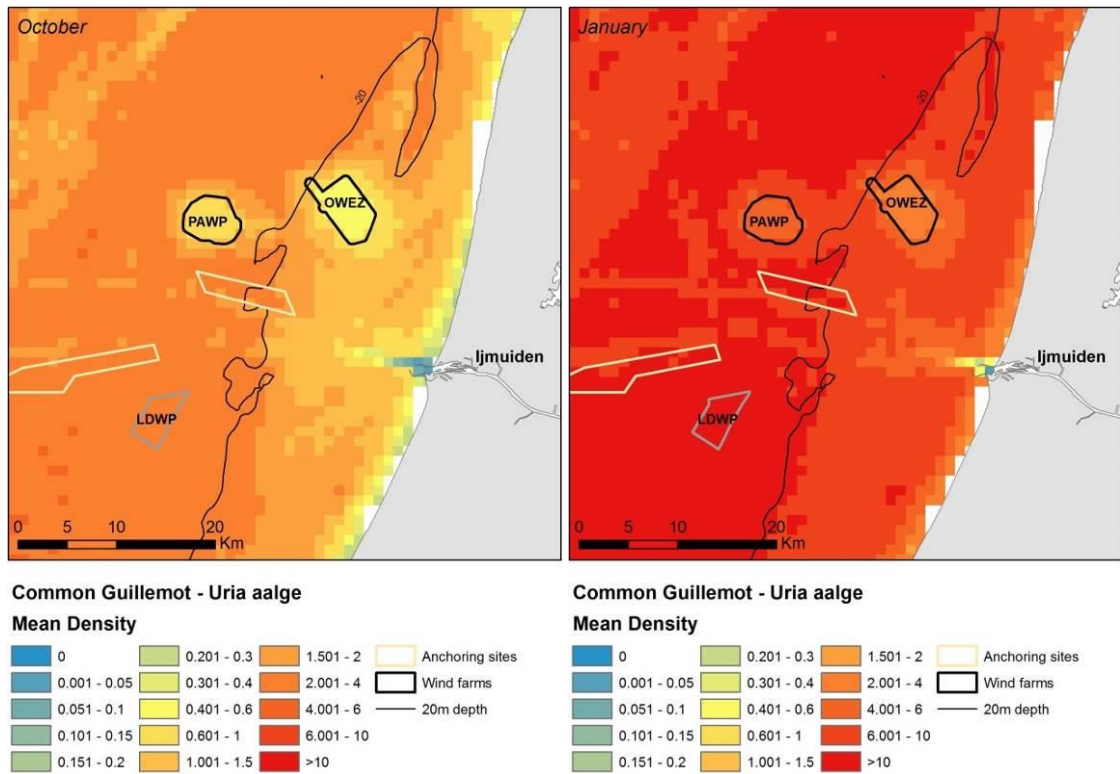


Figure 29. Predicted monthly distribution ( $n/km^2$ ) of wintering Common Guillemot during the baseline surveys 2013-2014.

#### 4.3.17 *Razorbill Alca torda*

The distribution of the Razorbill *Alca torda* in the area is rather similar to that of the Common Guillemot, and like this species the Razorbill is mainly using the area for wintering. Razorbills were observed all over the area during the PAWP-T0/ T1 and OWEZ-T0/T1 surveys though few birds were seen inshore (Appendix C). A negative effect of PAWP was detected during PAWP-T1 and IJmuiden anchorage area, not so during OWEZ-T1 where background densities were relatively high (Leopold et al. 2013).

During the LUD-T0 surveys in 2013-2014 the distribution of Razorbills was similar to the one found during the earlier surveys, and birds were seen over a large area, both in PAWP, OWEZ and LUD (Figure 30). Observed densities were generally at the same level during all three LUD-T0 surveys.

##### Model results

The explanatory power of the presence-absence part of the winter mean distribution model for the Razorbill was poor, whereas it was fair for the positive part of the model (Appendix B). The evaluation statistic indicated that the predictive accuracy of the model was poor. The modelling results indicated that the presence of the species was mainly associated with areas of low eddy activity and surface salinity, whereas higher densities were mainly associated with a sloping seafloor (Appendix B).

The predictions of mean densities showed disjoint patterns with peak densities in inshore waters and medium densities in a broad zone around the 20 m contour, including the LUD (Figure 31). The predicted densities inshore are extrapolations due to the associations with low eddy activity and surface salinity. The poor predictive power for the inshore part is also visualised by the high level of model uncertainty (Appendix B).

The modelled comparison between distributions during periods of different extent of the coastal water mass did not indicate major changes in the distribution of Razorbills between the periods (Appendix B).

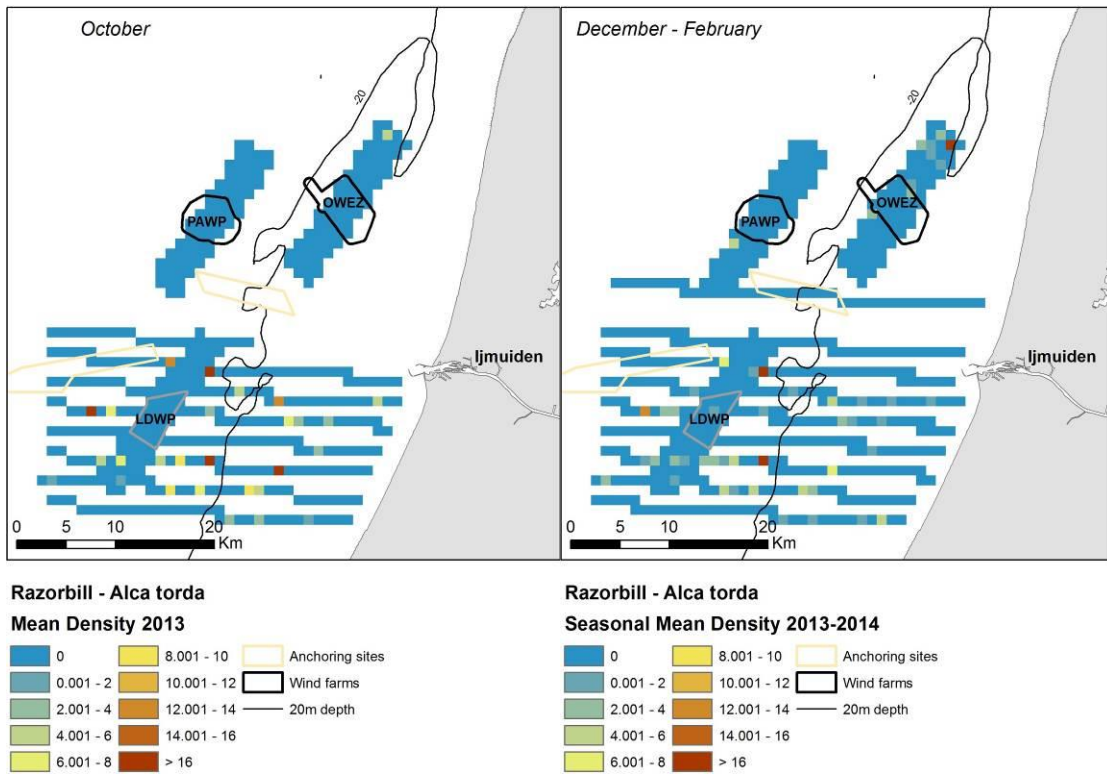


Figure 30. Seasonal mean observed density ( $n/km^2$ ) of Razorbill during baseline surveys 2013-2014. Densities have been corrected for distance bias.

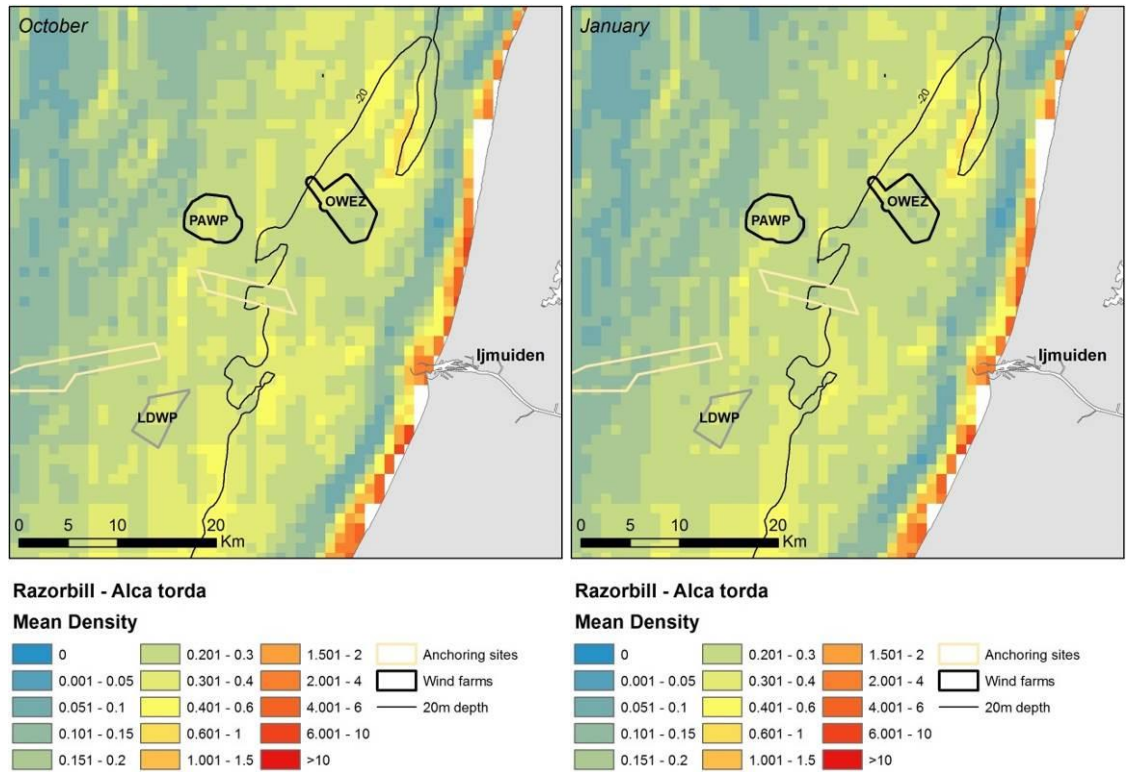


Figure 31. Predicted monthly distribution ( $n/km^2$ ) of wintering Razorbill during the baseline surveys 2013-2014.

#### 4.3.18 Marine mammal observations

During the three LUD-T0 surveys a number of marine mammal observations were made. Harbour Porpoise *Phocoena phocoena* was observed commonly in the whole area with most sightings in southern part, and by far more observations in January 2014 as compared to October 2013. Few seals were seen and the ones identified to species were Common Seal *Phoca vitulina*. One group of unidentified dolphins was also observed.

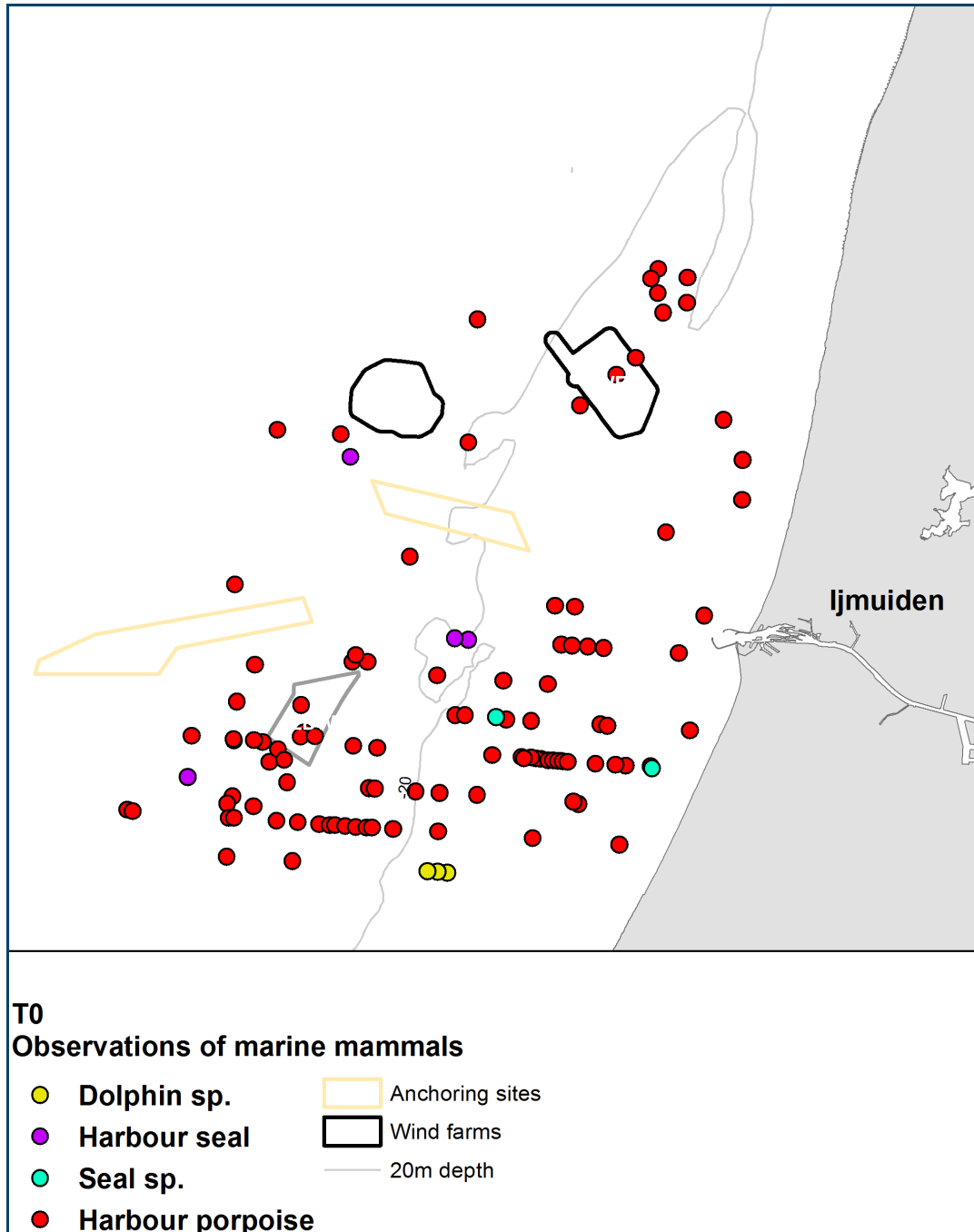


Figure 32. Observations of marine mammals during the LUD-T0 surveys 2013-2014. No corrections for possible double registrations have been made.

## 5 Discussion and Conclusions

### 5.1 Characterisation of LUD site

The LUD-T0 surveys added new knowledge about the distribution and abundance of seabirds at the planned location for the Offshore Wind Farm Eneco Luchterduinen LUD. The three surveys undertaken supplemented the PAWP-T0/ T1 and OWEZ-T0/T1 data near these two wind farms (Leopold et al. 2013), while the area south of PAWP and OWEZ received much more coverage compared to earlier surveys. Additionally, more data were collected on the utilisation of the wind farms by seabirds; data which largely corroborated earlier findings and now form part of LUD-T0. The LUD is located at 18-22 m water depth in an area characterised by being at the deeper end of the coastal-offshore gradient found along the Dutch mainland coast. Prominent concentrations of several species of seabirds are located in the shallow offshore zone. At the same time, higher densities of pelagic species are found in the deeper parts of the North Sea west of LUD. As the seabird density data which constitute the LUD-T0 data have been collected over a 10-year long period of time and during different seasons the description of the baseline situation for LUD had to be based on predictive distribution models which took account of the variability in the local oceanography.

The mean distribution models provided a good overview of the spatio-temporal trends in the winter distribution of seabirds at LUD based on predicted mean monthly densities. However, when compared to the results of the dynamic models based on observed densities during specific scenarios of a limited/extensive coastal current the mean predictions seem to have underestimated densities of seabird in LUD. Judged from the model results the winter distribution of seabirds at the LUD may be characterised by high densities of Common Guillemot and low densities of other species of seabirds. However, the distribution of several species of seabirds in the area is closely associated with features of the local current and hydrographic regime, especially surface salinity and eddy activity seem to be important features. Thus, distributions at the LUD may oscillate in response to the dynamics of currents and water masses. Diver densities at LUD are low, as the two species mainly occur in water of 10-15 m depth with intermediate eddy activity (low at LUD). Yet, the model scenarios indicated that densities at LUD may be three times higher during periods with an extensive coastal current. Great Crested Grebes prefer low water depth and surface salinity and an intermediate eddy activity, hence do not on average occur in LUD. However, the model scenarios indicated presence at the site during periods with an extensive coastal current.

The predicted patterns of mean density of Northern Gannets in the LUD showed a general increasing density gradient from the coast and offshore with the LUD located on the lower end of the gradient. As the Gannets are associated with water masses of higher surface salinity, the densities of Gannets at the LUD were predicted to increase during periods characterised by a narrow width of the coastal current. The highest densities of Great Cormorants were found in the shallowest areas with high eddy activity, as well as in PAWP and OWEZ. Very low densities were found in the projected LUD. In line with recent monitoring results, the surveys in 2013-2014 did not reveal any concentrations of feeding Common Scoter, and the species was mainly recorded flying along the coast (Leopold et al. 2013). Even if food resources (*Spisula subtruncata*) would recover to former levels along the Dutch coast, the LUD is not likely to host larger numbers of scoters.

Both Black-headed and Common Gulls are associated with estuarine water masses below 30 psu and a water depth shallower than 10 m, and few birds use the LUD site. The model scenarios indicated only slight increases in the abundance of these species at the LUD during periods with an extensive coastal current. Herring and Great Black-backed Gulls both display preferences to characteristics in both the coastal and offshore environments and associations with fishing activities, and were predicted to occur at low densities in the LUD. The model scenarios indicated slightly higher densities of Herring Gull during periods with an extensive coastal current.

Higher densities of Black-legged Kittiwake are related to areas of low salinity, high eddy potential and intermediate slope values, and the model predictions indicated low or medium densities at the LUD.

However, major changes in the overall abundance of Kittiwakes were predicted between the current scenarios with much higher densities occurring during periods with a narrow coastal current. The same distributional changes were predicted for the Common Guillemot, and may be linked to oceanographic processes at larger scale which were not taken into account by the local models. Guillemots were found in high densities at the LUD, and generally showed high use of areas deeper than 13 m with a prominent sloping terrain, and displayed a clear avoidance of PAWP and OWEZ and adjacent areas. Medium densities of Razorbills were found in a broad zone around the 20 m contour, including the LUD.

Ship traffic affected the distribution of several species of seabirds negatively, including Red- and Black-throated Diver, Great Crested Grebe, Herring and Great Black-backed Gull, Black-legged Kittiwake and Common Guillemot.

It is worth stressing that the specific baseline descriptions lack details of trends which are controlled by movements of seabirds rather than seabirds staging and wintering in the area. This is especially relevant in order to judge the seemingly important coastal zone along the 10 m depth contour. Since all seabirds were modelled irrespective of their behaviour, the potential bias induced by birds flying along the coast may be further investigated.

In conclusion, the baseline models for LUD have documented variability in the distribution of several seabird species. Species affined to the environment of the coastal current will penetrate offshore and occur more frequently in LUD during periods dominated by easterly winds and an extensive coastal current, while species with a predominating offshore distribution will have a tendency to occur in higher density during periods dominated by westerlies. These oscillations offer challenges for the post-construction monitoring (see below) by reducing the power of collected data and model predictions, unless the variations in the natural habitat of the different species can be accounted for. As the hydrodynamic models were set up and calibrated with the purpose to describe changes in water masses and mixing and in zones of eddies and fronts at the scale of a few kilometres the modelled distribution of seabird habitats is judged as satisfactory. Smaller scale frontal features may still play a role in shaping the local distribution of seabirds, yet they are less important determinants of the density gradients of these species (Schneider 1982, Skov & Prins 2001).

Not all mean distribution models performed well. The PA part of Gannet model and both parts of the models for Common Scoter and Razorbill had low levels of deviance explained (< 15%). More importantly, the predictive power clearly differed between the two model parts, as the predictive power of estimated patterns were generally better than predicted densities. This again stresses the need to base monitoring of post-construction effects on the dynamic models. Collection of detailed data within the primary zone of habitat displacement (3-5 kilometers) will be crucial to resolve gradients in density with distance from the wind farm. As the primary transects are prioritised during all LUD monitoring surveys sample sizes for target species are expected to allow for determination of gradients. As the three wind farms have different lay-outs differentiating the effect of each wind farm (rather than use all wind farms as a factor) on seabird densities might also strengthen the power of the models.

## 5.2 Monitoring design

The approved post-construction monitoring for LUD should be undertaken for at least one year, and possibly for two or three years. After LUD-T1, the power of the monitoring data will be assessed. All primary transects were covered, as were a number of the secondary transects, especially in the southern part of the area. Thus, the collected data should form a solid basis for assessing any habitat displacement of seabirds from the LUD. This can be determined by testing for changes in densities at increasing distances from the wind farms while taking account of changes in oceanographic properties of the area. The LUD-T0 results presented here documented negative responses of divers (2 km avoidance zone), Northern Gannets (2 km avoidance zone) and Common Guillemot (5 km avoidance zone) to the existing wind farms, as well as positive response of Great Cormorants.

Monitoring of seabirds is typically undertaken without consideration of the local oceanographic conditions. Our model scenarios stress the need to integrate in situ co-variables describing the variation in the location of feeding habitats into the LUD monitoring program. Almost all species which occur in higher densities inshore from LUD have a tendency to extend their distribution westwards during periods with a strong coastal current, whereas the more pelagic species show the opposite response and extend their distribution eastwards during periods with a weak coastal current. The estuarine dynamics responsible for the oscillations of the coastal current is probably wind driven and has a relatively short temporal scale (hours - few days). Accordingly, distribution of seabirds at the LUD may oscillate with a relatively high frequency which can only be described by coupling observations to hydrodynamic model data. In the absence of such dynamic descriptions, assessments of post-construction changes in the distribution of most of the wintering seabirds at the LUD may easily lead to a type II error – a result erroneously pointing at an impact, or a type I error – a result erroneously pointing at no impact.

## 6 References

- Austin, M.P. 2002. Spatial prediction of species distribution: an interface between ecological theory and statistical modelling. *Ecological Modelling*, 157, 101-118.
- Buckland, S.T., Anderson, D.R., Burnham, K.P. and Laake, J.L. 1993. *Distance sampling: estimating abundance of biological populations*. Chapman & Hall, London.
- Buckland ST, Anderson DR, Burnham KP, Laake JL, Borchers DL & Thomas L, 2001. *Introduction to Distance Sampling*, Vol. Oxford University Press, Oxford
- Burnham, K.P., and Anderson, D.R. 2002. *Model Selection and Multimodel Inference: A Practical Information-Theoretic Approach*, 2nd ed. Springer-Verlag. ISBN 0-387-95364-7.
- Camphuysen C.J. & Leopold M.F. 1994. Atlas of seabirds in the southern North Sea. IBN Research report 94/6, NIOZ Report 1994-8, Institute for Forestry and Nature Research, Netherlands Institute for Sea Research and Dutch Seabird Group, Texel.
- Camphuysen, C.J. & Garthe, S., 2004. Recording foraging seabirds at sea: standardised recording and coding of foraging behaviour and multi-species foraging associations. *Atlantic Seabirds* 5: 1-23.
- Camphuysen CJ, Fox TJ, Leopold MF & Petersen IK, 2004. Towards standardised seabirds at sea census techniques in connection with environmental impact assessments for offshore wind farms in the U.K. - A comparison of ship and aerial sampling methods for marine birds, and their applicability to offshore wind farm assessments. NIOZ Report to Cowrie / The Crown Estate.
- Camphuysen, C. J.; Scott, B. E.; Wanless, S.. 2006 Distribution and foraging interactions of seabirds and marine mammals in the North Sea: multispecies foraging assemblages and habitat-specific feeding strategies. In: Boyd, I.; Wanless, S.; Camphuysen, C. J., (eds.) *Top predators in marine ecosystems: their role in monitoring and management*. Cambridge, Cambridge University Press, 82-97.
- Camphuysen, C.J., 2009. Het gebruik van zeetrekellingen bij de analyse van populatie schommelingen Dwergmeeuwen *Larus minutus* langs de kust. *Sula* 22(2): 49-66.
- Hastie, T. & Tibshirani, R. 1990. *Generalized additive models*. Chapman & Hall, London.
- Keijl G.O. & Leopold M.F. 1997. Massaal fouragerende Dwergmeeuwen *Larus minutus* voor de Hollandse kust. *Sula* 11: 17-20.
- Kinder, T.H., Hunt, G.L. Jr., Schneider, D. & Schumacher, J.D. 1983. Correlations between seabirds and oceanic fronts around the Pribilof Islands, Alaska. *Est. Coast. Shelf Sci.* 16: 309-319.
- Krijgsveld K.L., Fijn R.C., Japink M., van Horssen P.W., Heunks C., Collier M.P., Poot M.J.M., Beuker D. & Dirksen S. 2011. Effect studies Offshore Wind Farm Egmond aan Zee: Final report on fluxes, flight altitudes and behaviour of flying birds. NoordzeeWind report nr WEZ\_R\_231\_T1\_20111114\_flux&flight, Bureau Waardenburg report 10-219.
- Leopold M.F., Baptist H.J.M., Wolf P.A. & Offringa H. 1995. De Zwarte Zeeëend *Melanitta nigra* in Nederland. *Limosa* 68: 49-64.
- Leopold M.F., Camphuysen C.J., ter Braak C.J.F., Dijkman E.M., Kersting K. & van Lieshout S.M.J. 2004. Baseline studies North Sea wind farms: Lot 5 marine birds in and around the future sites Nearshore Windfarm (NSW) and Q7. Alterra-rapport 1048.

- Leopold M.F., Dijkman E.M., Teal L. & the OWEZ Team 2011. Local birds in and around the Offshore Wind Farm Egmond aan Zee (OWEZ) (T-0 & T-1, 2002-2010). NoordzeeWind Report OWEZ\_R\_221\_T1\_20111220\_local\_birds, IMARES report C187/11.
- Leopold, M.F., van Bemmelen, R.S.A. & Zuur, A.F. 2013. Responses of Local Birds to the Offshore Wind Farms PAWP and OWEZ off the Dutch mainland coast. Report number C151/12. Imares Report.
- Maclean, I.M.D., Rehfisch, M.M., Skov, H. & Thaxter, C.B. 2012. Evaluating the statistical power of detecting changes in the abundance of seabirds at sea. *Ibis* 155: 113-126.
- Pearce, J. and Ferrier, S. 2000. Evaluating the predictive performance of habitat models developed using logistic regression. *Ecological Modelling*, 133, 225-245.
- Pebesma, E.J., 2004. Multivariable geostatistics in S: the gstat package. *Computers & Geosciences* 30: 683-691.
- Petersen I.K., Christensen T.K., Kahlert J., Desholm M. & Fox A.D. 2006. Final results of bird studies at the offshore wind farms at Nysted and Horns Rev, Denmark. NERI Report, commissioned by DONG energy and Vattenfall A/S.
- Piper, W., Kulik, G., Durinck, J., Skov, H., & Leonhard, S. 2008. Horns Rev II Offshore Wind Farm. Monitoring of Migrating Waterbirds. Baseline Studies 2007-2008. DONG Energy A/S.
- Potts, J. M. & Elith, J. 2006. Comparing species abundance models. *Ecological Modelling* 199: 153-163.
- Rasmussen, E.B. 1991. A finite difference scheme for three dimensional modelling of fluid dynamics. *Proceedings of IAHR, Madrid, Spain. 1991*, pp. 339-348.
- Schneider, D.C. 1982. Fronts and seabird aggregations in the southeastern Bering Sea. *Mar. Ecol. Prog. Ser.* 10: 101-103.
- Skov H., Durinck J., Leopold M.F. & Tasker M.L. 1995. Important bird areas in the North Sea, including the Channel and the Kattegat. BirdLife International, Cambridge.
- Skov, H. & Prins, E. 2001. Impact of estuarine fronts on the dispersal of piscivorous birds in the German Bight. *Mar. Ecol. Prog. Ser.* 214: 279-287.
- Skov, H., Piper, W. and Leonhard, S.B. 2009. Horns Reef II Wind Farm. Monitoring of waterbirds. Baseline Studies 2007-2008. Orbicon A/S, DHI Water, Environment and Health, Biola. s.l. : Dong Energy A/S, 2008.
- Skov, H., Heinänen, S., Žydelis, R., Bellebaum, J., Bzoma, S., Dagys, M., Durinck, J., Garthe, S., Grishanov, G., Hario, M., Kieckbusch, J. J., Kube, J., Kuresoo, A., Larsson, K., Luigujoe, L., Meissner, W., Nehls, H. W., Nilsson, L., Petersen, I.K., Roos, M. M., Pihl, S., Sonntag, N., Stock, A. and Stipniece, A. 2011. Waterbird populations and pressures in the Baltic Sea.
- Skov, H., Leonhard, S.B., Heinänen, S., Zydelis, R., Jensen, N.E., Durinck, J., Johansen, T.W., Jensen, B.P., Hansen, B.L., Piper, W., Grøn, P.N. 2012. Horns Rev 2 Monitoring 2010-2012. Migrating Birds. Orbicon, DHI, Marine Observers and Biola. Report commissioned by DONG Energy.
- Skov H, Heinänen S, Hansen DA, Ladage F, Schlenz B, Žydelis R, Thomsen, F. 2014. Chapter 14. Marine Habitat modelling for harbour porpoises in the German Bight In BSH & BMU (2014). *Ecological Research at the Offshore Windfarm alpha ventus - Challenges, Results and Perspectives*. Federal Maritime and Hydrographic Agency (BSH), Ministry for the Environment, Nature Conservation and Nuclear Safety (BMU). Springer Spektrum. 180 pp.
- Tasker M.L., Jones P.H., Dixon T.J. & Blake B.F. 1984. Counting seabirds at sea from ships: a review of methods employed and a suggestion for a standardized approach. *Auk* 101: 567-577.

Thomas L, Buckland ST, Rexstad EA, Laake JL, Strindberg S, Hedley SL, Bishop JRB, Marques TA & Burnham KP 2010. Distance software: design and analysis of distance sampling surveys for estimating population size. *Journal of Applied Ecology* 47: 5-14.

Wintle, B.A., Elith, J. and Potts, J.M. 2005. Fauna habitat modelling and mapping: A review and case study in the Lower Central Coast Region of NSW. *Austral Ecology*, 30, 719–738.

Wood, S. N. 2006. *Generalized Additive Models: An Introduction with R*. Chapman and Hall, London.

Wood, S. N. & Augustin, N. H. 2002. Gams with integrated model selection using penalized regression splines and applications to environmental modeling. *Ecological Modelling* 157: 157-177.

## APPENDICES

## APPENDIX A – Detailed description of species distribution models

## Overview

An overview of the model design is given in Figure A.1 outlining the different phases of the analyses. The model design was composed of a hydrodynamic model framework consisting of a 2D model producing time series of currents and associated variables and a 3D model producing time series of mixing regimes and associated variables, post-processing chains extracting dynamic habitat predictors and distribution models covering the winter (October-March) season and describing statistical responses of seabird densities to the habitat and pressure variables.

To be able to accurately describe the distribution of seabirds over time one needs to be able to take account of the actual oceanographic components realised during each observation; i.e. currents, fronts, salinity, mixing as well as the pressure components, as for example disturbance from ship traffic. Without these characteristics distribution models of seabirds will be unlikely to resolve the true variation in the distribution of the seabirds. A way to obtain instantaneous oceanographic factors is by linking observations to numerical hydrodynamic models. Hydrodynamic models enable mapping of locations, timing and movement of salinity fronts, eddies and upwelling which enhance the probability of prey detection for seabirds. These features are driven by daily and seasonal variations in weather, tidal cycles, run offs and major current systems and are key differentiators in the marine landscapes - and the associated biodiversity. The hydrodynamic model set-up is described in the following sub-chapter.

The spatio-temporal modelling is the crucial step of the species distribution models. In this step the corrected densities of seabirds were modelled as a response to their dynamic habitat and pressure variables. The temporal variation in the physical environment of the seabirds has been extracted from the hydrodynamic models based on both time and location to the species observations. This approach has allowed for prediction of the distribution of the species in space and time. Generalized Additive Models (GAMs) were chosen as the basis for spatio-temporal modelling due to the suitability of GAMs for this type of data as they can deal with non-linear relationships, non-normally distributed errors and over-dispersions.

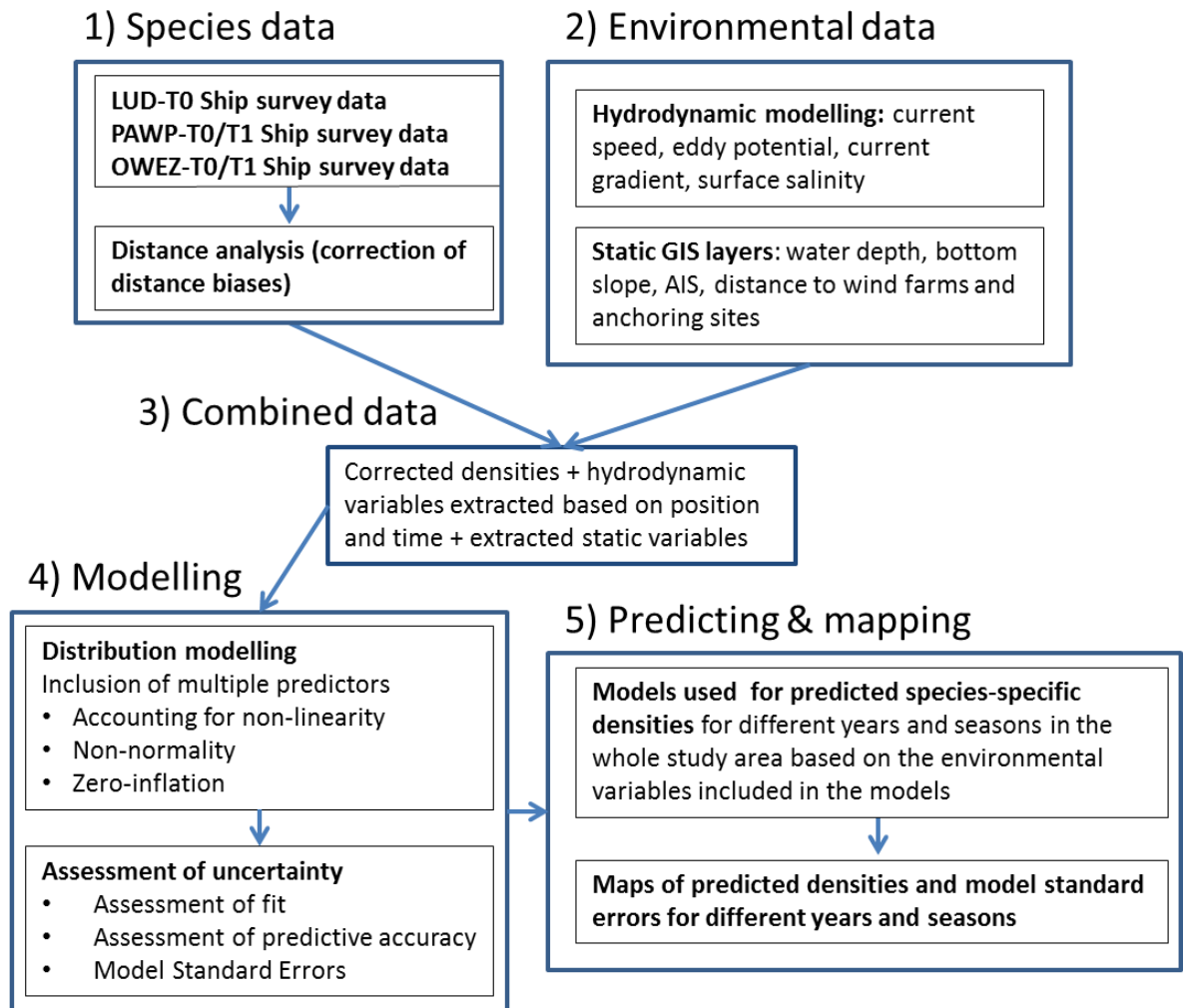


Figure A.1. Overview of design for species distribution models

## Hydrodynamic models

Two dedicated hydrodynamic models were designed for resolving currents and mixing regimes at the highest possible resolution achievable within the time constraints of the project. Time series of current patterns was developed using an integrated 2-dimensional model set-up in DHI's MIKE 21, while 3-dimensional density patterns were computed on the basis of a baroclinic model set up in DHI's MIKE 3. Both models were developed using finite-element grids with increasing spatial resolution in shallower areas, and were run at a temporal resolution of 1 hour between 2002 and 2012.

### Southern North Sea 2D flow model

Based on experience from other regions currents were expected to represent important predictor variables for the distribution of seabirds at medium and fine spatial scale. Thus, the dedicated Southern North Sea 2D flow model was set up with the purpose to describe fine-scale patterns of currents, including resolution of eddies and fronts. MIKE 21 FM HD computes on a flexible mesh the depth-integrated currents, driven by a combined forcing, which may comprise forces induced by tide, wind and waves. This model solves the depth-averaged shallow water equations of continuity and momentum and can reproduce temporal and spatial variations of water levels and currents. The applied driving forces can consist of wave forces (radiation stresses), water level differences or fluxes at the boundaries (tidal and river flow), wind and atmospheric pressure forces and Coriolis force. The MIKE 21 Flow Model used for the present study was Release 2012, Service Pack 1.

The model system is based on the numerical solution of the two dimensional incompressible Reynolds averaged Navier-Stokes equations subject to the assumptions of Boussinesq and of hydrostatic pressure. The model is applicable for the simulation of hydraulic and environmental phenomena in estuaries, bays, coastal areas, and seas wherever stratification can be neglected. The model can be used to simulate a wide range of hydraulic and related items, including tidal exchange and currents, storm surges, and water quality.

### Set-up and specifications

#### Bathymetry, domain and mesh

The model uses a flexible mesh (FM) based on unstructured triangular or quadrangular elements and applies a finite volume numerical solution technique. The extent of the model domain is seen in Figure A.2. The model bathymetry, taken from a previous study carried out by DHI, is based on a combination of interpolated GEBCO\_08<sup>1</sup> and C-map<sup>2</sup> data. Shorelines were adopted from the Global Self-consistent, Hierarchical, High-resolution Shoreline Database (GSHHS), version 2.2.2 provided by NOAA<sup>3</sup>.

The horizontal reference system used is longitude/latitude (WGS-84). The vertical reference system is mean sea level.

The mesh resolution is displayed in Figure A.3. The spatial resolution of the mesh varies from approximately 30-50 km off the shelf to 10-30 km over the slope and shelf edge to 5-10 km on the larger depths (>100 m) on the shelf, 3-5 km on the smaller depths (<100 m) on the shelf and between 1 and 3 km in the coastal areas.

---

<sup>1</sup> <http://www.gebco.net>

<sup>2</sup> <http://ww1.jeppesen.com/marine/lightmarine/index.jsp>

<sup>3</sup> <http://www.ngdc.noaa.gov/mgg/shorelines/gshhs.html>

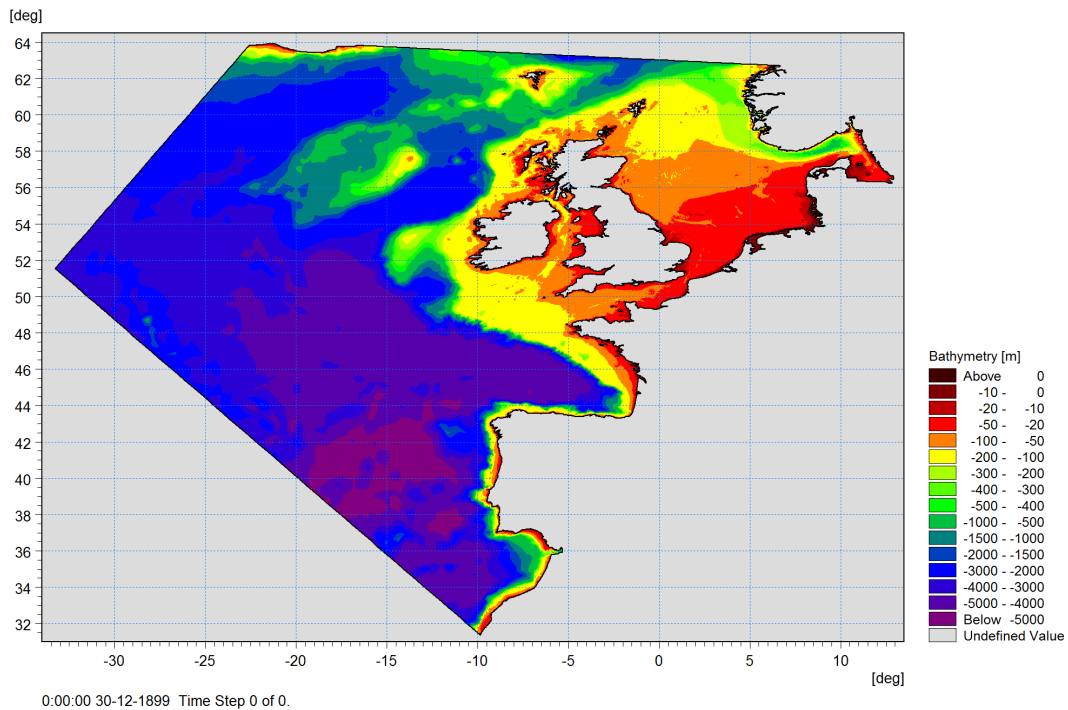


Figure A.2 Model domain

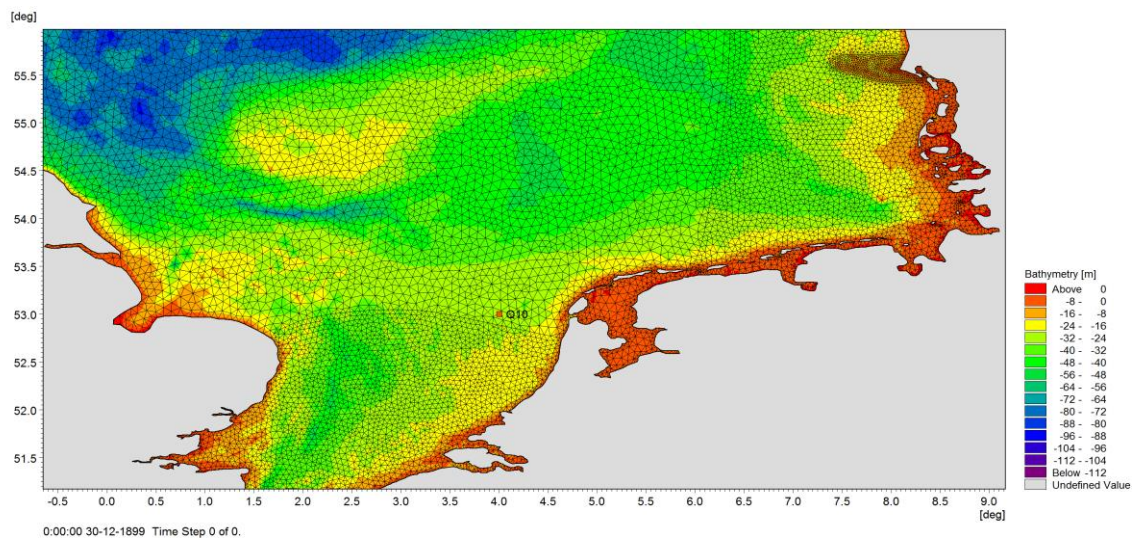


Figure A.3 Mesh resolution

## Boundary conditions

Spatial (1D) and time varying water level data were extracted from the global tide model (KMS) and applied to all four boundaries. The global tide model had obtained its tidal constituents from primarily satellite altimetry observations as described in Cheng & Andersen (2010). The global tide model included 8 constituents (M2, S2, K1, O1, N2, P1, K2 and Q1) and had a spatial resolution of 0.25 degrees. Boundary data was extracted with a temporal resolution of 15min.

## Meteorological forcing

The wind forcing and atmospheric pressure at MSL applied in the model were adopted from the Climate Forecast System Reanalysis (CFSR) numerical model provided by NOAA<sup>4</sup>. The CFSR data set was established by the National Centers for Environmental Prediction (NCEP). The data are available on an hourly basis from 1 January 1979 to present. The data set consists of Climate Forecast System Reanalysis (CFSR), covering the 31-year period from 1979 to 2009 and since then the operational data (CFSR2). The underlying model in CFSR2 is the same as for CFSR. The details of the CFSR are described in Saha et al. (2010). In the following “CSFR” will refer to the combined data of CFSR and CSFR2.

Table A.1 Spatial resolution of the applied meteorological data.

<i>Parameter</i>	<i>Temporal resolution</i>	<i>Spatial resolution CFSR</i>	<i>Spatial resolution CFSR2</i>
Wind (U,V)	1 h	0.30°	0.30°
Air pressure reduced to MSL	1 h	0.50°	0.50°

The wind data included parameters of wind speed and wind direction (or wind velocity vectors,  $u$  and  $v$ ) at height 10mMSL. The model values may be interpreted as representative of a 10-minute averaging period. The value in between the hourly values may attain a higher or lower value. However, the models produce a fairly smooth variation of the atmosphere, and the fluctuations within each time step are usually much smaller compared to what may be measured.

## General model specifications

Based on sensitivity studies and calibration experience from previous studies, the HD<sub>NE</sub> was set up with the following model specifications:

- Horizontal eddy viscosity: Smagorinsky formulation with constant = 0.28
- Bed resistance: Depth-dependent Manning map
  - < 30m:  $38\text{m}^{1/3}/\text{s}$
  - 30-100m:  $42\text{m}^{1/3}/\text{s}$
  - > 100m:  $45\text{m}^{1/3}/\text{s}$
- The wind stress  $\vec{\tau}_s$  is defined by  $\vec{\tau}_s = \rho_a c_d |\vec{U}| \vec{U}$ , where  $\rho_a$  is the density of the air,  $c_d$  represents the drag coefficient of the air and  $\vec{U} = (U, V)$  are the wind components specified by in the CFSR data.
- Wind drag (empirical factors):  $C_A = 1.255 \cdot 10^{-3}$ ,  $C_B = 2.425 \cdot 10^{-3}$ ,  $W_A = 7 \frac{\text{m}}{\text{s}}$ ,  $W_B = 25 \frac{\text{m}}{\text{s}}$  ( $C_A$ ,  $C_B$ ,  $W_A$ , and  $W_B$  are used to calculate the empirical drag coefficient of air.)

$$c_d = \begin{cases} c_a \\ c_a + \frac{c_b - c_a}{w_b - w_a} \cdot (w_{10} - w_a) \\ c_b \end{cases}$$

- Direct tidal potential from 11 constituents (M2, O1, S1, K2, N2, K1, P1, Q1, MF, MM, SSA)
- Boundary conditions: Tides from the global tidal model (8 constituents)

Discharges from rivers were not included. They were considered to have an insignificant influence on the water level and current in a 2D regional model where no baroclinic conditions were included.

<sup>4</sup> <http://journals.ametsoc.org/doi/pdf/10.1175/2010BAMS3001.1>

## Data assimilation

Data assimilation is a methodology that applies observed measurements in order to improve the skill and accuracy of the flow model. In this project, only assimilation of in situ water level data was considered.

The observations were used to update the model such that, broadly speaking, the model was used as an advanced interpolation and extrapolation tool. This allowed the model accuracy to be greatly improved also at non-observed positions and for additional variables such as the depth-averaged velocity.

The data assimilation scheme considered for this project was the Steady Kalman Filter approach based on the so-called Ensemble Kalman Filter. A time-varying temporally smoothed and distance regularized Ensemble Kalman Filter was used with a 8 ensemble member. The assimilation scheme assumes uncertainty in the open water level boundary conditions and wind forcing. The Ensemble Kalman Filter was used to construct a long-term averaged Kalman gain matrix based for January 2005. The Steady Kalman Filter then applies this time constant Kalman gain matrix, which has the advantage of reducing the computational cost significantly, while preserving good assimilation skills (Sørensen & Madsen 2004).

All measurements were corrected such that the datum approximately represents the model datum in order to allow proper comparison of observations and the model. The model datum was determined by the open boundary levels and a long-term average dynamical balance from a 1-year simulation without data assimilation. Note that the measurement-model difference could have a yearly mean variation. However, this was assumed to be insignificant.

A number of parameters need to be specified in the filter schemes. The assimilation system is very complex; hence, the parameters were based on experience and iterations (simulation tests). The standard deviation for most of the water level observations was in the range of 0.04-0.07. A lower valued of the standard deviation for a measurement station implies that more trust was put on the observation data and hence the model was pulled more towards it.

## Validation

### Quality indices

To obtain an objective and quantitative measure of how well the modelled water levels compared to the observed measurements, a number of statistical parameters, so-called quality indices (QI's), were calculated. Prior to the comparisons, the model data were synchronized to the time stamps of the observations so that both time series had equal length and overlapping time stamps. For each valid observation, measured at time  $t$ , the corresponding model value was found using linear interpolation between the model time steps before and after  $t$ . Only observed values that had model values within  $\pm$  the representative sampling or averaging period of the observations were included (e.g. for 10-min observed wind speeds measured every 10 min compared to modelled values every 1 hour, only the observed value every hour was included in the comparison).

The quality indices are described and defined in Table A.2. Most of the quality indices are based on the entire data set, and hence the quality indices should be considered averaged measures and may not be representative of the accuracy during rare conditions.

The BIAS is the mean difference between the modelled and observed data and AME is the mean of the absolute difference. RMSE is the root mean square of the difference.

The scatter index (SI) is a non-dimensional measure of the difference calculated as the unbiased root-mean-square difference relative to the mean absolute value of the observations. In open water, an SI below 0.2 is usually considered a small difference (excellent agreement) for significant wave heights. In

confined areas, where mean significant wave heights are generally lower, a slightly higher SI may be acceptable.

The correlation coefficient (CC) is a non-dimensional measure reflecting the degree to which the variation of the first variable is reflected in the variation of the second variable. A value close to 0 indicates very limited or no correlation between the two data sets, while a value close to 1 indicates a very high or perfect correlation. Typically, a CC above 0.9 is considered a high correlation (good agreement) for wave heights.

The hit rate (HR) quantifies how often (in percent) the modelled value is within +/- a given threshold of the observed value.

The Q-Q line slope and intercept are found from a linear fit to the data quantiles in a least square sense. The lower- and uppermost quantiles are not included on the fit. A regression line slope different from 1 may indicate a trend in the difference.

The peak ratio (PR) is the average of the  $N_{\text{peak}}$  highest model values divided by the average of the  $N_{\text{peak}}$  highest observations. The peaks are found individually for each data set through the peak-over-threshold (POT) method applying an average annual number of exceedance of 4 and an inter event time of 36 hours. A general underestimation of the modelled peak events results in PR below 1, while an over-estimation results in a PR above 1.

In the peak event plot, 'X' is representing the observed peaks, while 'Y' is representing the modelled peaks, based on the POT method. Joint peaks are defined as any X and Y peaks within +/-36 hours of each other.

Table A.2. Definition of quality indices (OBS = Observation, MOD = Model)

<i>Abbreviation</i>	<i>Description</i>	<i>Definition</i>
N	Number of valid and applied observations	–
MEAN	Mean of model data	$\frac{1}{N} \sum_{i=1}^N \mathbf{MOD}_i$
BIAS	Mean of difference	$\frac{1}{N} \sum_{i=1}^N (\mathbf{MOD} - \mathbf{OBS})_i$
AME	Mean of absolute difference	$\frac{1}{N} \sum_{i=1}^N ( \mathbf{MOD} - \mathbf{OBS} )_i$
RMSE	Root mean square of difference	$\sqrt{\frac{1}{N} \sum_{i=1}^N (\mathbf{MOD} - \mathbf{OBS})_i^2}$
SI	Scatter index (unbiased)	$\frac{\sqrt{\frac{1}{N} \sum_{i=1}^N (\mathbf{MOD} - \mathbf{OBS} - \mathbf{BIAS})_i^2}}{\mathbf{MEAN}(\text{of absolute values})}$
CC	Correlation coefficient	$\frac{\sum_{i=1}^N (\mathbf{OBS}_i - \mathbf{MEAN})(\mathbf{MOD}_i - \overline{\mathbf{MOD}})}{\sqrt{\sum_{i=1}^N (\mathbf{OBS}_i - \mathbf{MEAN})^2 \sum_{i=1}^N (\mathbf{MOD}_i - \overline{\mathbf{MOD}})^2}}$
HR(threshold)	Hit rate (threshold)	Percentage data points within +/- threshold
Q-Q line	Quantile-Quantile line	Linear least square fit to quantiles
PR(N <sub>peak</sub> )	Peak ratio of N <sub>peak</sub> events	$\mathbf{PR}(N_{\text{peak}}) = \frac{\sum_{i=1}^{N_{\text{peak}}} \mathbf{MOD}_i}{\sum_{i=1}^{N_{\text{peak}}} \mathbf{OBS}_i}$

## Validation results

The modelled water levels are reasonably predicted in terms of phase and amplitude. The RMSE is less than 0.25m at all stations. Figure A.4 gives examples of QIs computed for the validation stations at Dover and Port Erin. The vast majority of QIs indicate good correspondence between modelled and observed values.

From the above it can be concluded that the predictive power of the hydrodynamic model complex is strong and accurate hydrodynamic parameters have been supplied to the seabird distribution models.

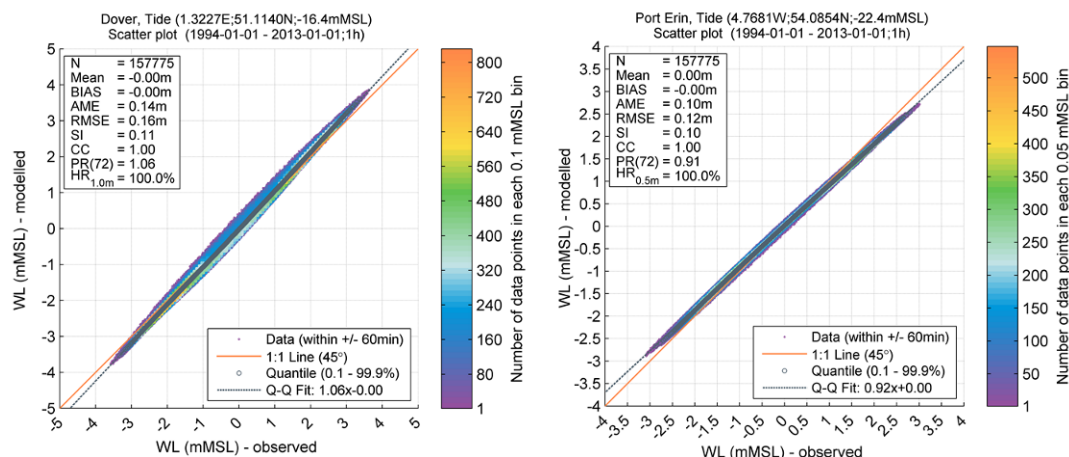


Figure A.4. Example of validations of modelled water levels (tide) for the stations at Dover and Port Erin.

### Southern North Sea 3D flow model

The purpose of the dedicated 3D flow model was to provide information on density changes, including determination of mean extent of estuarine water masses and tidally mixed water masses. The 3D baroclinic hydrodynamic model was set up with MIKE 3 Flexible Mesh (FM) HD. MIKE 3 FM is DHI's general 3D simulation engine. MIKE 3 HD describing elevations, current profiles and turbulence statistics (Rasmussen 1991) and is applicable for the study of a wide range of phenomena, including:

- Tidal exchange and currents, including stratified flows
- Heat and salt recirculation
- Mass budgets of different categories of solutes and other components such as particulate matter

MIKE 3 FM solves the time-dependent conservation equations of mass and momentum in three dimensions, the so-called Reynolds-averaged Navier-Stokes equations. The flow field and pressure variation are computed in response to a variety of forcing functions, when provided with the bathymetry, bed resistance, wind field, hydrographic boundary conditions, etc. The conservation equations for heat and salt are also included and provide among others the water temperature. MIKE 3 uses the UNESCO equation for the state of seawater (1980) as the relation between salinity, temperature and density. Hence, the model includes temperature and salinity such that baroclinic effects on the flow can be described.

MIKE 3 FM is based on an unstructured flexible mesh and uses a finite volume solution technique. The meshes are based on linear triangular elements. This approach allows for a variation of the horizontal resolution of the model grid mesh within the model area to allow for a finer resolution of selected sub-areas. The vertical discretization can be based on a combined sigma-z grid.

The numerical solution uses a finite-volume method, with a second order spatial representation, both in vertical and horizontal directions. The time marching is explicit, thus there is a strict Courant number criterion for stability. The relatively short time step enforced is balanced by a very efficient solution and ensures an accurate numerical solution.

## Set-up and specifications

### Bathymetry, domain and mesh

The North Sea model domain extends from Irish Sea around the Faroe Islands and the Shetland Islands into the central part of the Kattegat. Figure A.5 shows the extension of the entire model area and the bathymetry including mesh. The model bathymetry is based on a modified version of DHI's bathymetry for the North Atlantic using all available depth measurements. The spatial resolution of the mesh varies from approximately 10 km off the shelf to 6 km on the shelf and 1.5 km in the coastal areas. The vertical resolution is 2 m, and the temporal resolution of the output 1 hour.

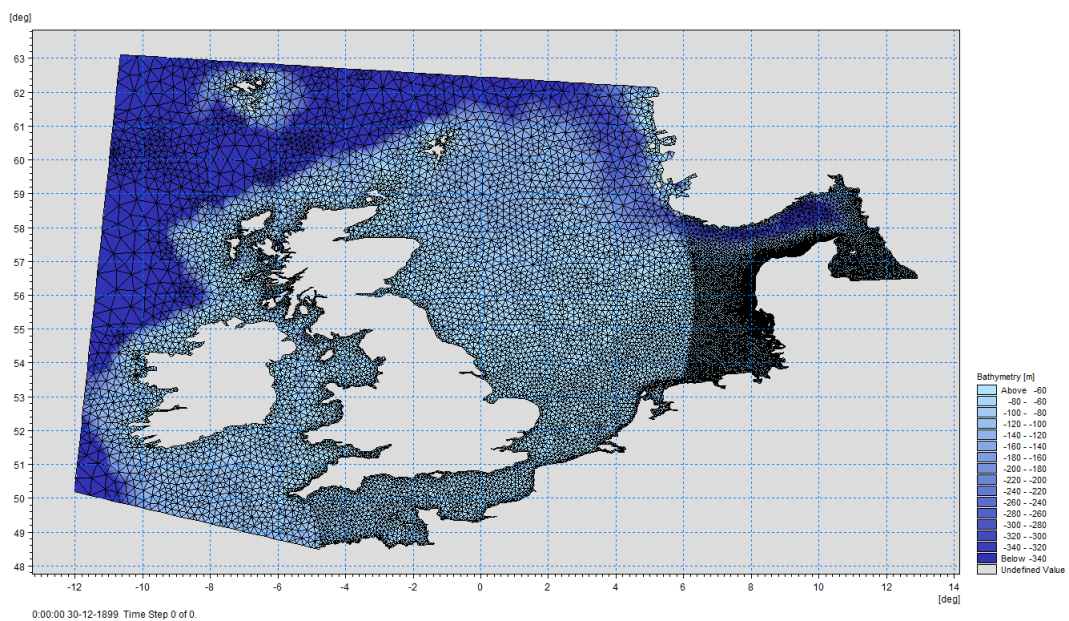


Figure A.5. North Sea model domain and bathymetry for the MIKE 3 FM model

### Meteorology and Runoff

The main weather model used as a basis for the 3D flow model is the regional WRF model run routinely by StormGeo for DHI. It is based on the global weather model run by ECMWF as illustrated in Figure A.6.

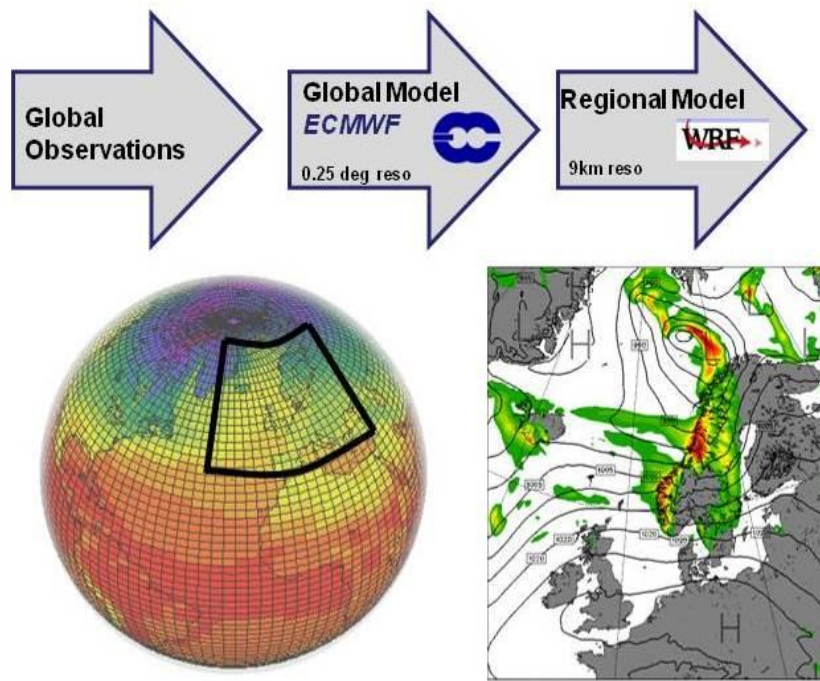


Figure A.6. Global and regional weather model applied in the UK 3D flow model

Runoff data from rivers have been included as daily or weekly values for British, German and Dutch rivers and as monthly values of flow for Danish, Swedish and Norwegian rivers.

### Open boundaries

The open boundaries for the 3D flow model were obtained from the Hybrid Coordinate Ocean Model (Hycom). Hycom is part of the multi-national Global Ocean Data Assimilation Experiment (GODAE) aiming for demonstrating real-time global ocean products in a way that will promote wide utility and availability for maximum benefit to the community. HYCOM is designed as a generalized (hybrid isopycnal/  $z$ ) coordinate ocean model. It is isopycnal in the open stratified ocean, but reverts to a terrain-following coordinate in shallow coastal regions, and to  $z$ -level coordinates near the surface in the mixed layer. The global model has  $1/12^\circ$  equatorial resolution and latitudinal resolution of  $1/12^\circ \cos(\text{lat})$  or  $\sim 7$  km for each variable at mid-latitudes. It has 32 coordinate surfaces in the vertical.

The data assimilation is performed using the Navy Coupled Ocean Data Assimilation (NCODA) (Cummings, 2005) system with a model forecast as the first guess. NCODA assimilates available satellite altimeter observations (along track obtained via the NAVOCEANO Altimeter Data Fusion Center), satellite and in situ sea surface temperature (SST) as well as available in situ vertical temperature and salinity profiles from XBTs, ARGO floats and moored buoys.

The HYCOM global ocean prediction system is designed to provide an advance over the existing operational global ocean prediction systems, since it overcomes design limitations of the present systems as well as limitations in vertical and horizontal resolution. The result should be a more streamlined system with improved performance and an extended range of applicability, especially for shallow water and in handling the transition from deep to shallow water.

As the boundaries from the Hycom model does not include tides and tide generated flows the boundaries for this North Sea model needs to be superimposed with tides and flows at the boundaries generated from the 2D flow model. The data generated with the 2D flow model was used together with the data obtained from the HYCOM model and added to construct the best possible boundaries for the 3D flow model.

## Water level data and assimilation

The 3D model includes assimilation of real-time water levels at 22 stations. This assimilation plays a major factor in the high accuracy of the water levels and currents produced by the 3D model.

Table A.3. Stations with online water level data

<i>Station</i>	<i>Longitude (deg E)</i>	<i>Latitude (deg N)</i>	<i>Country</i>	<i>Source</i>
Aberdeen	-2.0833	57.15	UK	DMI
Bournemouth	-1.87486	50.714333	UK	BODC
Cromer	1.30164	52.93419	UK	BODC
Devonport	-4.18525	50.36839	UK	BODC
Dover *	1.3167	51.117	UK	DMI
Esbjerg	8.45	55.467	Denmark	DMI
Felixstowe *	1.34655	51.95769	UK	BODC
Grenå	10.933	56.4	Denmark	DMI
Hanstholm	8.6	57.133	Denmark	DMI
Helgoland	7.883	54.183	Germany	DMI
Hirtshals	9.96	57.6	Denmark	DMI
Hornbæk	12.4667	56.1	Denmark	DMI
IJmuiden buitenhaven	4.555085	52.463335	The Netherlands	Rijkswaterstaat
Immingham	-0.187528	53.630417	UK	BODC
Lerwick	-1.14031	60.15403	Shetland Isles	BODC
Lowestoft *	1.75	52.467	UK	DMI
Måløy	5.116667	61.933333	Norway	IOC
Newhaven	0.05703	50.78178	UK	BODC
North Shields	-1.433	55.017	UK	DMI
Ostende	2.933	51.233	Belgium	DMI
Smögen	11.217	58.367	Sweden	DMI
Stavanger	5.733	58.967	Norway	DMI
Tredge	7.566667	58	Norway	IOC
Wick	-3.0833	58.433	UK	DMI
Wierumergronden	5.95882	53.51696	The Netherlands	Rijkswaterstaat

\*: Station not used for data assimilation.

## Validation

Comparisons of water levels from the regional 3D model are shown in the figure below.

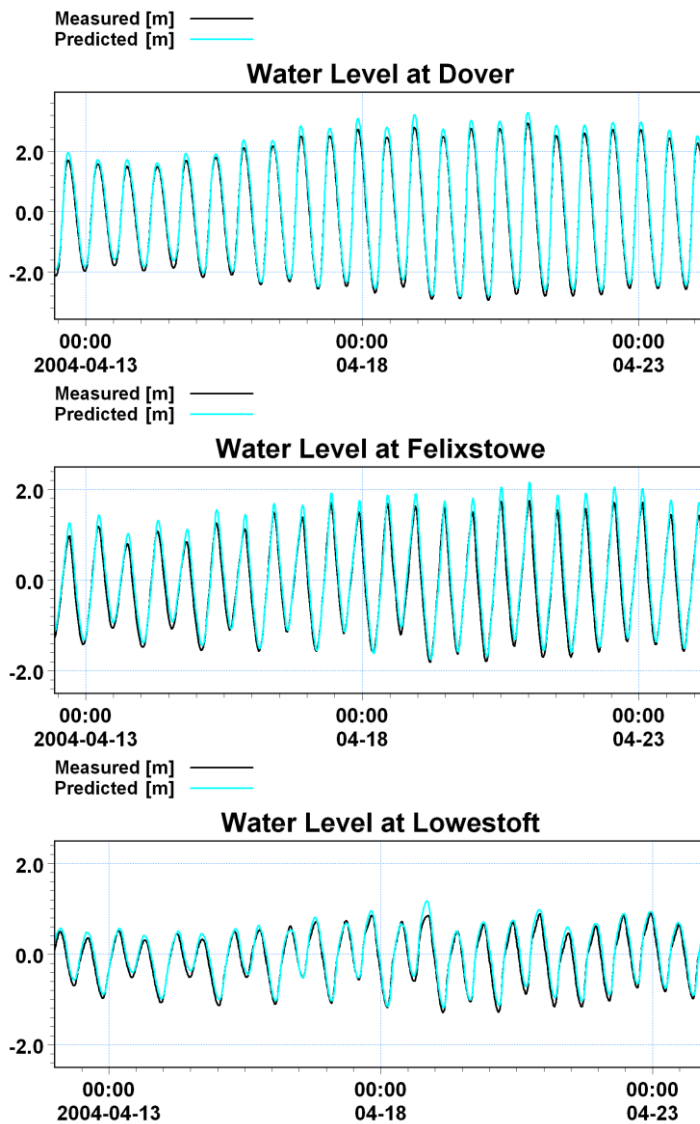


Figure A.7. Comparison of measured (black line) and predicted (blue line) water levels during validation period. Predicted data taken from the regional 3D hydrodynamic model.

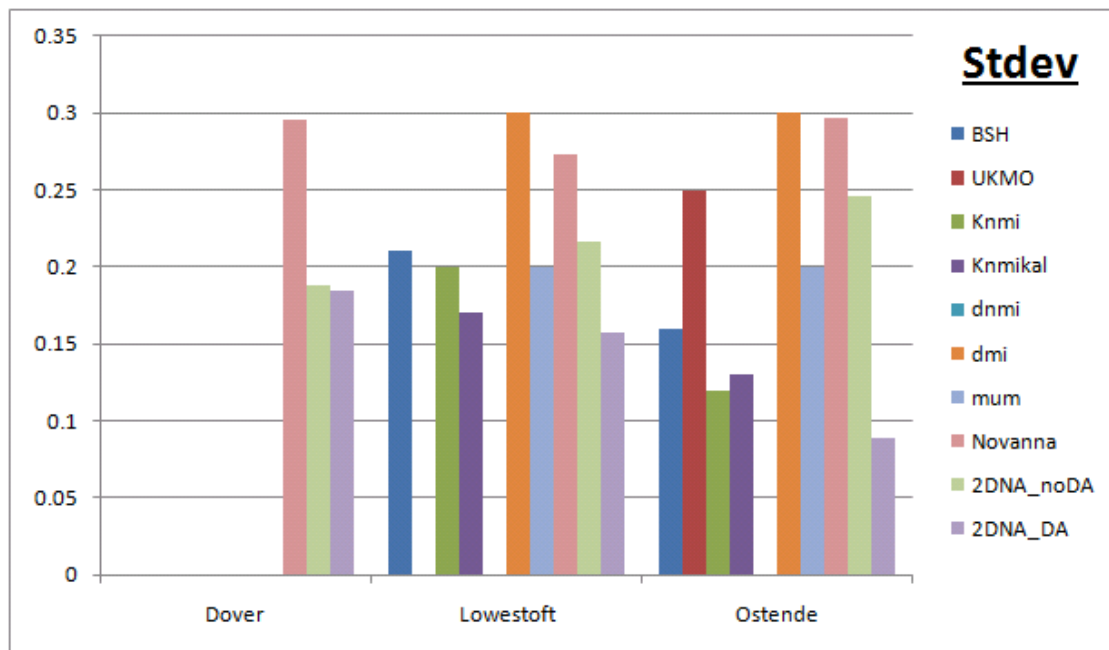


Figure A.8 Comparison of accuracy (standard deviation in m) between DHI's hydrodynamic model including data assimilation (denoted 2DNA\_DA) and without data assimilation (denoted 2DNA\_noDA) as well as other models from BSH (Germany) UKMO (UK), KNMI (Netherland) DNMI (Norway), DMI (Denmark), MUM (Belgium) and Novana (Denmark).

The comparisons between measurements and predicted (modeled) data shown both as time series and as profiles and in relation to other hydrodynamic models are very satisfactory.

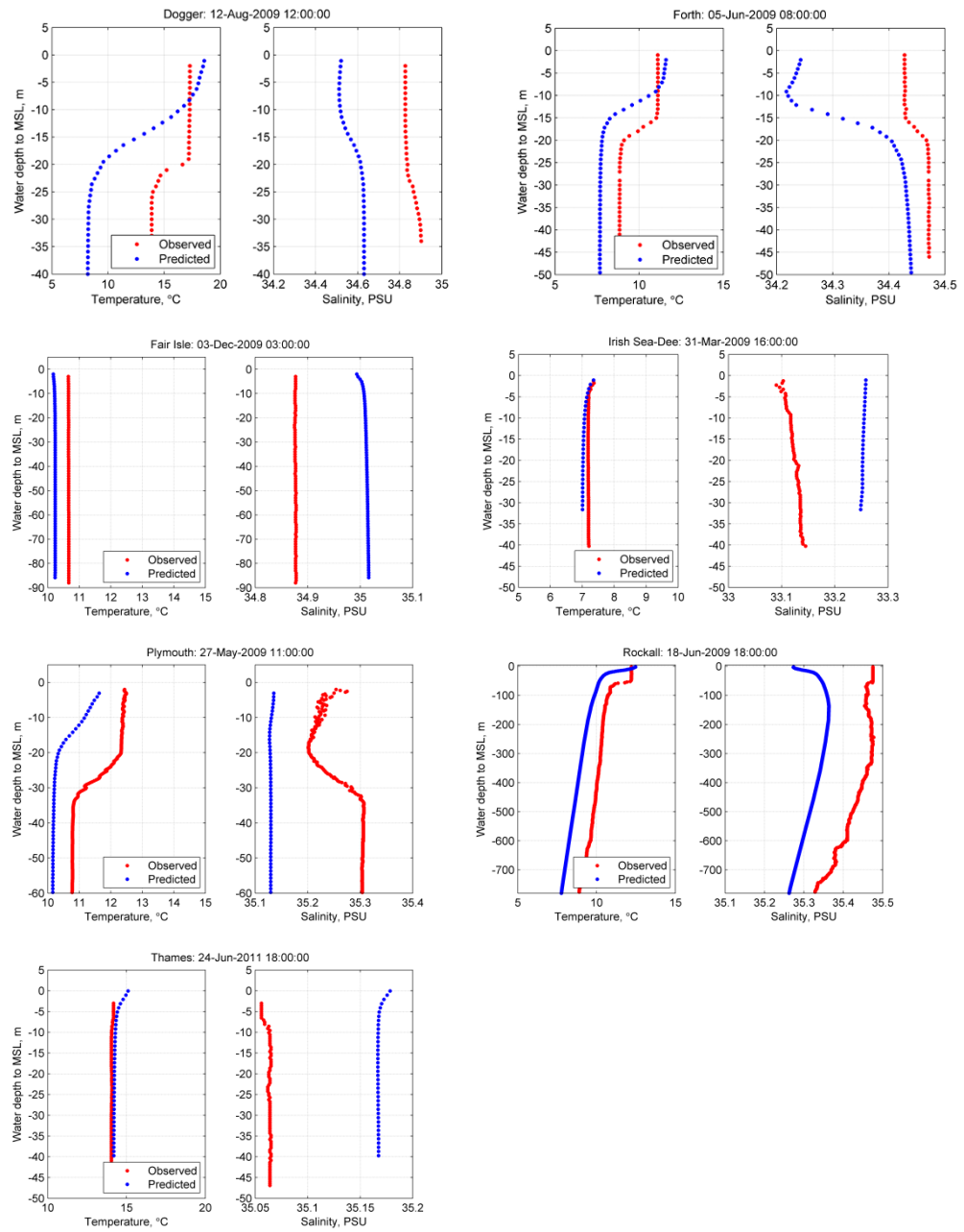


Figure A.9. Comparison between observed and modeled profiles of salinity and temperature at selected stations.

## GAM seabird distribution models

To account for zero inflation the seabird distribution models were based on a two-step model design consisting of a presence-absence model (binomial distribution with a logit link) and a positive model part where all zeroes were excluded (fitted with a gamma distribution and log link). One two-step model was fitted for each species using all available data, and included year (winter) and month as factor variables. All predictor variables were included in an initial “full” model, where after unimportant variables were dropped in a step-wise manner, starting with the least significant (Wood & Augustin, 2002). Variables contributing very little to the model fit (little change in UBRE/GCV; Wood & Augustin, 2002), and variables displaying ecologically meaningless responses (based on expert judgment) were also removed (Austin, 2002; Wintle et al., 2005). The GAM models were fitted using thin plate regression splines and the degree of smoothing (how closely the model fits the data) was automatically estimated by means of generalized cross validation (Wood, 2006). To reduce potential overfitting of the GAMs, smooth functions for each environmental variable were limited to 5 ( $k=5$ ). The models were fitted in R version 2.9.0 (R Development Core Team, 2004) using the R package “mgcv” (Wood, 2006).

Collinearity was checked between the predictor variables (see list in Table 3) before model fitting, as strong correlation between variables can result in inaccurate model parameterization and decreased predictive accuracy (Dormann et al., 2012). A Pearson’s pairwise correlation less than 0.75 was allowed. When using mean winter values (in the “mean model”, see description of model setup below) many predictors were highly correlated and therefore the following variables were included; mean eddy potential, mean salinity, water depth, slope, distance to wind farm (maximum 4 km) and distance to ship anchoring areas (maximum for km) in the initial full model. When using instantaneous data, (closest spatio-temporal match) the only excluded variable was current gradient which was highly correlated with eddy potential, however water depth and slope were also left out from these dynamic models, if possible, not to constrain the distribution to static conditions.

The fit of the GAMs was based on deviance explained and by inspecting residual plots. Diagnostic plots of the positive part, normality and homogeneity of variance (homoscedasticity) of the residuals as well as observed against fitted values were checked (Zuur et al. 2009). Model residuals were also checked for spatial autocorrelation by using variograms and checking for autocorrelation structures (R package “gstat”; Pebesma, 2004). The explanation degree of both model parts was judged as good with deviance explained exceeding 40%, as fair with deviance explained between 15% and 40% and as poor with deviance explained below 15%. For assessing the predictive accuracy of the models a 10-fold cross validation approach was used in which the data was randomly grouped into 10 groups of which one of the groups was left out for testing and the rest for fitting. The same procedure was repeated for all groups and the mean of the evaluation statistics was calculated. The binomial model was tested using AUC and the combined density predictions were evaluated using Spearman’s rank correlation (Pearce & Ferrier, Potts & Elith 2006). The binomial model predictions were judged as good with AUC values above 0.80, as fair with AUC values between 0.70 and 0.80 and as poor with AUC values below 0.70. Density predictions were judged as good with Spearman’s rank correlations above 0.4, as fair with correlations between 0.15 and 0.40 and as poor with correlations below 0.15.

The habitat predictor variables are visualised in the figures below. The parameter ‘current gradient’ or frontal strength (Figure A.10) was calculated by the local gradient ( $|dU/dx|+|dV/dy|$ ) in horizontal current from the eastern and northern current components (U and V). The horizontal eddy activity  $abs(dV/dx|-dU/dy|)$  (Figure A.10) was similarly calculated to represent the local ‘eddy potential’, with absolute values of anticlockwise and clockwise eddies. In the two expressions dx and dy indicate the horizontal grid spacing in the east and north direction, respectively. Examples of modelled salinity and eddy activity parameters used in the models covering different extent of the coastal water mass (extensive/narrow) are shown Figures A.14 and A.15.

Static, topographic predictors have also been shown before to be useful for describing the distribution of pelagic species. Water depth (Figure A.12) was included as a predictor. As the processes potentially enhancing the probability of prey encounter are expected to be associated with discontinuities of the seabed slope was included as a static variable (Figure A.12). The slope was calculated based on water depth using the standard slope tool in ArcGIS 10.1.

Dense ship traffic may cause displacement of seabirds from suitable habitats, hence in order to make reliable prediction of the distribution of seabirds it is important to include data on ship density in the distribution model. Patterns of ship traffic were deduced from historical AIS data provided by Anatec Ltd. for the two winter periods December-February 2011-2012 and 2013-2014 (Figure A.13). The data were split into two periods representing typical distributions of traffic during winter, as the traffic scheme in the region changed in 2013. The variation in shipping density has been estimated using a grid containing 5,584 cells with an average size of 1\*1 kilometre. Anatec's AIS shipping density model was then used to calculate the number of unique ship tracks passing through each cell based on the historical data.

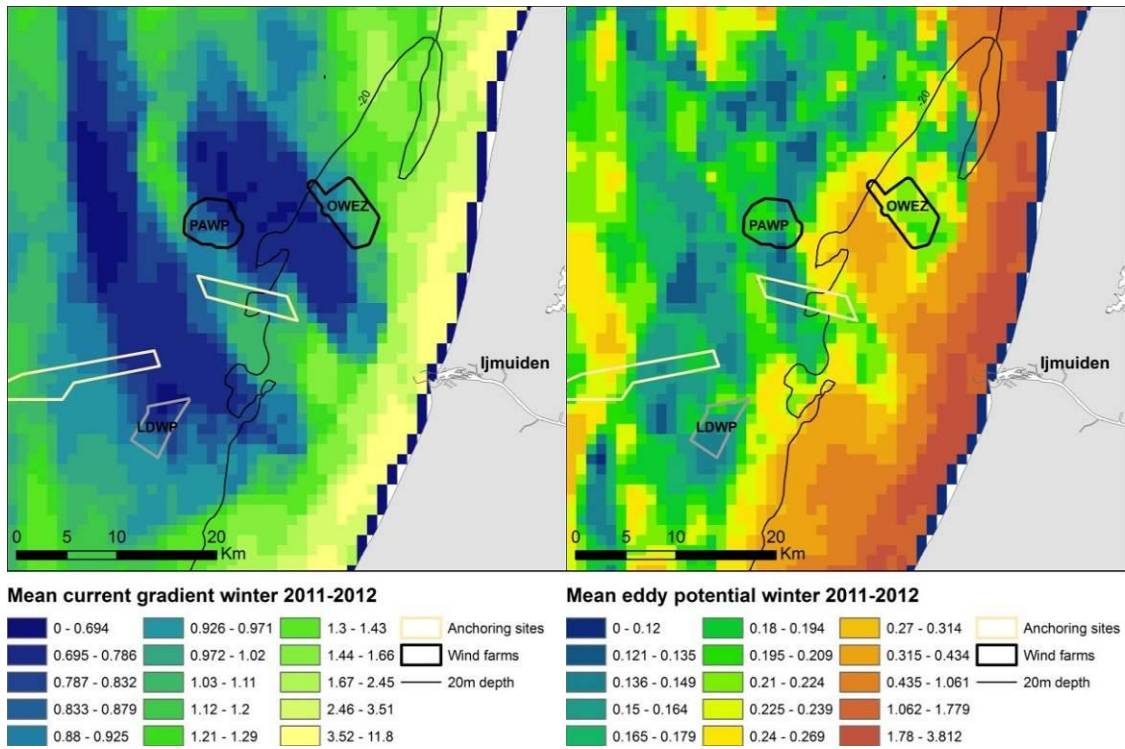


Figure A.10. Mean values of current gradient and eddy potential (m/s/m) for the winter season (2011-2012) used as predictor variables.

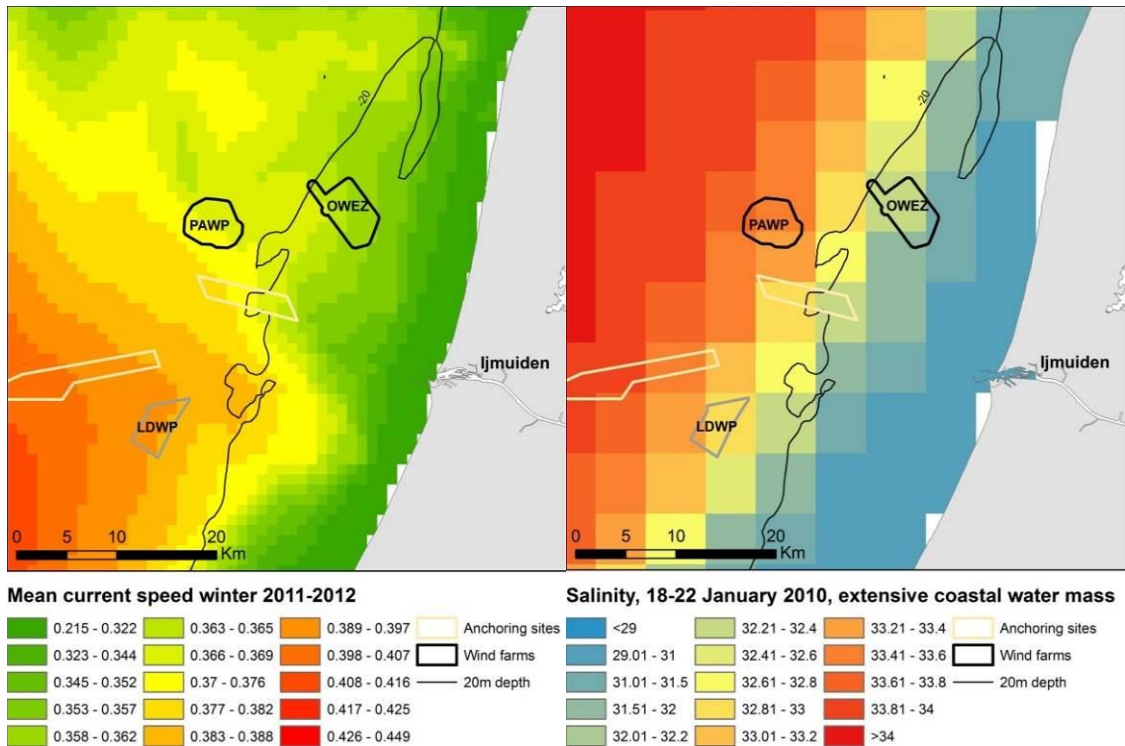


Figure A.11. Mean current speed (m/s) and surface salinity (psu) for the winter season (2011-2012) used as predictor variables.

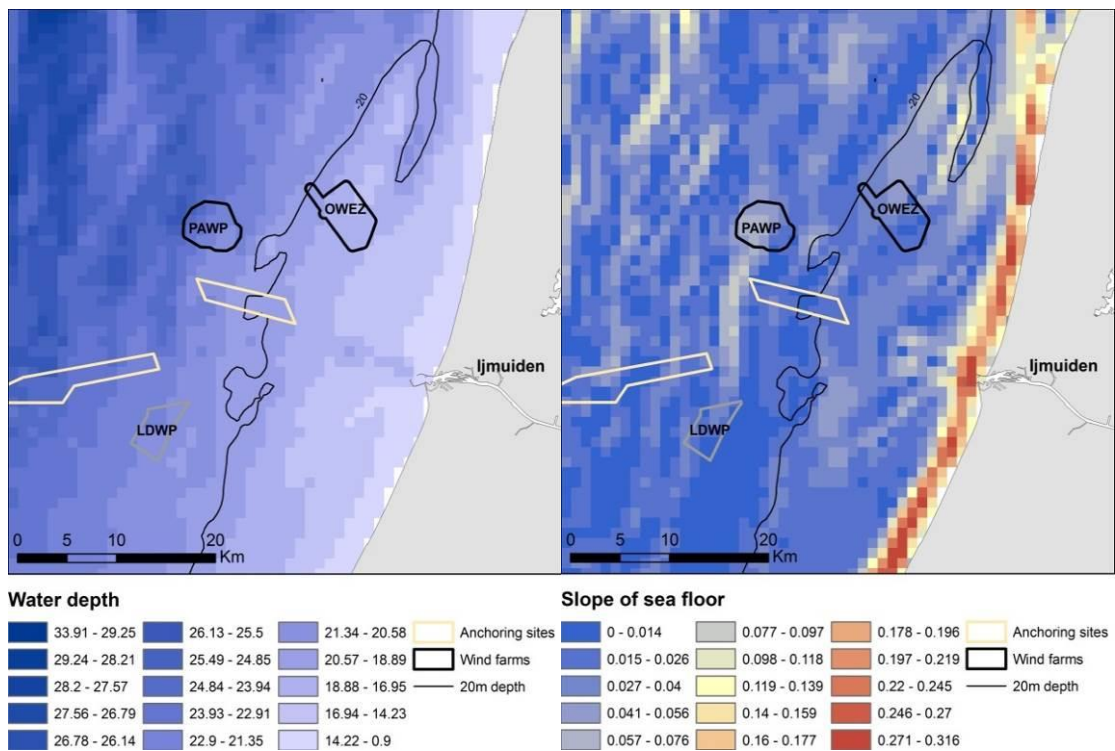


Figure A.12. Bathymetry (m) and slope (degrees) of sea floor used as predictor variables.

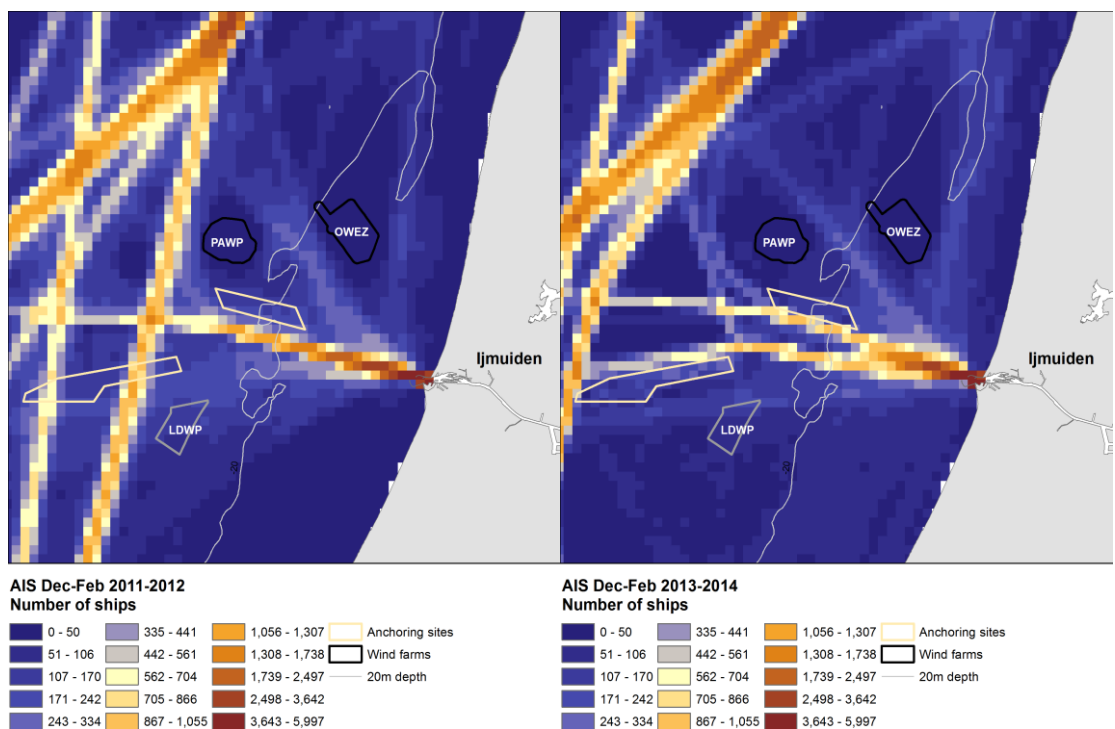


Figure A.13. Ship traffic winter 2011/2012 and 2013/2014. Total number of ships.

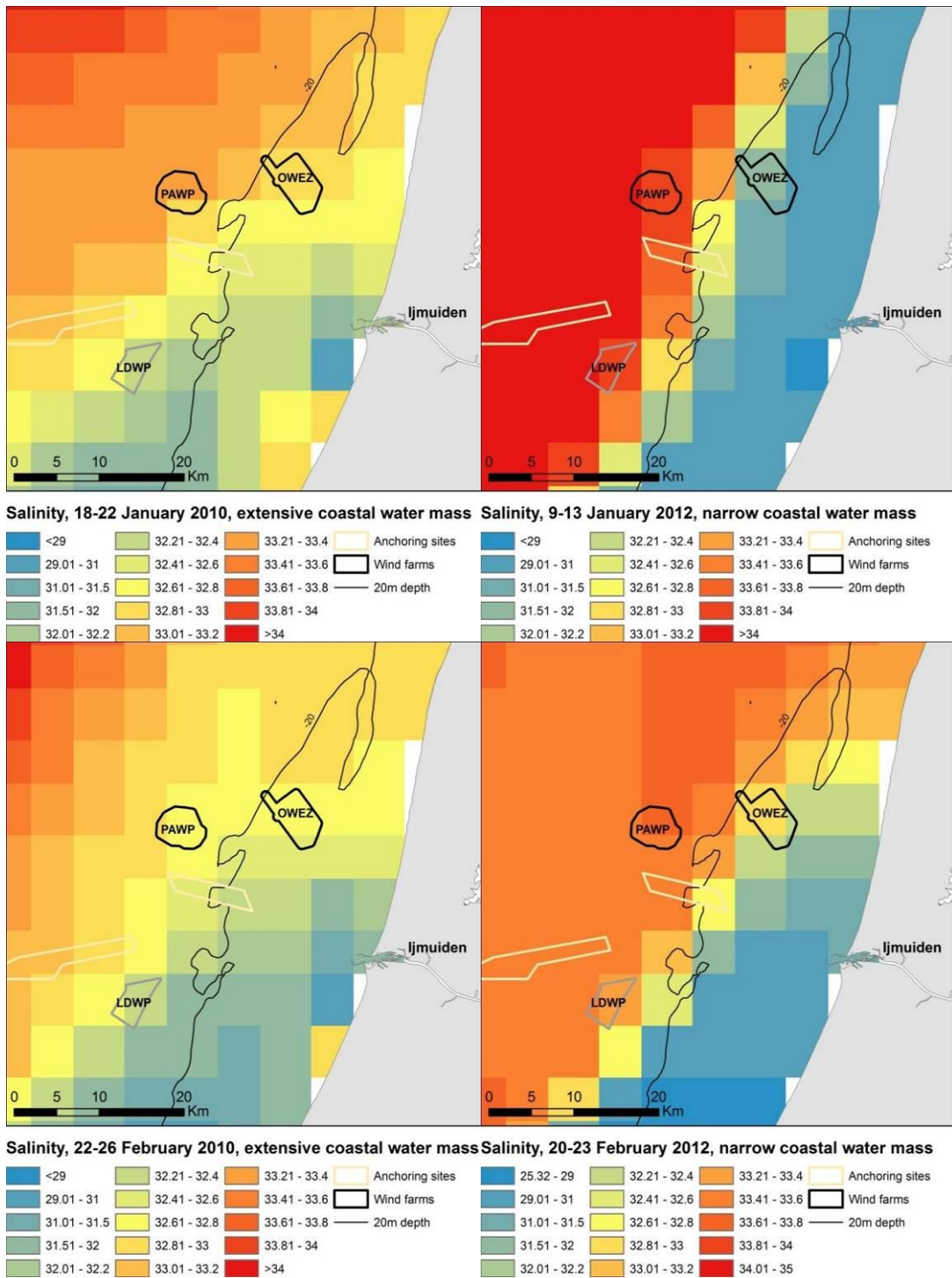


Figure A.14. Salinity (psu) for 4 different time periods, with “extensive” coastal water masses (to the left) and “narrow” coastal water masses (to the right)

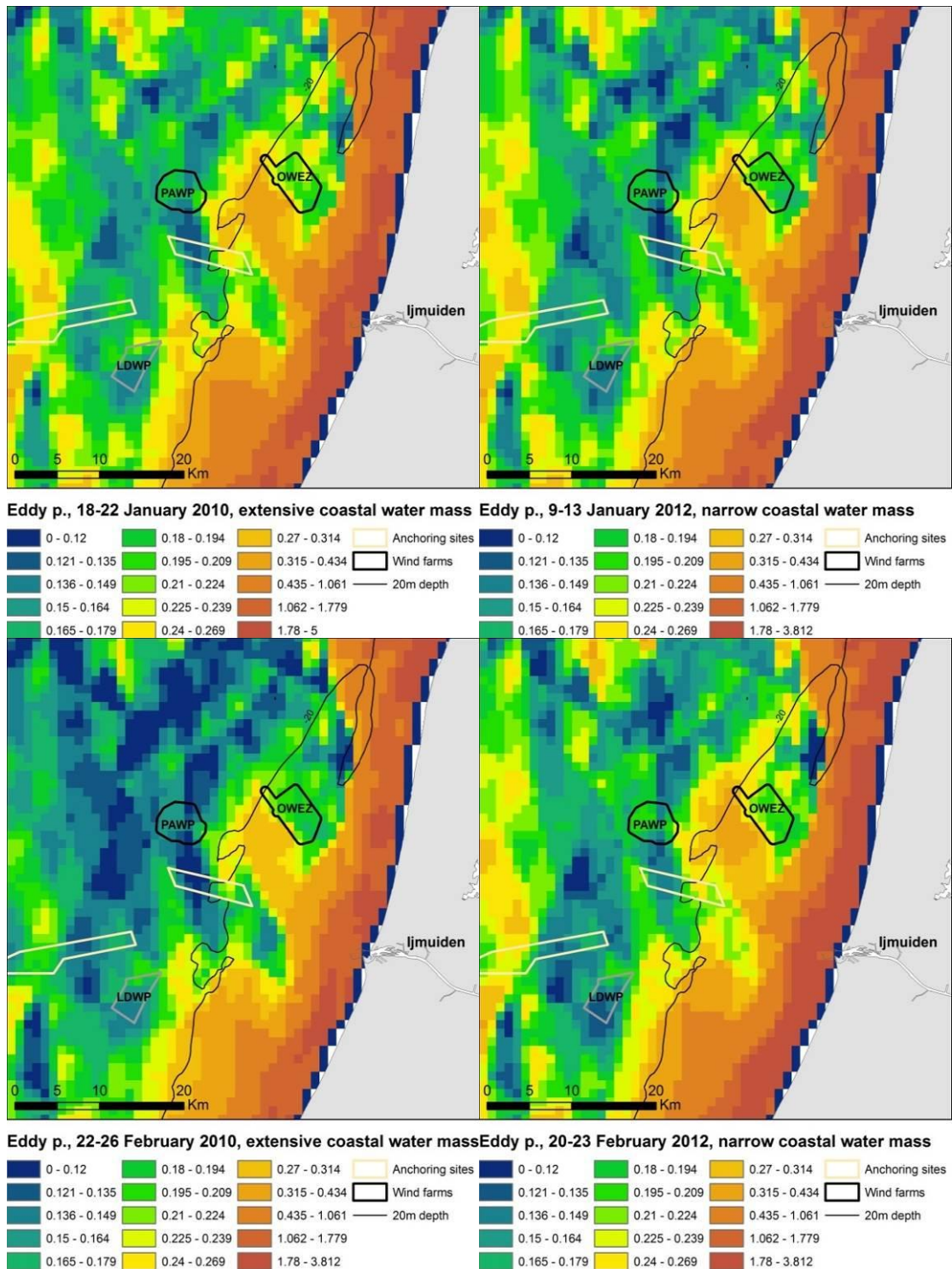


Figure A.15. Vorticity (m/s/m) for 4 different time periods, with “extensive” coastal water masses (to the left) and “narrow” coastal water masses (to the right)

## APPENDIX B – Supplementary results of species distribution models

In the following, supplementary results from the species distribution models to those described in chapter 4.3 are presented. For each species the following are provided:

1. Table showing the deviance explained and evaluation statistics for the presence/absence and the positive parts of the mean distribution models;
2. Map with proportion standard errors of predicted mean densities;
3. Predicted densities from the dynamic distribution models during different periods of contrasting extent of the coastal current are provided.

## Red-throated Diver/Black-throated Diver

Table B.1. Smooth terms, deviance explained and evaluation statistics for the diver distribution model. The z-values and significance for the parametric terms are shown and for the smooth terms the approximate significance and chi-square/F statistics. Variables not included in either the binomial or positive model part are indicated with a dash.

Smooth terms	Presence/absence		Positive density	
	chi-sqr	p	F	p
Current speed	-		-	
Eddy potential	17.688	<0.001	4.626	<0.01
Current gradient	-		-	
Surface salinity	-		4.261	<0.05
Water depth	52.407	<0.001	4.723	<0.05
Slope of seafloor	4.586	<0.05	-	
Distance to wind farm	18.043	<0.001	-	
Distance to anchoring site	-		-	
Density of ships	9.795	<0.01	-	
Parametric terms	<b>z</b>	<b>p</b>	<b>t</b>	<b>p</b>
Winter 2	2.04	<0.05	-0.264	
Winter 3	1.538		1.36	
Winter 4	0.562		0.691	
Winter 5	0.626		-0.608	
Winter 6	1.148		-0.287	
Winter 7	0.035		-1.697	
Month2	-2.337	<0.05	-4.672	<0.001
Month10	-6.081	<0.001	-3.888	<0.001
Month11	-7.821	<0.001	-6.804	<0.001
Sample size (n)	9071		395	
Dev. Exp.	19.60%		34.30%	
AUC	0.82			
Spearman's corr.	0.21			

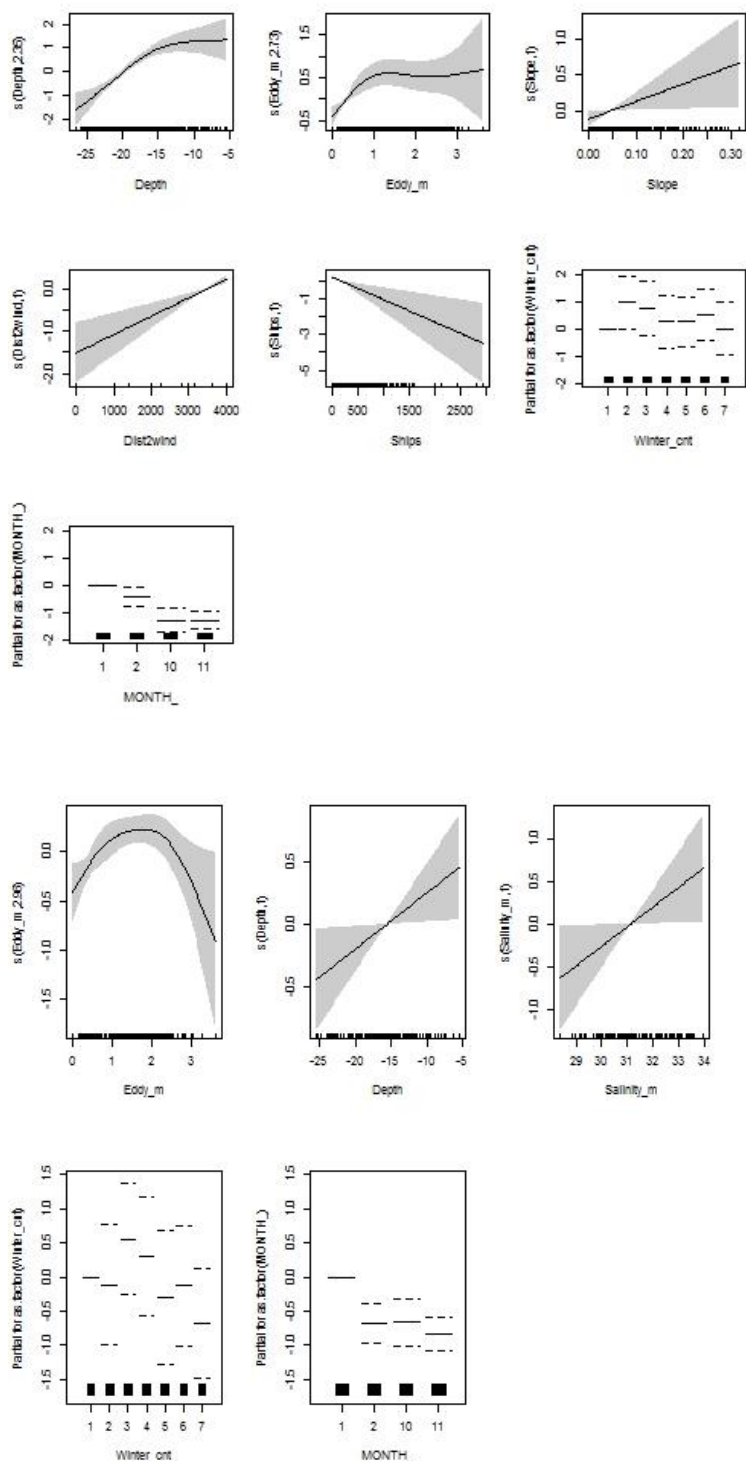


Figure B.1. Partial GAM plots for the diver distribution model – presence-absence (upper panel) and positive (lower panel) parts. The values of the environmental variables are shown on the X-axis and the probability on the Y-axis in the scale of the linear predictor. The grey shaded areas and the dotted lines (for factors) show the 95% Bayesian confidence intervals. The degree of smoothing is indicated in the legend of the Y-axis.

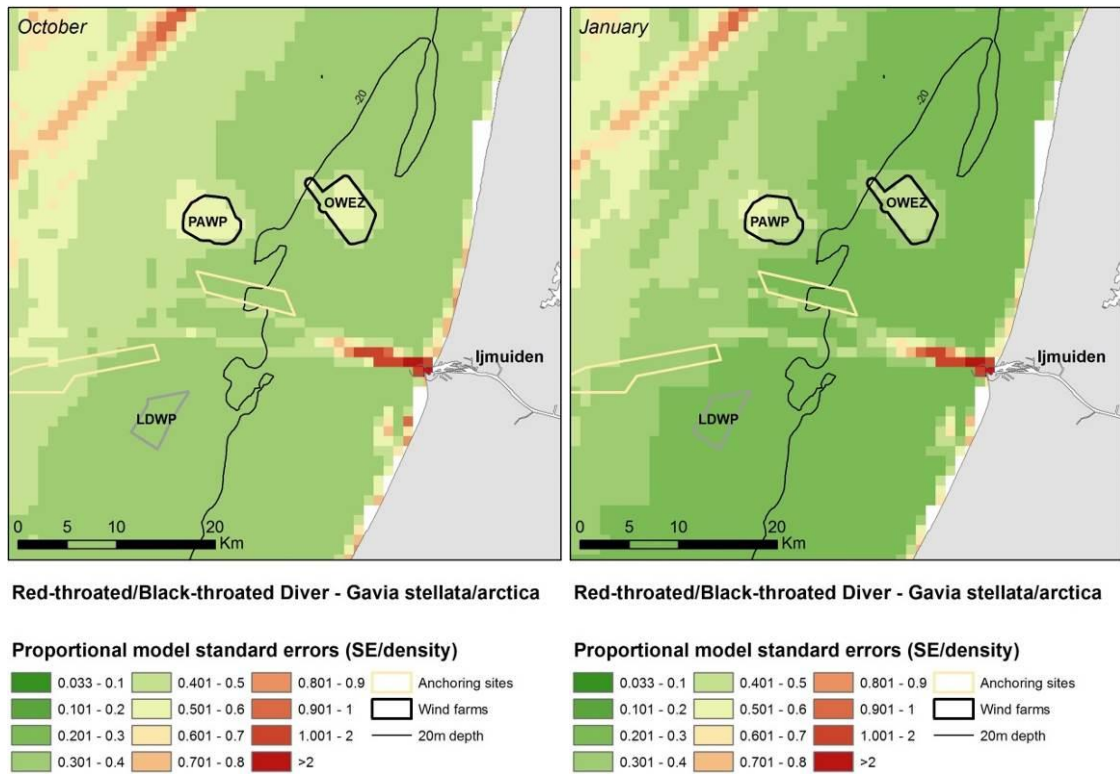


Figure B.2. Model uncertainty. Proportional model standard errors for the distribution (probability) model of wintering divers during the baseline surveys 2013-2014.

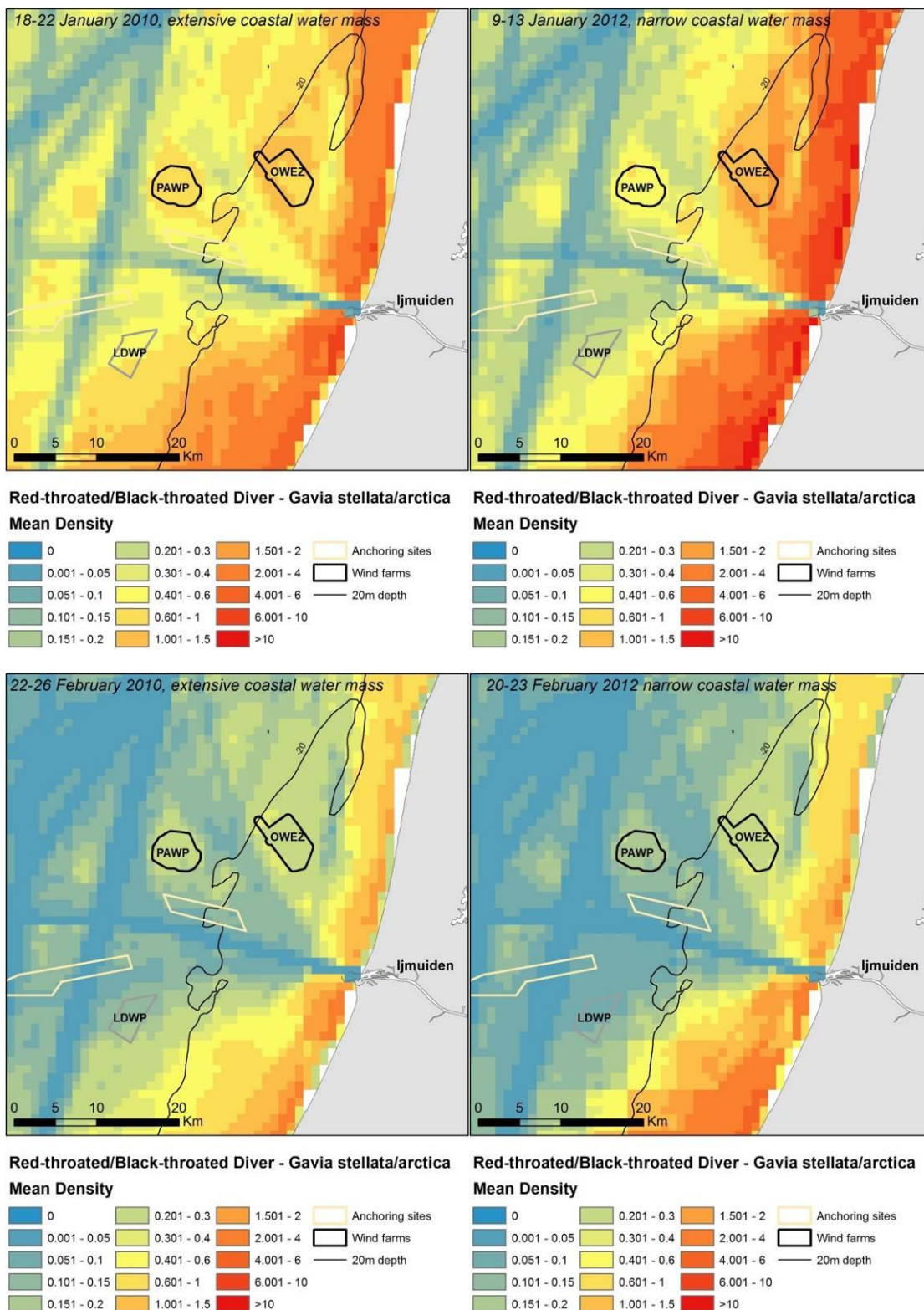


Figure B.3 Predicted variation in diver distribution during periods of limited and extensive coverage of the coastal water mass.

## Great Crested Grebe

Table B.2. Smooth terms, deviance explained and evaluation statistics for the Great Crested Grebe distribution model. The z-values and significance for the parametric terms are shown and for the smooth terms the approximate significance and chi-square/F statistics. Variables not included in either the binomial or positive model part are indicated with a dash. Due to low sample sizes in some months it was not possible to conduct the 10-fold cross-validation, a split sample (70/30 %) validation was carried out.

Smooth terms	Presence/absence		Positive density	
	chi-sqr	p	F	p
Current speed	-		-	
Eddy potential	13.899	<0.01	-	
Current gradient	-		-	
Surface salinity	-		10.955	<0.001
Water depth	99.153	<0.001	16.671	<0.001
Slope of seafloor	-		-	
Distance to wind farm	-		-	
Distance to anchoring site	-		-	
Density of ships	-		-	
Parametric terms	<b>z</b>	<b>p</b>	<b>t</b>	<b>p</b>
Winter 2	-		-	
Winter 3	-		-	
Winter 4	-		-	
Winter 5	-		-	
Winter 6	-		-	
Winter 7	-		-	
Month2	-		-	
Month10	-		-	
Month11	-		-	
Sample size (n)	9071		176	
Dev. Exp.	21.90%		15.90%	
AUC	0.87			
Spearman's corr.	0.18			

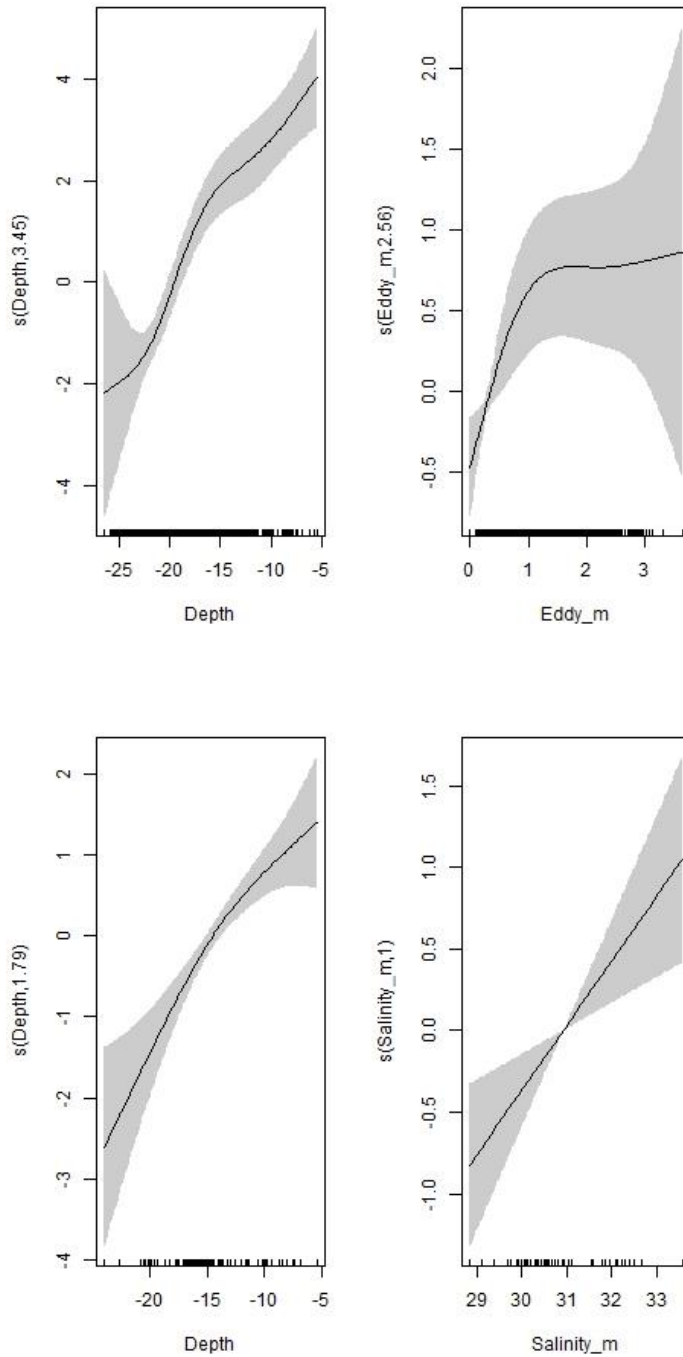


Figure B.4. Partial GAM plots for the Great Crested Grebe distribution model – presence-absence (upper panel) and positive (lower panel) parts. The values of the environmental variables are shown on the X-axis and the probability on the Y-axis in the scale of the linear predictor. The grey shaded areas and the dotted lines (for factors) show the 95% Bayesian confidence intervals. The degree of smoothing is indicated in the legend of the Y-axis.

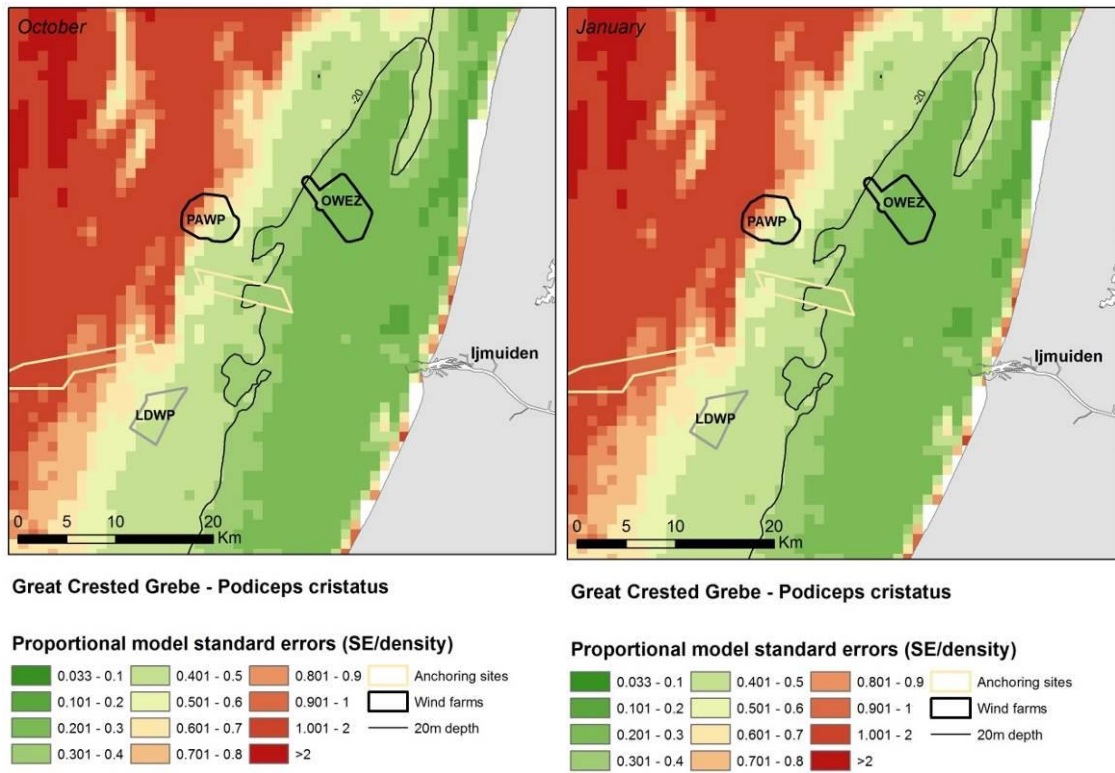


Figure B.5. Model uncertainty. Proportional model standard errors for the distribution (probability) model of wintering Great Crested Grebe during the baseline surveys 2013-2014.

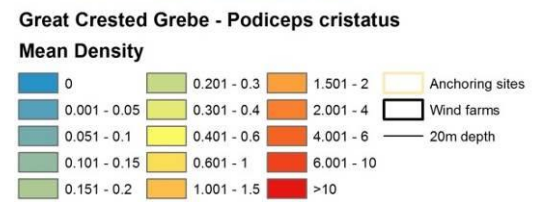
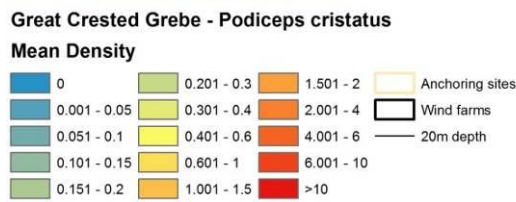
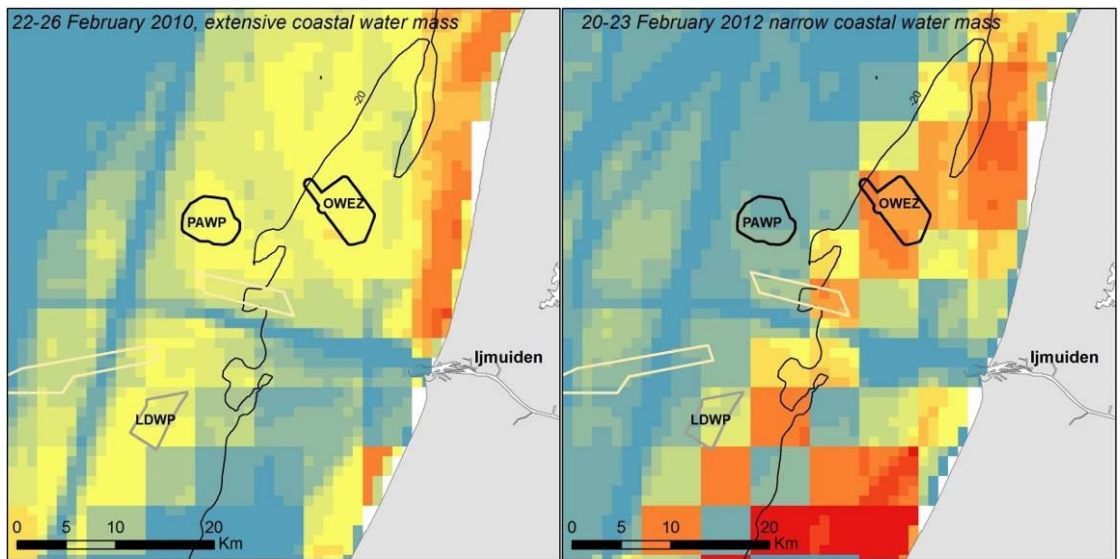
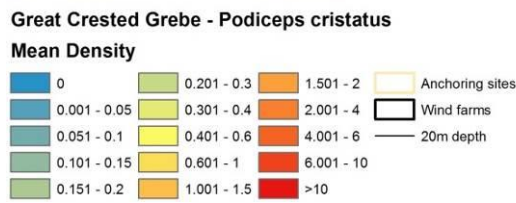
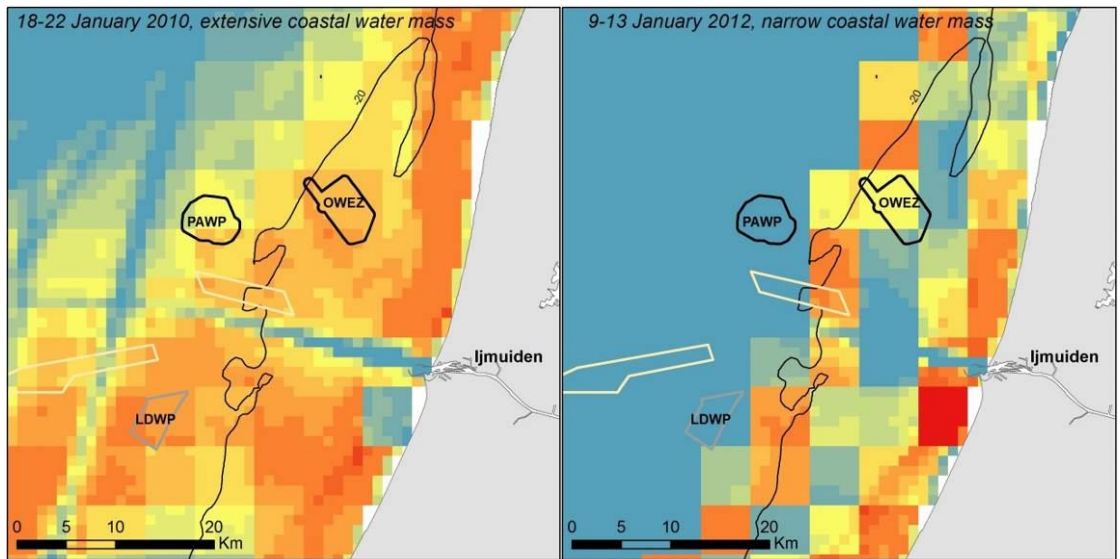


Figure B.6. Predicted variation in Great Crested Grebe distribution during periods of limited and extensive coverage of the coastal water mass.

## Northern Gannet

Table B.3. Smooth terms, deviance explained and evaluation statistics for the Northern Gannet distribution model. The z-values and significance for the parametric terms are shown and for the smooth terms the approximate significance and chi-square/F statistics. Variables not included in either the binomial or positive model part are indicated with a dash.

Smooth terms	Presence/absence		Positive density	
	chi-sqr	p	F	p
Current speed	-		-	
Eddy potential	4.69	<0.05	-	
Current gradient	-		-	
Surface salinity	87.549	<0.001	-	
Water depth	-		-	
Depth:Salinity	-		5.699	<0.001
Slope of seafloor	-		-	
Distance to wind farm	43.194	<0.001	-	
Distance to anchoring site	-		-	
Density of ships	-		-	
<b>Parametric terms</b>	<b>z</b>	<b>p</b>	<b>t</b>	<b>p</b>
Winter 2	-1.285		-3.311	<0.001
Winter 3	3.206	<0.001	2.731	<0.01
Winter 4	4.004	<0.001	-1.397	
Winter 5	-0.251		-3.366	<0.001
Winter 6	0.056		-2.938	<0.01
Winter 7	-1.298		-3.254	<0.001
Month2	2.374	<0.05	-6.189	<0.001
Month10	5.489	<0.001	-7.726	<0.001
Month11	7.321	<0.001	-10.088	<0.001
Sample size (n)	9071		806	
Dev. Exp.	10.00%		37.80%	
AUC	0.74			
Spearman's corr.	0.21			

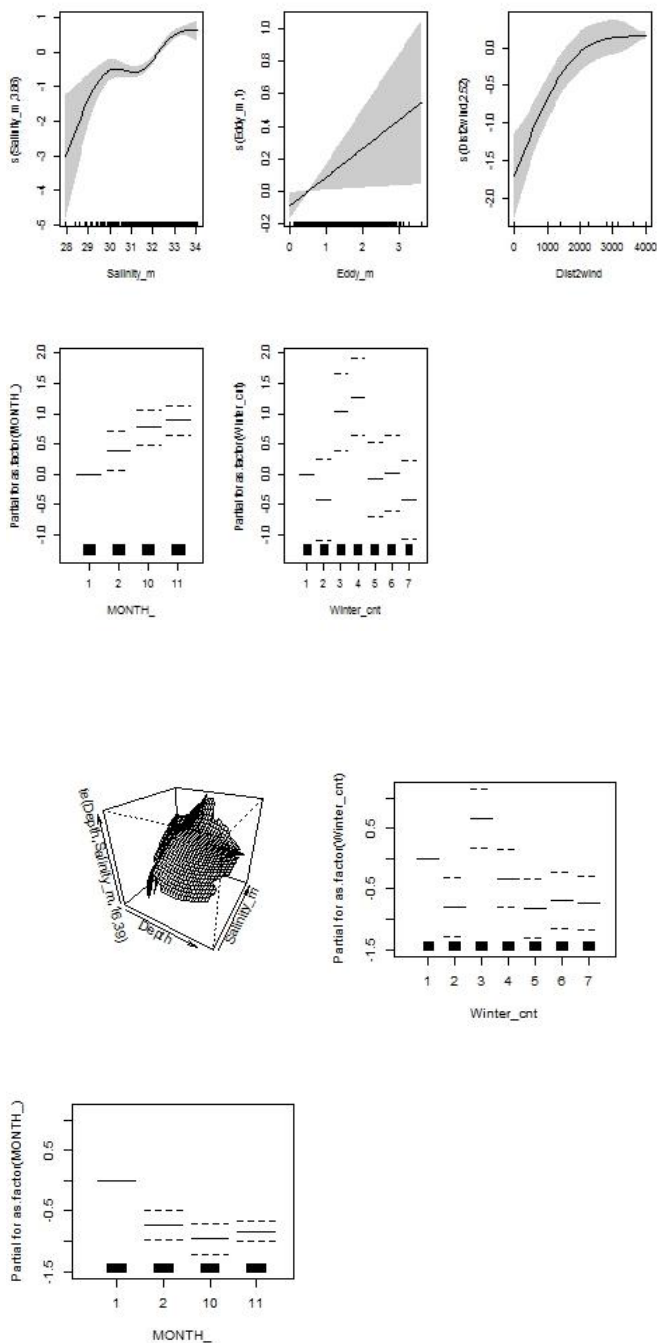


Figure B.7. Partial GAM plots for the Northern Gannet distribution model – presence-absence (upper panel) and positive (lower panel) parts. The values of the environmental variables are shown on the X-axis and the probability on the Y-axis in the scale of the linear predictor. The grey shaded areas and the dotted lines (for factors) show the 95% Bayesian confidence intervals. The degree of smoothing is indicated in the legend of the Y-axis.

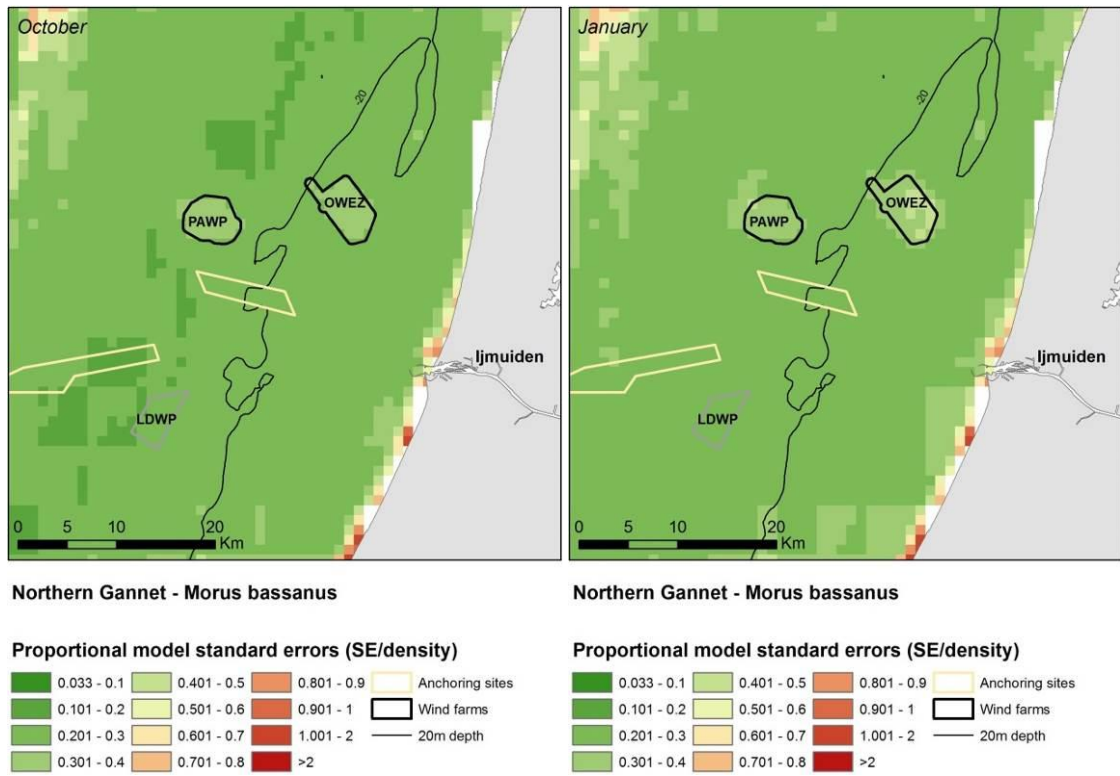


Figure B.8. Model uncertainty. Proportional model standard errors for the distribution (probability) model of wintering Northern Gannet during the baseline surveys 2013-2014.

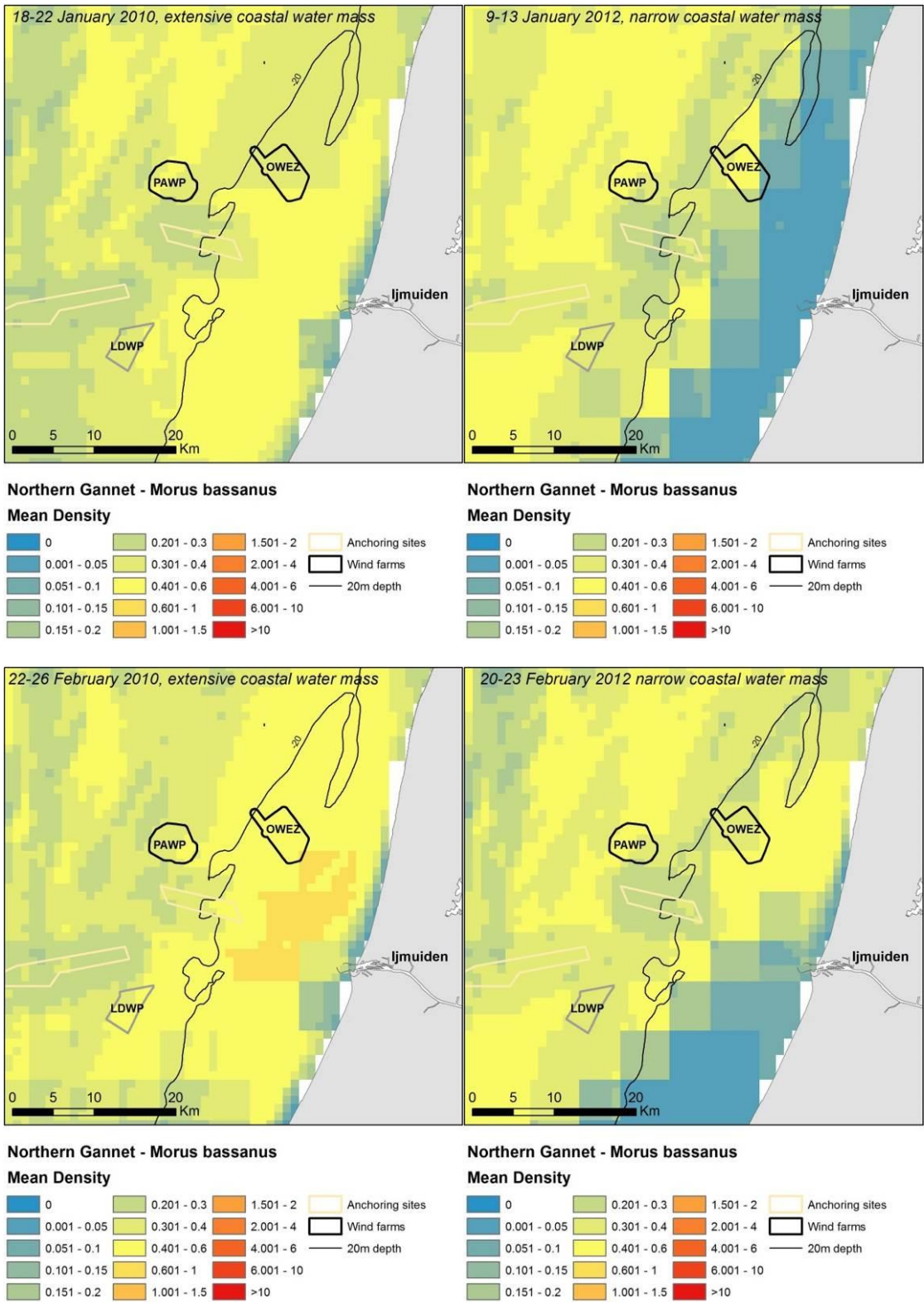


Figure B.9 Predicted variation in Northern Gannet distribution during periods of limited and extensive coverage of the coastal water mass.

## Great Cormorant

Table B.4. Smooth terms, deviance explained and evaluation statistics for the Great Cormorant distribution model. The z-values and significance for the parametric terms are shown and for the smooth terms the approximate significance and chi-square/F statistics. Variables not included in either the binomial or positive model part are indicated with a dash.

Smooth terms	Presence/absence		Positive density	
	chi-sqr	p	F	p
Current speed	-		-	
Eddy potential	28.678	<0.001	3.789	<0.01
Current gradient	-		-	
Surface salinity	-		-	
Water depth	50.044	<0.001	4.993	<0.001
Slope of seafloor	-		-	
Distance to wind farm	285.021	<0.001	25.028	<0.001
Distance to anchoring site	-		-	
Density of ships	-		-	
<b>Parametric terms</b>	<b>z</b>	<b>p</b>	<b>t</b>	<b>p</b>
Winter 2	-0.493		1.353	
Winter 3	-2.17	<0.05	0.229	
Winter 4	-1.497		3.928	<0.001
Winter 5	1.142		2.247	<0.05
Winter 6	-1.179		2.182	<0.05
Winter 7	-1.924		-0.308	
Month2	-1.669		2.297	<0.05
Month10	3.402	<0.001	4.868	<0.001
Month11	1.464		3.761	<0.001
Sample size (n)	9071		375	
Dev. Exp.	17.20%		28.30%	
AUC	0.82			
Spearman's corr.	0.21			

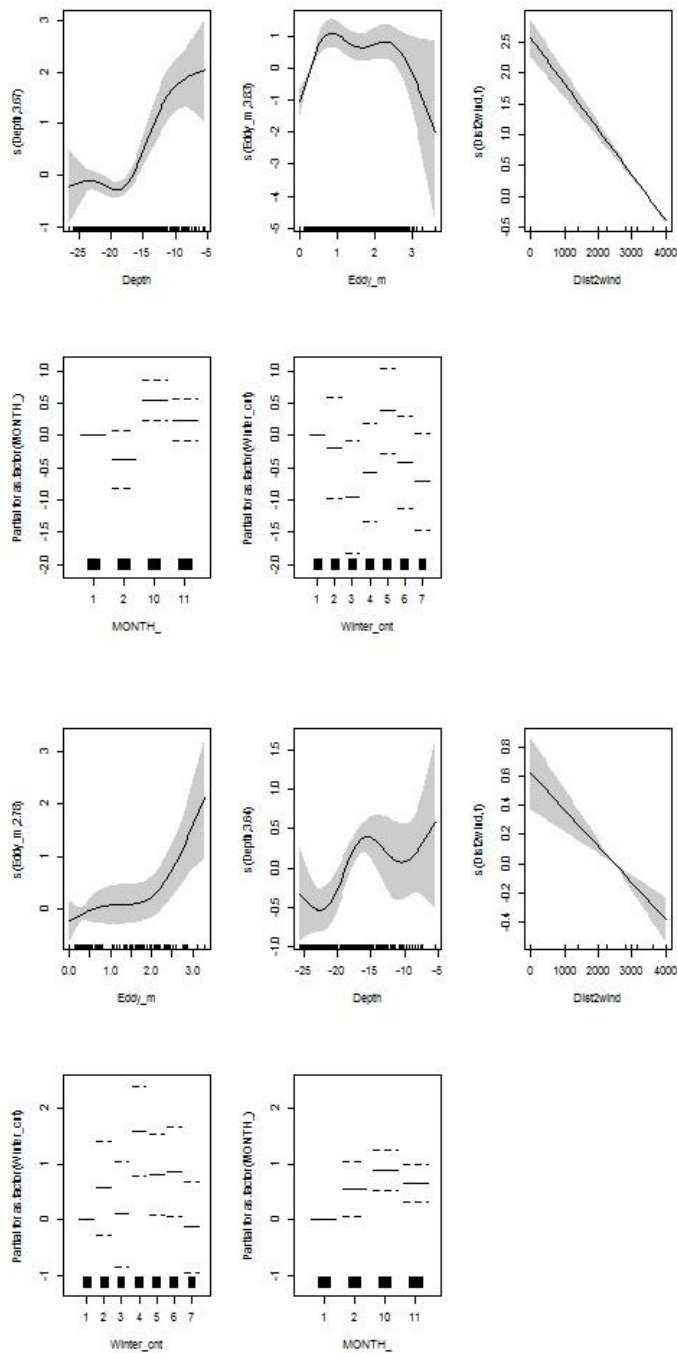


Figure B.10. Partial GAM plots for the Great Cormorant distribution model – presence-absence (upper panel) and positive (lower panel) parts. The values of the environmental variables are shown on the X-axis and the probability on the Y-axis in the scale of the linear predictor. The grey shaded areas and the dotted lines show the 95% Bayesian confidence intervals. The degree of smoothing is indicated in the legend of the Y-axis and for the interaction terms (Easting, Northing) in the heading.

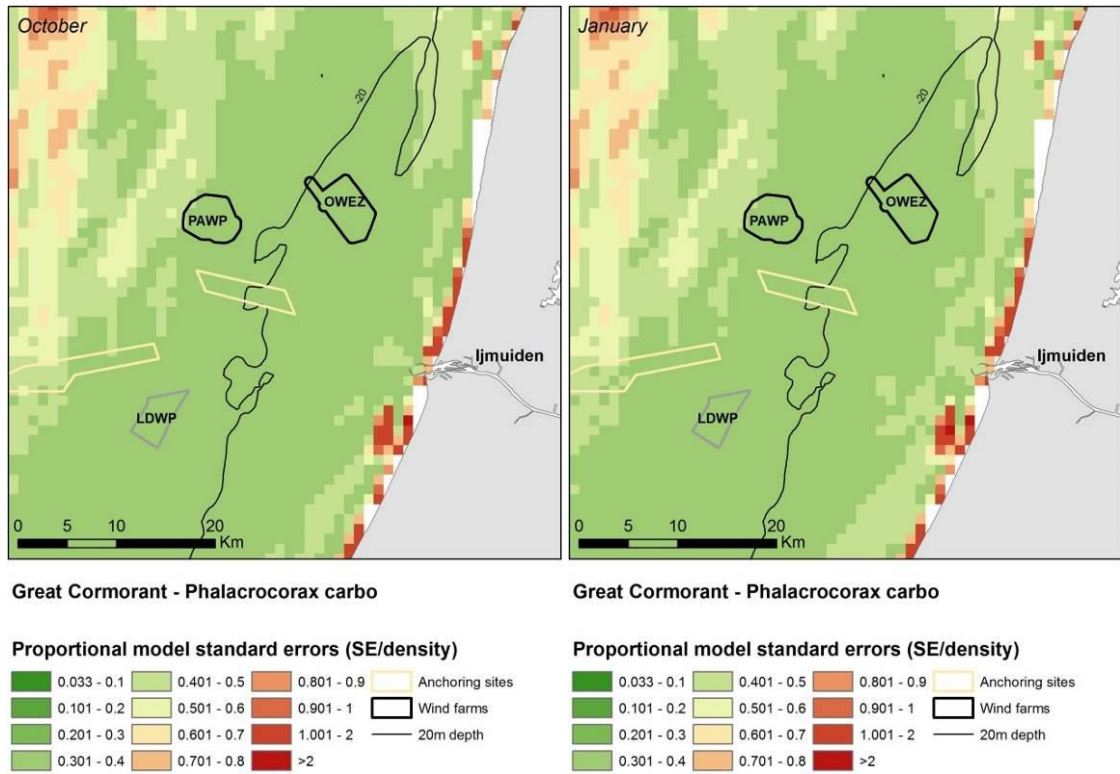


Figure B.11. Model uncertainty. Proportional model standard errors for the distribution (probability) model of wintering Great Cormorant during the baseline surveys 2013-2014.

## Common Scoter

Table B.5. Smooth terms, deviance explained and evaluation statistics for the Common Scoter distribution model. The z-values and significance for the parametric terms are shown and for the smooth terms the approximate significance and chi-square/F statistics. Variables not included in either the binomial or positive model part are indicated with a dash.

Smooth terms	Presence/absence		Positive density	
	chi-sqr	p	F	p
Current speed	-		-	
Eddy potential	-		-	
Current gradient	-		-	
Surface salinity	-		-	
Water depth	28.462	<0.001	-	
Slope of seafloor	19.296	<0.001	8.708	<0.01
Distance to wind farm	-		-	
Distance to anchoring site	-		-	
Density of ships	-		-	
<b>Parametric terms</b>	<b>z</b>	<b>p</b>	<b>t</b>	<b>p</b>
Winter 2	0.824		-1.236	
Winter 3	-0.915		-0.959	
Winter 4	0.033		-2.449	<0.05
Winter 5	-0.55		-0.465	
Winter 6	-1.488		-2.422	<0.05
Winter 7	-0.942		-2.439	<0.05
Month2	3.147	<0.01	0.689	
Month10	-1.421		-0.435	
Month11	-0.82		0.089	
Sample size (n)	9071		210	
Dev. Exp.	11.30%		19.00%	
AUC	0.76			
Spearman's corr.	0.12			

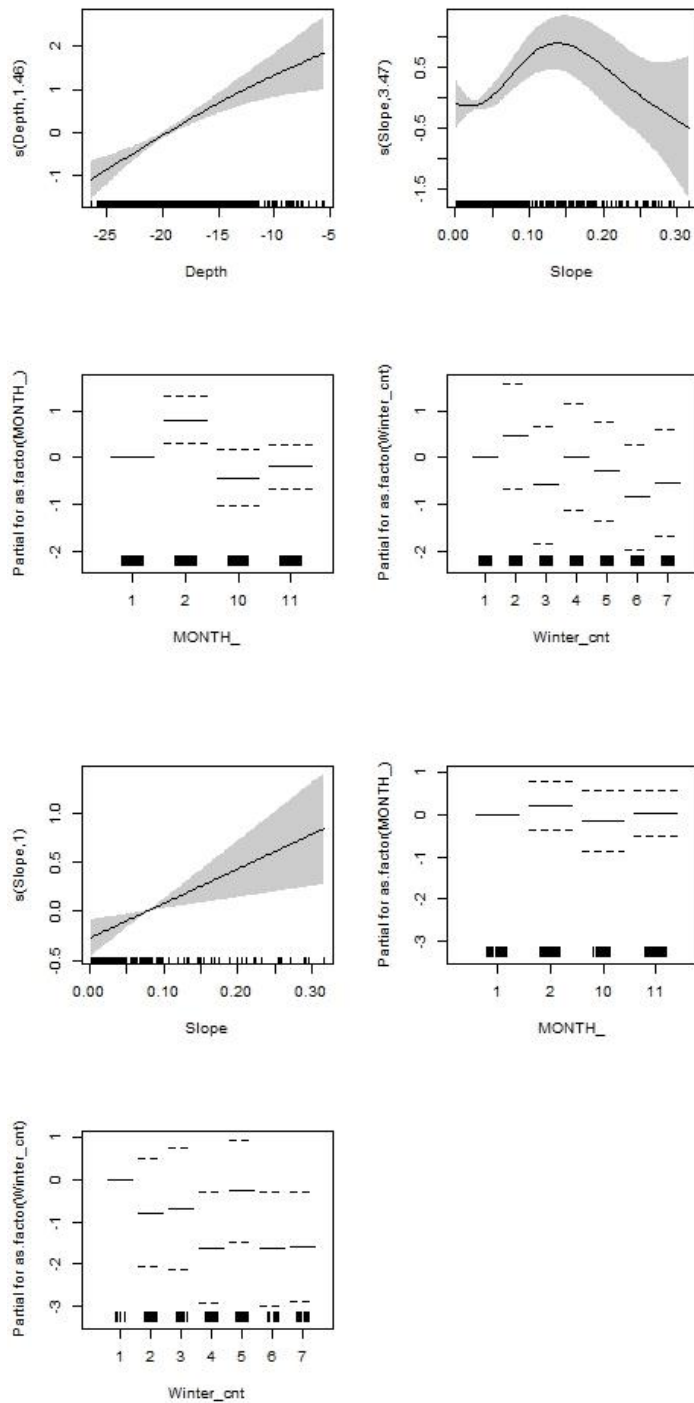


Figure B.12. Partial GAM plots for the Common Scoter distribution model – presence-absence (upper panel) and positive (lower panel) parts. The values of the environmental variables are shown on the X-axis and the probability on the Y-axis in the scale of the linear predictor. The grey shaded areas and the dotted lines (for factors) show the 95% Bayesian confidence intervals. The degree of smoothing is indicated in the legend of the Y-axis.

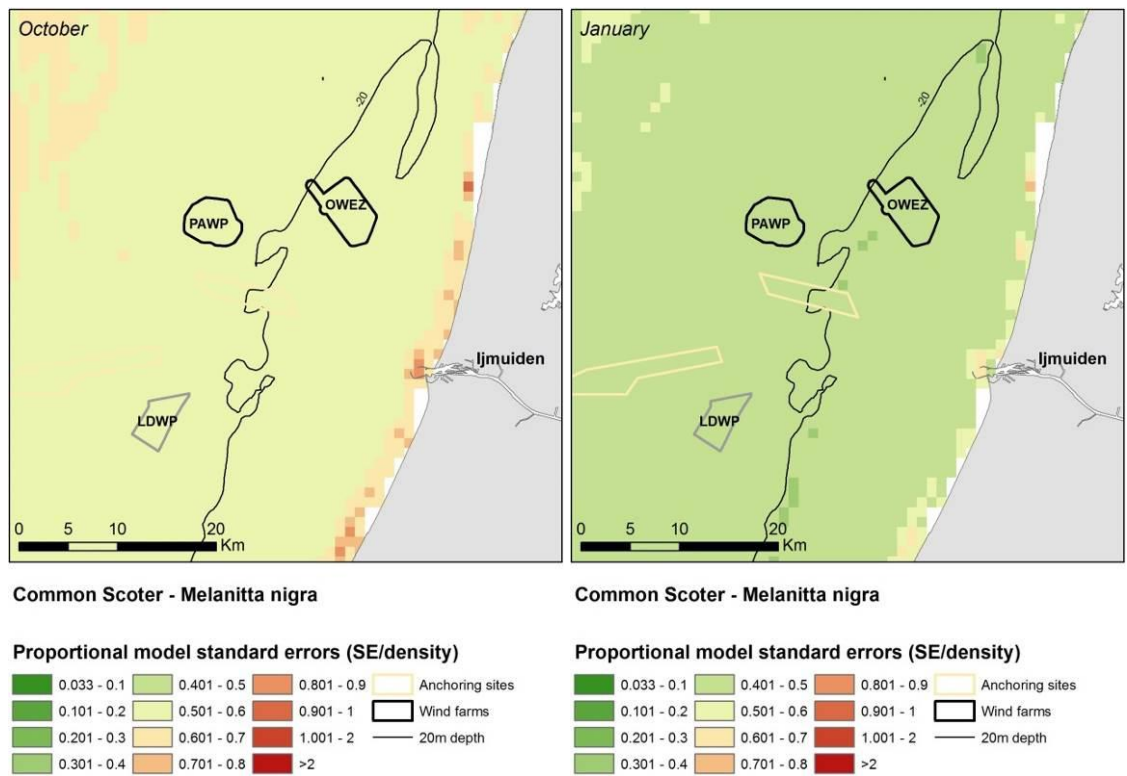


Figure B.13. Model uncertainty. Proportional model standard errors for the distribution (probability) model of wintering Common Scoter during the baseline surveys 2013-2014.

## Black-headed Gull

Table B.6. Smooth terms, deviance explained and evaluation statistics for the Black-headed Gull distribution model. The z-values and significance for the parametric terms are shown and for the smooth terms the approximate significance and chi-square/F statistics. Variables not included in either the binomial or positive model part are indicated with a dash.

Smooth terms	Presence/absence		Positive density	
	chi-sqr	p	F	p
Current speed	-		-	
Eddy potential	10.048	<0.05	6.063	<0.001
Current gradient	-		-	
Surface salinity	18.557	<0.001	-	
Water depth	18.976	<0.001	18.413	<0.001
Slope of seafloor	-		-	
Distance to wind farm	-		4.515	<0.05
Distance to anchoring site	-		-	
Density of ships	-		-	
<b>Parametric terms</b>	<b>z</b>	<b>p</b>	<b>t</b>	<b>p</b>
Winter 2	2.649	<0.01	-2.304	<0.05
Winter 3	-0.629		-4.735	<0.001
Winter 4	-0.841		-4.325	<0.001
Winter 5	-0.163		-3.459	<0.001
Winter 6	-1.572		-3.045	<0.01
Winter 7	-0.651		-2.47	<0.05
Month2	-4.507	<0.001	-3.471	<0.001
Month10	2.069	<0.05	-4.032	<0.001
Month11	-0.276		-1.86	
Sample size (n)	9071		254	
Dev. Exp.	18.40%		40.10%	
AUC	0.81			
Spearman's corr.	0.17			

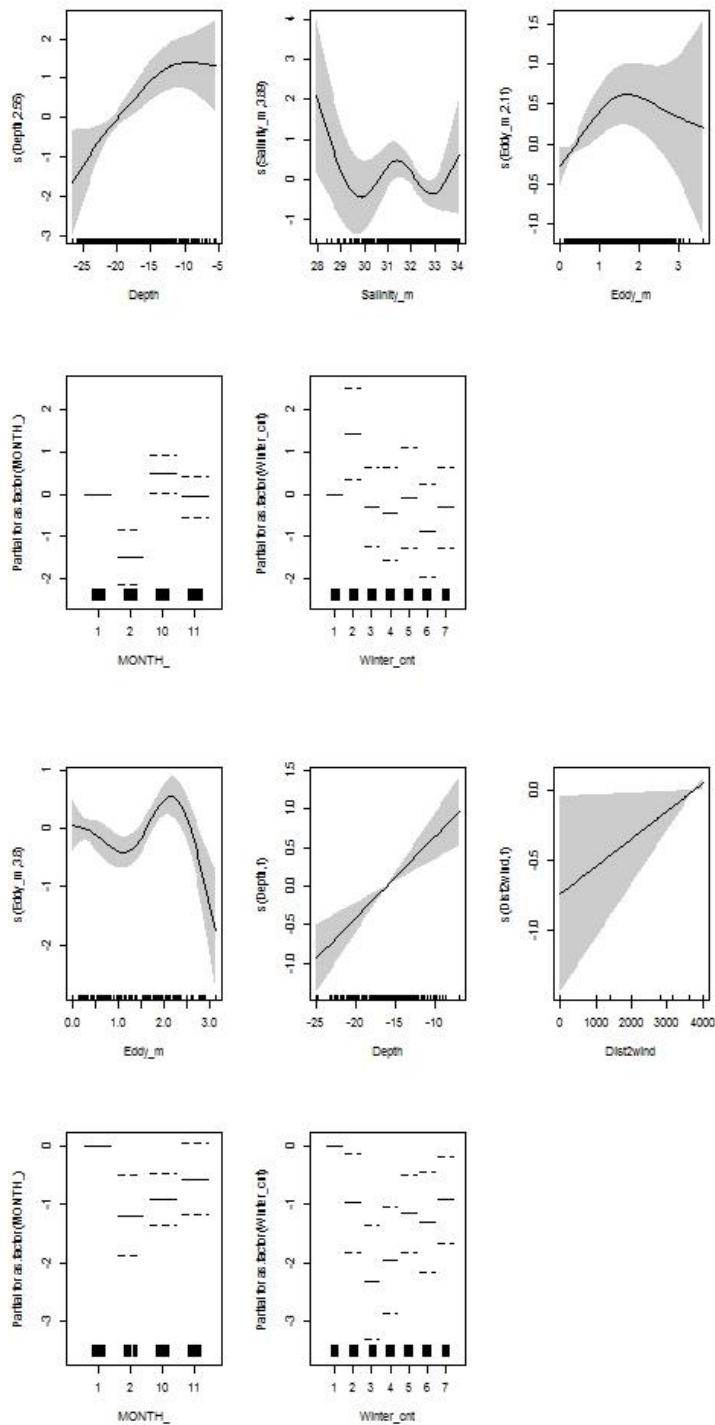


Figure B.14. Partial GAM plots for the Black-headed Gull distribution model – presence-absence (upper panel) and positive (lower panel) parts. The values of the environmental variables are shown on the X-axis and the probability on the Y-axis in the scale of the linear predictor. The grey shaded areas and the dotted lines (for factors) show the 95% Bayesian confidence intervals. The degree of smoothing is indicated in the legend of the Y-axis.

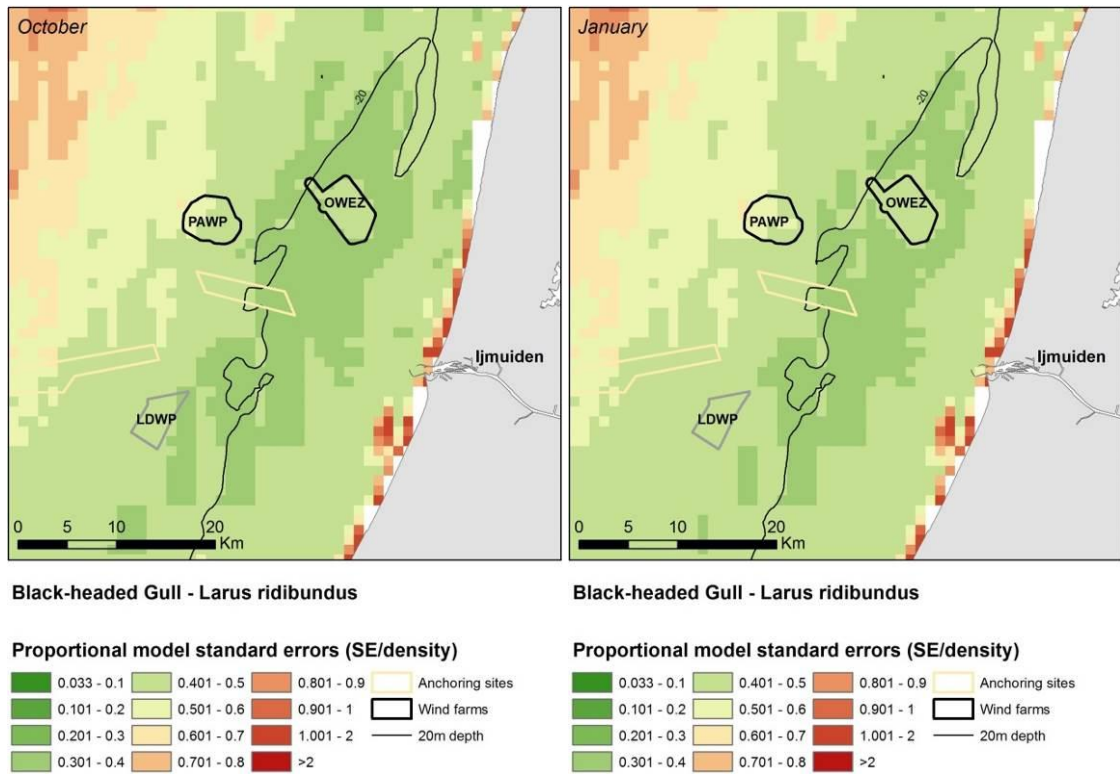


Figure B.15. Model uncertainty. Proportional model standard errors for the distribution (probability) model of wintering Black-headed Gull during the baseline surveys 2013-2014.

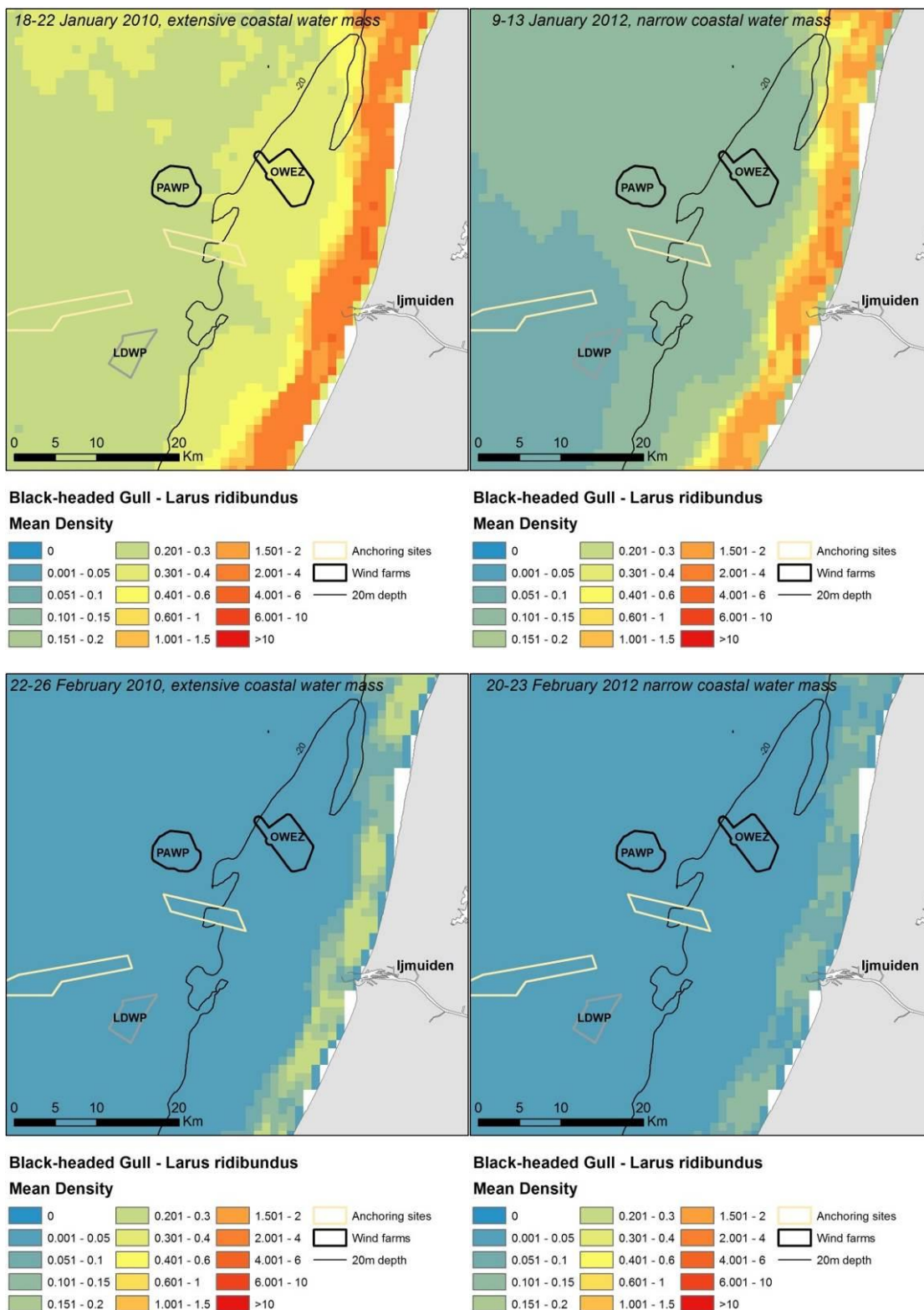


Figure B.16. Predicted variation in Black-headed Gull distribution during periods of limited and extensive coverage of the coastal water mass.

## Common Gull

Table B.7. Smooth terms, deviance explained and evaluation statistics for the Common Gull distribution model. The z-values and significance for the parametric terms are shown and for the smooth terms the approximate significance and chi-square/F statistics. Variables not included in either the binomial or positive model part are indicated with a dash.

Smooth terms	Presence/absence		Positive density	
	chi-sqr	p	F	p
Current speed	-		-	
Eddy potential	23.509	<0.001	16.667	<0.001
Current gradient	-		-	
Surface salinity	39.139	<0.001	11.501	<0.001
Water depth	8.652	<0.05	-	
Slope of seafloor	-		21.223	<0.001
Distance to wind farm	-		-	
Distance to anchoring site	-		-	
Density of ships	-		-	
<b>Parametric terms</b>	<b>z</b>	<b>p</b>	<b>t</b>	<b>p</b>
Winter 2	6.138	<0.001	1.978	<0.05
Winter 3	1.707		-2.663	<0.01
Winter 4	5.432	<0.001	-0.826	
Winter 5	3.931	<0.001	-0.341	
Winter 6	2.958	<0.01	-0.293	
Winter 7	-1.029		-2.523	<0.05
Month2	-7.195	<0.001	-12.081	<0.001
Month10	-9.394	<0.001	-5.274	<0.001
Month11	-7.927	<0.001	-5.903	<0.001
Sample size (n)	9071		1595	
Dev. Exp.	12.30%		41.60%	
AUC	0.74			
Spearman's corr.	0.32			

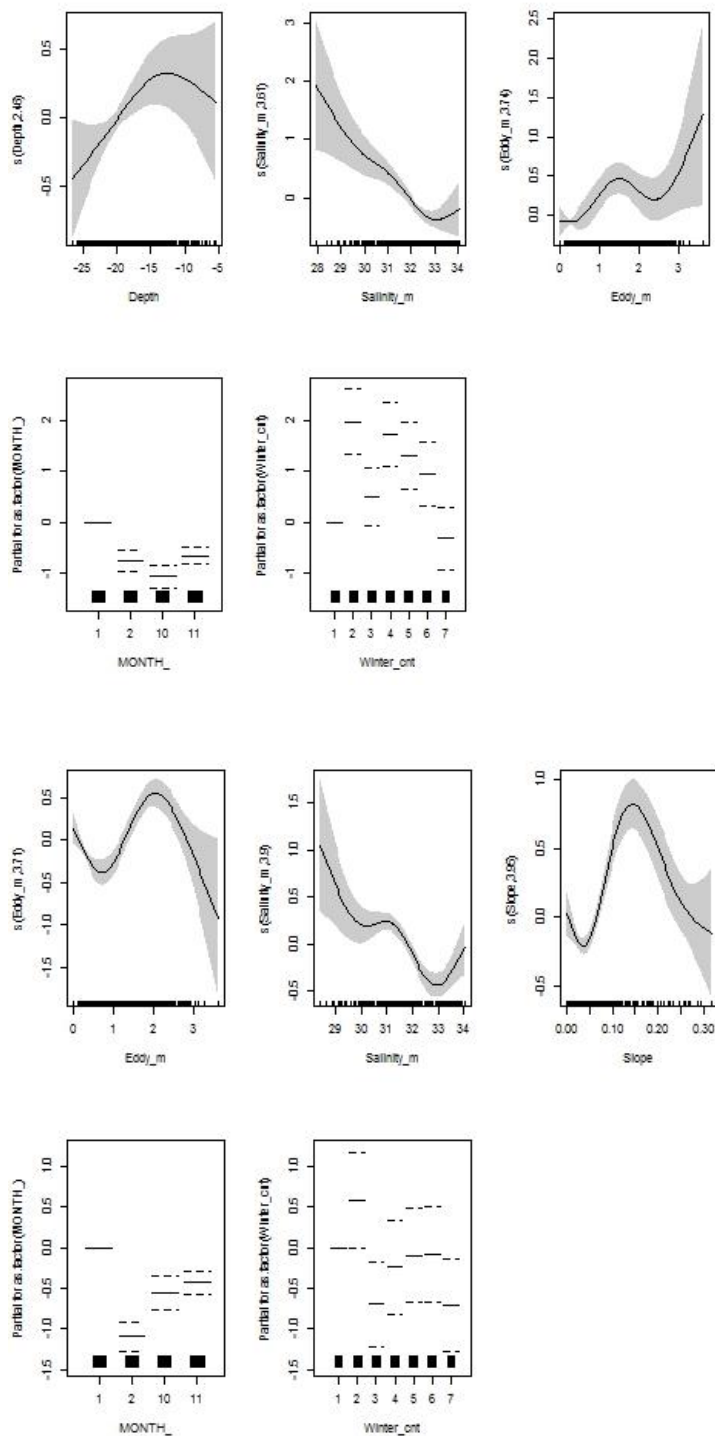


Figure B.17. Partial GAM plots for the Common Gull distribution model – presence-absence (upper panel) and positive (lower panel) parts. The values of the environmental variables are shown on the X-axis and the probability on the Y-axis in the scale of the linear predictor. The grey shaded areas and the dotted lines (for factors) show the 95% Bayesian confidence intervals. The degree of smoothing is indicated in the legend of the Y-axis.

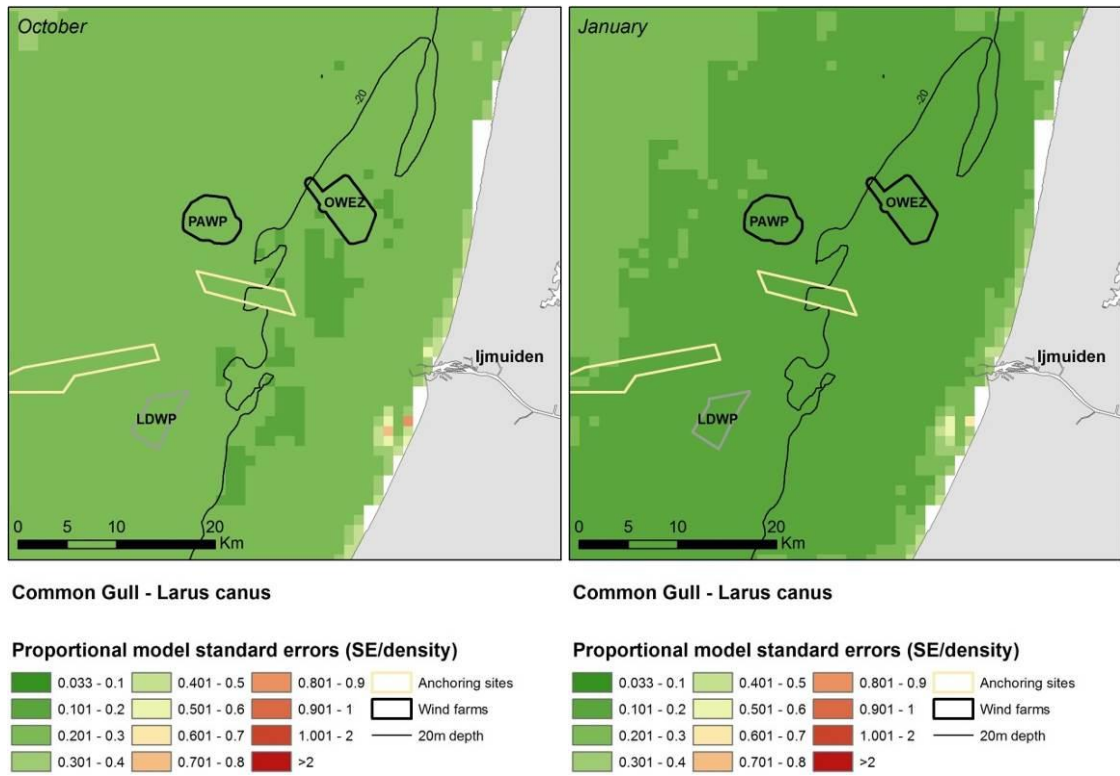


Figure B.18. Model uncertainty. Proportional model standard errors for the distribution (probability) model of wintering Common Gull during the baseline surveys 2013-2014.

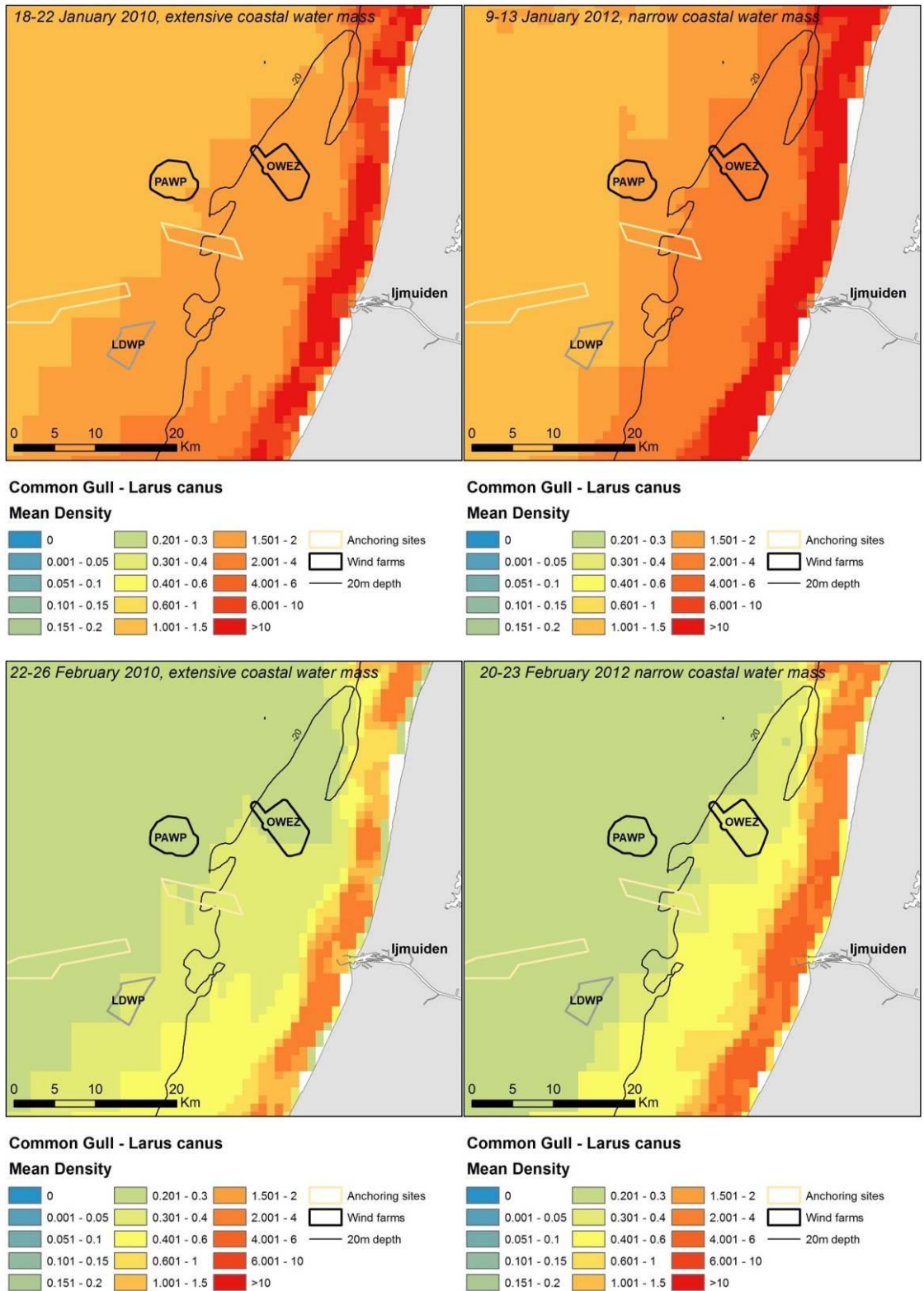


Figure B.19. Predicted variation in Common Gull distribution during periods of limited and extensive coverage of the coastal water mass.

## Herring Gull

Table B.8. Smooth terms, deviance explained and evaluation statistics for the Herring Gull distribution model. The z-values and significance for the parametric terms are shown and for the smooth terms the approximate significance and chi-square/F statistics. Variables not included in either the binomial or positive model part are indicated with a dash.

Smooth terms	Presence/absence		Positive density	
	chi-sqr	p	F	p
Current speed	-		-	
Eddy potential	34.108	<0.001	3.307	<0.05
Current gradient	-		-	
Surface salinity	14.867	<0.001	13.435	<0.001
Water depth	10.015	<0.05	-	
Slope of seafloor	6.317	<0.05	10.136	<0.001
Distance to wind farm	-		-	
Distance to anchoring site	-		-	
Density of ships	-		9.423	<0.001
<b>Parametric terms</b>	<b>z</b>	<b>p</b>	<b>t</b>	<b>p</b>
Winter 2	1.569		2.984	<0.01
Winter 3	-4.123	<0.001	-1.844	
Winter 4	-0.75		-2.338	<0.05
Winter 5	-3.409	<0.001	-0.62	
Winter 6	-4.778	<0.001	-0.47	
Winter 7	-5.909	<0.001	-2.077	<0.05
Month2	-3.447	<0.001	-10.104	<0.001
Month10	-0.718		-1.527	
Month11	-3.904	<0.001	-2.225	<0.05
Sample size (n)	9071		787	
Dev. Exp.	17.20%		51.60%	
AUC	0.79			
Spearman's corr.	0.25			

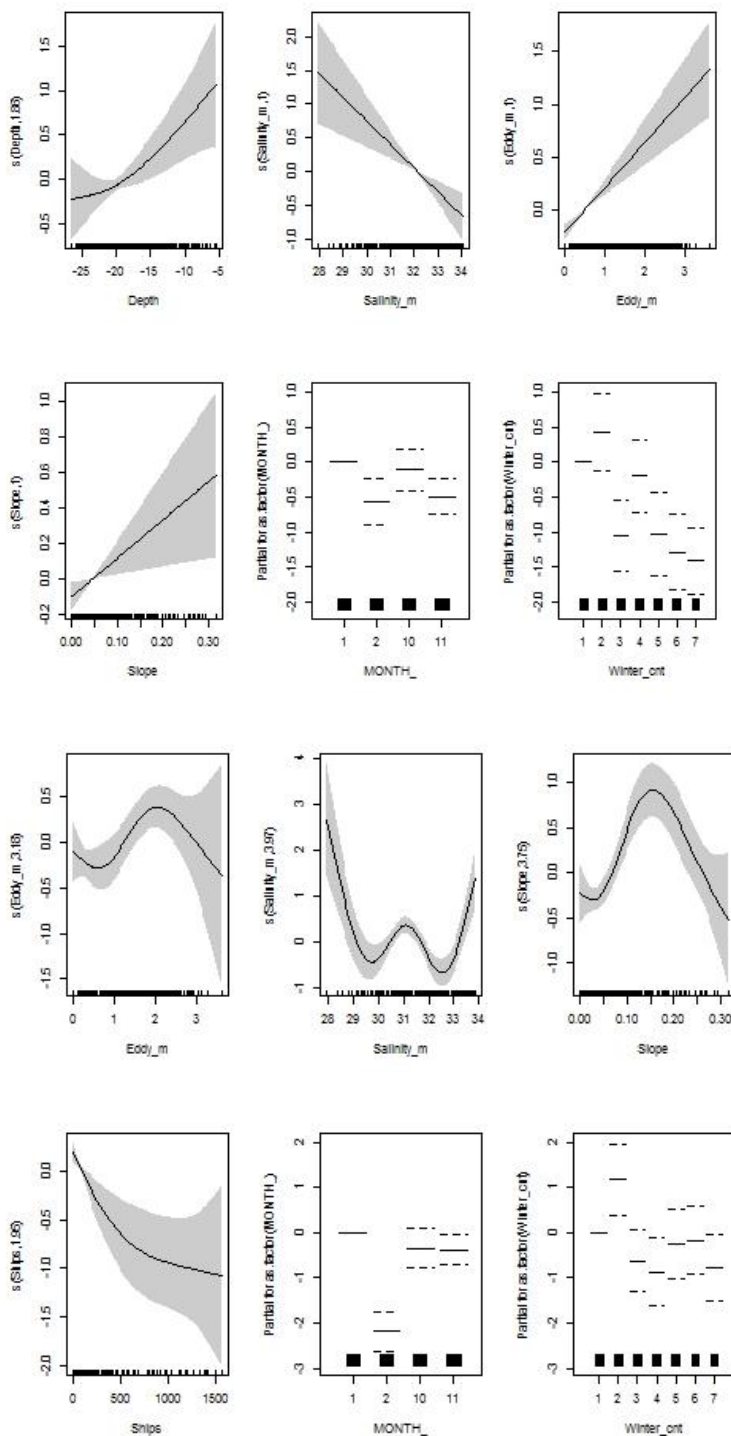


Figure B.20. Partial GAM plots for the Herring Gull distribution model – presence-absence (upper panel) and positive (lower panel) parts. The values of the environmental variables are shown on the X-axis and the probability on the Y-axis in the scale of the linear predictor. The grey shaded areas and the dotted lines (for factors) show the 95% Bayesian confidence intervals. The degree of smoothing is indicated in the legend of the Y-axis.

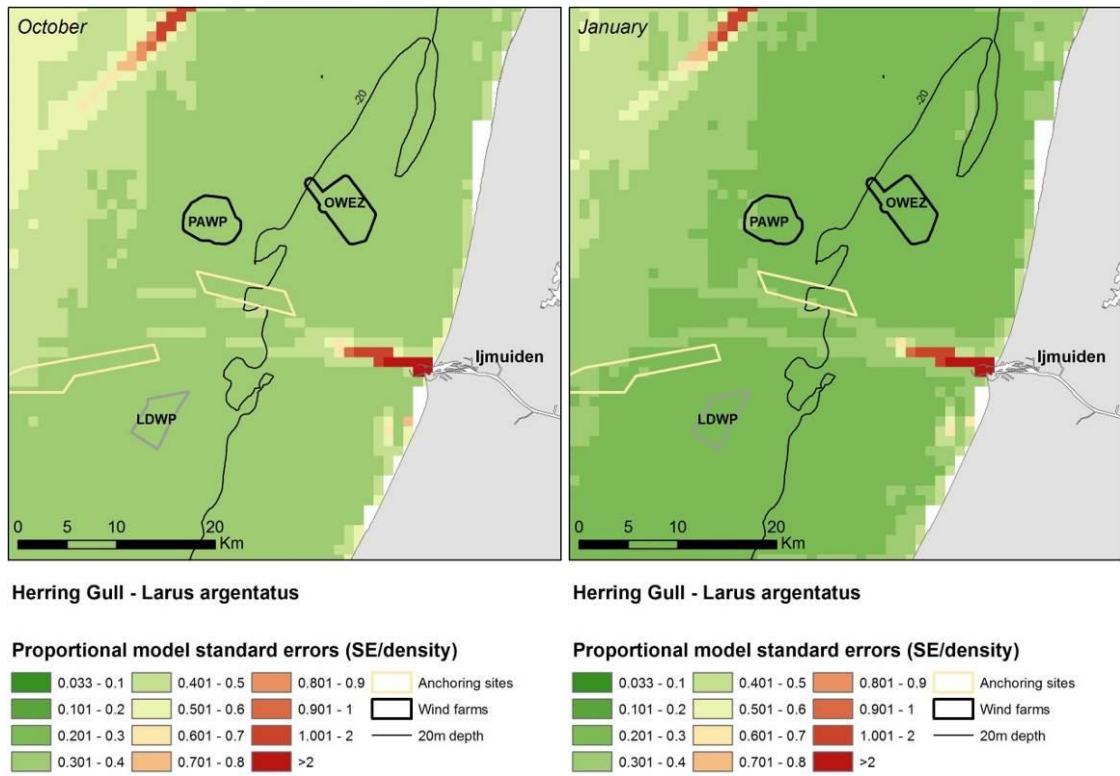


Figure B.21. Model uncertainty. Proportional model standard errors for the distribution (probability) model of wintering Herring Gull during the baseline surveys 2013-2014.

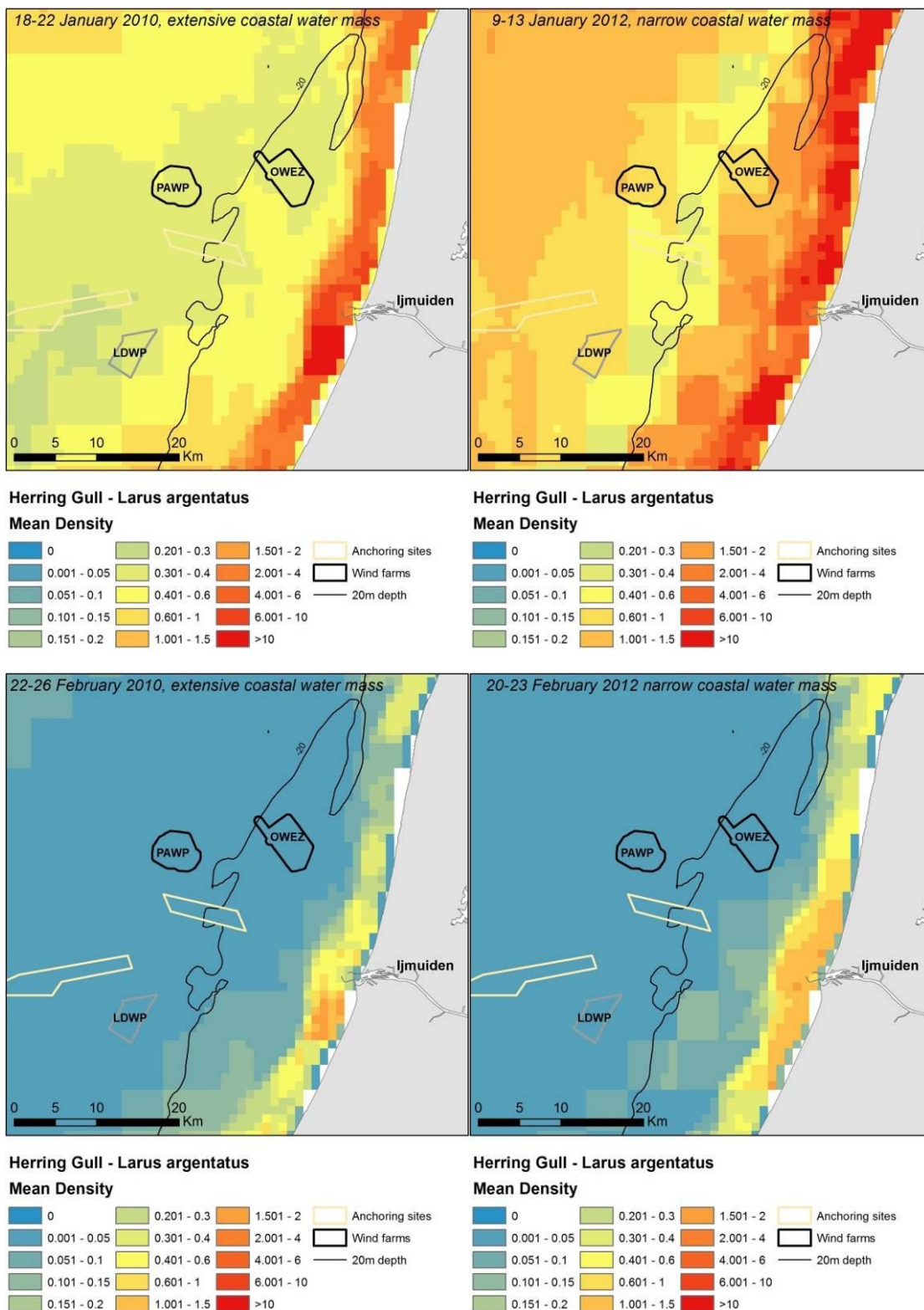


Figure B.22. Predicted variation in Herring Gull distribution during periods of limited and extensive coverage of the coastal water mass.

## Great Black-backed Gull

Table B.9. Smooth terms, deviance explained and evaluation statistics for the Great Black-backed Gull distribution model. The z-values and significance for the parametric terms are shown and for the smooth terms the approximate significance and chi-square/F statistics. Variables not included in either the binomial or positive model part are indicated with a dash.

Smooth terms	Presence/absence		Positive density	
	chi-sqr	p	F	p
Current speed	-		-	
Eddy potential	9.878	<0.05	16.667	<0.001
Current gradient	-		-	
Surface salinity	-		8.937	<0.001
Water depth	44.047	<0.001	20.156	<0.001
Slope of seafloor	-		3.59	<0.01
Distance to wind farm	-		-	
Distance to anchoring site	8.28	<0.01	-	
Density of ships	4.139	<0.05	9.176	<0.001
<b>Parametric terms</b>	<b>z</b>	<b>p</b>	<b>t</b>	<b>p</b>
Winter 2	2.453	<0.05	4.406	<0.001
Winter 3	0.317		-3.495	<0.001
Winter 4	3.546	<0.001	2.431	<0.05
Winter 5	-0.952		1.252	
Winter 6	-0.343		1.395	
Winter 7	-4.921	<0.001	-1.047	
Month2	-7.618	<0.001	-6.622	<0.001
Month10	8.146	<0.001	-1.887	
Month11	4.612	<0.001	-5.712	<0.001
Sample size (n)	9071		1290	
Dev. Exp.	10.30%		39.90%	
AUC	0.73			
Spearman's corr.	0.26			

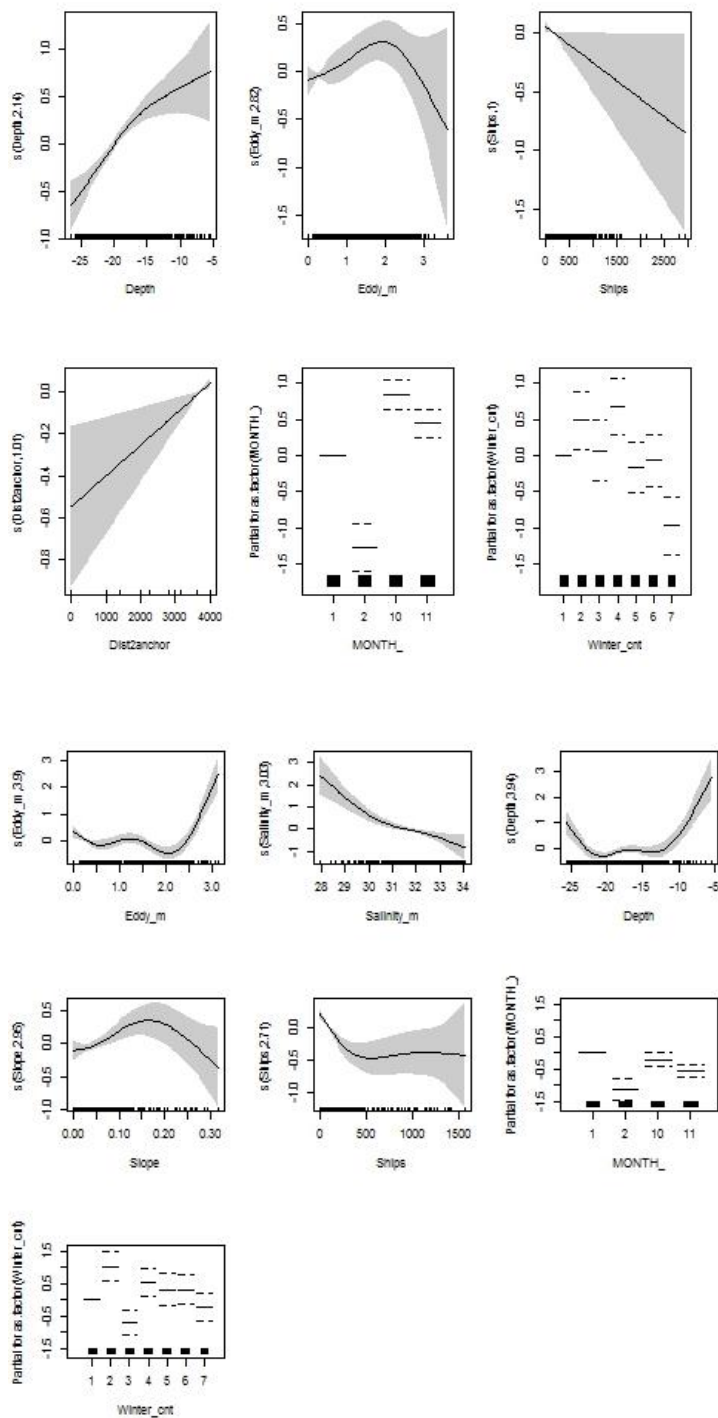


Figure B.23. Partial GAM plots for the Great Black-backed Gull distribution model – presence-absence (upper panel) and positive (lower panel) parts. The values of the environmental variables are shown on the X-axis and the probability on the Y-axis in the scale of the linear predictor. The grey shaded areas and the dotted lines (for factors) show the 95% Bayesian confidence intervals. The degree of smoothing is indicated in the legend of the Y-axis.

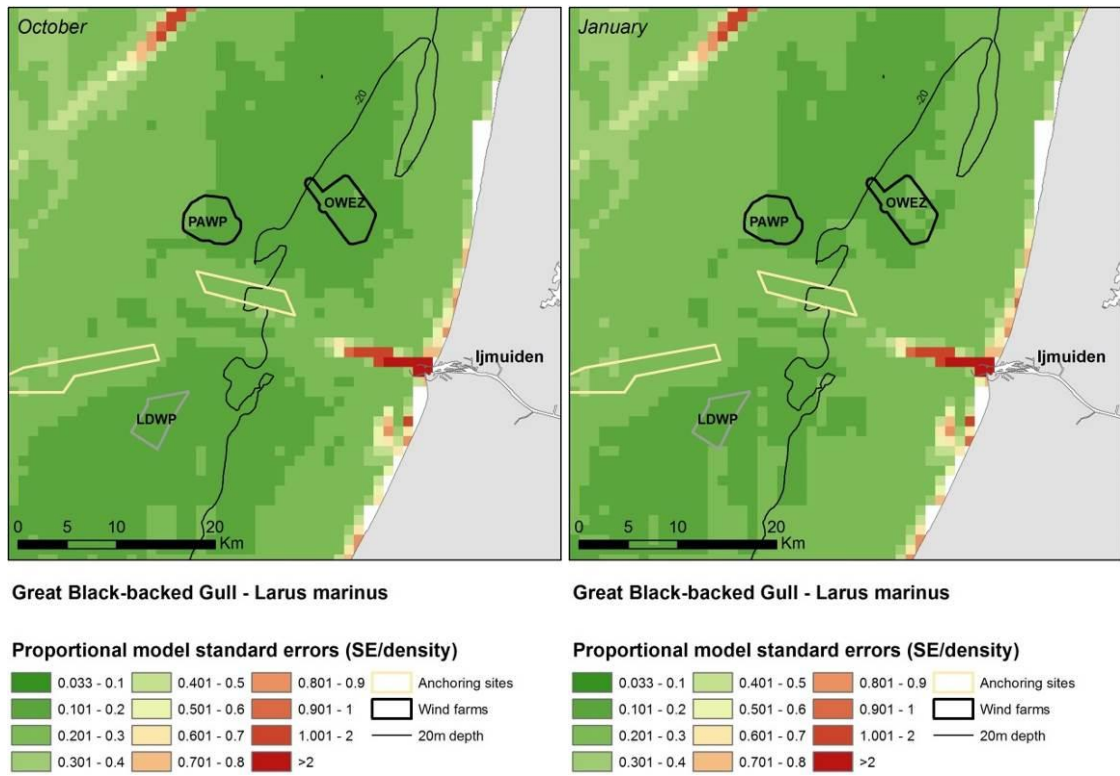


Figure B.24. Model uncertainty. Proportional model standard errors for the distribution (probability) model of wintering Great Black-backed Gull during the baseline surveys 2013-2014.

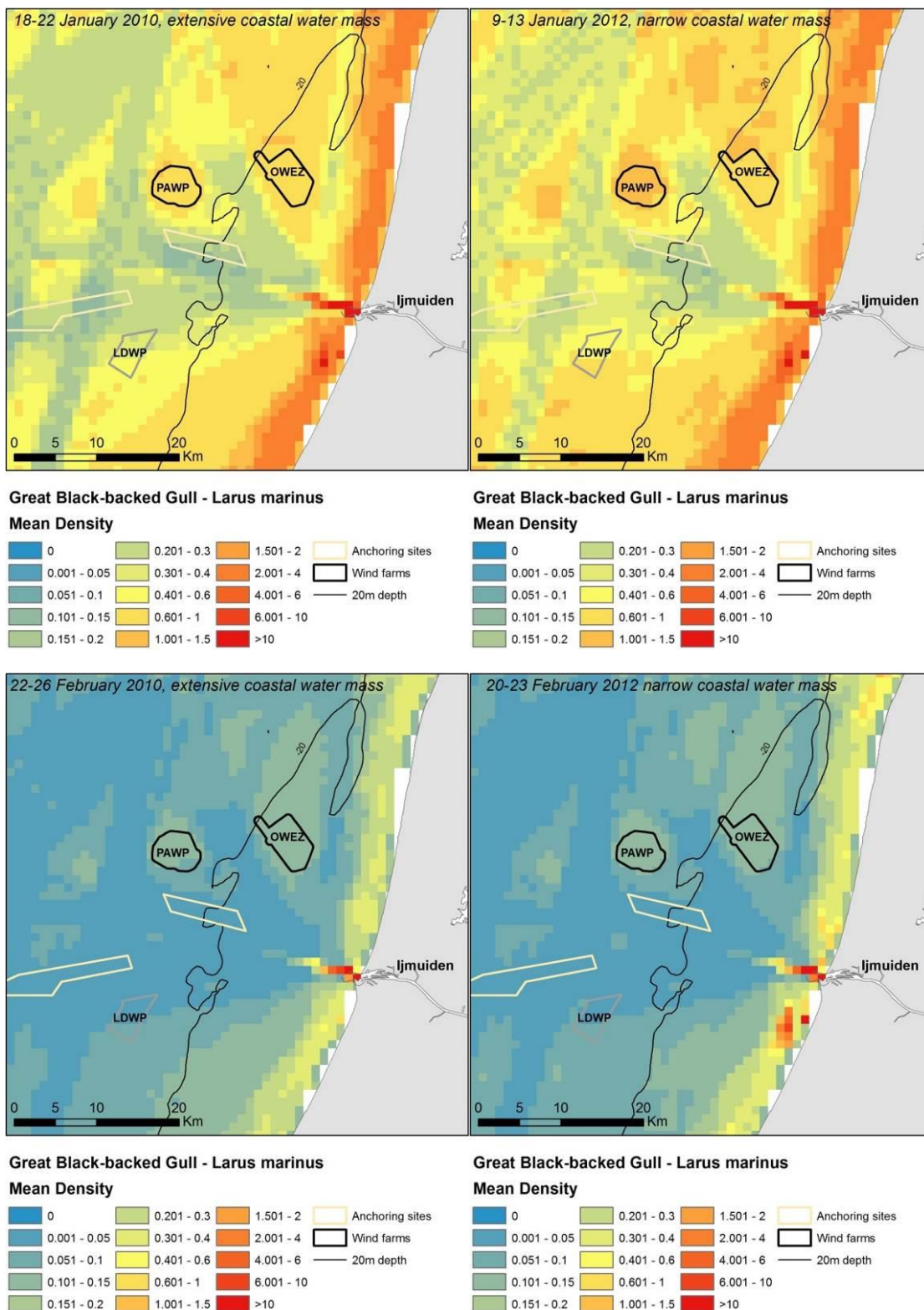


Figure B.25. Predicted variation in Great Black-backed Gull distribution during periods of limited and extensive coverage of the coastal water mass.

## Black-legged Kittiwake

Table B.10. Smooth terms, deviance explained and evaluation statistics for the Black-legged Kittiwake distribution model. The z-values and significance for the parametric terms are shown and for the smooth terms the approximate significance and chi-square/F statistics. Variables not included in either the binomial or positive model part are indicated with a dash.

Smooth terms	Presence/absence		Positive density	
	chi-sqr	p	F	p
Current speed	-		-	
Eddy potential	-		19.136	<0.001
Current gradient	-		-	
Surface salinity	24.75	<0.001	-	
Water depth	14.751	<0.001	4.057	<0.01
Slope of seafloor	-		13.138	<0.001
Distance to wind farm	-		2.947	
Distance to anchoring site	4.925	<0.05	-	
Density of ships	-		14.183	<0.001
<b>Parametric terms</b>	<b>z</b>	<b>p</b>	<b>t</b>	<b>p</b>
Winter 2	3.97	<0.001	0.987	
Winter 3	4.035	<0.001	0.268	
Winter 4	0.918		-1.192	
Winter 5	-0.405		0.095	
Winter 6	4.086	<0.001	0.14	
Winter 7	0.655		-2.473	<0.05
Month2	-10.644	<0.001	-8.263	<0.001
Month10	-10.575	<0.001	-7.439	<0.001
Month11	-1.116		-7.071	<0.001
Sample size (n)	9071		1304	
Dev. Exp.	11.90%		23.80%	
AUC	0.74			
Spearman's corr.	0.26			

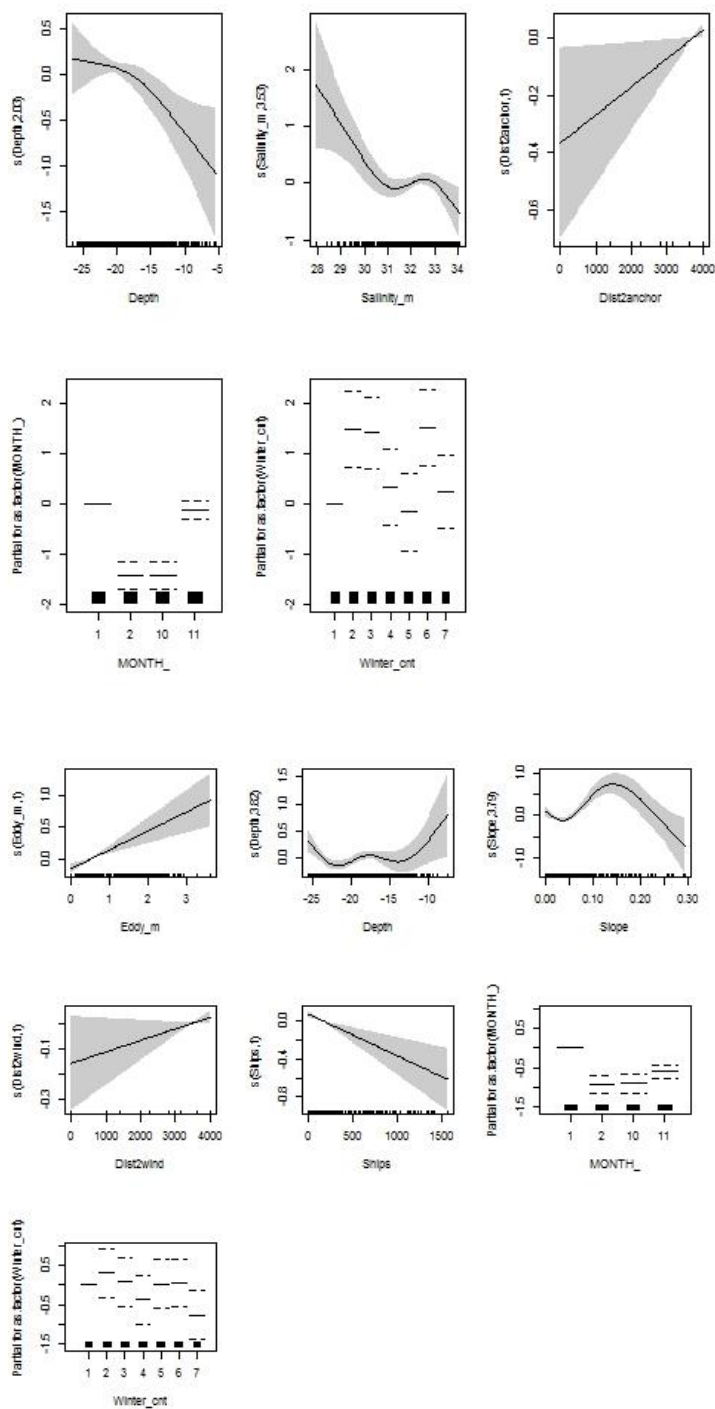


Figure B.26. Partial GAM plots for the Black-legged Kittiwake distribution model – presence-absence (upper panel) and positive (lower panel) parts. The values of the environmental variables are shown on the X-axis and the probability on the Y-axis in the scale of the linear predictor. The grey shaded areas and the dotted lines (for factors) show the 95% Bayesian confidence intervals. The degree of smoothing is indicated in the legend of the Y-axis.

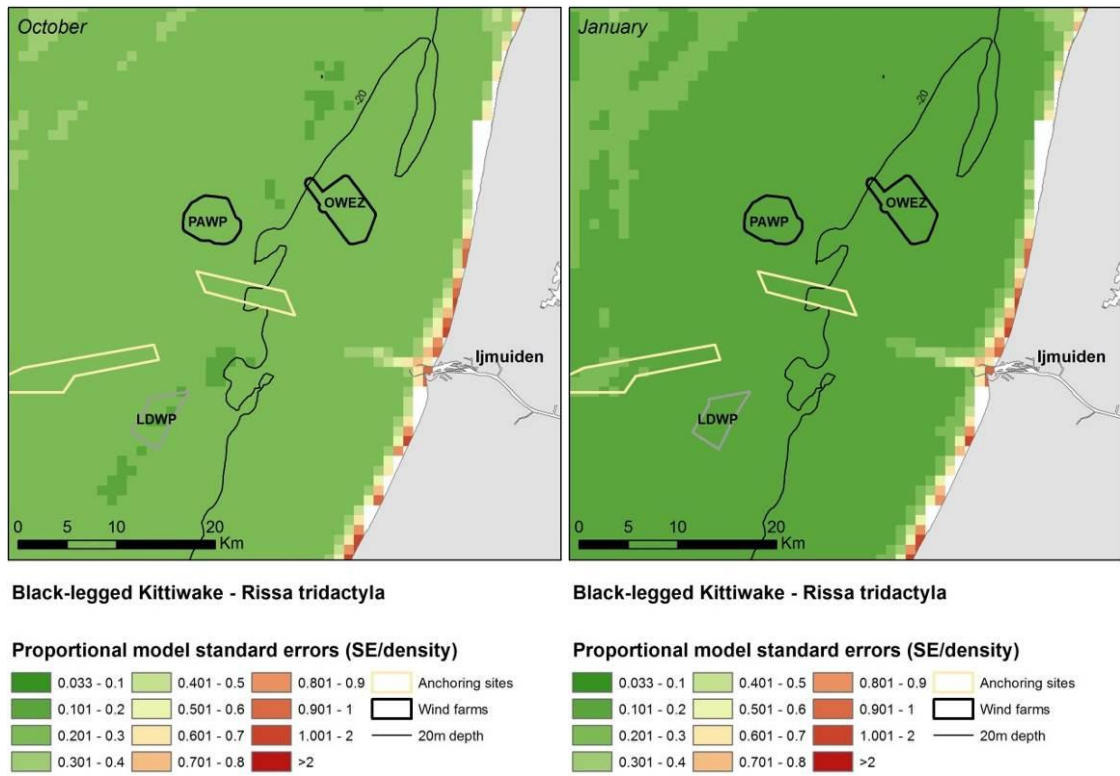


Figure B.27. Model uncertainty. Proportional model standard errors for the distribution (probability) model of wintering Black-legged Kittiwake during the baseline surveys 2013-2014.

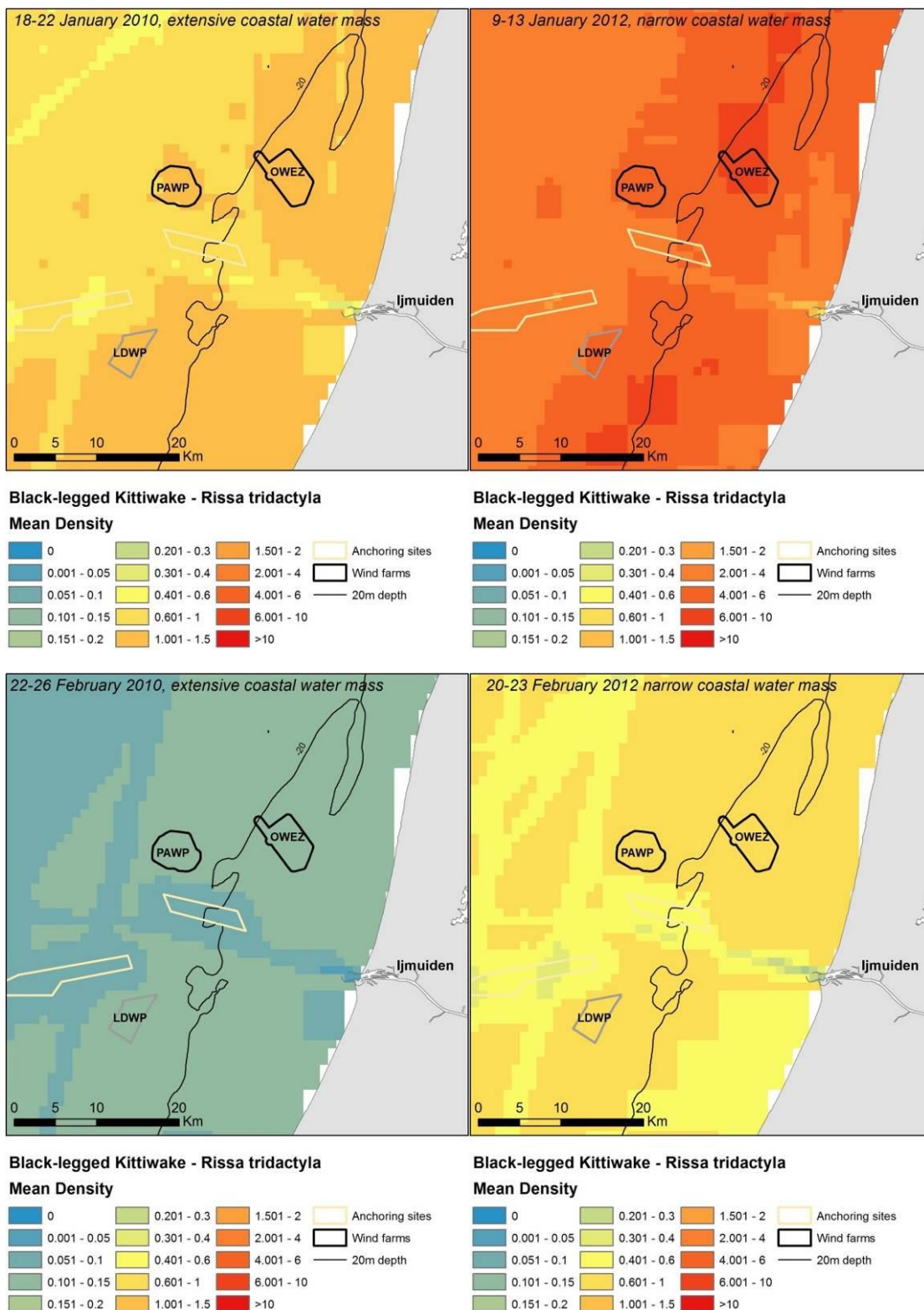


Figure B.28. Predicted variation in Black-legged Kittiwake distribution during periods of limited and extensive coverage of the coastal water mass.

## Common Guillemot

Table B.11. Smooth terms, deviance explained and evaluation statistics for the Common Guillemot distribution model. The z-values and significance for the parametric terms are shown and for the smooth terms the approximate significance and chi-square/F statistics. Variables not included in either the binomial or positive model part are indicated with a dash.

Smooth terms	Presence/absence		Positive density	
	chi-sqr	p	F	p
Current speed	-		-	
Eddy potential	-		-	
Current gradient	-		-	
Surface salinity	-		-	
Water depth	77.2	<0.001	8.286	<0.001
Slope of seafloor	-		3.863	<0.01
Distance to wind farm	43.914	<0.001	45.877	<0.001
Distance to anchoring site	-		-	
Density of ships	3.911		8.589	<0.001
<b>Parametric terms</b>	<b>z</b>	<b>p</b>	<b>t</b>	<b>p</b>
Winter 2	-1.279		-0.558	
Winter 3	-2.257	<0.05	1.766	
Winter 4	-3.987	<0.001	-0.225	
Winter 5	-4.93	<0.001	-2.502	<0.05
Winter 6	0.078		-0.95	
Winter 7	5.184	<0.001	-0.448	
Month2	-10.569	<0.001	-5.108	<0.001
Month10	-16.433	<0.001	-8.994	<0.001
Month11	-4.158	<0.001	-6.101	<0.001
Sample size (n)	9071		1591	
Dev. Exp.	21.40%		23.10%	
AUC	0.79			
Spearman's corr.	0.38			

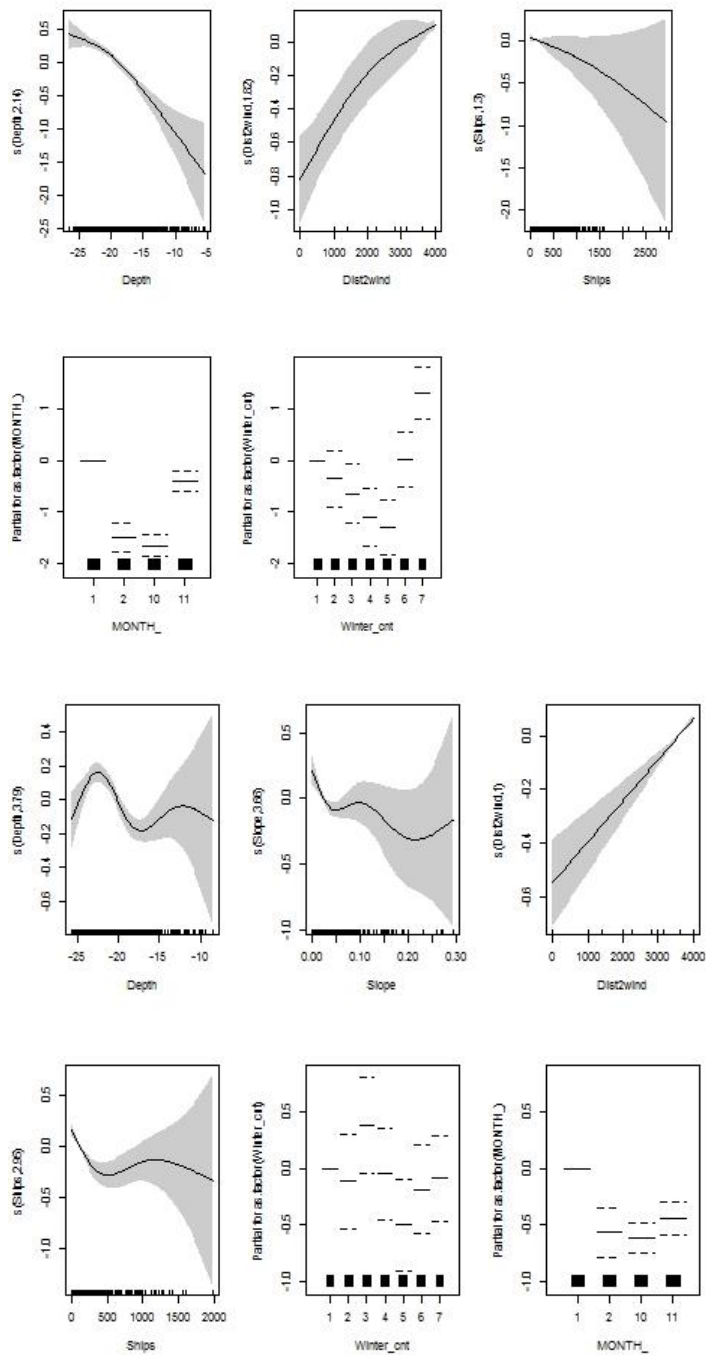


Figure B.29. Partial GAM plots for the Common Guillemot distribution model – presence-absence (upper panel) and positive (lower panel) parts. The values of the environmental variables are shown on the X-axis and the probability on the Y-axis in the scale of the linear predictor. The grey shaded areas and the dotted lines (for factors) show the 95% Bayesian confidence intervals. The degree of smoothing is indicated in the legend of the Y-axis.

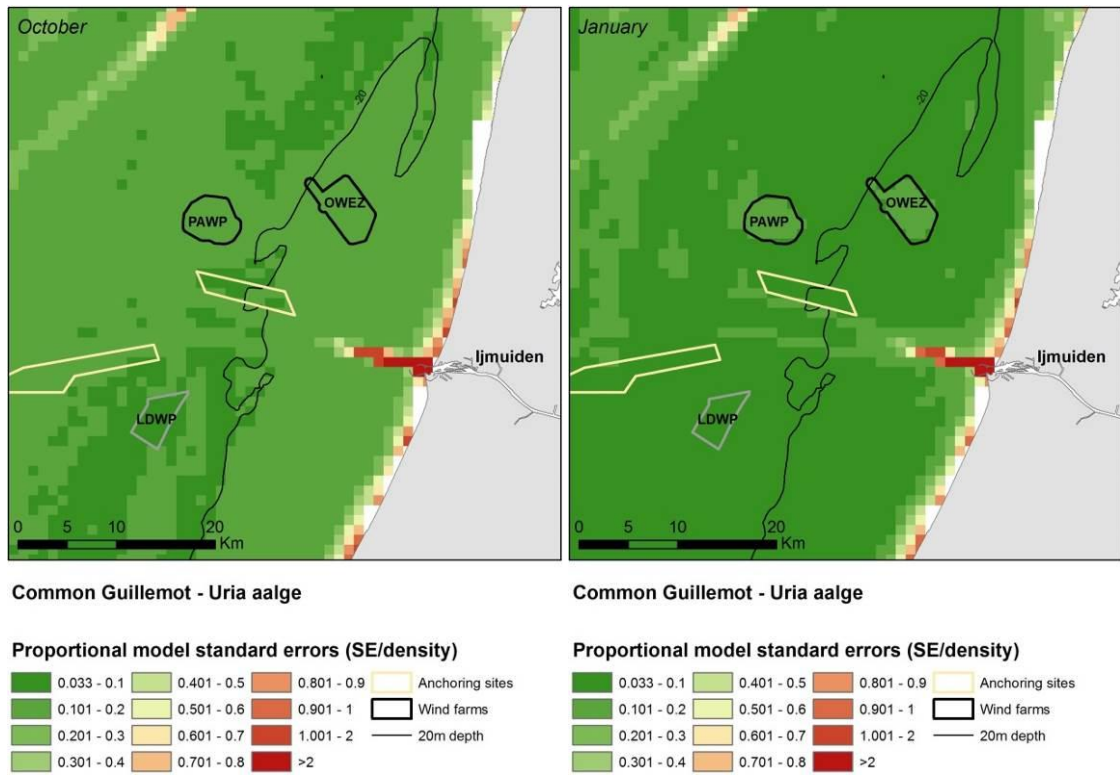


Figure B.30. Model uncertainty. Proportional model standard errors for the distribution (probability) model of wintering Common Guillemot during the baseline surveys 2013-2014.

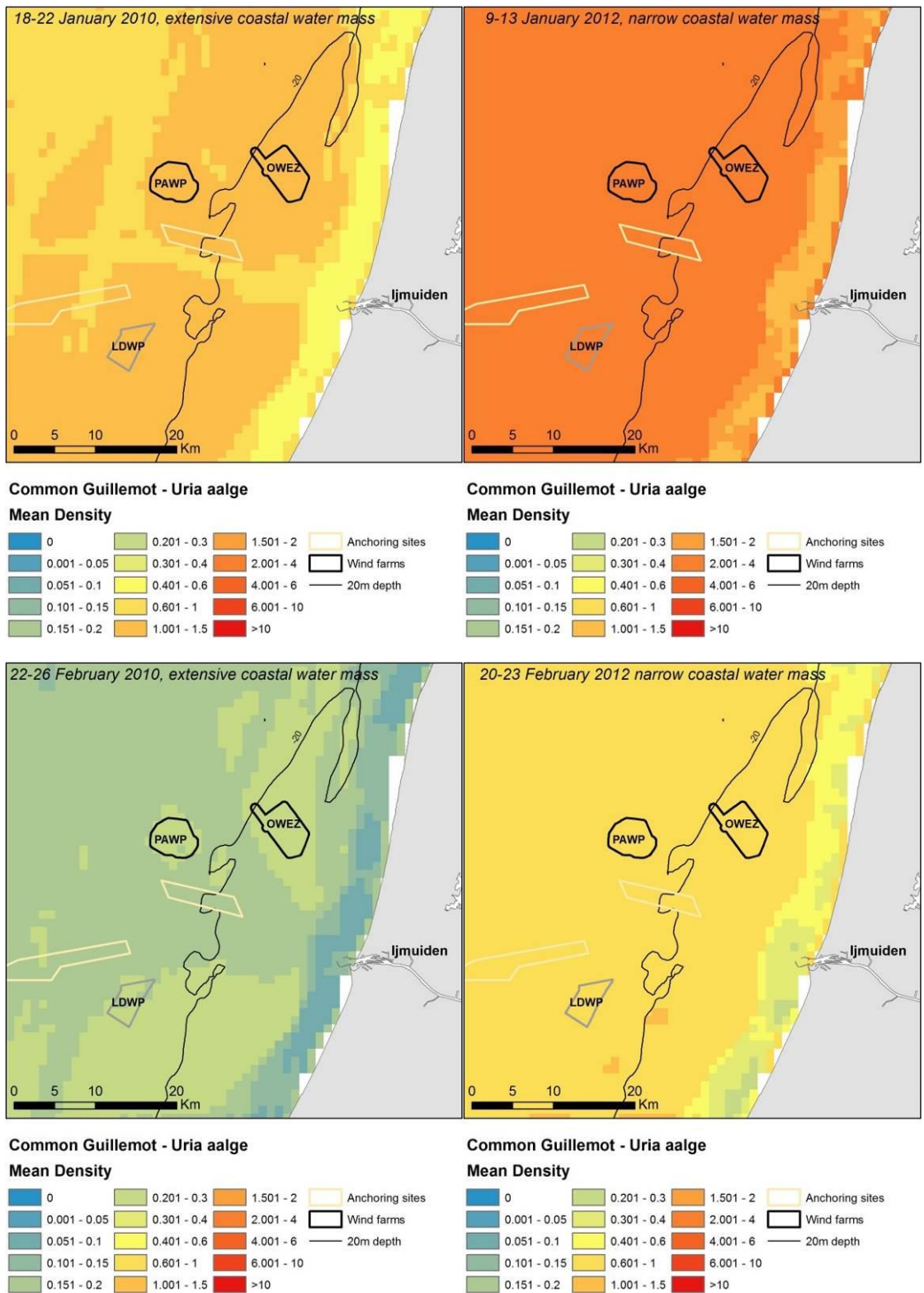


Figure B.30. Predicted variation in Common Guillemot distribution during periods of limited and extensive coverage of the coastal water mass.

## Razorbill

Table B.12. Smooth terms, deviance explained and evaluation statistics for the Razorbill distribution model. The z-values and significance for the parametric terms are shown and for the smooth terms the approximate significance and chi-square/F statistics. Variables not included in either the binomial or positive model part are indicated with a dash.

Smooth terms	Presence/absence		Positive density	
	chi-sqr	p	F	p
Current speed	-		-	
Eddy potential	20.042	<0.001	-	
Current gradient	-		-	
Surface salinity	34.685	<0.001	-	
Water depth	-		5.341	<0.001
Slope of seafloor	-		23.287	<0.001
Distance to wind farm	-		-	
Distance to anchoring site	-		-	
Density of ships	-		-	
Parametric terms	<b>z</b>	<b>p</b>	<b>t</b>	<b>p</b>
Winter 2	-		-	
Winter 3	-		-	
Winter 4	-		-	
Winter 5	-		-	
Winter 6	-		-	
Winter 7	-		-	
Month2	-2.241	<0.05	0.14	
Month10	-1.215		2.204	<0.05
Month11	-4.578	<0.001	0.243	
Sample size (n)	9071		158	
Dev. Exp.	4.20%		27.70%	
AUC	0.67			
Spearman's corr.	0.06			

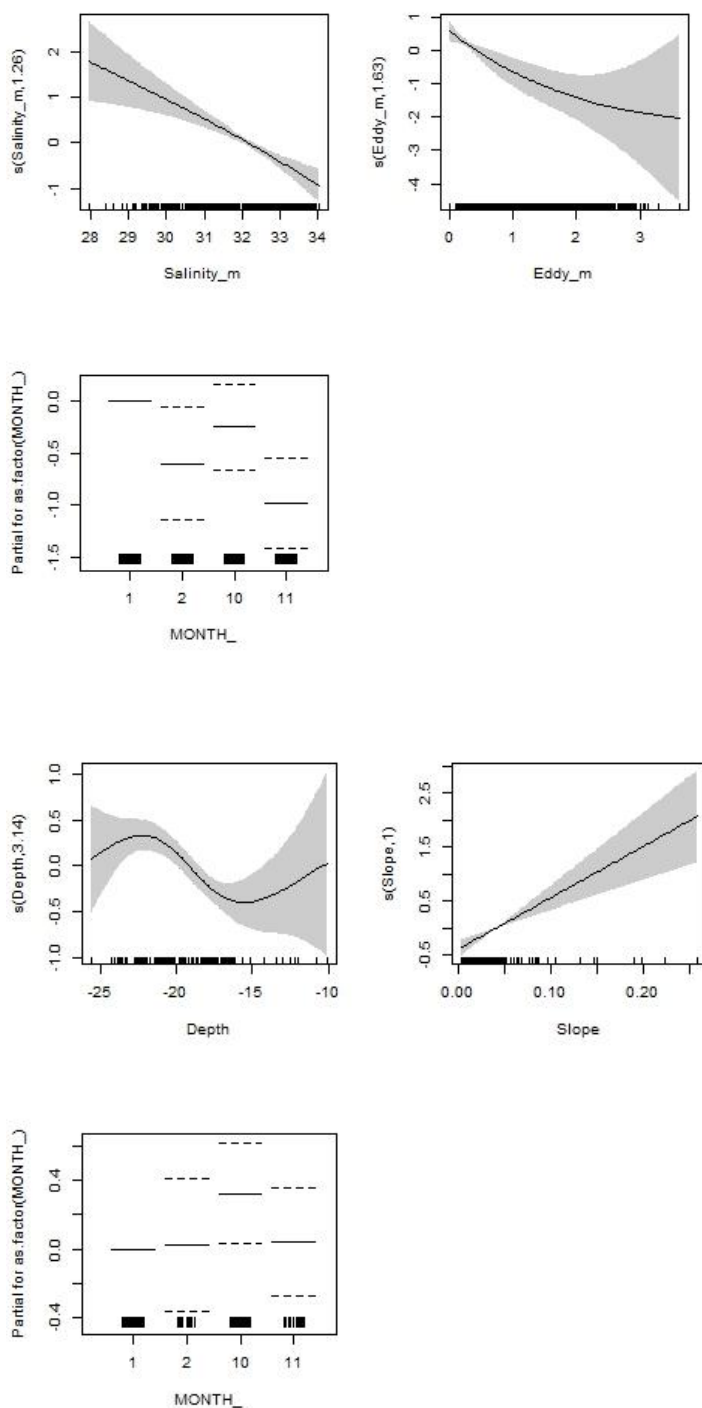


Figure B.31. Partial GAM plots for the Razorbill distribution model – presence-absence (upper panel) and positive (lower panel) parts. The values of the environmental variables are shown on the X-axis and the probability on the Y-axis in the scale of the linear predictor. The grey shaded areas and the dotted lines (for factors) show the 95% Bayesian confidence intervals. The degree of smoothing is indicated in the legend of the Y-axis.

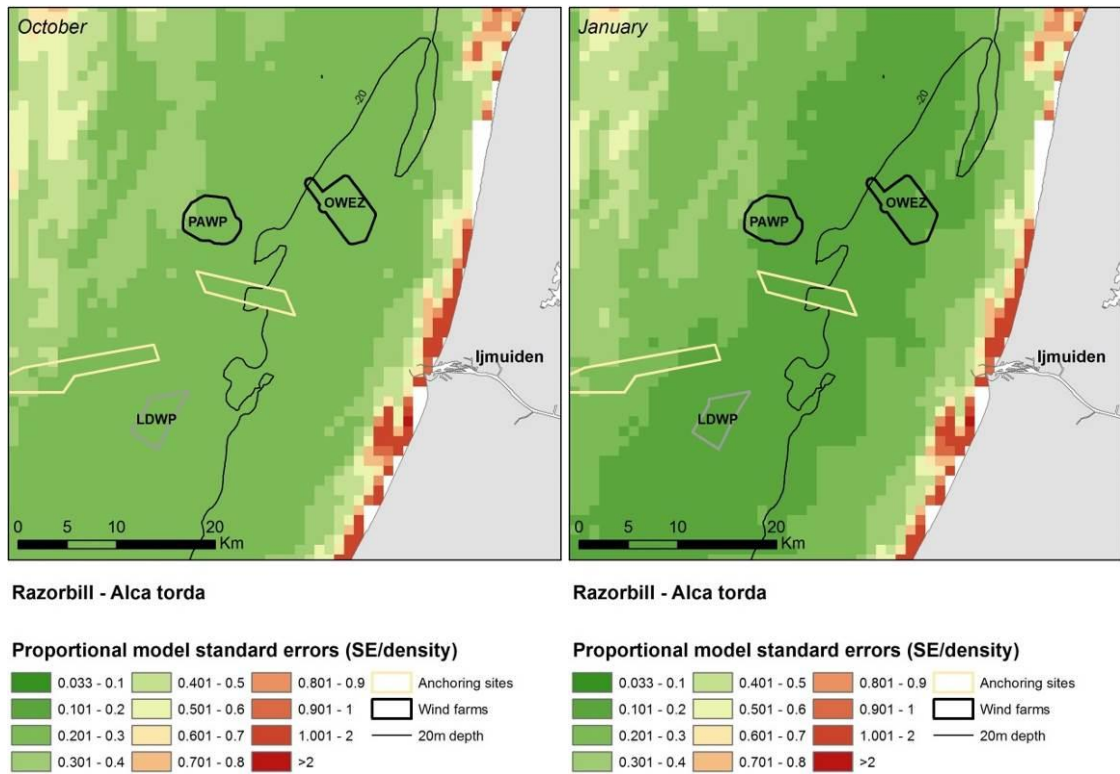
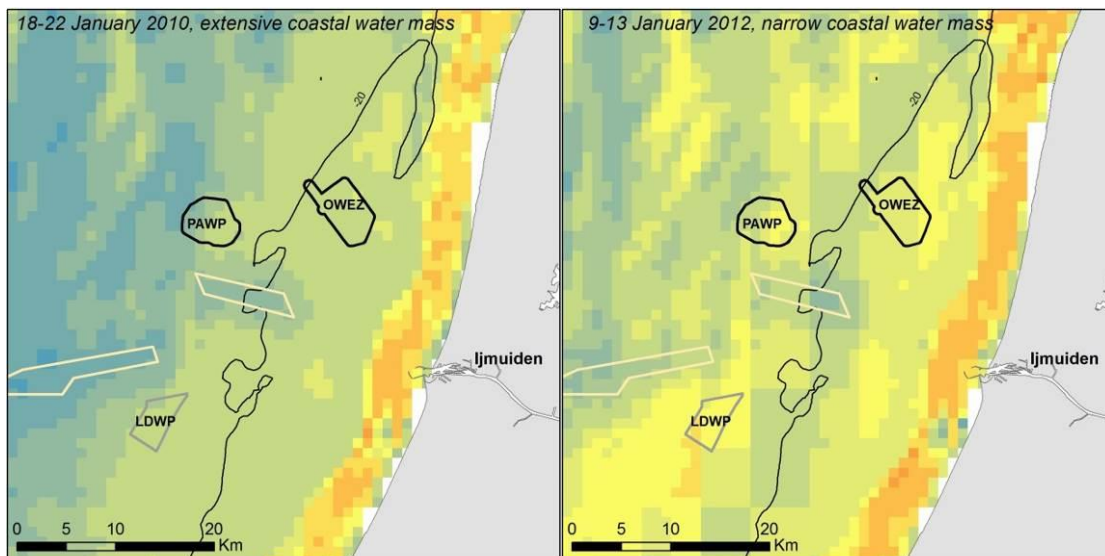
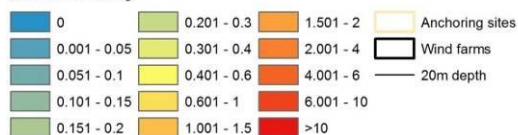


Figure B.32. Model uncertainty. Proportional model standard errors for the distribution (probability) model of wintering Razorbill during the baseline surveys 2013-2014.



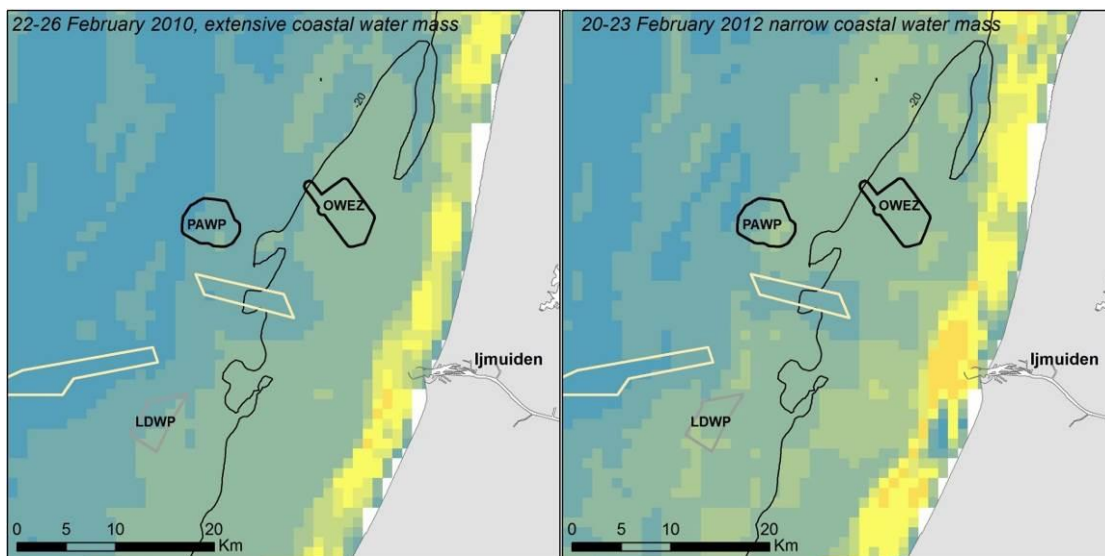
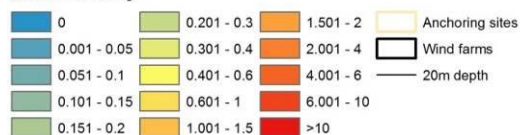
**Razorbill - Alca torda**

**Mean Density**



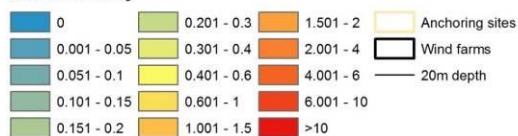
**Razorbill - Alca torda**

**Mean Density**



**Razorbill - Alca torda**

**Mean Density**



**Razorbill - Alca torda**

**Mean Density**

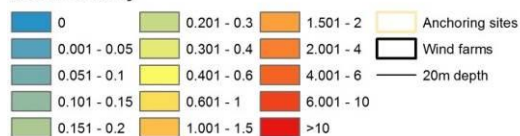
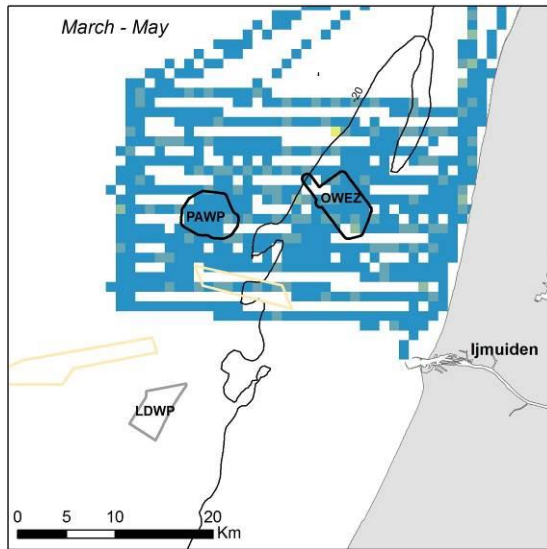
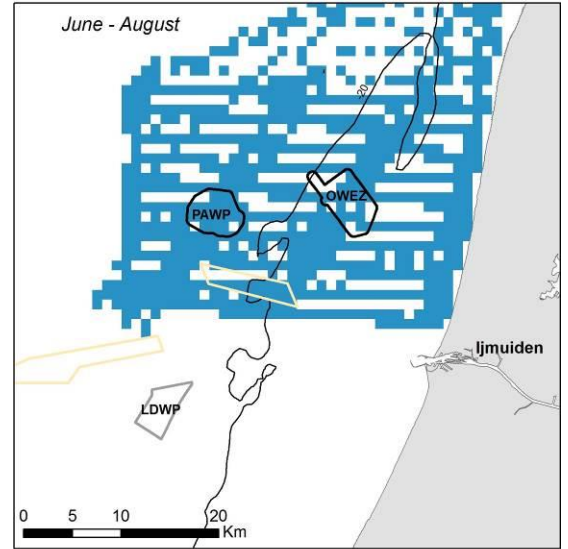
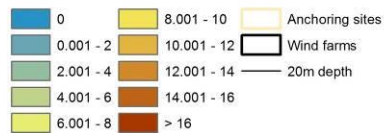


Figure B.33. Predicted variation in Razorbill distribution during periods of limited and extensive coverage of the coastal water mass.

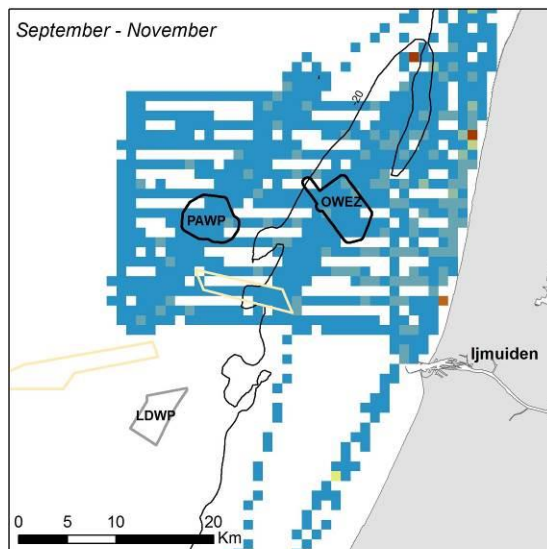
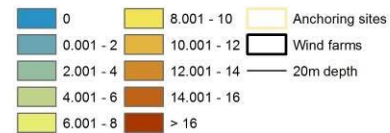
## APPENDIX C – Historic LUD T0 data



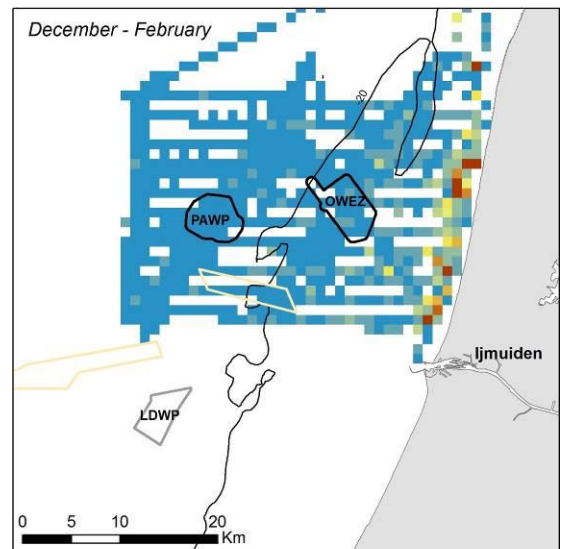
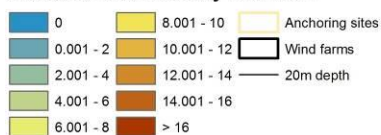
Red-throated/Black-throated Diver - *Gavia stellata/arctica*  
Seasonal Mean Density 2002-2011



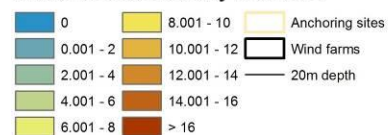
Red-throated/Black-throated Diver - *Gavia stellata/arctica*  
Seasonal Mean Density 2002-2011



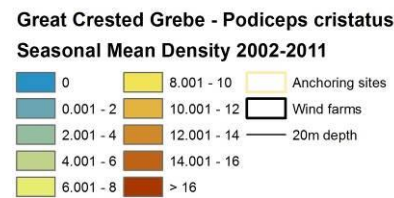
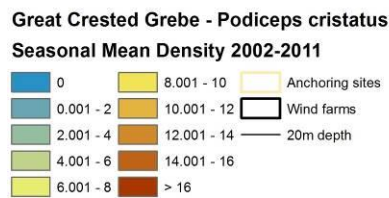
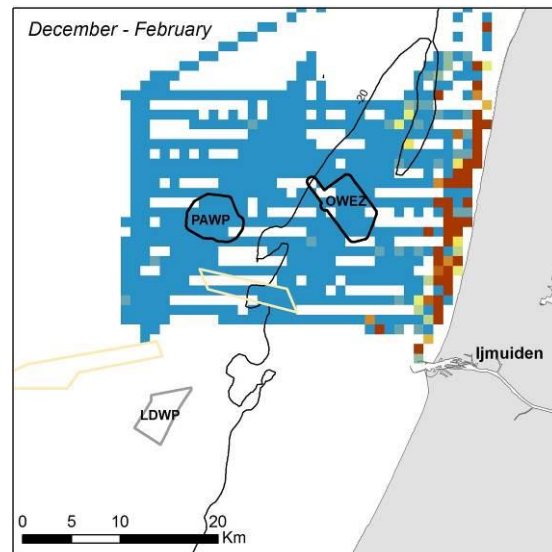
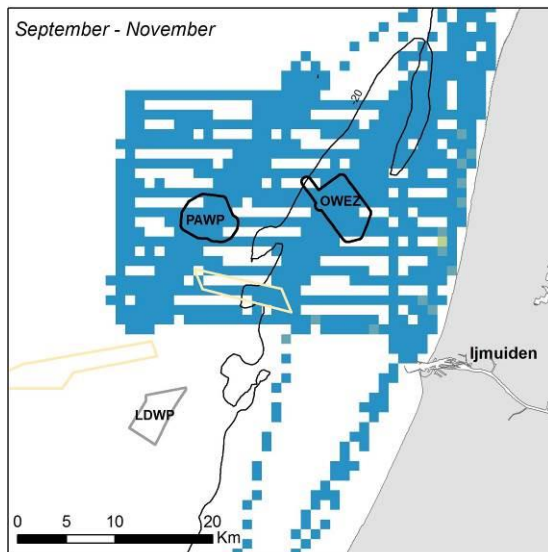
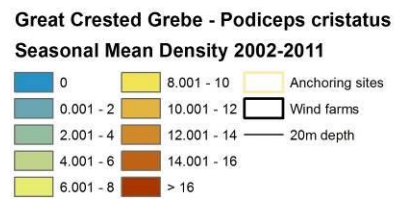
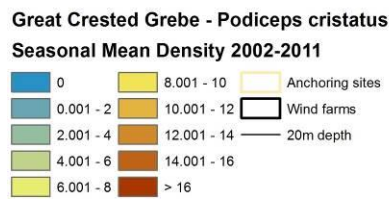
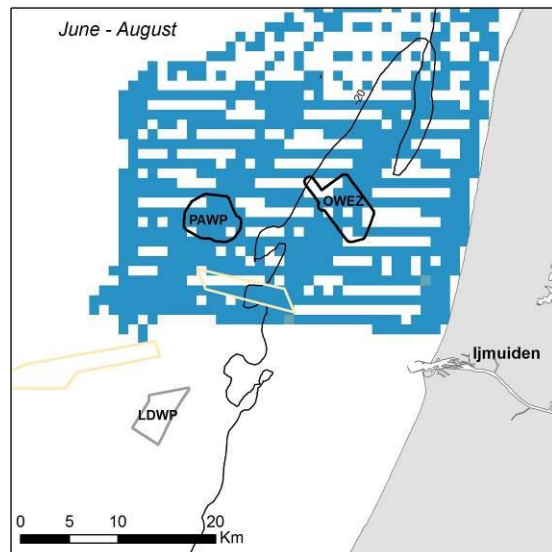
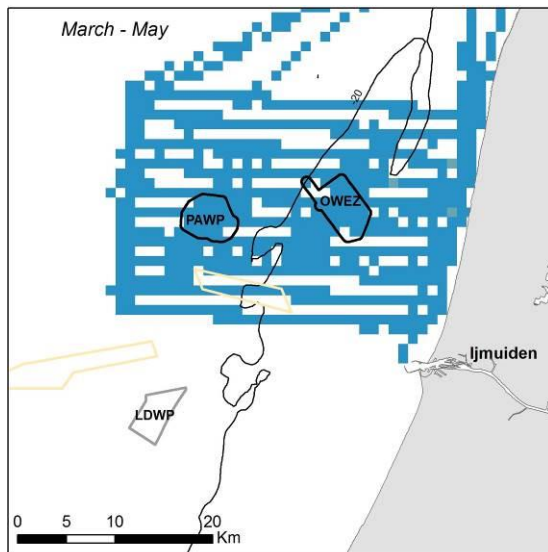
Red-throated/Black-throated Diver - *Gavia stellata/arctica*  
Seasonal Mean Density 2002-2011



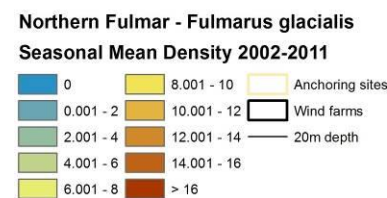
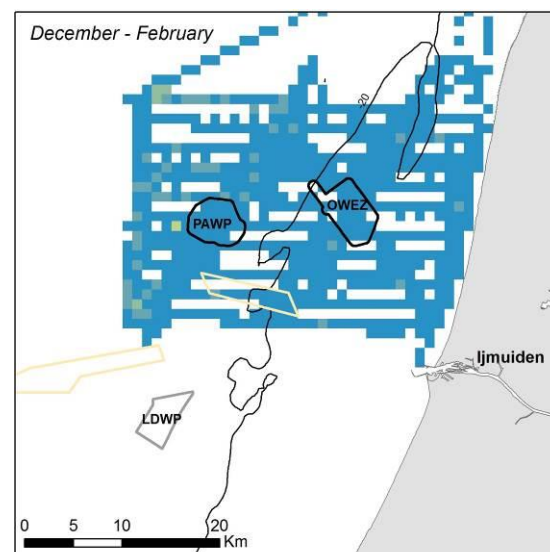
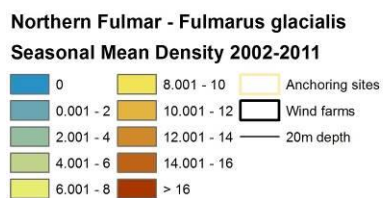
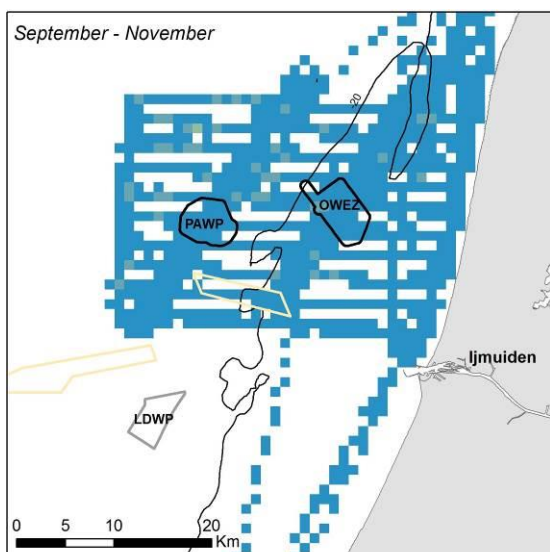
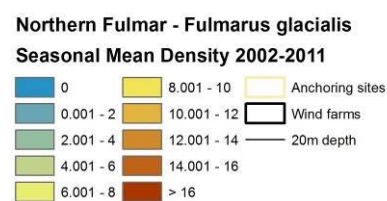
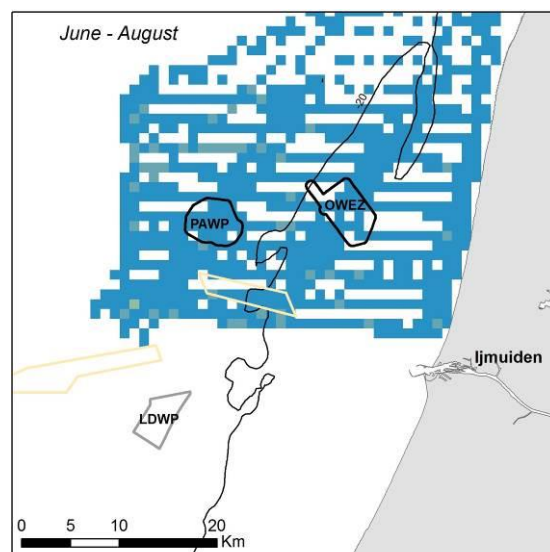
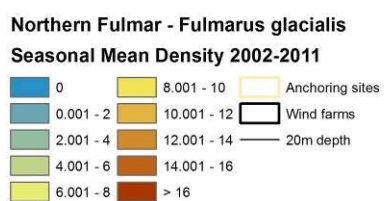
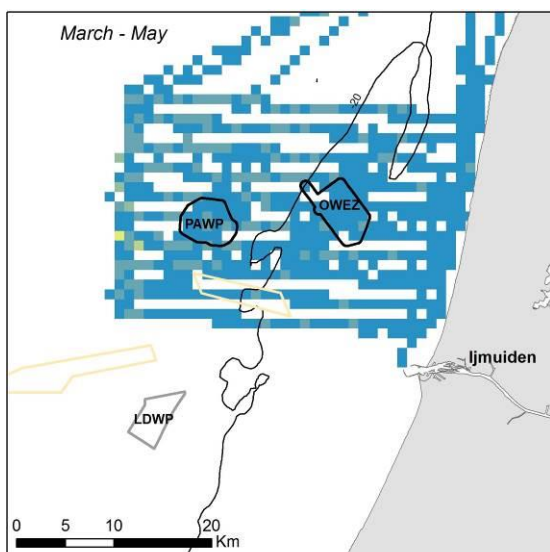
Red-throated/Black-throated Diver - *Gavia stellata/arctica*  
Seasonal Mean Density 2002-2011



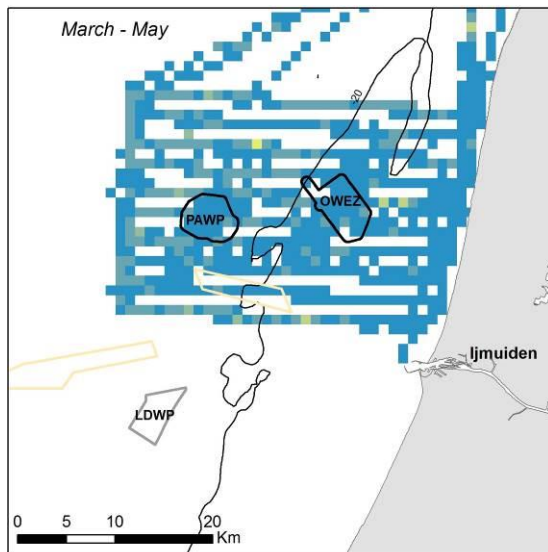
Seasonal mean observed density ( $n/km^2$ ) of Red-/Black-throated Diver during ship-based surveys 2002-2011.  
Densities have been corrected for distance bias.



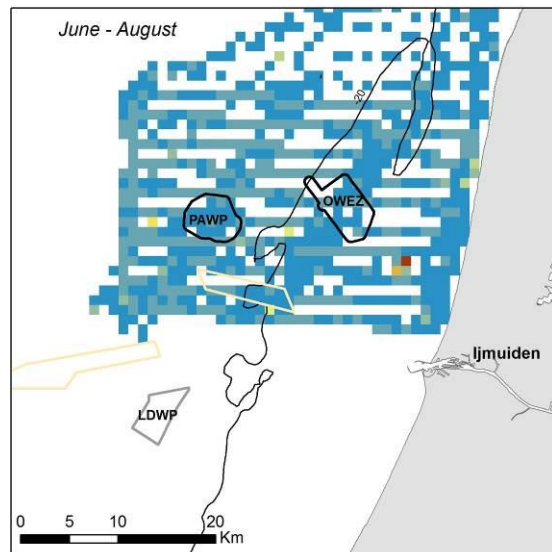
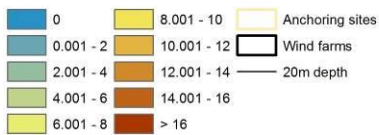
Seasonal mean observed density ( $n/km^2$ ) of Great Crested Grebe during ship-based surveys 2002-2011. Densities have been corrected for distance bias.



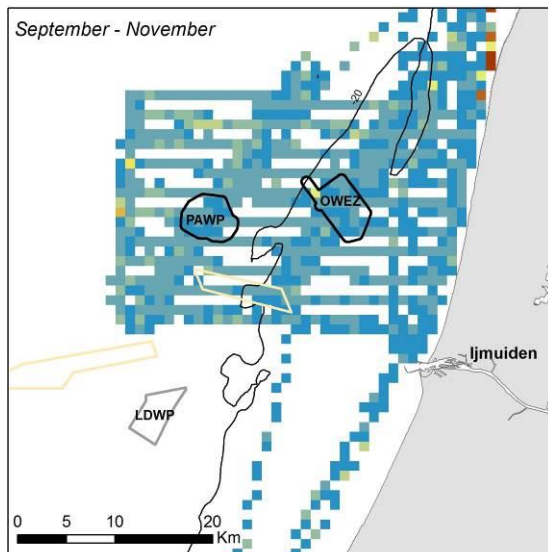
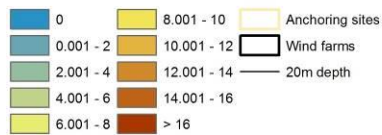
Seasonal mean observed density ( $n/km^2$ ) of Northern Fulmar during ship-based surveys 2002-2011. Densities have been corrected for distance bias.



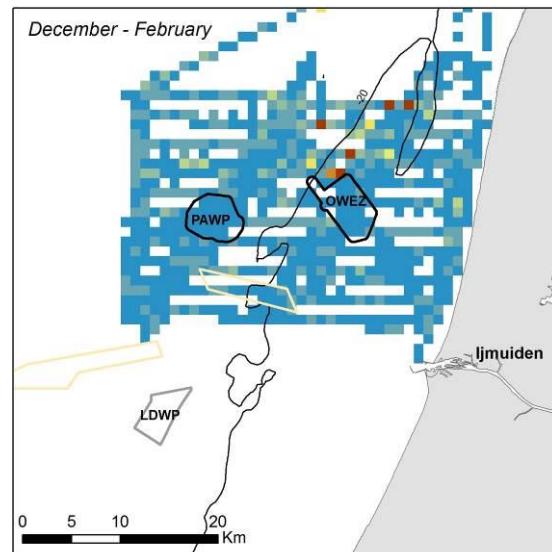
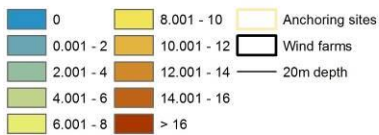
**Northern Gannet - *Morus bassanus***  
**Seasonal Mean Density 2002-2011**



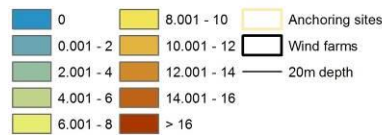
**Northern Gannet - *Morus bassanus***  
**Seasonal Mean Density 2002-2011**



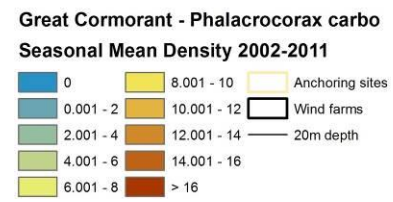
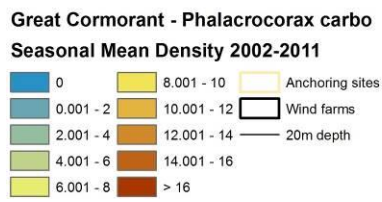
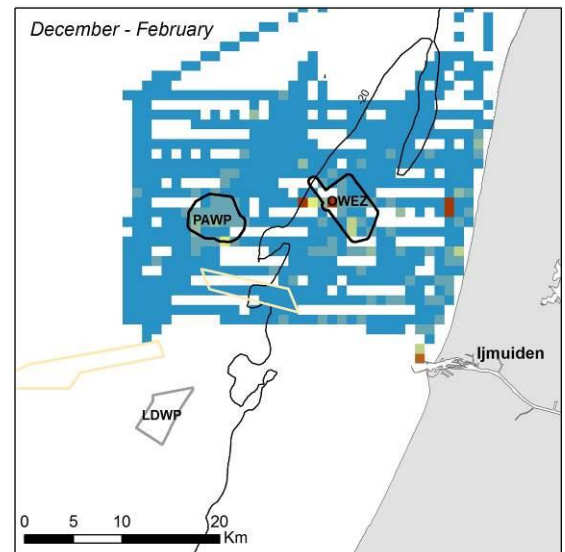
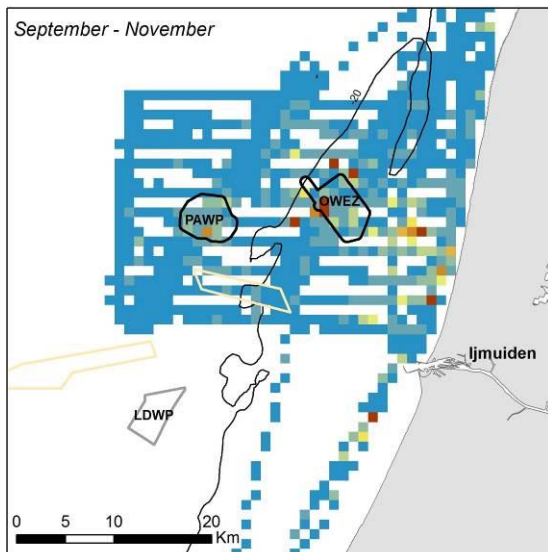
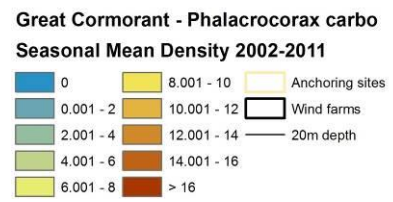
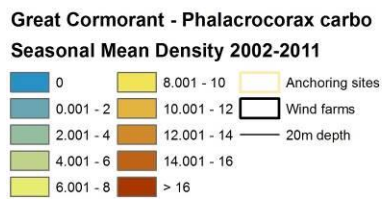
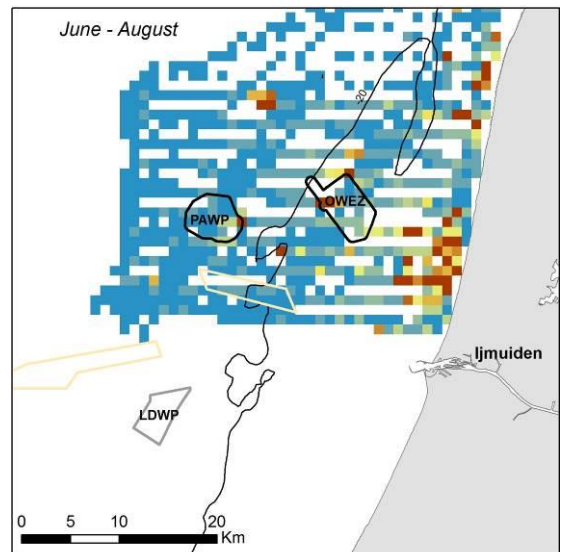
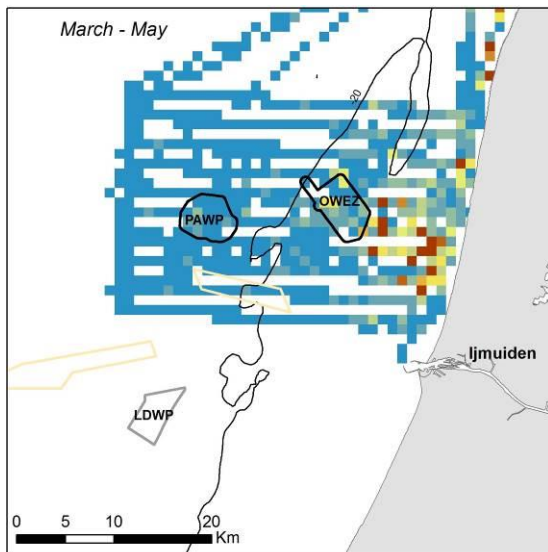
**Northern Gannet - *Morus bassanus***  
**Seasonal Mean Density 2002-2011**



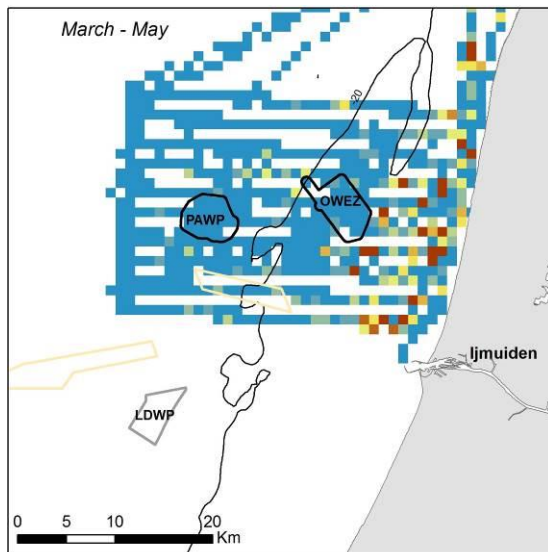
**Northern Gannet - *Morus bassanus***  
**Seasonal Mean Density 2002-2011**



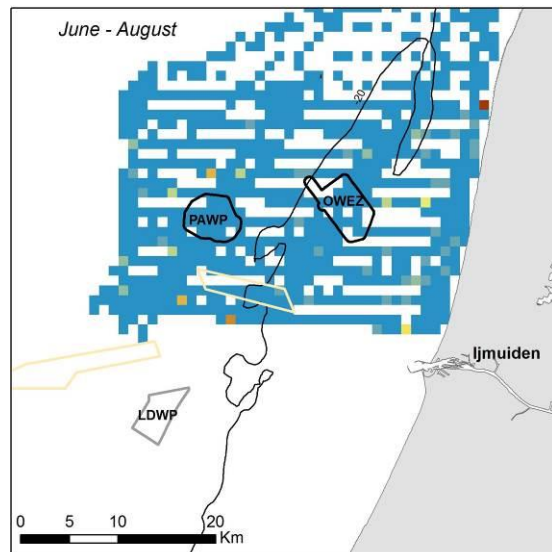
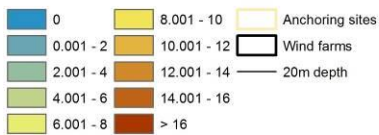
Seasonal mean observed density ( $n/km^2$ ) of Northern Gannet during ship-based surveys 2002-2011. Densities have been corrected for distance bias.



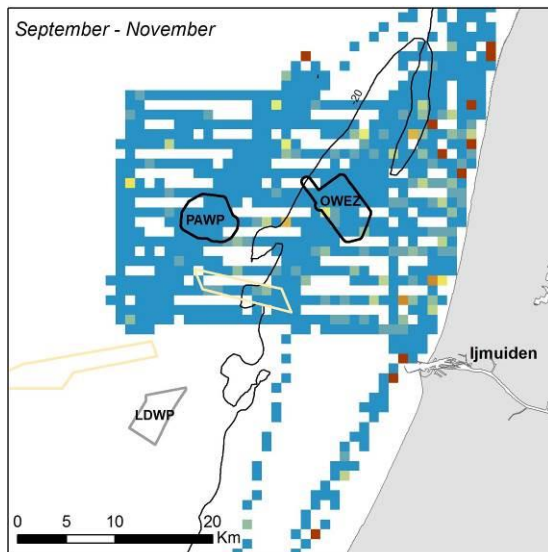
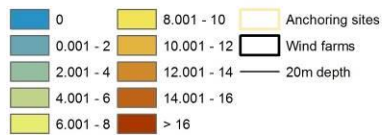
Seasonal mean observed density ( $n/km^2$ ) of Great Cormorant during ship-based surveys 2002-2011. Densities have been corrected for distance bias.



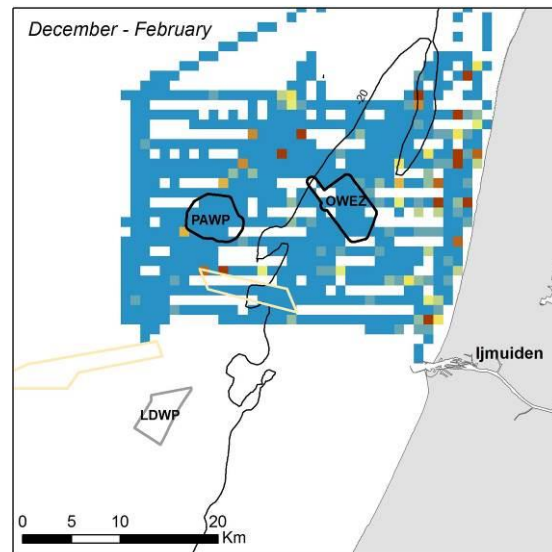
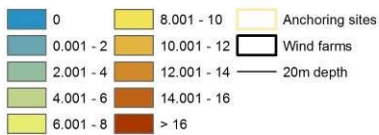
**Common Scoter - *Melanitta nigra***  
**Seasonal Mean Density 2002-2011**



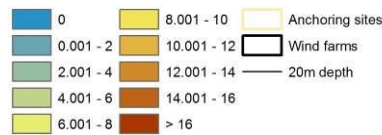
**Common Scoter - *Melanitta nigra***  
**Seasonal Mean Density 2002-2011**



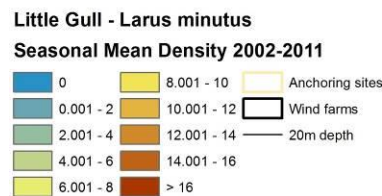
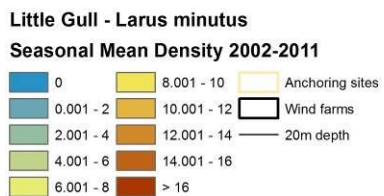
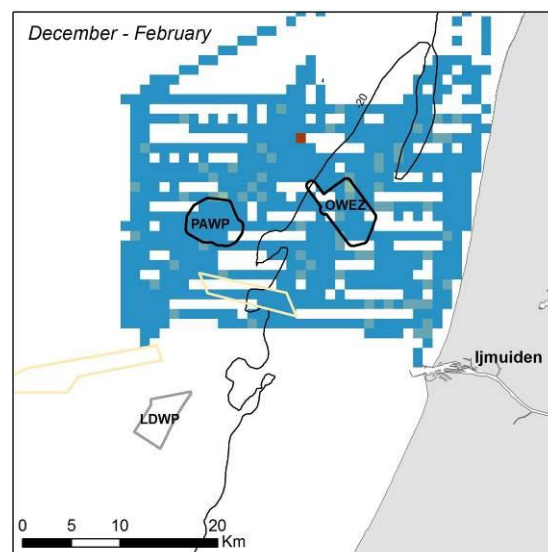
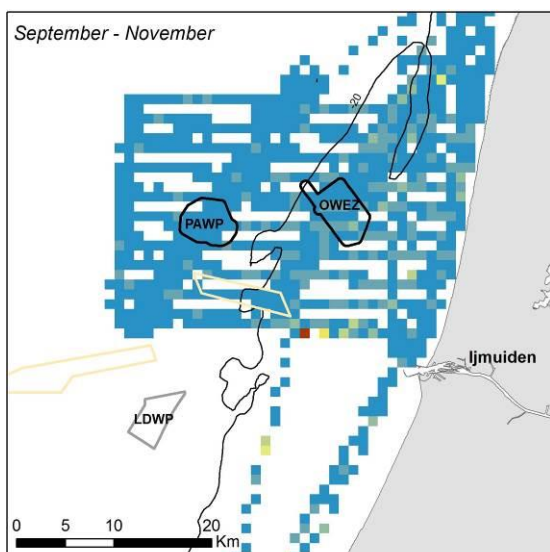
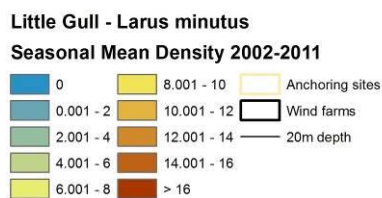
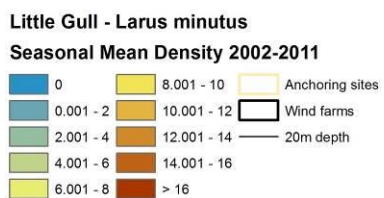
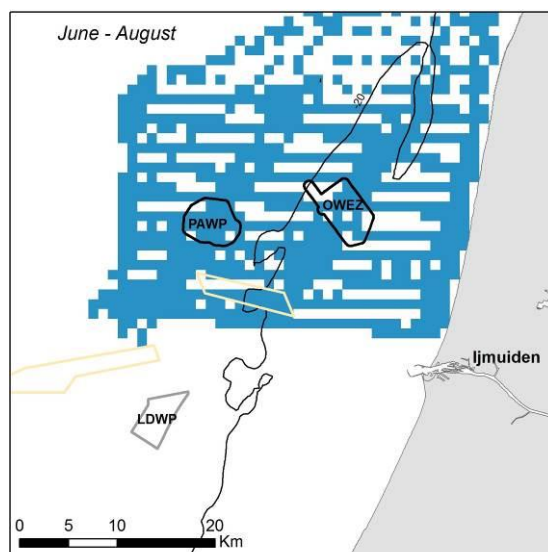
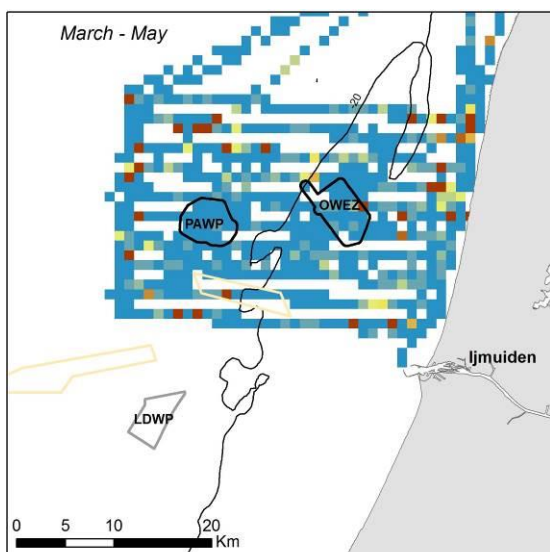
**Common Scoter - *Melanitta nigra***  
**Seasonal Mean Density 2002-2011**



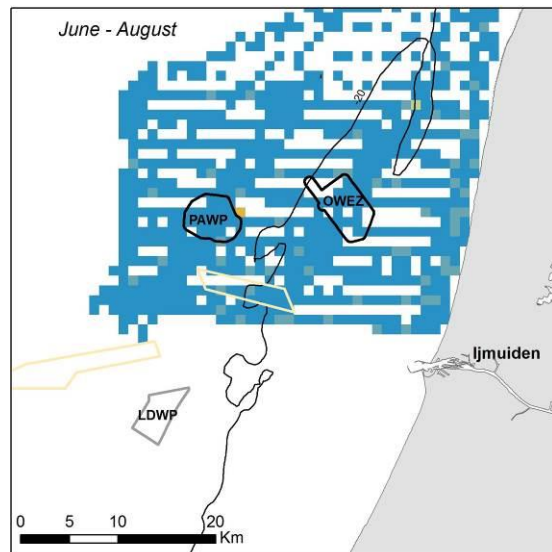
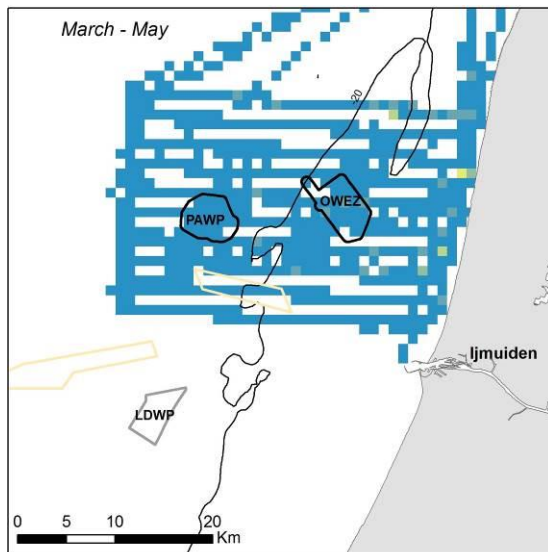
**Common Scoter - *Melanitta nigra***  
**Seasonal Mean Density 2002-2011**



Seasonal mean observed density ( $n/km^2$ ) of Common Scoter during ship-based surveys 2002-2011. Densities have been corrected for distance bias.

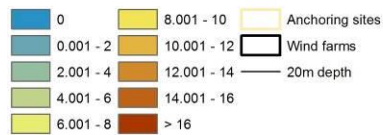


Seasonal mean observed density ( $n/km^2$ ) of Little Gull during ship-based surveys 2002-2011. Densities have been corrected for distance bias.



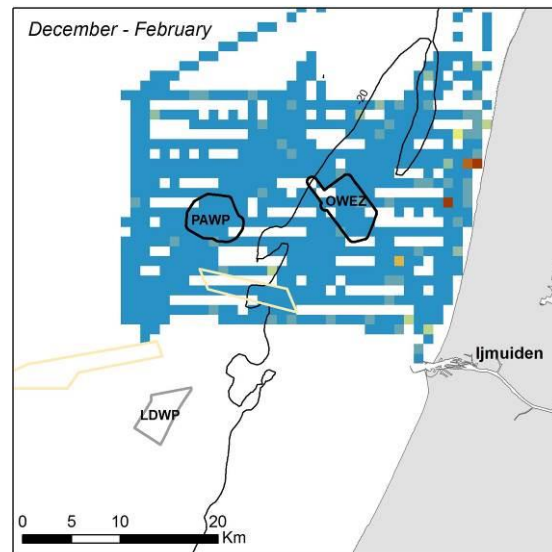
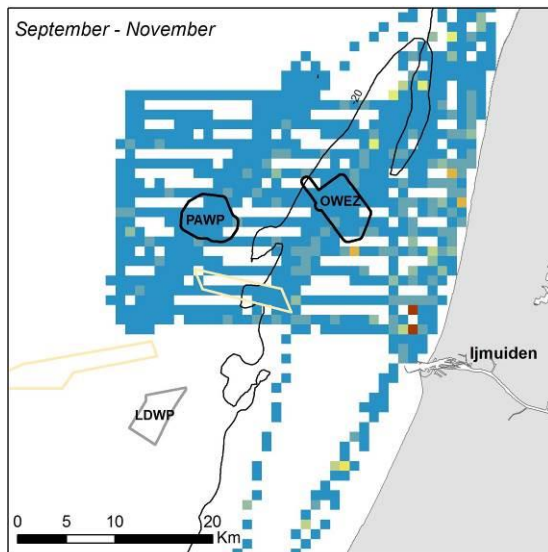
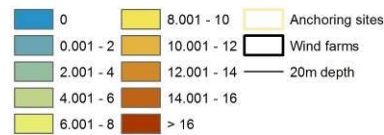
**Black-headed Gull - *Larus ridibundus***

**Seasonal Mean Density 2002-2011**



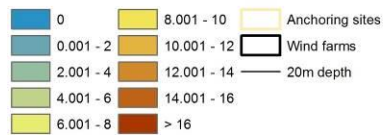
**Black-headed Gull - *Larus ridibundus***

**Seasonal Mean Density 2002-2011**



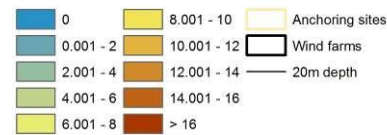
**Black-headed Gull - *Larus ridibundus***

**Seasonal Mean Density 2002-2011**

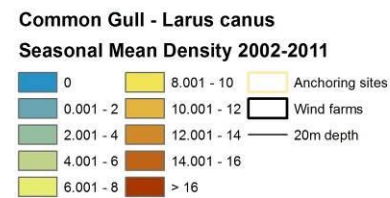
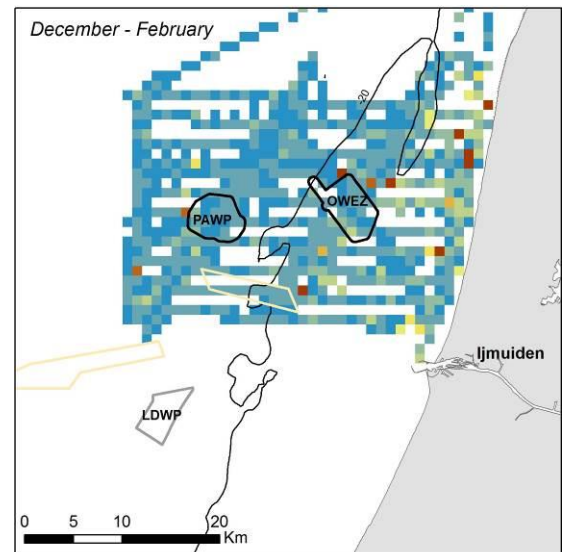
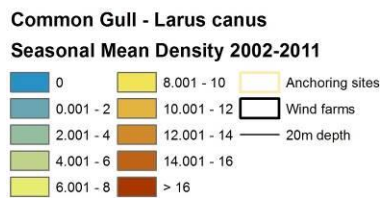
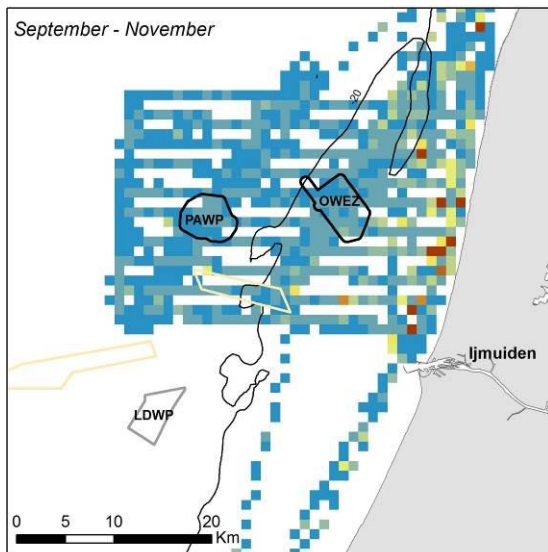
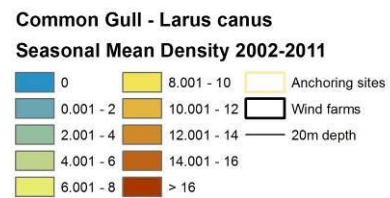
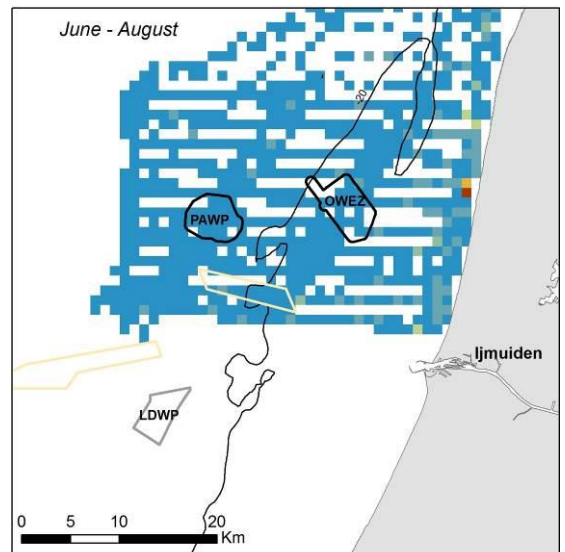
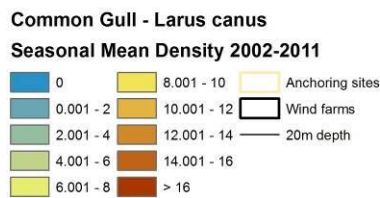
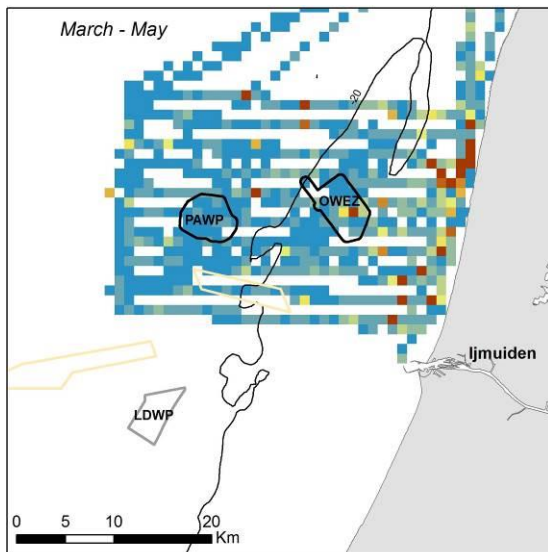


**Black-headed Gull - *Larus ridibundus***

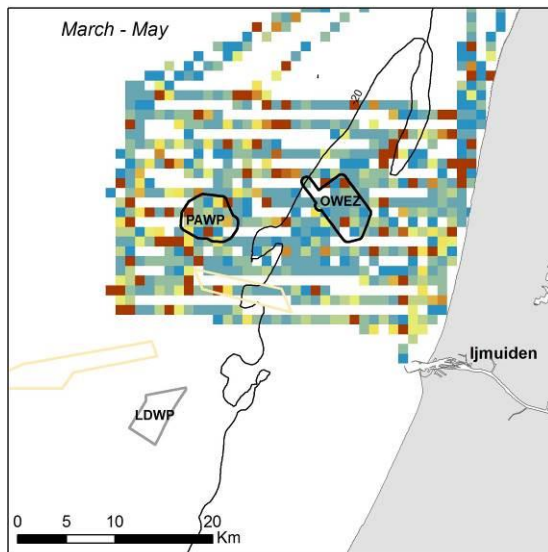
**Seasonal Mean Density 2002-2011**



Seasonal mean observed density ( $n/km^2$ ) of Black-headed Gull during ship-based surveys 2002-2011. Densities have been corrected for distance bias.

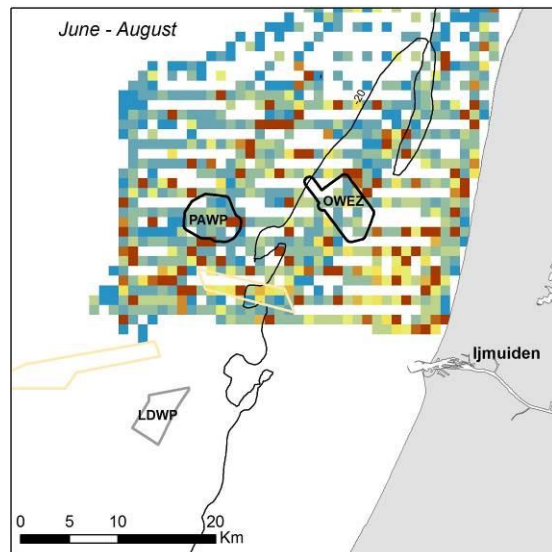
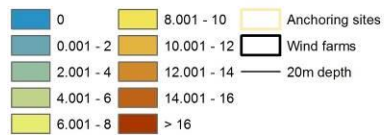


Seasonal mean observed density ( $n/km^2$ ) of Common Gull during ship-based surveys 2002-2011. Densities have been corrected for distance bias.



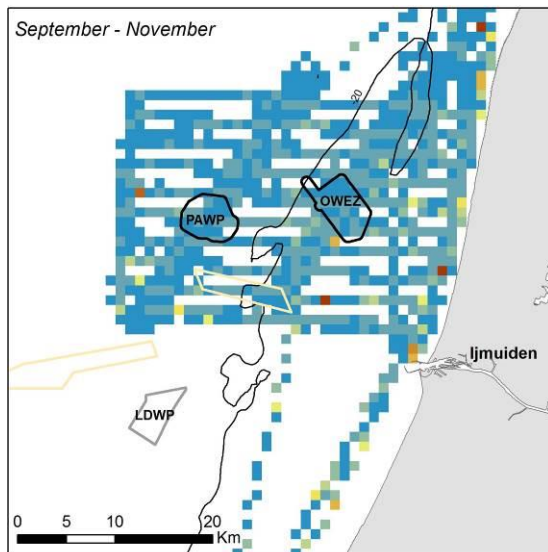
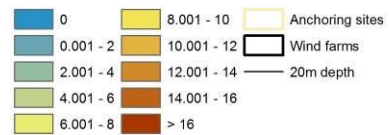
**Lesser Black-backed Gull - *Larus fuscus***

**Seasonal Mean Density 2002-2011**



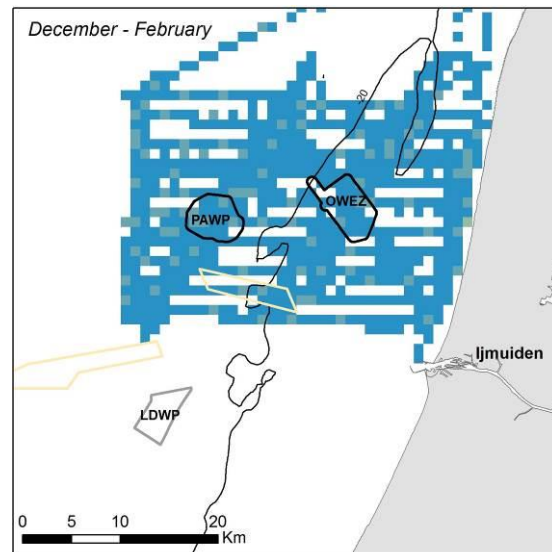
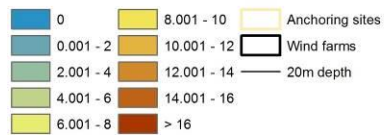
**Lesser Black-backed Gull - *Larus fuscus***

**Seasonal Mean Density 2002-2011**



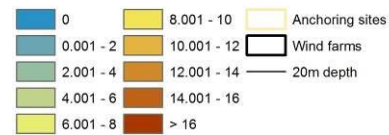
**Lesser Black-backed Gull - *Larus fuscus***

**Seasonal Mean Density 2002-2011**

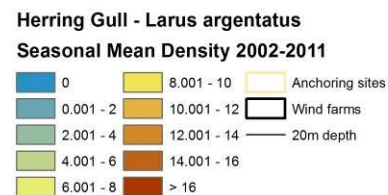
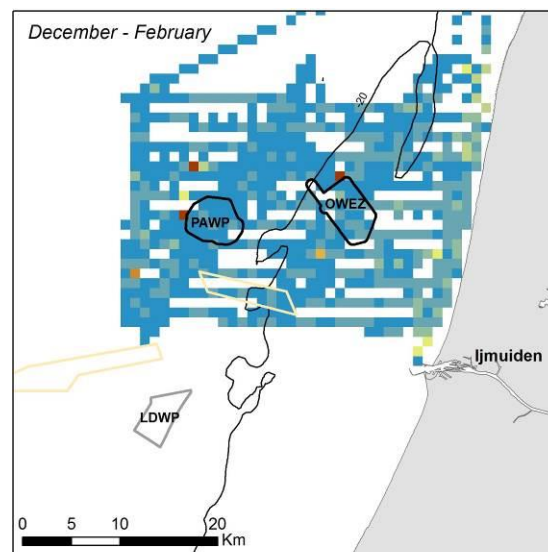
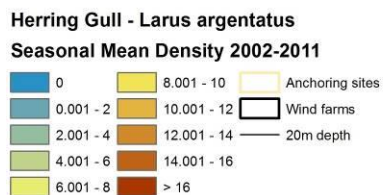
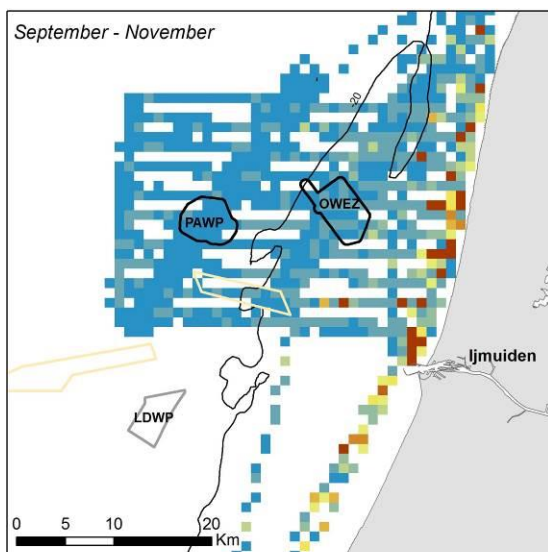
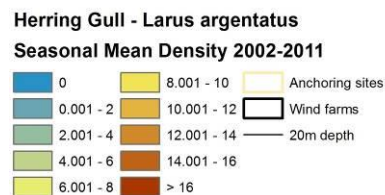
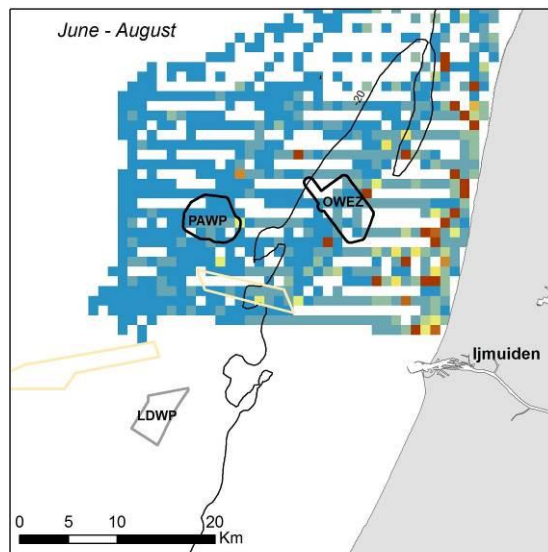
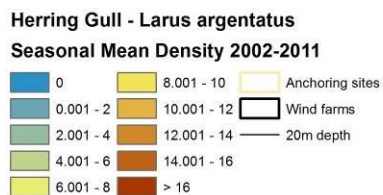
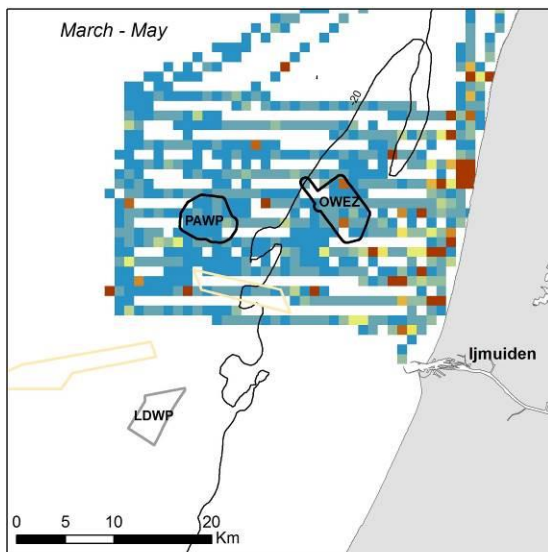


**Lesser Black-backed Gull - *Larus fuscus***

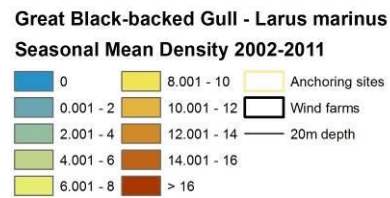
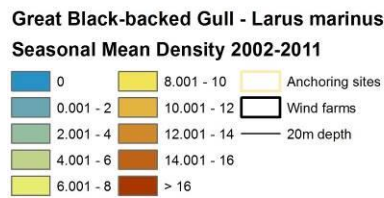
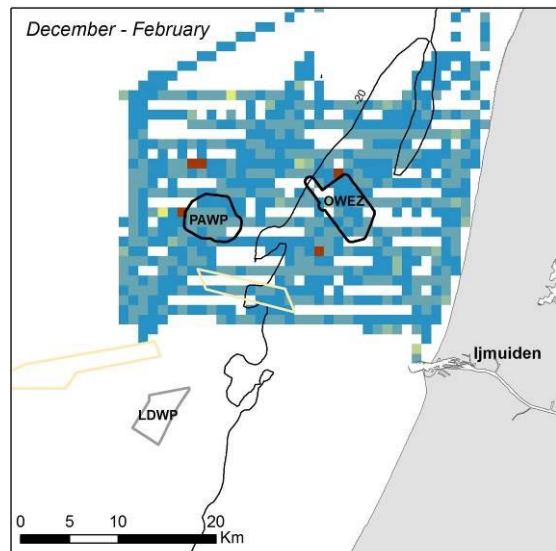
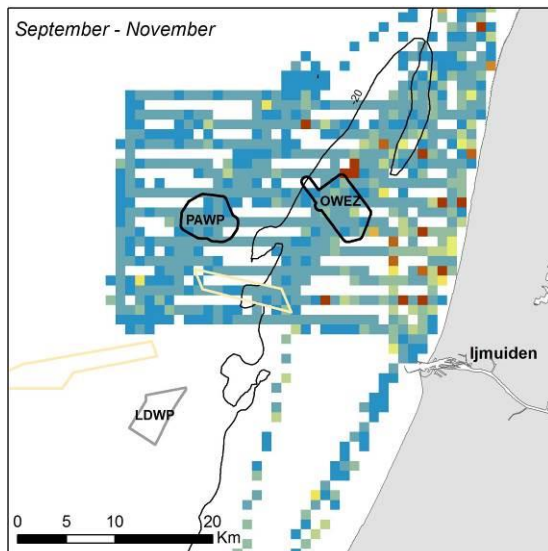
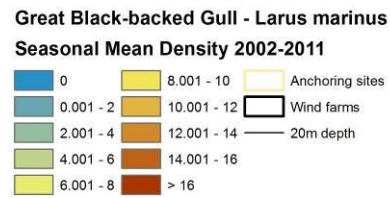
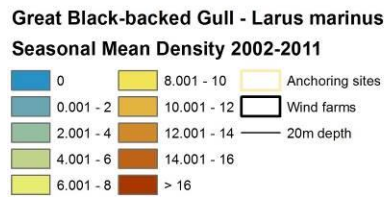
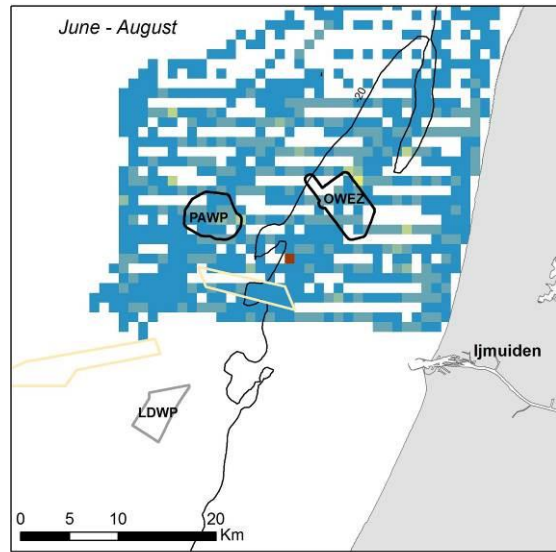
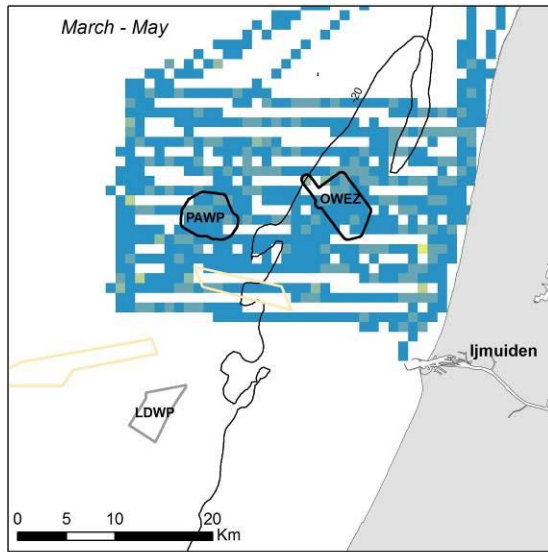
**Seasonal Mean Density 2002-2011**



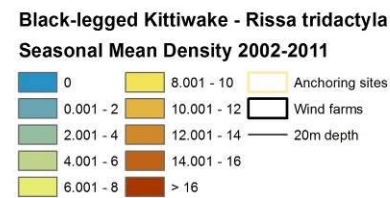
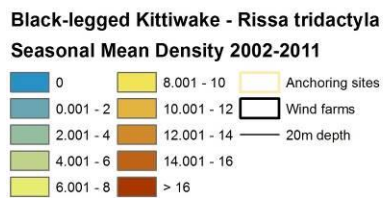
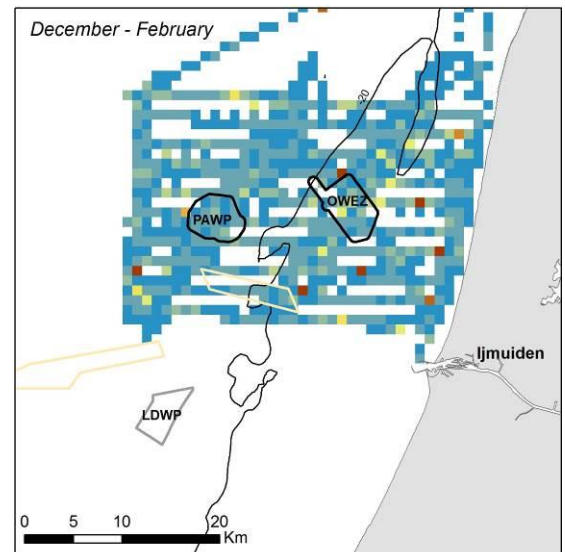
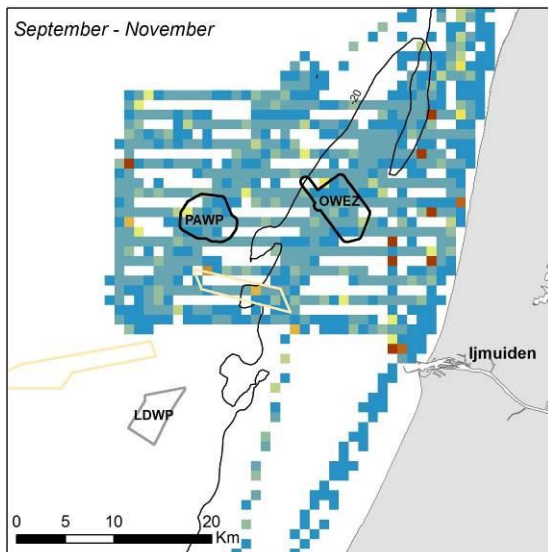
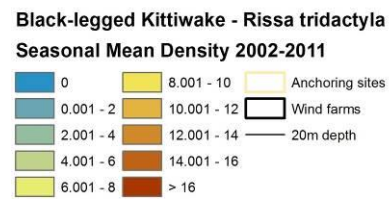
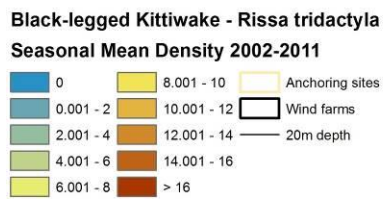
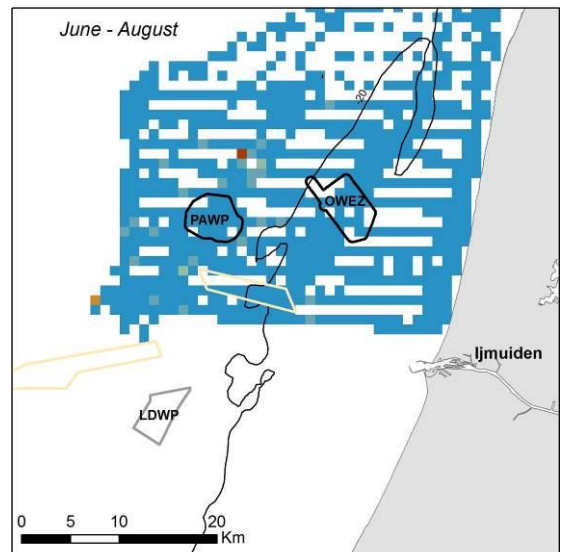
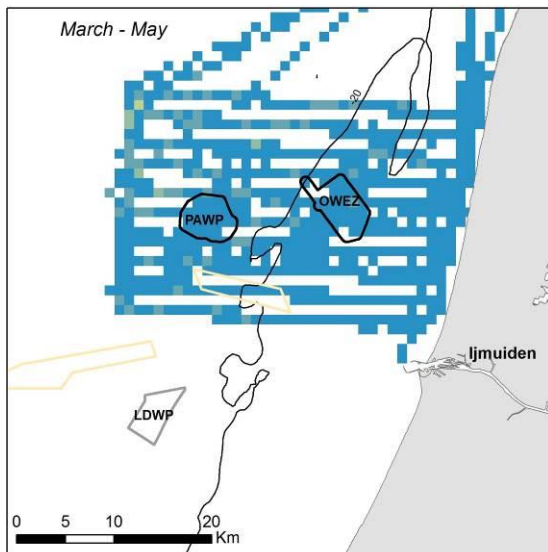
Seasonal mean observed density ( $n/km^2$ ) of Lesser Black-backed Gull during ship-based surveys 2002-2011. Densities have been corrected for distance bias.



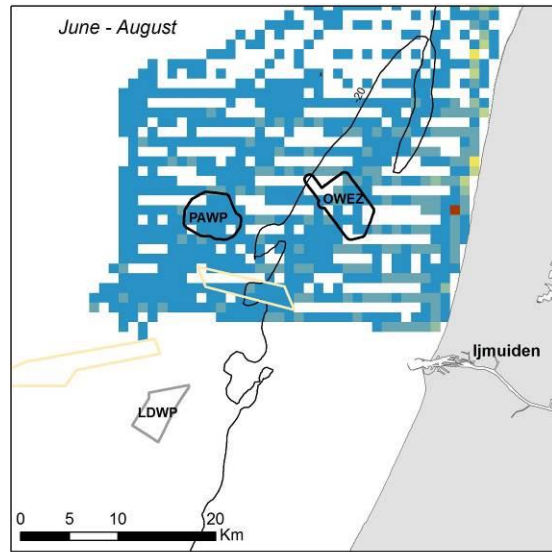
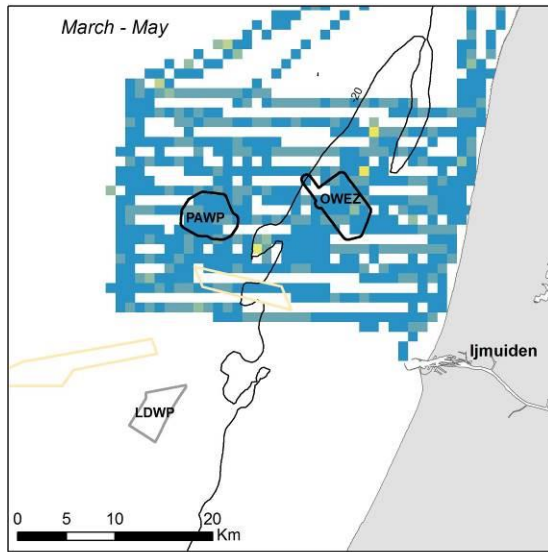
Seasonal mean observed density ( $n/km^2$ ) of Herring Gull during ship-based surveys 2002-2011. Densities have been corrected for distance bias.



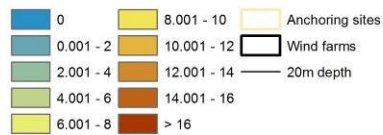
Seasonal mean observed density ( $n/km^2$ ) of Great Black-backed Gull during ship-based surveys 2002-2011. Densities have been corrected for distance bias.



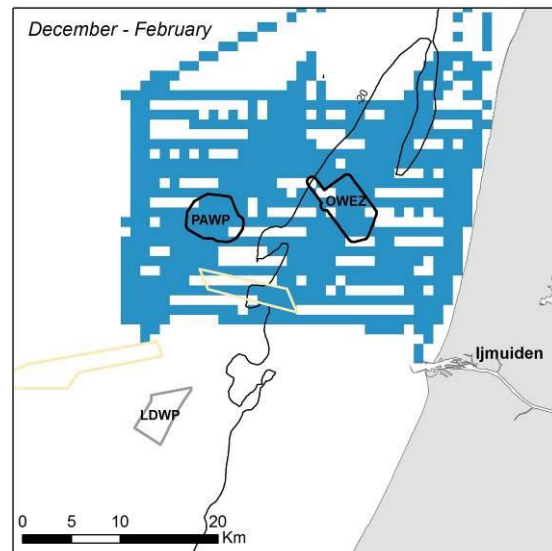
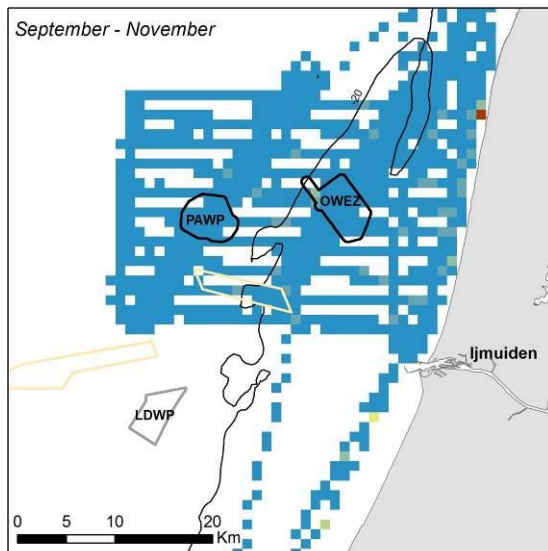
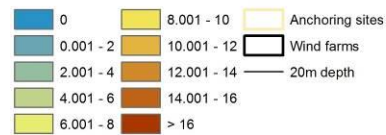
Seasonal mean observed density (n/km<sup>2</sup>) of Black-legged Kittiwake during ship-based surveys 2002-2011. Densities have been corrected for distance bias.



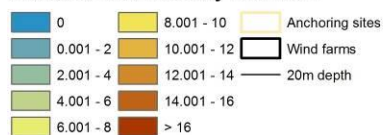
**Sandwich Tern - *Sterna sandvicensis***  
**Seasonal Mean Density 2002-2011**



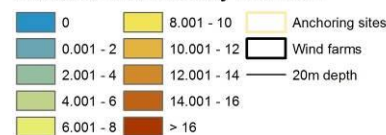
**Sandwich Tern - *Sterna sandvicensis***  
**Seasonal Mean Density 2002-2011**



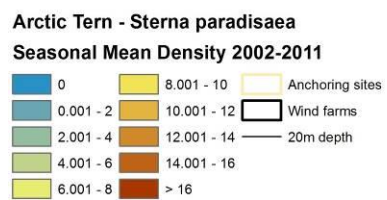
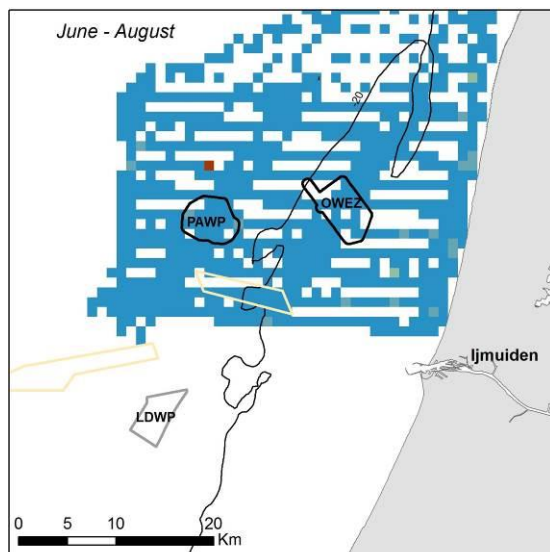
**Sandwich Tern - *Sterna sandvicensis***  
**Seasonal Mean Density 2002-2011**



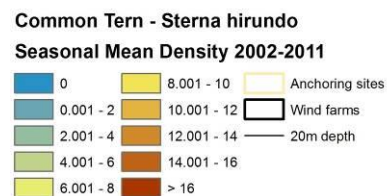
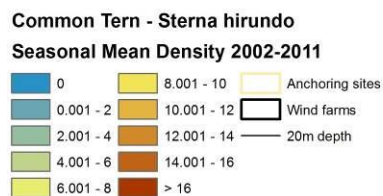
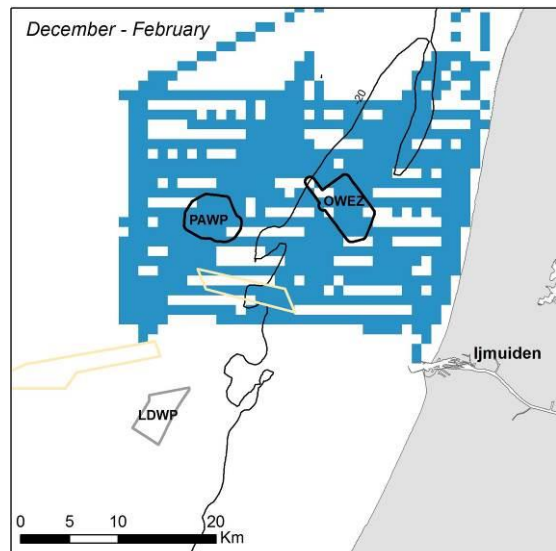
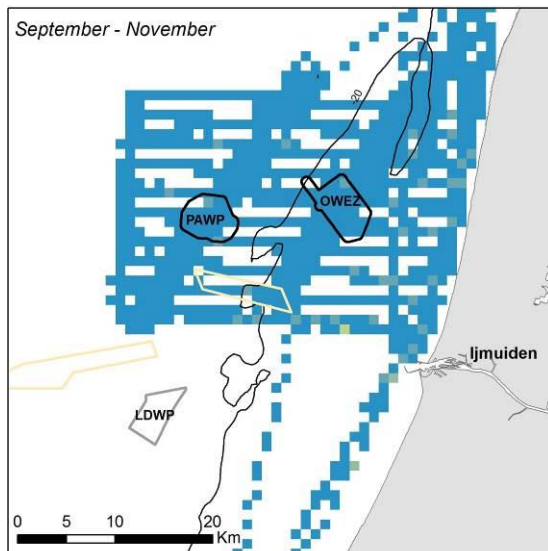
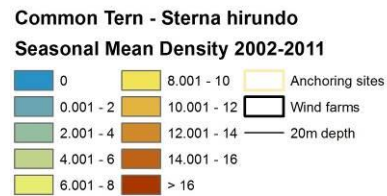
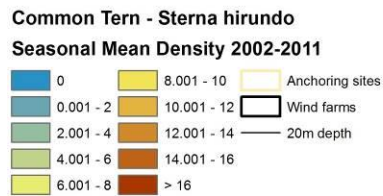
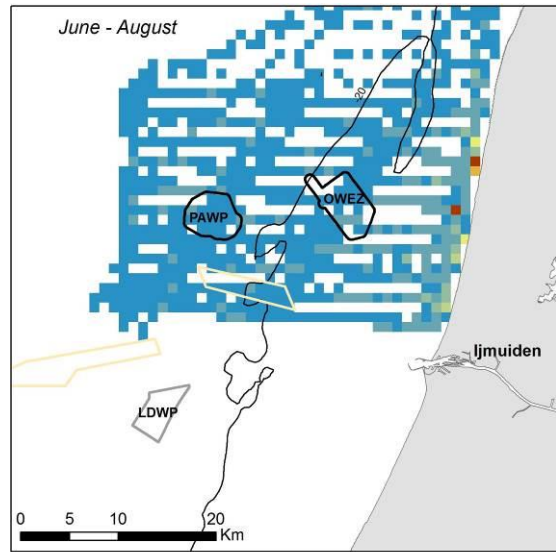
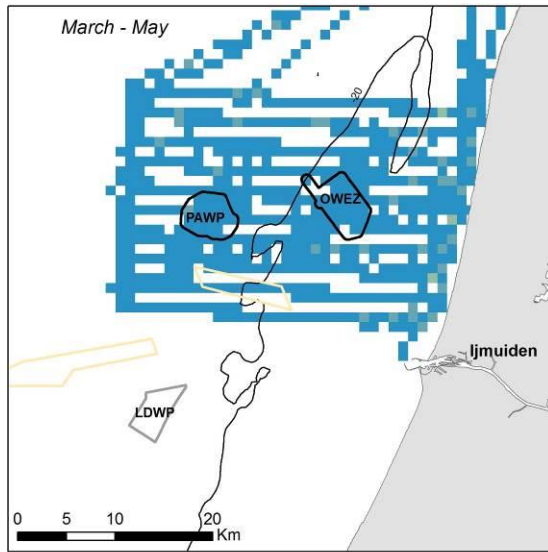
**Sandwich Tern - *Sterna sandvicensis***  
**Seasonal Mean Density 2002-2011**



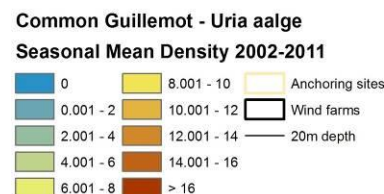
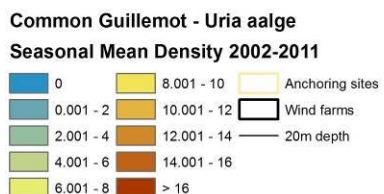
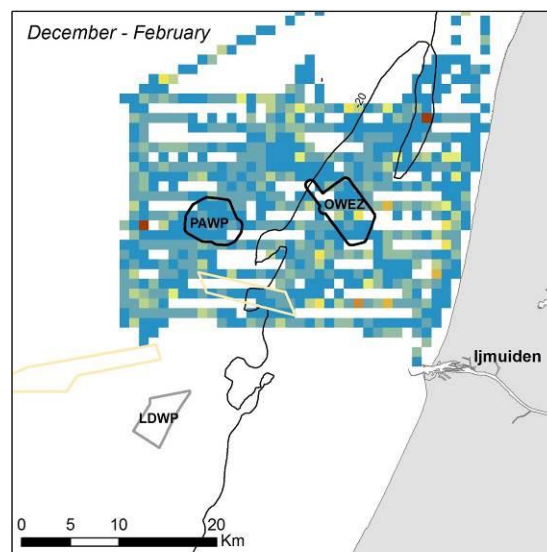
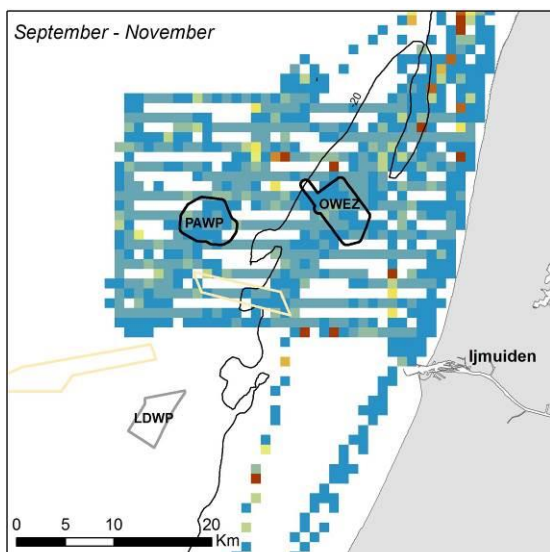
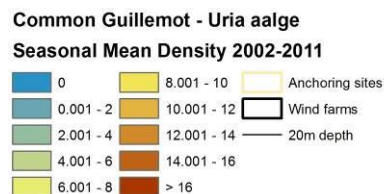
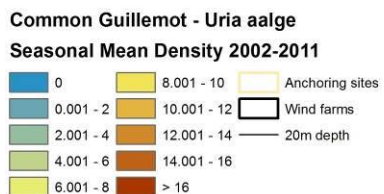
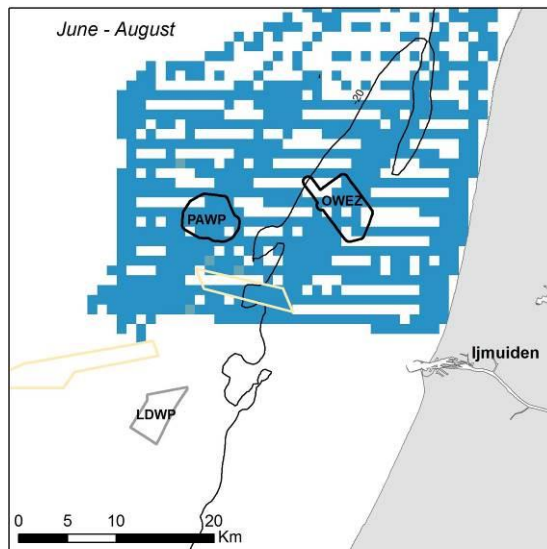
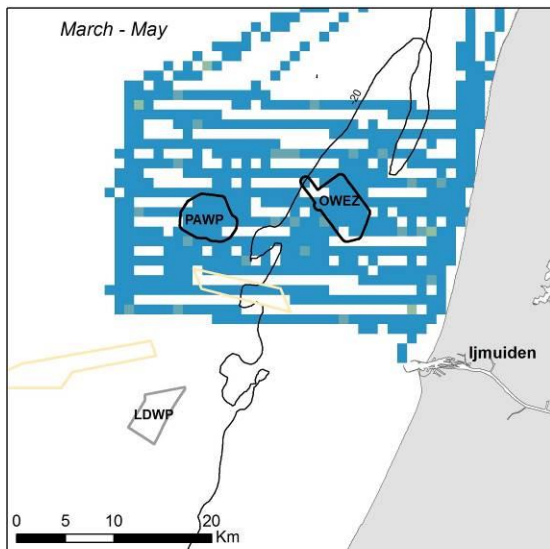
Seasonal mean observed density ( $n/km^2$ ) of Sandwich Tern during ship-based surveys 2002-2011. Densities have been corrected for distance bias.



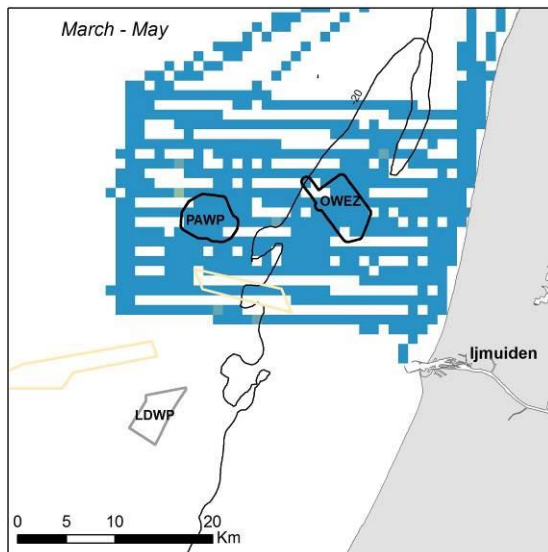
Mean observed density during summer ( $n/km^2$ ) of Arctic Terns during ship-based surveys 2002-2011. Densities have been corrected for distance bias.



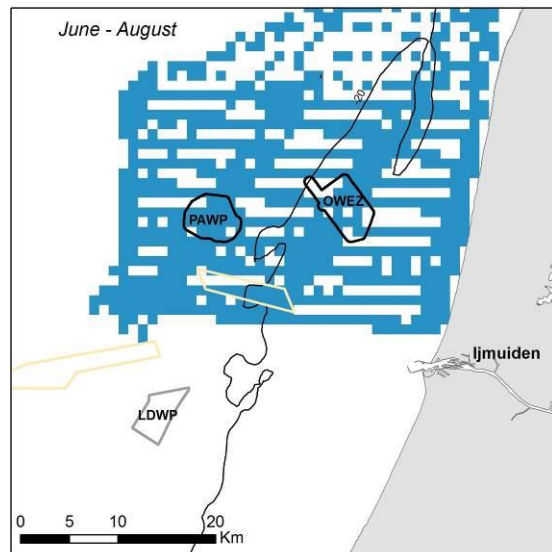
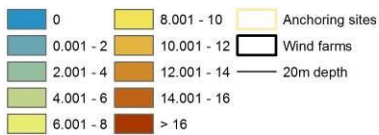
Mean observed density during summer ( $n/km^2$ ) of Common Terns during ship-based surveys 2002-2011. Densities have been corrected for distance bias.



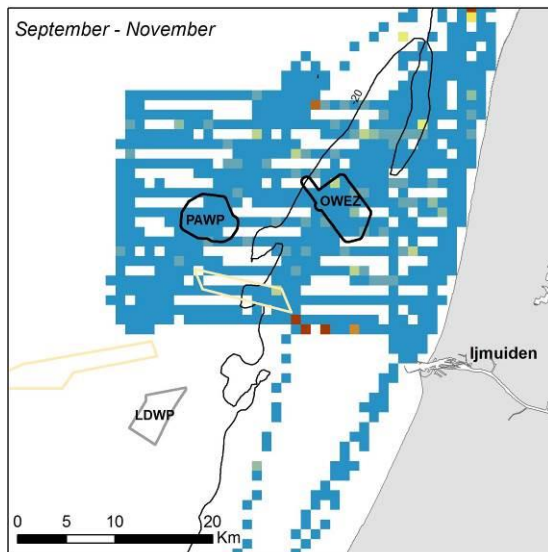
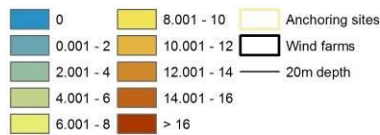
Seasonal mean observed density ( $n/km^2$ ) of Common Guillemot during ship-based surveys 2002-2011. Densities have been corrected for distance bias.



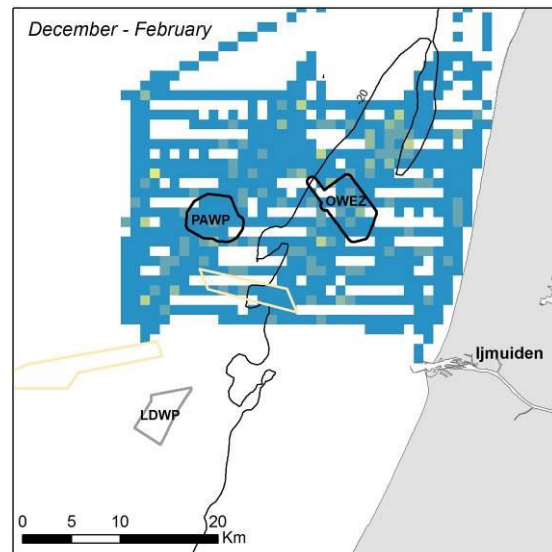
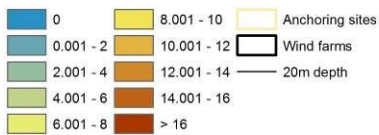
**Razorbill - Alca torda**  
**Seasonal Mean Density 2002-2011**



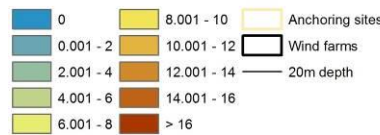
**Razorbill - Alca torda**  
**Seasonal Mean Density 2002-2011**



**Razorbill - Alca torda**  
**Seasonal Mean Density 2002-2011**

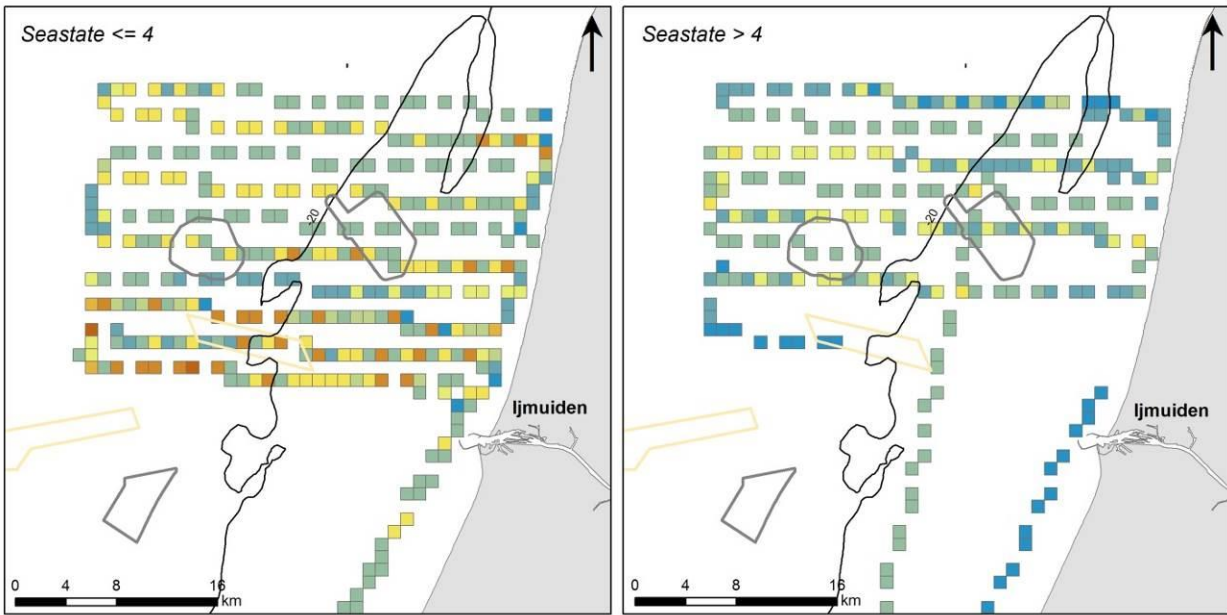


**Razorbill - Alca torda**  
**Seasonal Mean Density 2002-2011**

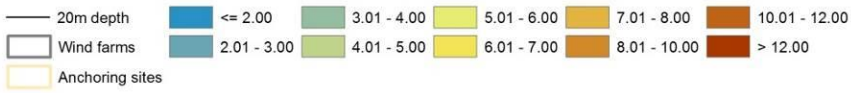


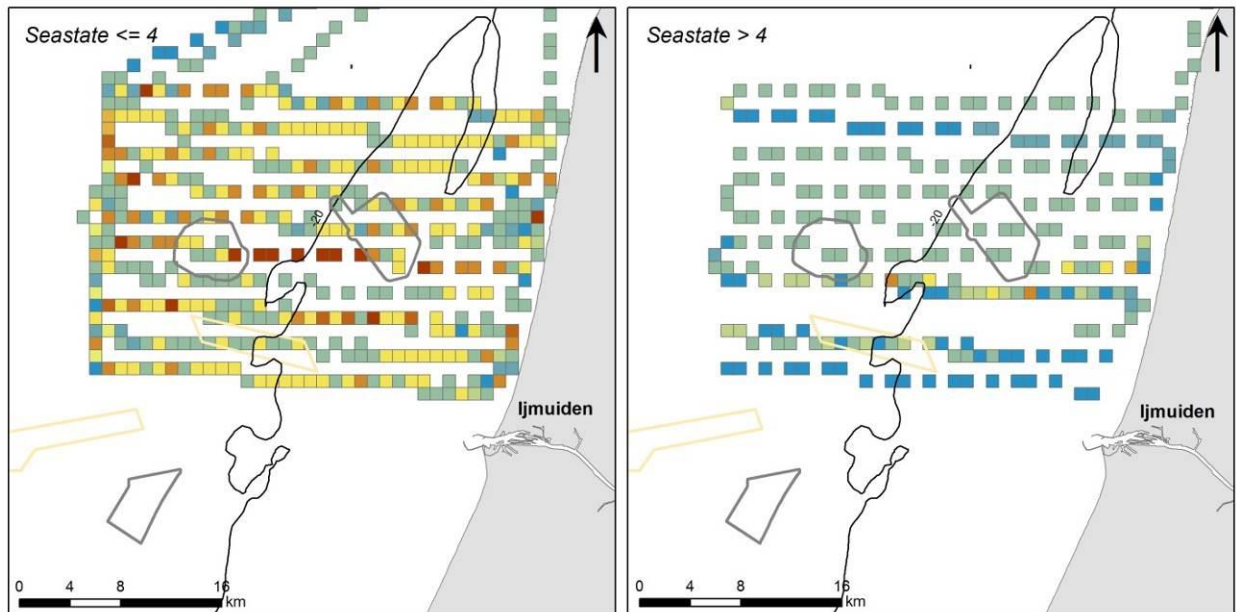
Seasonal mean observed density ( $n/km^2$ ) of Razorbill during ship-based surveys 2002-2011. Densities have been corrected for distance bias.

## APPENDIX D – Survey effort 2002-2010

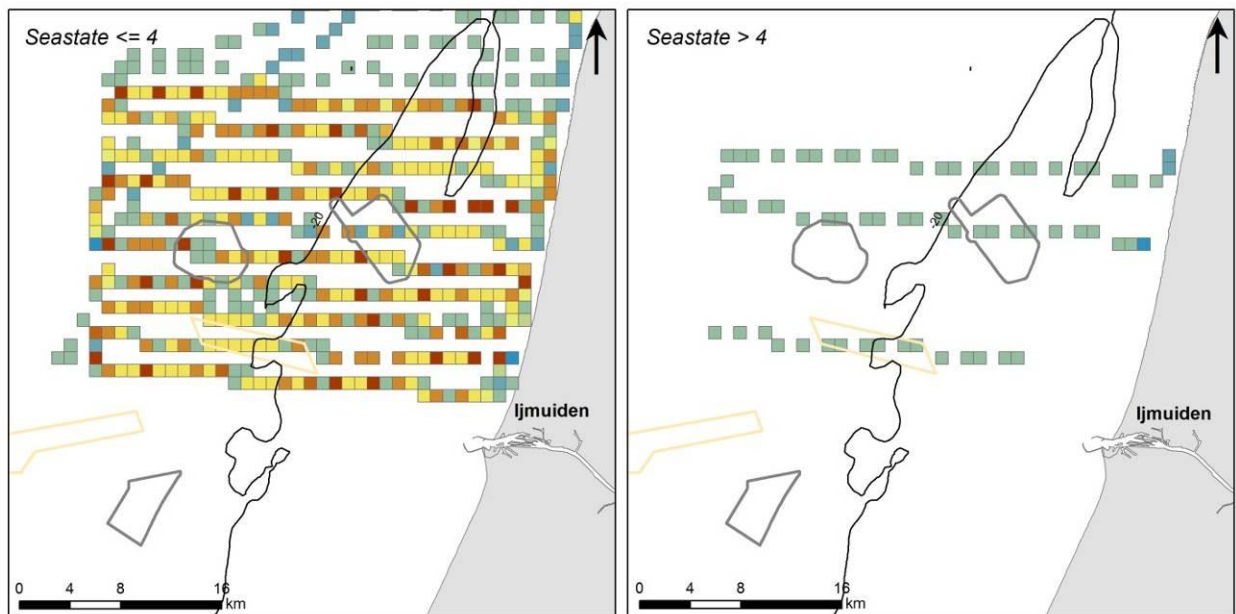


**2002 Autumn - Km surveyed**

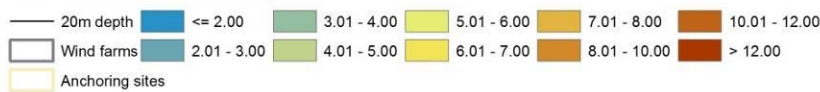


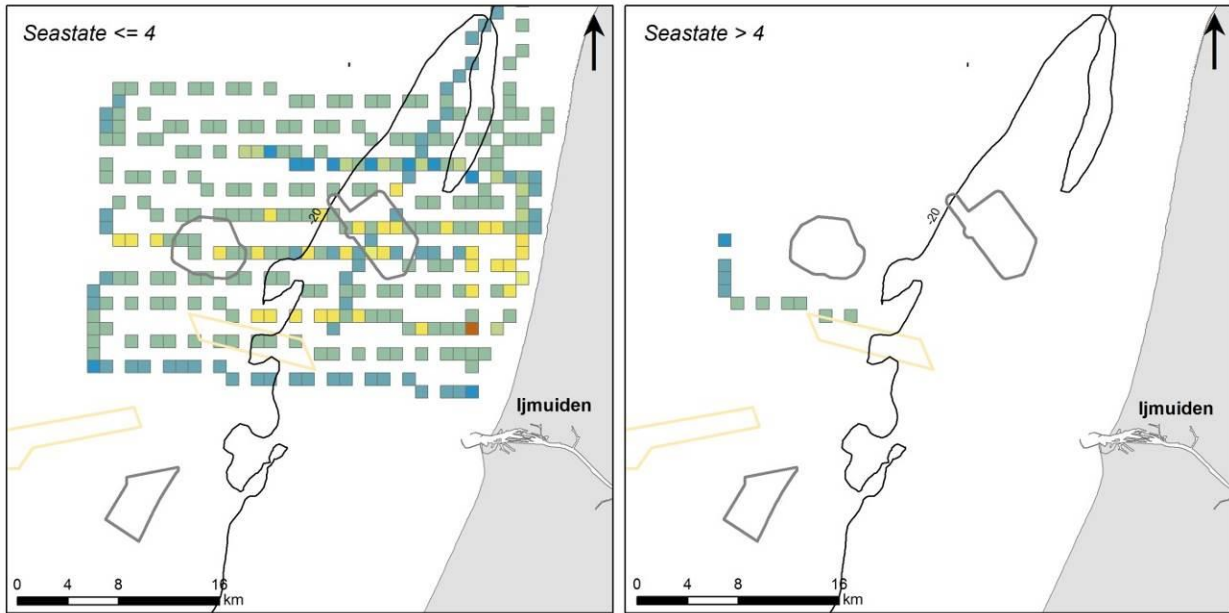


**2003 Spring - Km surveyed**

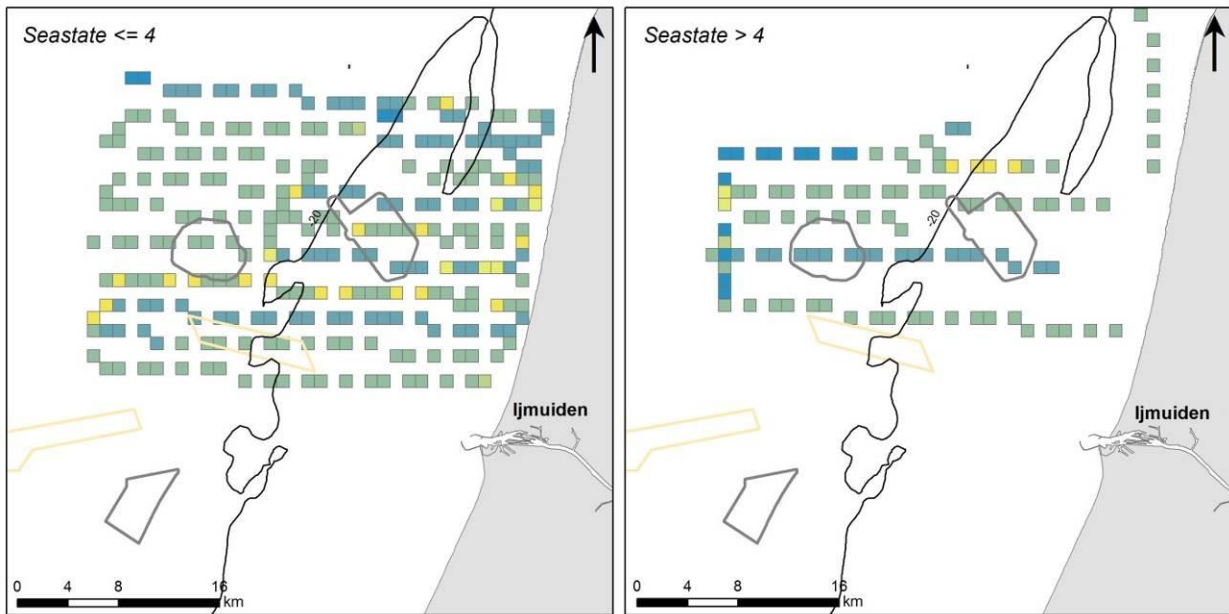
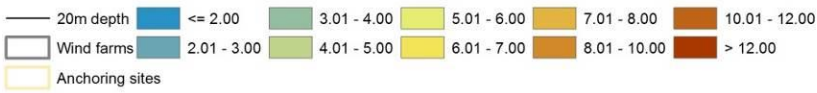


**2003 Summer - Km surveyed**



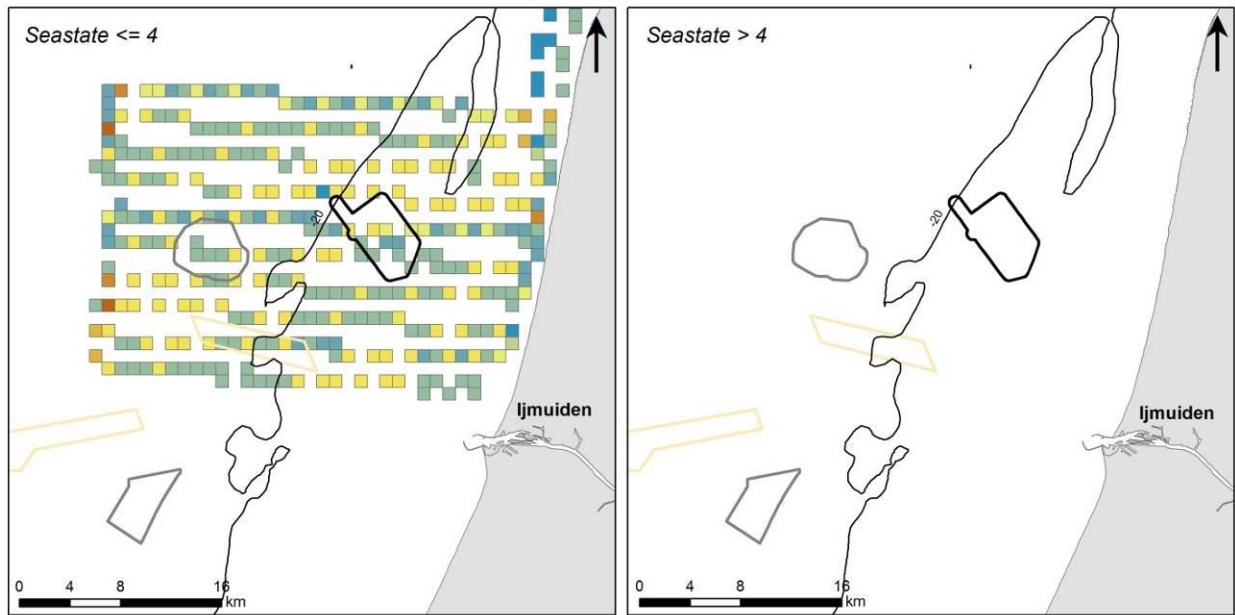


**2003 Autumn - Km surveyed**

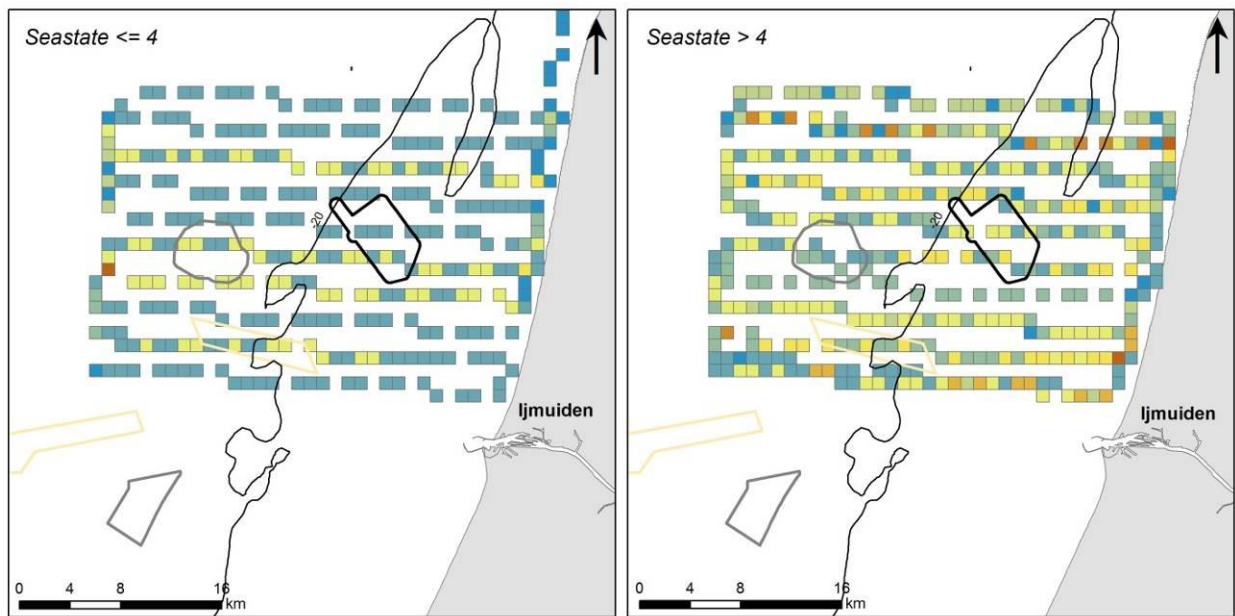


**2004 Winter - Km surveyed**



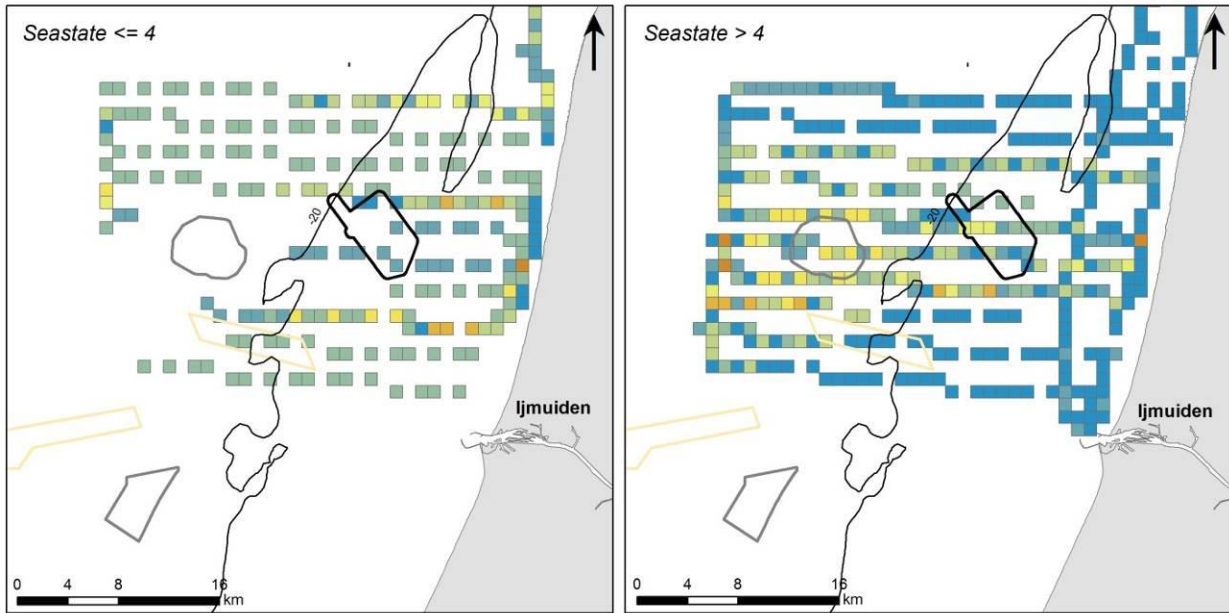


**2007 Spring - Km surveyed**

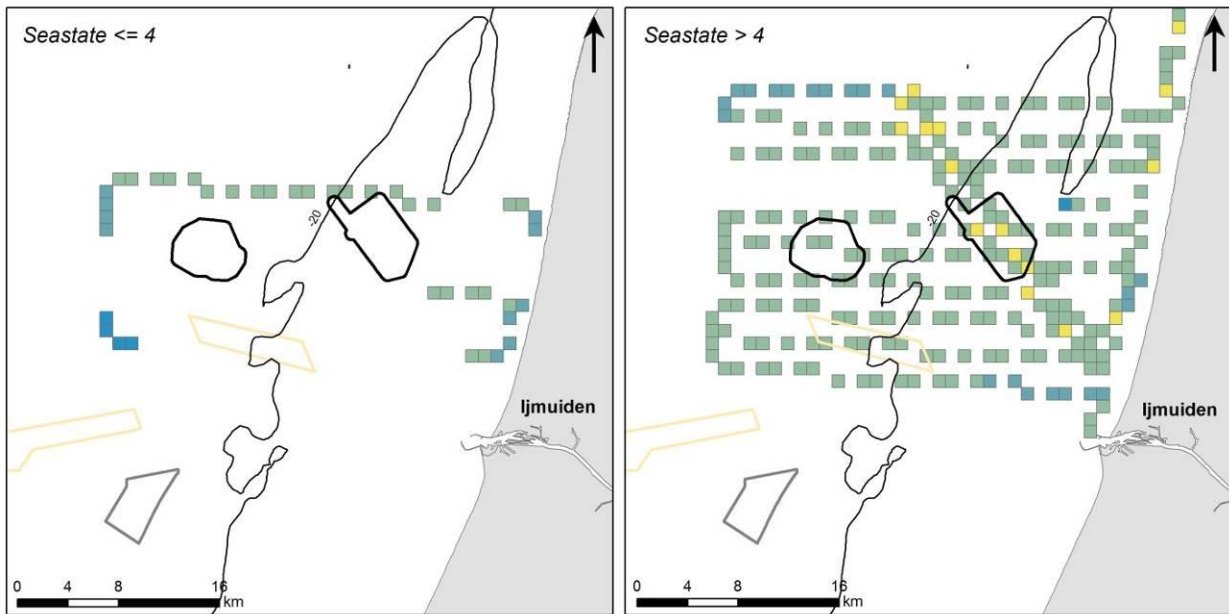
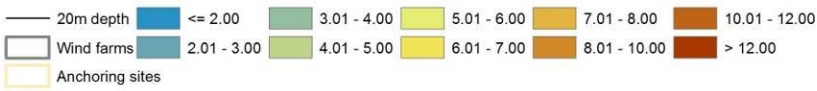


**2007 Summer - Km surveyed**



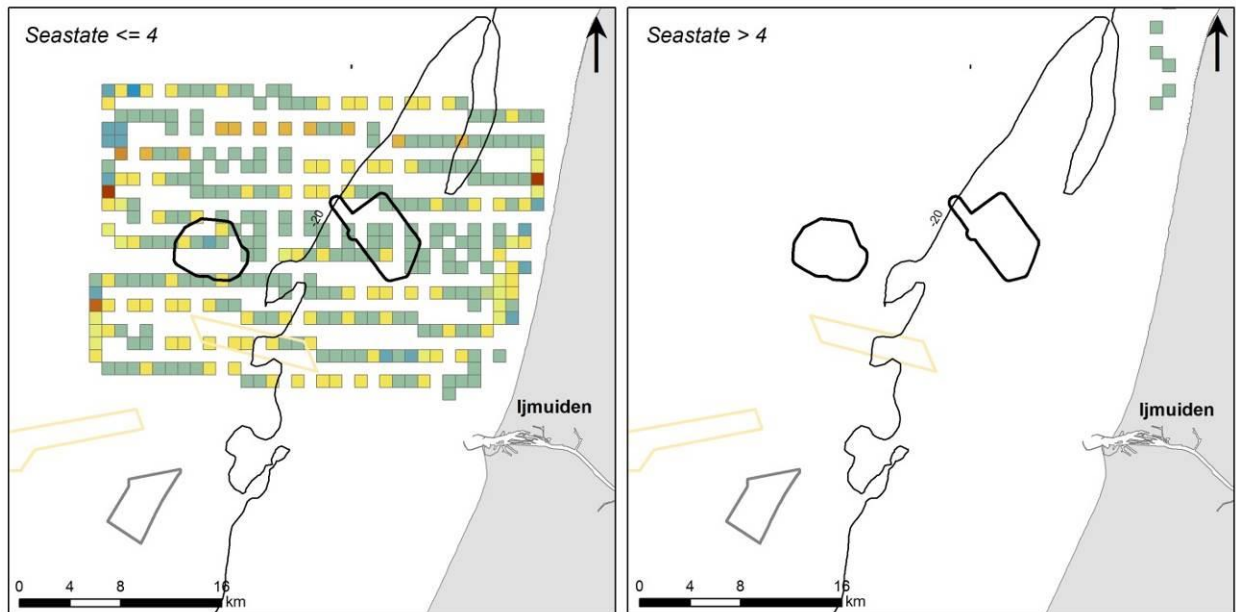


**2007 Autumn - Km surveyed**

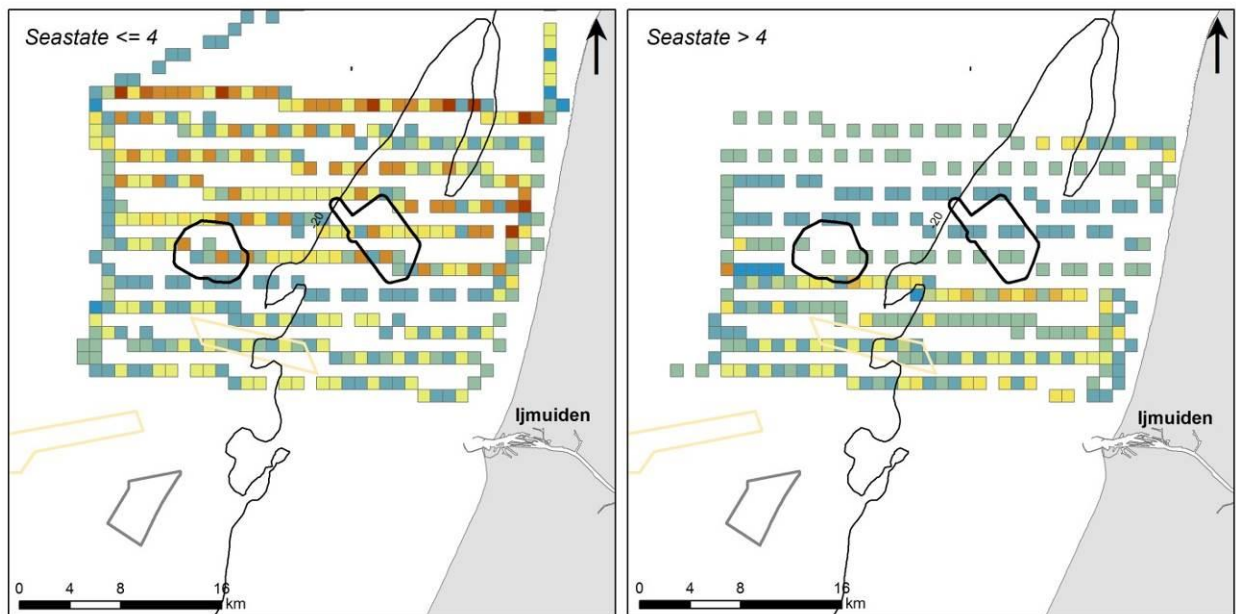


**2008 Winter - Km surveyed**



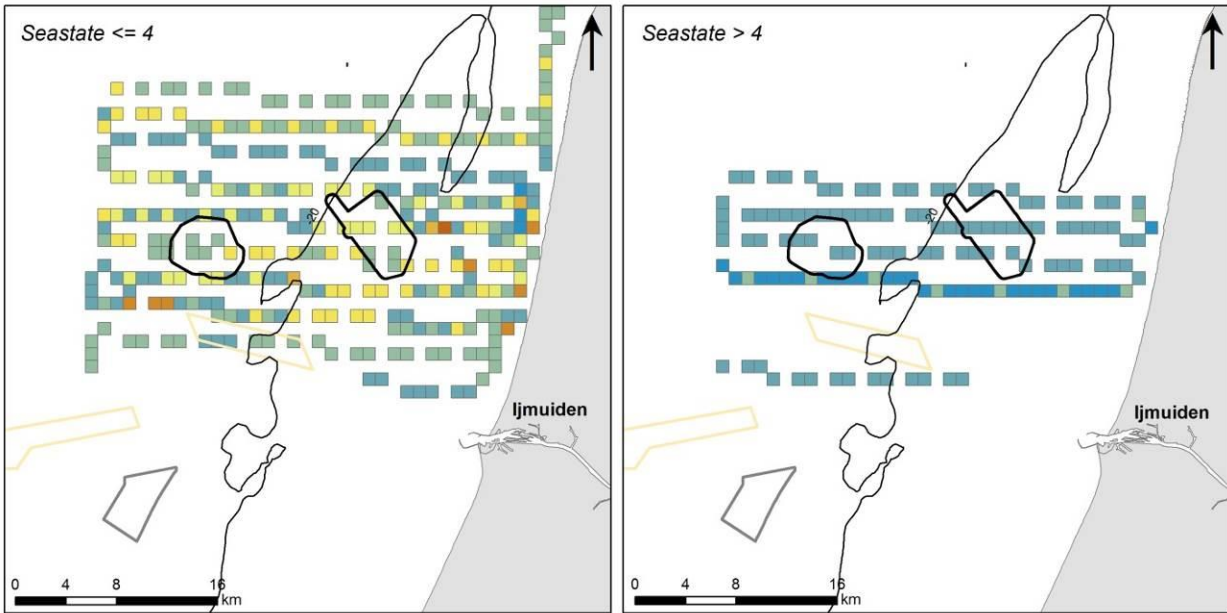


**2008 Spring - Km surveyed**

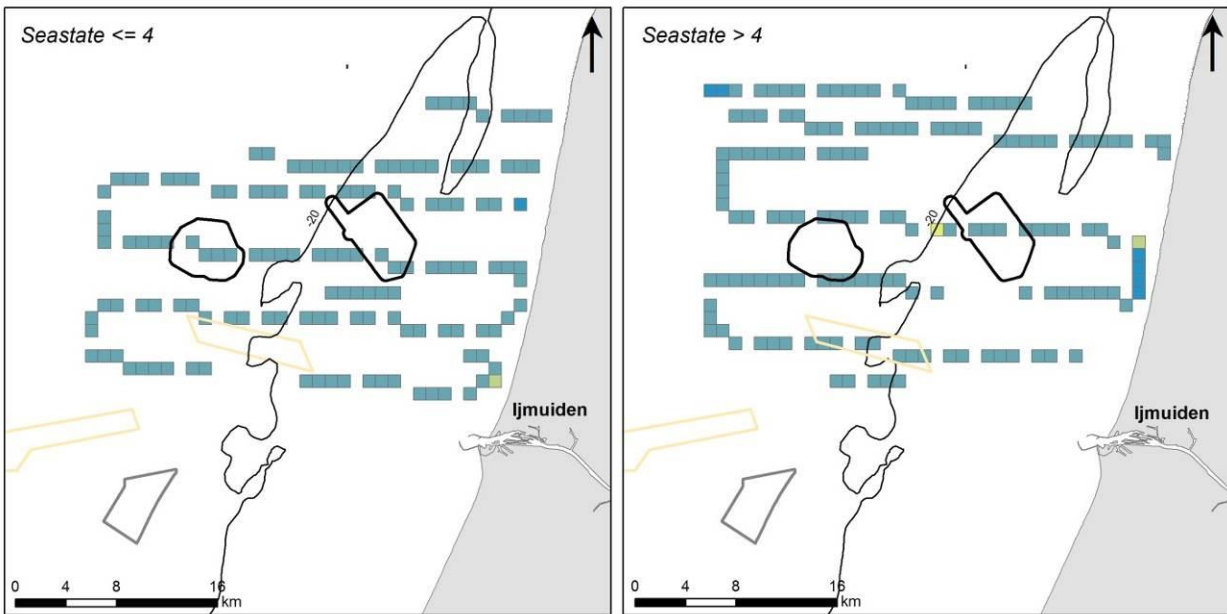
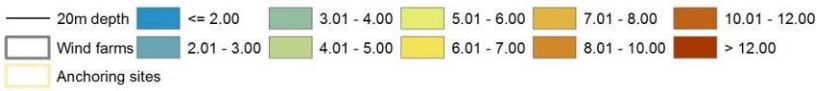


**2008 Summer - Km surveyed**



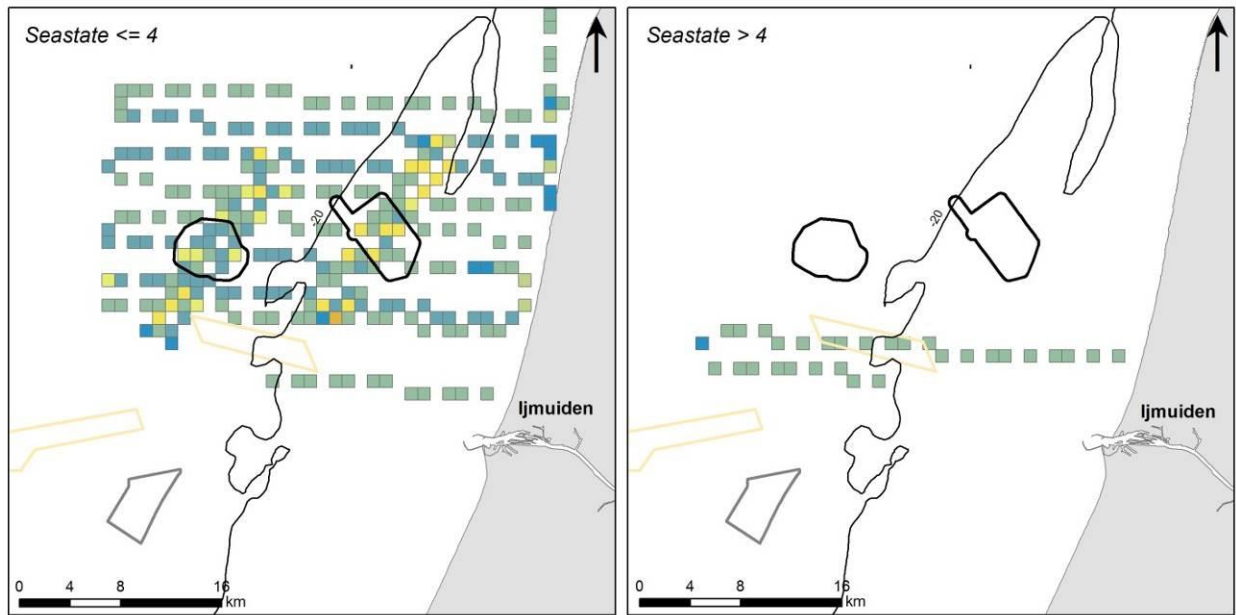


**2008 Autumn - Km surveyed**

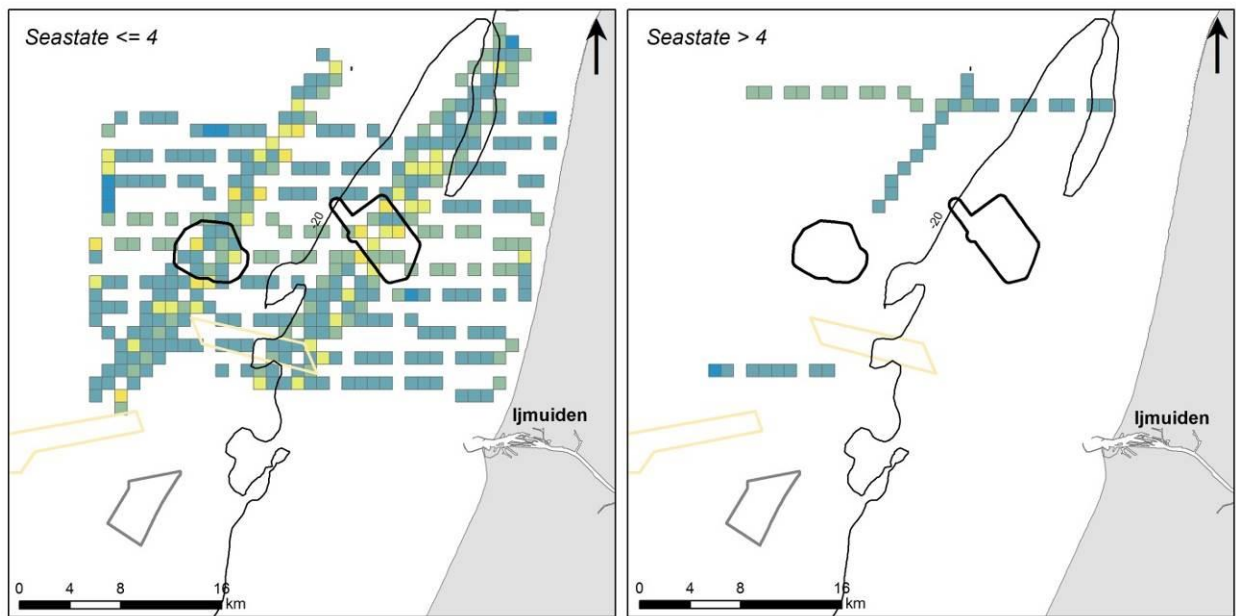


**2009 Winter - Km surveyed**



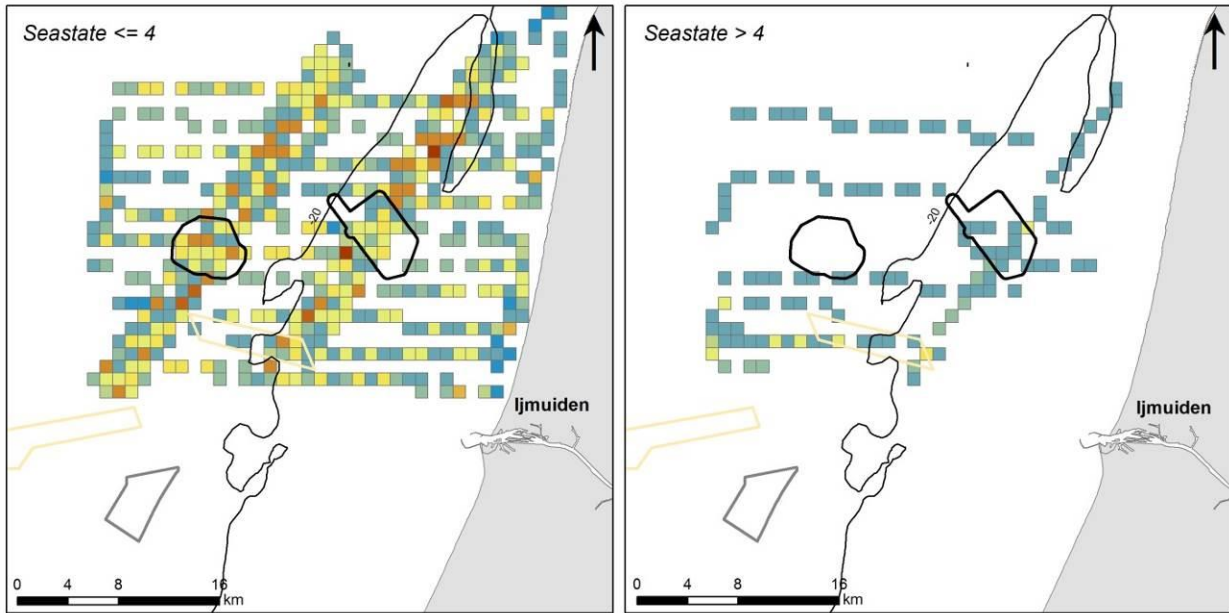


**2009 Spring - Km surveyed**

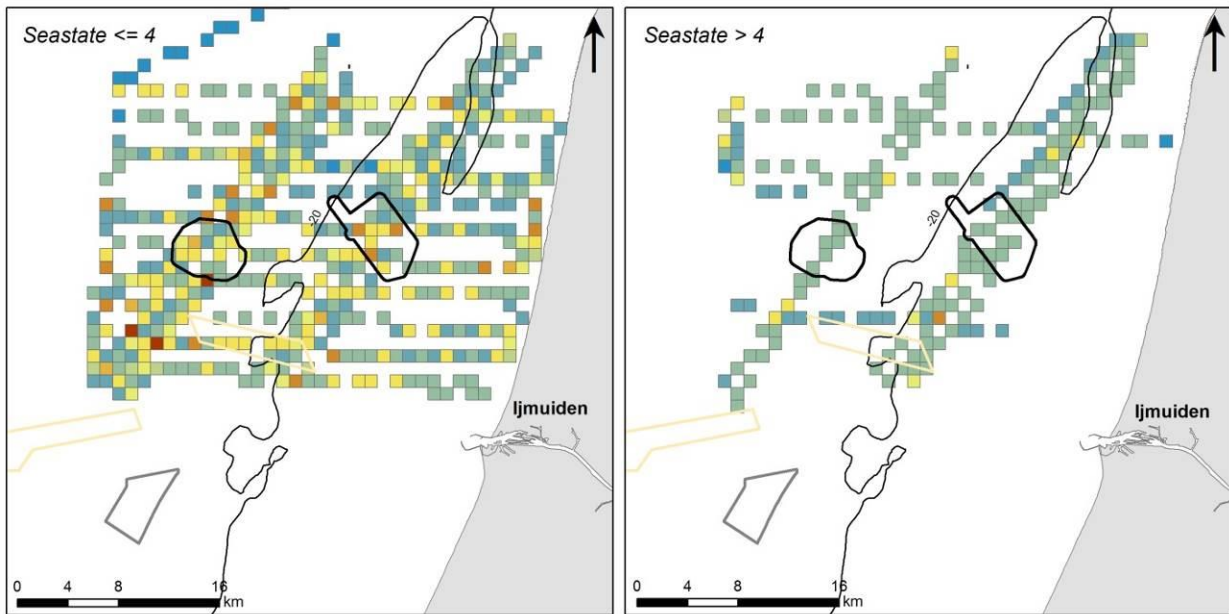
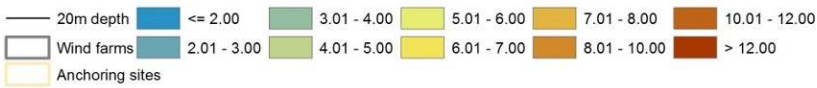


**2009 Summer - Km surveyed**





**2009 Autumn - Km surveyed**



**2010 Winter - Km surveyed**

